Automation and Traction Control of Articulated Vehicles

Ulf Andersson

LULEÅ
UNIVERSITY
OF TECHNOLOGY

Automation and Traction Control of Articulated Vehicles

Ulf Andersson

Luleå University of Technology
Department of Computer Science, Electrical and Space Engineering
Division of Systems and Interaction

To my family

ABSTRACT

Articulated machines such as load-haul-dump machines, wheel loaders and haulers operate in many different environments and driving conditions. In particular they need to be able to perform well with road conditions and loads that can change drastically, setting hard requirements on performances and robustness. The control challenges for off-road vehicles are hence quite different from standard cars or trucks, which mostly drive on regular roads.

An important aspect characterising this is the fact that wheel slip may cause severe damage to the wheels and ground. Particularly, tyre lifespan is a serious problem since for instance in a modern hauler the tyres often represents 20%-25% of a hauler overall operating cost. Better traction control algorithms can strongly contribute to reducing tyre wear and hence operating costs.

Increasing fuel prices and increasing environmental awareness have influenced all the main vehicle manufacturers so that the commitment towards less fuel consumption has become one of the main goals for development. During the last few years' hybrid vehicles have been vigorously developed. For wheel loaders, in particular, the series hybrid concept seems to be suitable whereby a diesel engine generates electricity for a battery that serves as the power source of the individual wheel motors, enabling regenerative braking as well as partial recovery of the energy necessary to lift the load. Hence, traction control algorithms should be adapted for use with individual wheel drives.

Load-haul-dump machines, wheel loaders and haulers are sometimes used in cyclic operations in isolated areas, which is a typical driver for automation. The use of the load-haul-dump machine in underground hard rock mines such as iron ore mines is one example where the conditions for automation are excellent. The working conditions for a driver in the cabin are monotone. The working conditions are improved by moving the driver from the machine to a control room and alternate between different remote operations, for instance between load-haul-dump machines and remote controlled rock breaker. Moving the driver from the cabin to the control room also have a positive effect on the personnel costs since one operator can handle several machines.

However, for the automation to be successful, the cycle time and loading capacity of an automated machine has to match a manual machine operated by skilled drivers. A challenge is the remote bucket filling, where traditional tele remote loading is based only on slightly delayed video feedback from the machine. This is in sharp contrast to the manual loading where the driver close the loop based on non-delayed 3D vision of the machine relative the pile as well as listening to the noise and sensing the vibrations of the machine.

II

THESIS INTRODUCTION

The author of this thesis was a PhD student from 1986 to 1989 at Luleå University of Technology, working in a research project that developed a laser based navigation system for automatic guided vehicles (AGVs). The project resulted in a spinoff company, AutoNavigator AB, with the goal to commercialise the laser navigation system, two licentiate theses - Wiklund (1988) and Andersson (1989) - and one doctoral thesis Hyyppä (1993).

The laser navigation system was adapted to automation of the load-haul-dump (LHD) vehicles at the LKAB Kiruna iron ore mine in Sweden in 1996 and used in production from 1999 to 2009. LHD automation is the subject of the first part of the thesis.

The second part of the thesis deals with traction control for articulated vehicles. The need for traction control became clear during the production period. Wheel spin during remote controlled loading of fragmented rock had a negative impact on the production.

Volvo Construction Equipment initiated 2009 a VINNOVA research project with focus on traction control for off-road construction vehicles at Luleå University of Technology in which the author re-started the work as a PhD student. The first part of the traction control project finished in mid 2013. VINNOVA has granted a two-year extension of the project with focus on traction control for construction vehicles propelled by individual wheel drives. Work in the second part of the traction control project is not part of the thesis.

The common factor for both parts of the thesis is the articulated vehicle. An introduction to this type of vehicle is found in chapter 1. Readers familiar with the articulated vehicle can skip this part of the thesis.

The history of the laser navigation system since the founding of AutoNavigator AB up until today is discussed in Andersson (2013) with focus on commercialisation aspects.

References

Andersson, U. (2013). Laser navigation system for automatic guided vehicles – From research project to commercial product, Research Report, Luleå University of Technology, Luleå, Sweden.

Andersson, U. (1989). Trajectory estimation and control of autonomous guided vehicles, Licentiate Thesis, Luleå University of Technology, Luleå, Sweden.

Hyyppä, K. (1993). On a laser anglemeter for mobile robot navigation, Doctoral thesis, Luleå University of Technology, Luleå, Sweden.

Wiklund, U. (1988). Algorithms for navigation of autonomous guided vehicles, Licentiate Thesis, Luleå University of Technology, Luleå, Sweden.

ACKNOWLEDGEMENTS

There have been many people that over the years in some way or the other have affected the course of my professional career leading up to this thesis. My warmest thanks and thoughts to: Staffan Backén, Jan Björkman, Henrik Berghäll, Lasse Bergström, Roger Bergström, Glenn Bergqvist, Wolfgang Birk, Mikael Boman, Gianantonio Bortolin, Peter Broman, Fredrik Broström, Anders Dahlgren, Tommy Efraimsson, Lars Ehrenbom, Håkan Fredriksson, Tomas From, Anders Fröberg, Anders Grennberg, Thomas Gustafsson, Arne Hedström, Fredrik Holmquist, Kalevi Hyyppä, Ronny Hägg, Daniel Jannok, Daniel Jatko, Anders OE Johansson, Jan Jutander, Stigge Karpinen, Åke Kruukka, Magnus Lindgren, Torsten L. Lindström, Gunnar Lofgren, Magnus Lundqvist, Johan Markdahl, Pär-Erik Martinsson, Jan-Erik Moström, Kent Mrozek, Rikard Mäki, Göran Netzler, Johan Nordlander, Peter Olofsson, Lars Orvinder, Kenneth Palm, Carina Persson, Maj Petersen, Jonas Rahm, Johan Rooseniit, David Rosendahl, Stefan Rönnbäck, Risto Stenberg, Jan Sternby, Mats Strömsten, Jan Sundqvist, Håkan Tyni, Björn Wahlström, Peter Wallin, Åke Wernersson, Kirthi Walgama, Ingemar Westin, Irving Wigdén, Urban Wiklund, Kalle Åström.

Bensbyn 2013-11-09

Ulf Andersson

APPENDED PAPERS

Papers relating to part I - LHD automation

[A] Wiklund, U., Andersson, U. and Hyyppä, K. (1988). AGV navigation by angle measurements. In Proceedings of the 6th International Conference on Automated Guided Vehicle Systems, Brussels, Belgium.

[B] Andersson, U., Mrozek, K., Åström, K., & Hyyppä, K. (1997). Path design and control algorithms for articulated mobile robots. In Proceedings of the International Conference on Field and Service Robotics, 1997, Canberra, Australia.

[C] Andersson, U. & Strömsten. M. (2013). LHD automation at the LKAB Kiruna iron ore mine. Paper submitted to IEEE Robotics & Automation Magazine.

Papers relating to part II - Traction Control

[D] Markdahl, J., Bortolin G., and Andersson U. (2010). Traction control for articulated off-road vehicles. Reglermöte 2010, Lund, Sweden.

[E] Andersson, U., Bortolin, G., Backén, S. and Gustafsson, T. (2011) Estimation of Sideslip Angles of a Volvo A25E Articulated All-Wheel Drive Hauler Based on GPS/INS Measurements, SAE Technical Paper Series 2011-01-2156, Commercial Vehicle Engineering Congress, September 13-14, 2011, Chicago, Illinois, United States.

[F] Andersson, U. & Broström, F. (2013). Tyre parameter estimation based on control of individual wheel drives. Paper submitted to International Journal of Vehicle Autonomous Systems.

Paper relating to the spinoff company AutoNavigator AB

[G] Andersson, U. (2013). Laser navigation system for automatic guided vehicles – From research prototype to commercial product. Research Report, Luleå University of Technology, Luleå, Sweden.

CONTENTS

CHAPTER 1

Articulated vehicles

1.1 Introduction

An articulated vehicle consists of two or more frames where neighbouring frames are connected to each other with vertical hinges. The yaw angles of the hinges can be directly or indirectly controlled. Each frame has at least one wheel axle with steered or non-steered wheels. This type of vehicle has some typical characteristics.

- The vehicle can fold – "jack knife effect" - if the forward frame in the driving direction is subject to lateral forces that exceed the counteracting torque in the hinge. Reversing a trailer with a personal car is an example of when this phenomenon can occur. This is an example of an articulated vehicle where the yaw angle of the hinge is indirectly controlled via the steered wheels of the car.

- Steering the vehicle is done by changing the yaw angle of the hinge in case of vehicles with non-steered wheels. The steering causes the wheels to rotate which in turn causes a motion of the vehicle. This is in contrast to the steering of single frame vehicles such as passenger cars where the steering affects only the steered wheels and not the frame. If the frame is at a standstill when the steering starts, it will remain at standstill during the steering manoeuvring.

- Each frame has a fixed centre of gravity, but the resulting centre of gravity of the vehicle changes as a function of the yaw angle of the hinge. This implies that the vehicle can roll over if the centre of gravity of each frame is close to the hinge for large yaw angles since the resulting centre of gravity of the vehicle is located somewhere on the axis going through the centre of gravity of each frame.

1.1.1 Frame steering system

A typical steering system of construction types of articulated vehicles is a hydro-mechanical system that directly controls the yaw angle – also referred to as the articulation angle - of the hinge connecting the two frames. There are two cylinders on each side of the hinge. One end of the cylinder is attached to the front frame and the other end is attached to the rear frame. Counter clockwise steering implies that the left cylinder is pulled in and the right cylinder is

pulled out and vice versa for clockwise steering. This type of system is referred to as *frame steering system*.

The steering system can be modelled as a spring and a damper. Lateral forces acting in the contact patch between the tyres and the ground can cause *snaking* while driving if the system is not controlled properly, Azad (2006).

1.1.2 Mechanical drivelines

A vehicle with a single engine, a diesel engine for instance, and two or more driving wheels has a *driveline,* which is the mechanical system that connects the transmission to the driving wheels. The main components of the driveline are shafts and power-dividing units (PDUs) also referred to as differentials. The number of PDUs equals the number of driving wheels minus one, Andreev, Kabanau and Vantsevich (2010). A four-wheel drive vehicle (4x4) has for instance three PDU's, one for each wheel axle and one for the longitudinal axle connecting the wheel axles. The typical PDU has one input – characterized by the torque T_0 and the rotational velocity ω_0 − and two outputs - torques T' and T'' respectively with corresponding rotational velocities ω' and ω''. The input power to the PDU is $P_{in} = T_0\omega_0$ and the output power from the PDU are $P_{out'} = T'\omega'$ and $P_{out''} = T''\omega''$. The following relation holds when the PDU is in *open mode.*

$$\omega_0 = p'\omega' + p''\omega'' \tag{1}$$

where the coefficients, p' and p'', are constants. The values of the constants can be determined by stopping one of the outputs according to

$$p' = \frac{\omega_0}{\omega'}, \ \omega'' = 0 \qquad p'' = \frac{\omega_0}{\omega''}, \ \omega' = 0 \tag{2}$$

If the PDU is in *locked mode,* also referred to as positively engaged, the following holds

$$\omega' = \omega'' \tag{3}$$

which implies that both wheels on the same axle rotates with the same velocity. This will cause wear on the tyres if the vehicle at the same time is negotiating a turn. On the other hand, if the vehicle is at a standstill on a slippery surface with one wheel spinning, locking the PDU and thereby forcing both wheels to rotate might result in a tractive force that starts moving the vehicle. The locking of the PDU is done by a clutch. If a so called dog-clutch is used, the operating mode its either open or locked. The PDU can also be in *sliding mode* if a wet disc clutch is used. This mode represents the transient between the open and the locked mode of the clutch.

1.1.3 Individual wheel drives

A vehicle with individual motors for each driving wheel, electric motors for instance, lack a traditional driveline. The *hub motor* incorporated in the hub of the wheel is one example of an individual wheel drive. The maximum number of individual wheel drives equals the number of wheels.

1.1.4 Construction vehicles

The hauler and the wheel loader are two common constructions vehicles that are both articulated. They are mainly used for *earthmoving*. Both types consist of two frames and non-steered wheels. The main differences are the wheel configuration and the distance from the hinge to the axles. The distance between the axles and the hinge differs on a hauler, which is typically not the case for the wheel loader where the axles are at the same distance from the hinge. These types of vehicles are referred to as centre articulated vehicles. The bigger haulers are six-wheelers where the rear frame – also referred to as the trailer – has two wheel axles in a bogie arrangement. The front frame is referred to as the tractor.

Figure 1. A conceptual wheel loader model as illustrated by Volvo Construction Equipment.

Figure 2. A conceptual hauler model as illustrated by Volvo Construction Equipment.

Another difference between the wheel loader and the hauler is that the hauler has only one hinge around which the tractor and trailer can rotate freely both in the yaw direction and in the roll direction. The wheel loader has two vertical hinges implying that the two frames

cannot roll relative each other. The rear axle can typically pivot around the centre axis of the rear frame to ensure that all wheels have ground contact.

The vehicle types are characterized by pronounced pitching due to high pitching inertia. The axle loads varies considerably between loaded and unloaded conditions. The tyres have low vertical stiffness, implying that the tyres have a large impact on the dynamics of the suspended mass, Rehnberg (2011).

1.1.5 Load-haul-dump vehicles

The LHD vehicle, where LHD stands for Load, Haul and Dump, is a type of wheel loader machine adapted for use in underground mines. The LHD is articulated frame steered to reduce the sweep area when turning. The main difference compared to a wheel loader is that the cabin is placed on the side of the machine to reduce the height. Most LHDs are equipped with a diesel engine. LHDs where an electric motor is used instead of a diesel engine also exists but are less common.

Figure 3. The photograph shows one of eight automated LHD's at the LKAB iron ore mine in Kiruna, Sweden. The photograph is published with permission of LKAB.

The electric LHD in figure 3 is 14 meters long. The width of the bucket is approximately 4 meters. It weighs 77.5 tonnes unloaded. The approximately 300-metre long cable of the machine is connected to a 1000 [VAC] outlet. The cable is rolled in or out depending on the travelling direction of the LHD, on a drum in the rear of the machine. It has a nominal loading capacity of 25 ton in a 10 [m^3] bucket. The rubber tyres are filled with both compressed air and water to reduce the explosion at puncture.

The laser anglemeter for the navigation system is placed on the pole above the rear wheels and rotates the laser beam above the cabin roof 3.20 meter above the ground.

1.2 Kinematic model

Kinematic models are compared to dynamic models simple and can be used in some applications such as motion models for automatic guided vehicles, see for instance Wiklund, Andersson and Hyyppä (1988), Larsson, Zell, Hyyppä and Wernersson (1994), Scheding, Dissanayake, Nebot and Durrant-Whyte (1997) and Marshall, Barfoot and Larsson (2008).

The base for the kinematic model is presented in section 2.1.1. A kinematic model for articulated vehicles is derived in the section 2.1.2. Some limitations and test results of the kinematic model in real vehicle applications are discussed in section 2.1.3.

1.2.1 Base model

The base for the kinematic model is a work by Larsson, Zell, Hyyppä and Wernersson (1994).
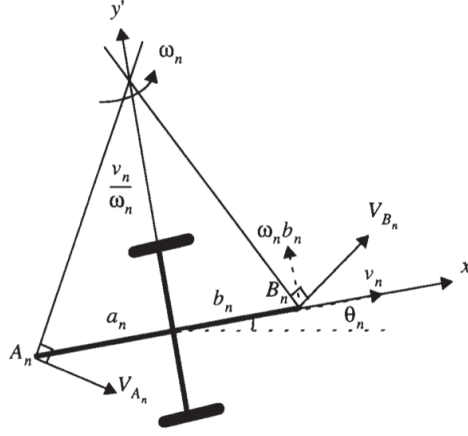
Figure 4. The figure illustrates a wheel axis and the mid axis perpendicular to the wheel axis. The rotational speed is ω_n and the transversal speed is v_n. The figure is taken from Larsson, Zell, Hyyppä and Wernersson (1994).

The speed components of the mid axis at the distance a_n in the rearward direction of the wheel axis and at the distance b_n in the forward direction of the wheel axis in figure 4 are given by

$$V_{An} = \begin{pmatrix} 1 & 0 \\ 0 & -a_n \end{pmatrix} \begin{pmatrix} v_n \\ \omega_n \end{pmatrix}, \quad V_{Bn} = \begin{pmatrix} 1 & 0 \\ 0 & b_n \end{pmatrix} \begin{pmatrix} v_n \\ \omega_n \end{pmatrix} \tag{4}$$

Denote the crossing of the two axes in figure 4 O. From (4) we get

$$V_{On} = \begin{pmatrix} 1 & 0 \\ 0 & 0 \end{pmatrix} \begin{pmatrix} v_n \\ \omega_n \end{pmatrix} \tag{5}$$

which implies that the model assumes no sideslip of the wheels since the speed component in the y' direction is zero. This assumption is referred to as a *nonholonomic constraint*, Altafini (1999).

Equation (4) can be used to define the relation between the frames of an articulated vehicle. If we assume the distance from the hinge to the wheel axis of the frames to be L and the articulation angle to be γ we get

$$\begin{pmatrix} 1 & 0 \\ 0 & L \end{pmatrix} \begin{pmatrix} v_r \\ \omega_r \end{pmatrix} = T_f \begin{pmatrix} 1 & 0 \\ 0 & -L \end{pmatrix} \begin{pmatrix} v_f \\ \omega_f \end{pmatrix}, \quad T_f = \begin{pmatrix} \cos(\Upsilon) & -\sin(\Upsilon) \\ \sin(\Upsilon) & \cos(\Upsilon) \end{pmatrix} \tag{6}$$

where index r is used for the rear frame and index f is used for the front frame. T_f is the transformation matrix from the co-ordinate system of the front frame to the co-ordinate system of the rear frame. The articulation angle defines the rotations of the frames relative each other. The articulation angle is positive counter clockwise. If the articulation angle is zero, the frames aligns and the vehicle will drive straight implying that $\omega_f = \omega_r = 0$.

1.2.2 Kinematic model for articulated vehicles

From (6) we get

$$\begin{pmatrix} v_r \\ \omega_r \end{pmatrix} = \begin{pmatrix} \cos{(\Upsilon)} & L\sin(\Upsilon) \\ \sin{(\Upsilon)}/L & -\cos{(\Upsilon)} \end{pmatrix} \begin{pmatrix} v_f \\ \omega_f \end{pmatrix} \tag{7}$$

$$\dot{\Upsilon} = \omega_f - \omega_r \tag{8}$$

7) and 8) gives

$$\begin{pmatrix} v_r \\ \dot{\Upsilon} \end{pmatrix} = \begin{pmatrix} \cos{(\Upsilon)} & L\sin(\Upsilon) \\ -\sin{(\Upsilon)}/L & 1 + \cos{(\Upsilon)} \end{pmatrix} \begin{pmatrix} v_f \\ \omega_f \end{pmatrix} \tag{9}$$

Assume point contact between the wheels and the ground and the distance between the wheels on the same axis to be e. Then we get for the front axis

$$\begin{pmatrix} v_f \\ \omega_f \end{pmatrix} = \begin{pmatrix} \frac{1}{2} & \frac{1}{2} \\ \frac{-1}{e} & \frac{1}{e} \end{pmatrix} \begin{pmatrix} v_1 \\ v_2 \end{pmatrix} \tag{10}$$

where index 1 is used for the front left wheel and index 2 is used for the front right wheel. (9) and 10) gives

$$\begin{pmatrix} v_r \\ \dot{\Upsilon} \end{pmatrix} = \begin{pmatrix} \frac{\cos(\Upsilon)}{2} - \frac{L\sin(\Upsilon)}{e} & \frac{\cos(\Upsilon)}{2} + \frac{L\sin(\Upsilon)}{e} \\ \frac{-\sin{(\Upsilon)}}{2L} - \frac{1+\cos{(\Upsilon)}}{e} & \frac{-\sin{(\Upsilon)}}{2L} + \frac{1+\cos{(\Upsilon)}}{e} \end{pmatrix} \begin{pmatrix} v_1 \\ v_2 \end{pmatrix} \tag{11}$$

$$\begin{pmatrix} v_1 \\ v_2 \end{pmatrix} = \frac{e}{1+\cos{(\Upsilon)}} \begin{pmatrix} \frac{-\sin{(\Upsilon)}}{2L} + \frac{1+\cos{(\Upsilon)}}{e} & \frac{-\cos(\Upsilon)}{2} - \frac{L\sin(\Upsilon)}{e} \\ \frac{\sin{(\Upsilon)}}{2L} + \frac{1+\cos{(\Upsilon)}}{e} & \frac{\cos(\Upsilon)}{2} - \frac{L\sin(\Upsilon)}{e} \end{pmatrix} \begin{pmatrix} v_r \\ \dot{\Upsilon} \end{pmatrix} \tag{12}$$

$$v_1 = \left(1 - \frac{e/(2L)\sin(\Upsilon)}{1+\cos(\Upsilon)}\right) v_r - \left(\frac{e/2\cos(\Upsilon)}{1+\cos{(\Upsilon)}} + \frac{L\sin(\Upsilon)}{1+\cos{(\Upsilon)}}\right) \dot{\Upsilon} \tag{13}$$

$$v_2 = \left(1 + \frac{e/(2L)\sin(\Upsilon)}{1+\cos(\Upsilon)}\right) v_r + \left(\frac{e/2\cos(\Upsilon)}{1+\cos{(\Upsilon)}} - \frac{L\sin(\Upsilon)}{1+\cos{(\Upsilon)}}\right) \dot{\Upsilon} \tag{14}$$

For the rear axis with index 3 denoting the rear left wheel and index 4 denoting the rear right wheel, we have

$$\begin{pmatrix} v_r \\ \omega_r \end{pmatrix} = \begin{pmatrix} \frac{1}{2} & \frac{1}{2} \\ \frac{-1}{e} & \frac{1}{e} \end{pmatrix} \begin{pmatrix} v_3 \\ v_4 \end{pmatrix} \tag{15}$$

$$\begin{pmatrix} v_3 \\ v_4 \end{pmatrix} = \begin{pmatrix} 1 & \frac{-e}{2} \\ 1 & \frac{e}{2} \end{pmatrix} \begin{pmatrix} v_r \\ \omega_r \end{pmatrix} \tag{16}$$

From (8)

$$\omega_r = \omega_f - \dot{\Upsilon} \tag{17}$$

Use $\omega_f = (v_2 - v_1)/e$ and (13) and (14), then we get

$$\omega_f = \frac{\sin(Y)/L}{1+\cos(Y)} v_r + \frac{\cos(Y)}{1+\cos(Y)} \dot{Y} \tag{18}$$

(17) and (18) gives

$$\omega_r = \frac{\sin(Y)/L}{1+\cos(Y)} v_r - \frac{1}{1+\cos(Y)} \dot{Y} \tag{19}$$

16) and 19) gives

$$v_3 = \left(1 - \frac{e/(2L)\sin(Y)}{1+\cos(Y)}\right) v_r + \frac{e/2}{1+\cos(Y)} \dot{Y} \tag{20}$$

$$v_4 = \left(1 + \frac{e/(2L)\sin(Y)}{1+\cos(Y)}\right) v_r - \frac{e/2}{1+\cos(Y)} \dot{Y} \tag{21}$$

Remark. From (13), (14), (20) and (21) we have

$$v_1 - v_3 = -\left(\frac{e}{2} + \frac{L\sin(Y)}{1+\cos(Y)}\right) \dot{Y} \tag{22}$$

$$v_2 - v_4 = \left(\frac{e}{2} - \frac{L\sin(Y)}{1+\cos(Y)}\right) \dot{Y} \tag{23}$$

(22) and (23) implies that if $\dot{Y} = 0$, we get $v_1 = v_3$ and $v_2 = v_4$.

(13), (14) and (20), (21) can be summarised as

$$\begin{pmatrix} v_1 \\ v_2 \\ v_3 \\ v_4 \end{pmatrix} = \begin{pmatrix} -\left(\frac{e/2\cos(Y)}{1+\cos(Y)} + \frac{L\sin(Y)}{1+\cos(Y)}\right) & \left(1 - \frac{e/(2L)\sin(Y)}{1+\cos(Y)}\right) \\ \left(\frac{e/2\cos(Y)}{1+\cos(Y)} - \frac{L\sin(Y)}{1+\cos(Y)}\right) & \left(1 + \frac{e/(2L)\sin(Y)}{1+\cos(Y)}\right) \\ \frac{e/2}{1+\cos(Y)} & \left(1 - \frac{e/(2L)\sin(Y)}{1+\cos(Y)}\right) \\ -\frac{e/2}{1+\cos(Y)} & \left(1 + \frac{e/(2L)\sin(Y)}{1+\cos(Y)}\right) \end{pmatrix} \begin{pmatrix} \dot{Y} \\ v_r \end{pmatrix} \tag{24}$$

The potential conflict of control is clear when studying the right hand side and the left hand side of equation (24). If the speed of each wheel can be individually controlled as well as the rate of change of the articulation angle based on control of the steering system, contradictory control can easily be implemented. The kinematic model in (24) is discussed in chapter 3 section 3.5.1.

1.2.3 Limitations of the kinematic model

1.2.3.1 Sideslip
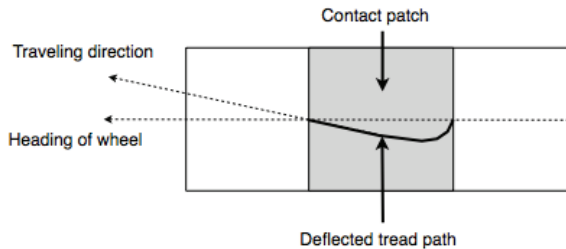
Figure 5. The figure illustrates the sideslip of a pneumatic tyre subject to a side force.

A property of pneumatic tyres is the sideslip, which occurs if a lateral force acts in the contact patch between the wheel and the ground, see figure 5. Lateral forces occur for instance when turning because of the Coriolis force, implying that the nonholonomic constraint does not hold for articulated vehicles with pneumatic tyres.

Remark. The kinematic model can be used to estimate the sideslip if there is one frame with free rolling rigid wheel(s).

Assume that the axis with sideslip in figure 6 is the rear axis of an articulated vehicle and that the axis with no sideslip is a measuring device. There is a joint at a distance b_m in front of the wheel axis of the measuring device that is connected to a joint at a distance a_r behind the wheel axis of the rear part. Both a_r and b_m are known. The point on the mid axis of the rear frame with no sideslip is at a distance $\bar{a}_r$ from the joint that connects the rear frame to the measuring device. The task is to calculate the sideslip angle α_r based on the measurements from the measuring device.
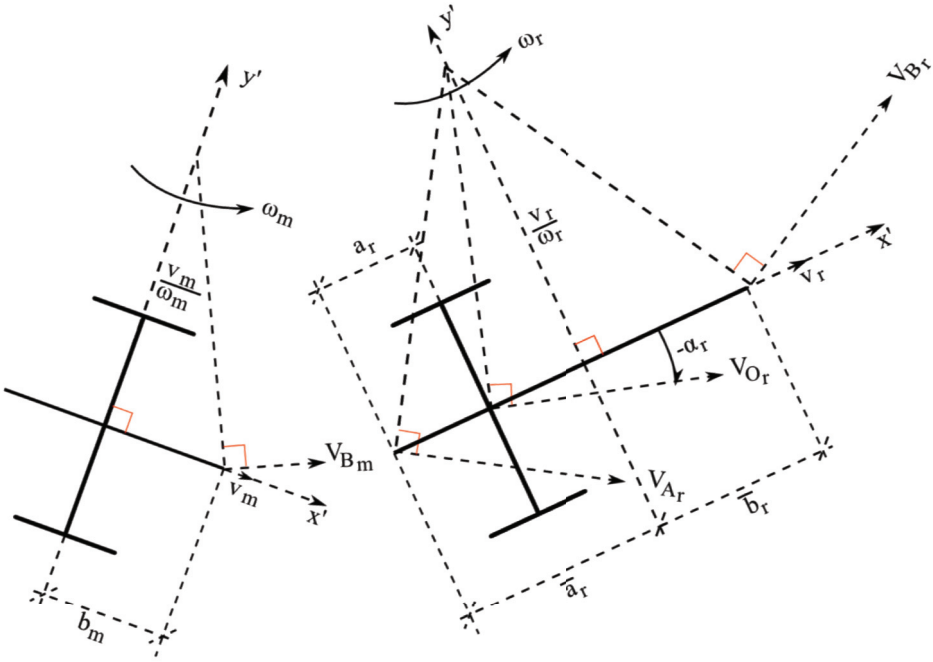
Figure 6. The figure illustrates the resulting sideslip angle α_r of an axis with pneumatic tyres subject to a side force and an axis with no sideslip.

Denote the articulation angle between the measuring device and the rear frame of the articulated vehicle γ_m. (6) gives

$$\begin{pmatrix} 1 & 0 \\ 0 & b_m \end{pmatrix}\begin{pmatrix} v_m \\ \omega_m \end{pmatrix} = \begin{pmatrix} \cos(\gamma_m) & -sin(\gamma_m) \\ \sin(\gamma_m) & \cos(\gamma_m) \end{pmatrix}\begin{pmatrix} 1 & 0 \\ 0 & -\bar{a}_r \end{pmatrix}\begin{pmatrix} v_r \\ \omega_r \end{pmatrix} \tag{25}$$

The rotational speed of the rear frame equals the rotational speed of the measuring device if the articulation angle is constant. From (25) we get with $\omega_m = \omega_r = \omega$

$$\begin{pmatrix} v_r \\ \bar{a}_r \end{pmatrix} = \begin{pmatrix} 1 & 0 \\ 0 & -\omega^{-1} \end{pmatrix} \begin{pmatrix} \cos(Y_m) & \sin(Y_m) \\ -\sin(Y_m) & \cos(Y_m) \end{pmatrix} \begin{pmatrix} 1 & 0 \\ 0 & b_m \end{pmatrix} \begin{pmatrix} v_m \\ \omega \end{pmatrix} \quad (26)$$

The sideslip angle is

$$\alpha_r = \tan^{-1} \frac{(a_r - \bar{a}_r)\omega}{v_r} \quad (27)$$

Once $\bar{a}_r$ is calculated $\bar{b}_r$ can be calculated and thereby the sideslip angle for the front axis using the same method as for the sideslip of the rear axis.

Sideslip is discussed in chapter 3 section 3.3.

1.2.3.2 Load transfer

Jannok and Petersen (1992) mounted pendulums at the centre of the wheels on an LHD at the LKAB Kiruna iron ore mine. The LHD was lined up and the positions of the pendulums were marked on the ground. The LHD was then turned with the brakes off and gear in neutral implying that the LHD was freewheeling during the tests. The positions of each pendulum were marked on the ground with and without load in the bucket for articulation angles ±10, ±20, ±30 and ±40 degree. The change in distance for each wheel was measured. The results are summarised in table 1.

Table 1. The table shows the distance travelled by the front left wheel (FL), the front right wheel (FR), the rear left wheel (RL) and the rear right wheel (RR) as a function of the articulation angle γ with unloaded and loaded bucket (14 tonnes).

γ [Degree]	Bucket	FL [mm]	FR [mm]	RL [mm]	RR [mm]
-40	Unloaded	155	-138	150	120
	Loaded	150	-146	84	106
-30	Unloaded	110	-100	120	94
	Loaded	115	-108	76	96
-20	Unloaded	80	-64	88	62
	Loaded	80	-70	60	77
-10	Unloaded	40	-30	40	36
	Loaded	35	-36	32	40
+10	Unloaded	-34	25	34	42
	Loaded	-26	85	74	22
+20	Unloaded	-64	74	66	76
	Loaded	-20	145	140	-10
+30	Unloaded	-88	106	104	104
	Loaded	-18	208	212	-20
+40	Unloaded	-132	152	130	150
	Loaded	12	264	282	-50

The conclusion from this practical test is that the nonholonomic constraint does not hold is negligible since the measured distances differ between the unloaded and the loaded cases. The differences in distances implies that the (x,y)-trajectory of the wheels when turning to a certain articulation angle depends not only in the kinematic variables but also on the load in the bucket.

The differences in measured distances are explained by different frictional forces acting in the contact patch of the wheels and the ground in the case of unloaded and loaded bucket. The load transfer between the wheel axles that occurs when loading the bucket changes the normal forces acting on the tyres and thereby the resistance to motion when turning the LHD.

The influence of load transfer is discussed in chapter 3 sections 3.2 and 3.4.

1.2.3.3 Rotational speed

The rotational speed of the frames can be derived from the kinematic model as a function of the longitudinal speed, articulation angle and the steering rate. From (6) we get

$$v_r = \cos(\varUpsilon)\, v_f + L \sin(\varUpsilon)\, \omega_f \tag{28}$$

Inserting (24) in (17) gives

$$\omega_f = \frac{\sin(\varUpsilon)/L}{1+\cos(\varUpsilon)} v_f + \frac{1}{1+\cos(\varUpsilon)}\dot{\varUpsilon} \tag{29}$$

which is the rotational speed of the front frame that is referred to by Corke and Ridley (2001) as *the full kinematic model*.

Corke and Ridley compare the full kinematic with a simpler model discussed by Scheding, Dissanyake and Durrant-Whyte (1999) referred to as the *bicycle model* which omits the $\dot{\varUpsilon}$ term in (29).

The models are evaluated using a 28.5 tonnes LHD equipped with two IMU units, one unit mounted on the front frame and one unit mounted on the rear frame. The conclusion is that the full kinematic model predicts the rotational speed more accurate than the bicycle model when comparing with the data from the IMUs. The articulation angle varied ±20 degrees and the front yaw rate and the rear yaw rate varied between ±20 degree/s. The speed of the LHD was 2 m/s. The root mean square (RMS) errors were 2.3 degree/s for the full kinematic model and 5.0 degree/s for the bicycle model.

Remark. A motion model describing the 2D pose of the front frame can be derived from (29). Denote the heading of the front frame θ_f. Assume the heading to be positive counter clockwise relative the x-axis of the 2D co-ordinate system. We get

$$\begin{pmatrix} \dot{x}_f \\ \dot{y}_f \\ \dot{\theta}_f \end{pmatrix} = \begin{pmatrix} 0 & \cos(\theta_f) \\ 0 & \sin(\theta_f) \\ \frac{1}{1+\cos(\varUpsilon)} & \frac{\sin(\varUpsilon)/L}{1+\cos(\varUpsilon)} \end{pmatrix} \begin{pmatrix} \dot{\varUpsilon} \\ v_f \end{pmatrix} \tag{30}$$

The kinematic motion model in (30) is the base for the navigation system discussed in chapter 2 section 2.2.1.

1.3 ArtiTRAX

ArtiTRAX is a 240 kg articulated vehicle with 24 [VDC] electric motors. ArtiTRAX consists of two TRAX wheelchairs from the Swedish company Permobil. ArtiTRAX is developed at Luleå University of Technology in collaboration with Volvo Construction Equipment.

Many construction machines are articulated, for instance haulers and wheel loaders. ArtiTRAX is considered to be a downscaled version of such a vehicle in many test scenarios. The main advantage with ArtiTRAX is the small size, which makes initial tests easy to perform, Rehnberg, Edrén, Eriksson, Drugge, Stensson Trigell (2011).

Figure 7. ArtiTRAX, the small wheel in the rear is the measuring wheel used to measure the actual velocity. Holders for weightlifting weights are placed above each wheel making it possible to change the static normal load in a controlled manner.

The two TRAX units are connected with a hinge, and thereby making ArtiTRAX articulated. The joint angle is controlled with an electric motor connected to the joint via a chain. Each wheel has its own 500 [W] motor. The motor is connected to the wheel axle via a gearbox. The gearbox reduces the rotational speed of the motor 18 times. The controls of the motors are done in an on-board PC104 computer that sends the control reference values over a CAN bus to the drive electronic units of each motor. The drive electronic units control the motor currents.

ArtiTRAX is equipped with various sensors, encoders that measure the rotational angle and velocity of the motors, encoder that measure the rotational angle and velocity of the measuring wheel and inbuilt sensors in the drive electronics that measures the motor currents. Two units containing 3D gyros and 3D accelerometers are also installed; one in the centre of the front part above the wheel axis and one unit in the centre of the rear part above the wheel axis.

The input to the drive electronic unit is a reference value for the motor current. The units control the motor currents with high accuracy. All five encoders are of the same type, an absolute encoder with a 12-bit single turn and 12-bit multi turn resolution.

Three weight distributions of extra weights on the front axis and the rear axis has been used in tests. The static front axis weight and rear axis weight for these cases is specified in table 2.

Table 2.

Axis	F/R 80/0	F/R 60/20	F/R 0/80
Front	180 kg	160 kg	100 kg
Rear	140 kg	160 kg	220 kg

The x,y-location of the centre of gravity can be estimated using individual scales for each wheel using the method described below.
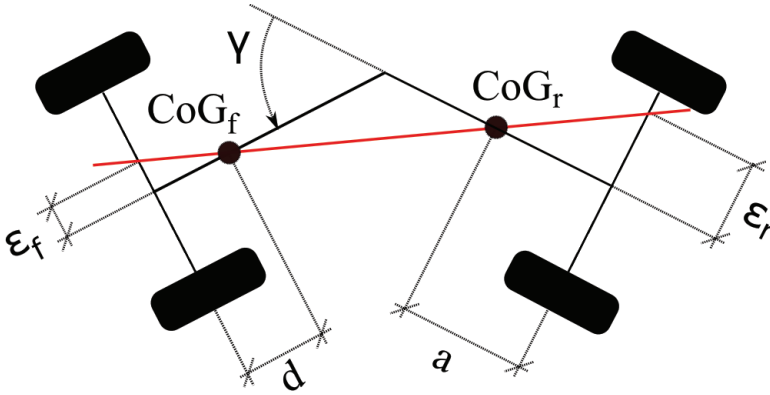
Figure 7. The centre of gravity (CoG) of the front and the rear frame is illustrated in the figure. The centre of gravity of the vehicle lie somewhere on the red line between the centre of gravity of the front frame and the centre of gravity of the rear frame.

d in figure 7 is the distance from the centre of gravity of the front frame to the front axis. a is the distance from the center of gravity of the rear frame to the rear axis. ε_f and ε_r are the distances from the middle of the front and the rear axis respectively to the balancing points on the axis. ε_f and ε_r depends on the articulation angle.

The first step is to make sure that the centre of gravity lies on the mid axis of the vehicle. This can be verified by weighing the vehicle with articulation angle at zero degrees and making sure that the weight of the front left wheel w_1 equals the weight of the front right wheel w_2 and that the weight of the rear left wheel w_3 equals the weight of the rear right wheel w_4.

The next step is to weigh the vehicle for a number of articulation angles different from zero degrees.

12
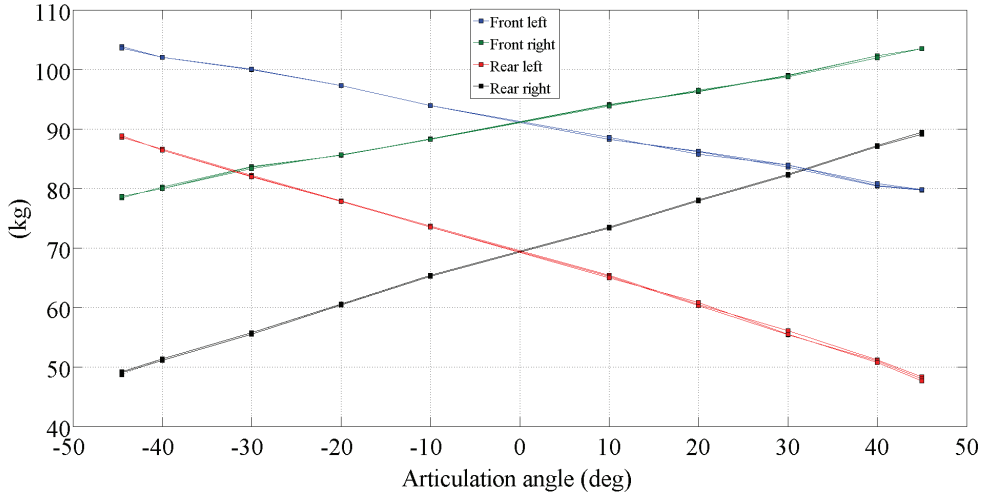
Figure 8. The figure shows weights of each wheel for 10 articulation angles. The front wheels were each loaded with 40 kg extra weights.

The third step is to estimate the distances from the centres of gravity to respective wheel axis and thereafter calculate the mass of each frame.

Denote the distance from the axis to the hinge L and the distance between the wheels on the same axis e, then the distance d from the center of gravity of the front frame to the front axis and the distance a from the center of gravity of the rear frame to the rear axis are given by

$$d = \varepsilon_f \frac{(\tan(\beta)\sin(\gamma/2)+\cos(\gamma/2))}{\sin(\gamma/2)-\tan(\beta)\cos(\gamma/2)} \tag{31}$$

$$a = \varepsilon_r \frac{(-\tan(\beta)\sin(\gamma/2)+\cos(\gamma/2))}{\sin(\gamma/2)+\tan(\beta)\cos(\gamma/2)} \tag{32}$$

where the distances from the centre of the wheels axis to the balancing points, ε_f and ε_r, and $\tan(\beta)$ are given by

$$\varepsilon_f = \frac{w_2-w_1}{w_2+w_1}\frac{e}{2} \tag{33}$$

$$\varepsilon_r = \frac{w_4-w_3}{w_4+w_3}\frac{e}{2} \tag{34}$$

$$\tan(\beta) = \frac{(\varepsilon_r-\varepsilon_f)\cos(\gamma/2)}{2L\cos(\gamma/2)+(\varepsilon_r+\varepsilon_f)\sin(\gamma/2)} \tag{35}$$

Remark

Note from (35) that $\tan(\beta)$ is zero if $\varepsilon_f = \varepsilon_r$ which implies that $d = a$. Note also from (31) – (35) that the centre of gravity is in the centre of the axis if $\varepsilon_i = 0$ for $\gamma \neq 0$. A negative value of the distance from the centre of gravity to the wheel axis implies that the wheel axis lies between the centre of gravity and the hinge. The vehicle is balancing on the outer wheels if $\varepsilon_f = \varepsilon_r = e/2$.

13
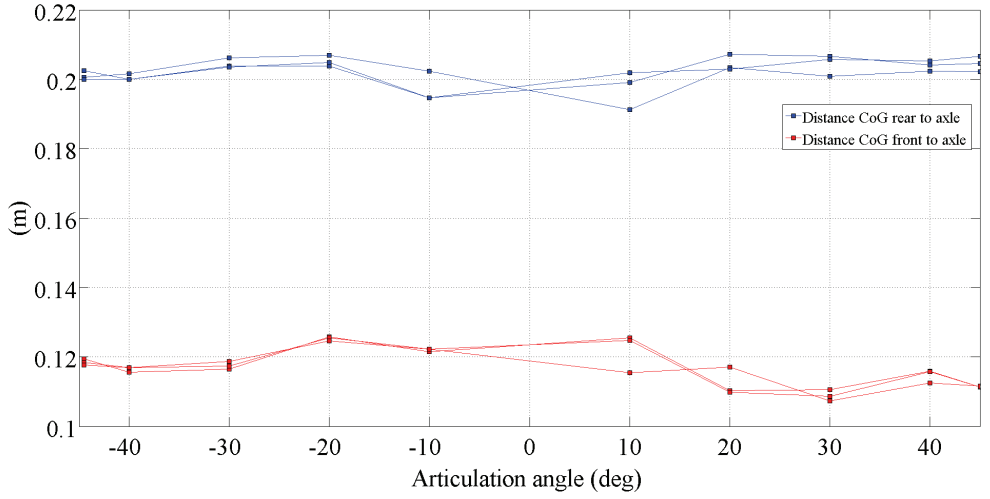
Figure 9. The figure shows estimated distances from the centre of gravity for each frame to respective wheel axis for 10 different articulation angles based on three sets of measurements. The front wheels were each loaded with 40 kg extra weights.

Note from figure 9 that the centre of gravity or the rear frame is further away from the rear axis than the corresponding distance for the front frame. This is reasonable since the batteries are located in the rear frame between the rear axis and the hinge.

The mass of each frame is based on the estimated distances from the centre of gravity to the axis. The mass of the front and rear frame respectively can be calculated as

$$m_f = \frac{w_f(\bar{L}-\bar{a})-w_r\bar{a}}{\bar{L}-\bar{a}-\bar{d}} \tag{36}$$

$$m_r = \frac{w_r(\bar{L}-\bar{d})-w_f\bar{d}}{\bar{L}-\bar{a}-\bar{d}} \tag{37}$$

where

$$w_f = w_1 + w_2 \tag{38}$$

$$w_r = w_3 + w_4 \tag{39}$$

$$\bar{L} = \frac{2L\cos(\gamma/2)+(\varepsilon_r+\varepsilon_f)\sin(\gamma/2)}{\cos(\beta)} \tag{40}$$

$$\bar{a} = \frac{\varepsilon_r\sin(\gamma/2)+a\cos(\gamma/2)}{\cos(\beta)} \tag{41}$$

$$\bar{d} = \frac{\varepsilon_f\sin(\gamma/2)+d\cos(\gamma/2)}{\cos(\beta)} \tag{42}$$

14
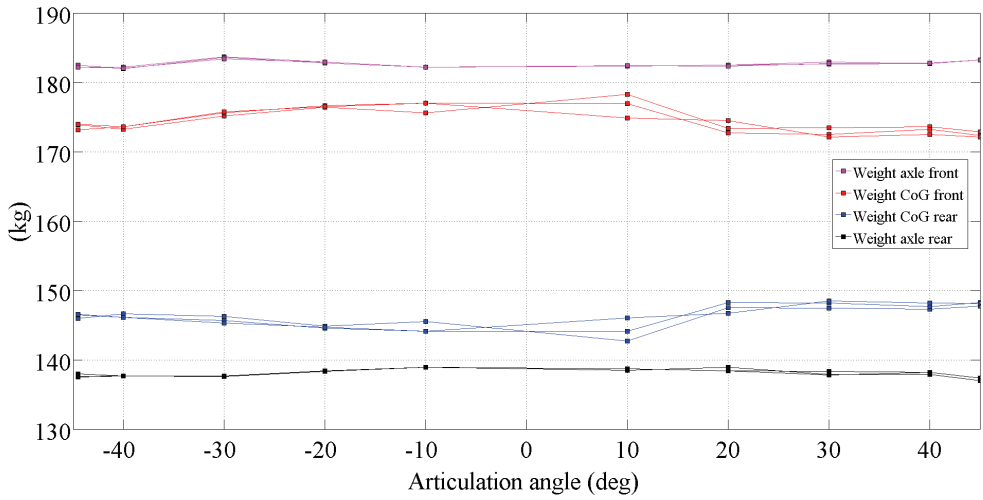
Figure 10. Estimated mass of the centre of gravity of each frame and the wheel axes loads.

The method to estimate the centre of gravity is part of an on-going work to estimate the normal forces acting on the tyres. The normal forces have a significant influence on the tractive performance of the vehicle for instance the energy efficiency, which is discussed in chapter 3 section 3.2.
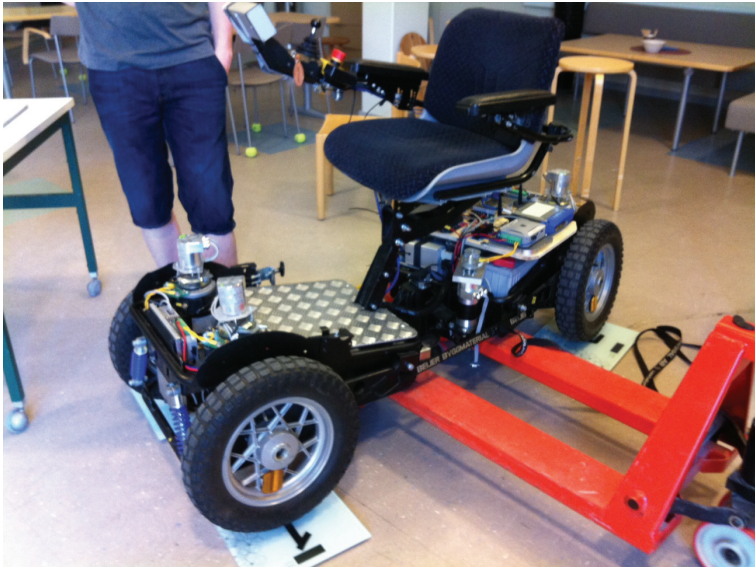
Figure 11. Weighing of ArtiTRAX using four bathroom scales.

References

Altafini, C. (1999). A path-tracking criterion for an LHD articulated vehicle. *International Journal of Robotics Research*, 18(5):435–441.

Andreev, A. F., Kabanau, K. I., & Vantsevich, V.V. (2010). Driveline Systems of Ground Vehicles - Theory and Design, CRC Press, Boca Raton, FL, United States.

Azad, N. L. (2006). Dynamic modelling and stability controller development for articulated steer vehicles. Doctoral Thesis, University of Waterloo, Waterloo, ON, Canada.

Corke, P.I., & Ridley, P. (2001). Steering kinematics for a center articulated mobile robot. *IEEE Transaction on Robotics and Automation*, 17(2):215-218.

Jannok, D., & Petersen, M. (1992). Lasernavigering av midjestyrda gruvlastare. Master's Thesis, Luleå University of Technology, Luleå, Sweden.

Larsson, U., Zell, C., Hyyppä, K., & Wernersson, Å. (1994). Navigating an articulated vehicle and reversing with a trailer. *In Proceedings of IEEE International Conference on Robotics and Automation*, San Diego, CA, USA.

Markdahl, J., Bortolin G., & Andersson U. (2010). Traction control for Articulated off-road vehicles. Reglermöte 2010, Lund, Sweden.

Marshall, J., Barfoot, T., & Larsson, J. (2008). Autonomous underground tramming for center-articulated vehicles. *Journal of Field Robotics*, 25(6-7):400-421.

Rehnberg, A., Edrén, J., Eriksson, M., Drugge, L., & Stensson Trigell, A. (2011). Scale model investigation of the snaking and folding stability of an articulated frame steer vehicle. *Int. J. Vehicle Modelling and Testing*, Vol. 6, No. 2, 126-144.

Rehnberg, A. (2011). Suspension design for off-road construction machines. Doctoral Thesis, Royal Institute of Technology, Stockholm, Sweden.

Scheding, S., Dissanayake, G., Nebot, E., & Durrant-Whyte, H. (1997). Slip modelling and aided inertial navigation of an LHD. In *Proceedings of IEEE International Conference on Robotics and Automation*, Albuquerque, New Mexico, USA.

Scheding, S., Dissanayake, G., Nebot, E. M., & Durrant-Whyte, H. (1999). An experiment in autonomous navigation of an underground mining vehicle. *IEEE Transactions on Robotics and Automation*, 15(1):85–95.

Wiklund, U., Andersson, U., & Hyyppä, K. (1988). AGV navigation by angle measurements. In *Proceedings of the 6th International Conference on Automated Guided Vehicle Systems*, Brussels, Belgium.

Part I - LHD automation

2.1 Introduction

This part of the thesis focus on the reflector based laser navigation system used in an LHD automation system at the iron ore mine in Kiruna Sweden owned by the mining company Luossavaara-Kiirunavaara Aktiebolag - LKAB. The laser navigation system is referred to as HUNS, High speed Underground Navigation System.

The system was tested in 1996/97 and used in production from 1999 to 2009. At its peak, the system consisted of eight LHD's operating in seven production areas in the sublevel cave mine.

LHD automation systems have its origin in the automatic guided vehicle (AGV) industry. An AGV system (AGVS) is a material handling system that uses independently operated, self-propelled vehicles (AGVs) guided along defined pathways.

The distances from the walls of the drifts to the machine are very small and unlike traditional AGV applications in factories / warehouses, it is not possible to have external safety systems that will stop the vehicle in case of navigation error unless the speed is limited. A limitation of the speed increases the cycle time and thereby the production, which is not acceptable. The speed of the AGVs is low - typically 1 – 1.5 m/s - since AGVs often operates in areas where people work so that specially designed safety systems can stop them in a controlled manner.

Figure 1. The photograph shows the LHD used in the underground field trials in 1996/97. The margin for errors in the motion control is small. The photograph is published with permission of LKAB.

LHD automation systems are not considered to be a part of the AGVS market. The market for LHD automation systems is not known, but is significantly less than the AGVS market.

A number of attempts to automate LHD's have been done since the 80's in underground mines, Mäkelä (2001a), Roberts, Duff and Corke (2002), Bakambu and Polotski, (2007), Marshall, Barefoot and Larsson (2008) and Gustafson (2011).

LKAB has since the late 80's conducted a series of LHD automation projects. A driving force has been the large-scale operations in the Kiruna sublevel cave iron ore mine, which is one of the world's largest underground mines.

Today, at least three major suppliers of underground mining equipment have developed LHD automation systems of their own that are commercially available, Mäkelä (2001a, 2001b), Duff, Roberts and Corke (2002, 2003), Duff and Roberts (2003), Roberts, Duff and Corke (2002), Marshall, Barfoot and Larsson (2008), Larsson, Appelgren, Marshall and

Barfoot (2008) and Larsson, Appelgren and Marshall (2010). This is in contrast to the situation in the late 90's when mining companies had to develop their own systems, Wylie (1996).

A state of the art review is found in Andersson and Strömsten (2013) in comparison with the navigation system used at the LKAB Kiruna iron ore mine.

2.1.1 Background - LHD automation at LKAB

The test vehicle - Luleå Turbo Turtle, Andersson (2013) - used in the research project that developed the laser navigation system project at Luleå University of Technology in the late 80's was demonstrated live in the LKAB Kiruna iron ore mine in the autumn of 1989. The demonstration resulted in a master thesis project in 1991 in which adaptation questions were highlighted and algorithms proposed for the pose estimator and the guidance controller for the LHD application, Jannok and Petersen (1992).

LTT was demonstrated in the production area of the SALT2 project where SALT stands for Semi-Automatic Loading and Transport, in which a wire guided based navigation system was used for the automation of an electric LHD, Eriksson and Kitok (1991), Nilsson, Wigdén and Tyni (2001). Wires connected to line drivers creating a magnetic field around the wires were buried in the concrete roads of the drifts in the production area. Sensors on the LHD sensed the magnetic field emitted from the wires and were able to detect the distance from the wires. The navigation system aimed at controlling the articulation angle such that the distance was at a minimum implying that the LHD was "on track". The speed of the LHD was limited mainly because of the basic principal of a wire guidance system that does not separate the guidance from the localization of the vehicle, which is key to enable high speed driving. One can compare the wire guidance technique with a person driving a car looking down through a hole in the floor trying to follow the lane separating line. Doing so makes it very difficult to separate distance errors and heading errors to the line that is necessary to be able to go with full speed. This separation is easily done when looking out through the front window of the car. The driver weight distance errors and heading errors differently in the closed loop control of the steering angle of the car. Another benefit by looking out through the front window is that it is possible to plan for curves beforehand by reducing the speed when approaching a curve so that the speed of the car is reduced appropriately when negotiating the curve.

The adaption of the pose estimator suggested by Jannok and Petersen, was tested on an electric TORO501E LHD in the Kiruna iron ore mine in the spring of 1995. Sensors measuring the articulation angle and the rotational speed of the longitudinal drive shaft together with a laser scanner were mounted on the LHD and retro-reflectors were mounted on the walls of the drifts in the production area. The (x,y) positions of the reflectors were surveyed and stored in the navigation computer so that the pose of the LHD while driving manually in the drifts could be estimated. The pose test convinced LKAB to proceed with a test of the automatic tramming function of the LHD in their SALT3 project in which the loop was closed with the guidance controller to enable the automatic tramming function. The work with the automatic tramming function of the LHD was started in 1996.

One reason LKAB became interested in the laser navigation system was due to the fact that it fulfilled the requirements for high speed driving as discussed, implying that the guidance

function and the localization functions were separated, the distance and heading errors to the reference path were calculated separately and used with different weights in the feedback control loop. The references path consisted of "virtual wires" – polynomials - referred to as segments making it possible to reduce the speed before entering a sharp curve. The main work was to adapt the guidance and localization functions to articulated vehicles (Andersson, Mrozek, Åström and Hyyppä, 1997). The initial tests were done during the summer and autumn of 1996 using CALMAN - Computerized Articulated Lawn Mower with Automatic Navigation – (Larsson, Zell, Hyyppä and Wernersson, 1994). In December of 1996, the navigation system was installed on a TORO501E LHD and tested in a production area in the Kiruna mine during December 1996 and January 1997. The results from the tests, convinced LKAB that the performance of the navigation system, referred to as HUNS (High speed Underground Navigation System), was sufficient for use in the SALT4 project which aimed at automation of the big TORO2500E's introduced in the Kiruna mine in the later part of the 90's.

LKAB's role in the SALT4 project was as the "systems integrator". Sandvik was the supplier of the automation prepared TORO2500E, the Finnish company Elektrobit Oy was the supplier of the communication system WUCS, the Swedish company Pronyx (now ÅF) was the supplier of the remote control system LRCS and the traffic control system LUCS, a system that interfaced the planning system of the mine. The Swedish company Q Navigator AB was the supplier of the navigation system HUNS. The functionality in the navigation system was significantly extended compared to the version used for the underground field trials in 1996/97. Automatic handling of the bucket for tramming and hauling was for instance added, Lundqvist (1999).

The first TORO2500E to be equipped with the automation system was the sixth machine (TORO595) delivered to LKAB in 1998.
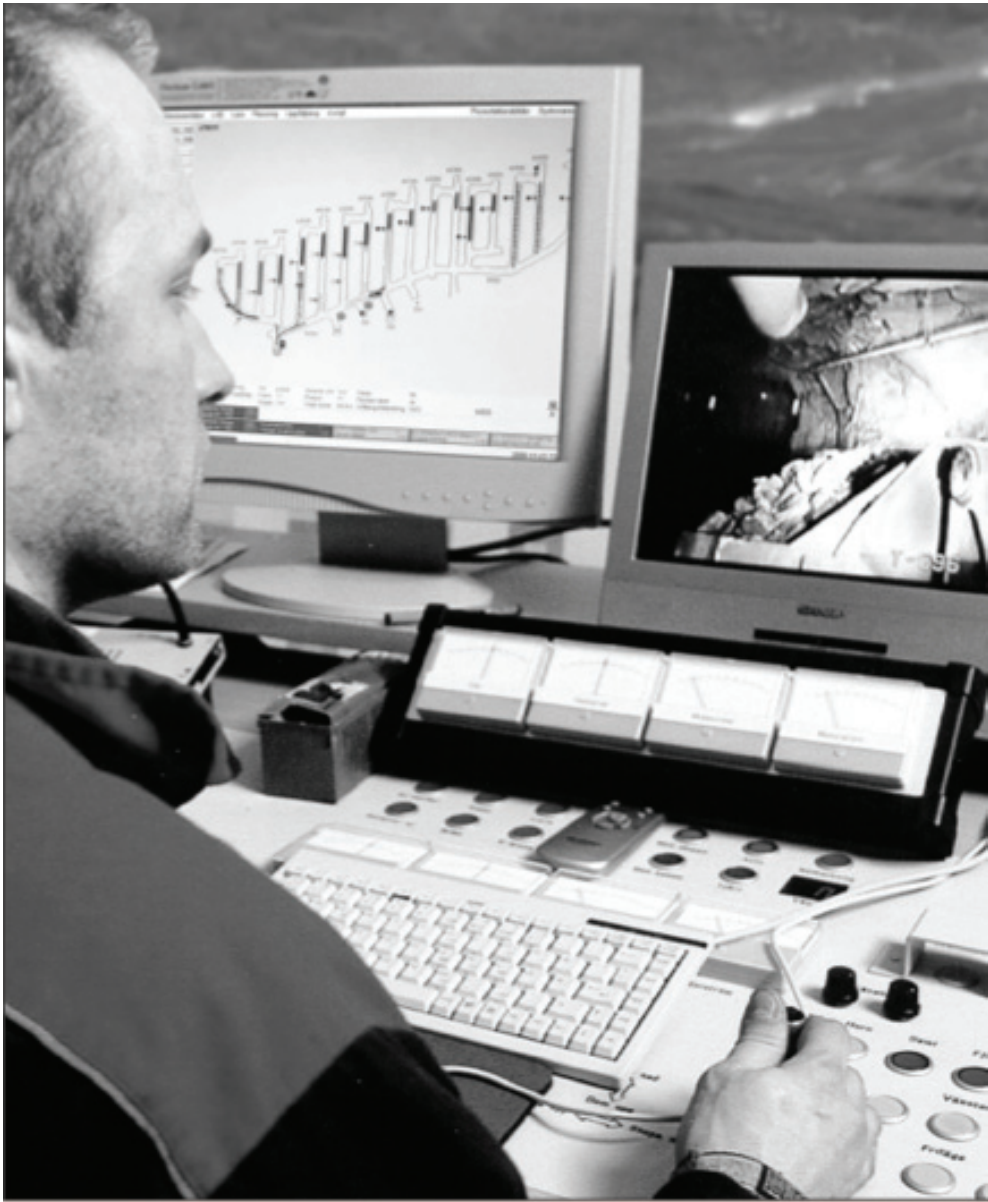
Figure 2. The photograph shows one of three operators' desks of the production system (SALT4). The photograph is published with permission of LKAB.

The user interface of the traffic control system is visible to the left in figure 2 displaying one production area in the mine, the video from the LHD is visible on the monitor to the right and some of the remote controls are visible in the lower part of the picture. The right hand joystick is used for control of the bucket height (boom) and angle (tilt). The identity of the LHD connected to the operator's desk is displayed on the video monitor.

2.2 Laser navigation system

A brief description of the laser navigation system is given in this section. The basic functions are discussed in Wiklund, Andersson and Hyyppä (1988) and Hyyppä (1993).

It should be noted that the loading is considered to be an integrated part of the navigation system. The reason simply being the completely integrated load, haul and dump functions of the machine itself. Therefore, systems controlling these functions have to be integrated for the cyclic operation to be efficient.

2.2.1 Pose estimator

Figure 3. The photograph shows the LHD used in the underground field trials in 1996/97. Eight retro-reflectors reflect back the flashlight to the camera.

The laser anglemeter rotates a laser beam counter-clockwise at 6 rev/s. When the laser beam hits a retro-reflector, a single stripe of tape, it is reflected back in the same direction, thus "hitting" the laser anglemeter which then registers the angle of the rotating head relative to the axis of the laser anglemeter. The measured angle is transmitted to the on-board navigation computer. Since the 2D positions of the retro-reflectors are known and stored in a reflector map, the measured angle can be associated to a retro-reflector in the map if the pose of the laser anglemeter is known or estimated with high accuracy.

An "abundance" of retro-reflectors can be installed since they are not space demanding to ensure redundancy in case of blocked or lost retro-reflectors.

When the navigation system is powered on, the pose of the vehicle is unknown and an initialisation of the pose estimate is necessary. The initialization procedure requires the vehicle to be standing still during the time measured angles from one revolution of the rotating head of the laser anglemeter are used to triangulate the pose, a method that requires at least four measured angles. The triangulated pose is used as the initial 2D pose estimate $(\hat{x}, \hat{y}, \hat{\theta})$ of the vehicle. (Estimates are denoted by the "hat" symbol.) It should be noted that the pose initialisation is done automatically with no requirements of complementing systems or that the vehicle should be positioned in certain spot as long as the laser anglemeter is surrounded by four well spread out retro-reflectors.

Figure 4. The sketch illustrates measurement of angles to retro-reflectors. Note that only one angle at a time is measured because of the rotation of the laser beam, implying that the pose of the vehicle changes between the measurements if the vehicle is in motion.

After the initial pose has been calculated, single measured angles are used one at a time to correct the estimated pose based on the Kalman filter method, which allows the vehicle to be in motion. The difference between the measured angle and the expected angle to the retro-reflector causing the reflection is used to correct the pose estimate.
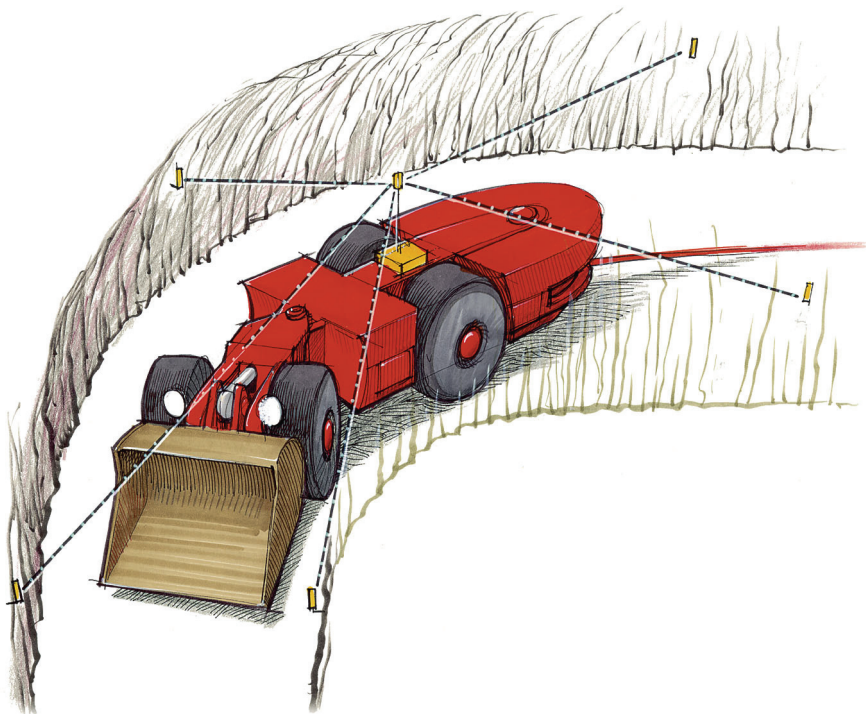
Measurements of the steering angle and the speed of the vehicle are used to update a kinematic model that describes the motion of the vehicle. The kinematic model is initiated to the pose estimate that was last corrected by a measured angle to a retro-reflector. A rough pose is then estimated, based on the kinematic model, at the time of the measured angle so that expected angles to retro-reflectors can be calculated. If the deviation between the measured angle and the expected angle to a reflector is small, the measured angle is associated to that reflector and the deviation is used to correct the rough estimate of the pose.

The association of a measured angle to the object causing the reflection is a key function in the navigation technique. There are several possible scenarios a few are listed below.

- The angle originates from a surveyed retro-reflector with a correct position in the reflector map.
- The angle originates from a stainless steel tube with a position not corresponding to the retro-reflector positions in the reflector map.
- The angle originates from a retro-reflector with a correct position in the reflector map but there are one or more reflector positions in the map giving the same expected angle.
- The angle originates from a retro-reflector that has been moved after the survey so that the measured angle and the expected angle differ significantly.

If a measured angle is wrongly associated to a retro-reflector in the map and thereby used for correction, the resulting pose estimate can be totally erroneous resulting in collisions with fixed installations at the site or with other vehicles. Therefore, it is of importance that the angle used for correction originates from the true retro-reflector with a correct position in the reflector map to avoid production disturbances.

A pose estimation safety system handles the lack of measured angles or angles that cannot be associated to retro-reflectors in the reflector map. Such measurements or lack of measurements causes the safety level to drop and when the level reaches 0% the vehicle is stopped. The vehicle will come to a stop in less than a second if consecutive measurements cannot be associated to retro-reflectors. Measured angles that are associated to retro-reflectors in the map increase the safety level up to 100%. The safety level is not updated if the safety level is at 100% and the measured angle is associated to a retro-reflector in the map.

Note that a measured angle can be disregarded even though it actually originates from a retro-reflector with a correct position in the map. This can happen if the sensors measuring the speed and steering angle gives inaccurate readings, resulting in incorrectly calculated expected angles to the retro-reflectors.

The estimator is based on the Extended Kalman Filter (EKF) discussed by Wiklund, Andersson and Hyyppä (1988) and the kinematic model of articulated vehicles discussed by Larsson, Zell, Hyyppä and Wernersson (1994), see chapter 1. The input to the estimator is the articulation angle and the speed of the LHD. If the difference between a measured

bearing and an expected bearing is small enough, the measurement is associated to that retro-reflector, provided that there is only one candidate retro-reflector, and used to correct the pose estimate in the EKF, Hyyppä (1989, 1991). In case of no measurements or no measurement possible to associate to a retro-reflector in the map, the pose estimate is not corrected and simply updated by the dead-reckoning system to the next sampling instant.

The time discrete state space model used in the pose estimator is, with k denoting the sampling instance

$$x_k = x_{k-1} + \Delta x \tag{1}$$

$$y_k = y_{k-1} + \Delta y \tag{2}$$

$$\theta_k = \theta_{k-1} + \Delta\theta_1 + \Delta\theta_2 \tag{3}$$

where the increments $\Delta x, \Delta y, \Delta\theta_1, \Delta\theta_2$ depends on the velocity v, the sampling period h, the articulation angle γ and the distance between the hinge and the wheel axles L according to

$$\Delta x = \bar{d}\cos(\theta_{k-1} + \overline{\Delta\theta})\,(1 - \overline{\Delta\theta}^2/6) \tag{4}$$

$$\Delta y = \bar{d}\sin(\theta_{k-1} + \overline{\Delta\theta})\,(1 - \overline{\Delta\theta}^2/6) \tag{5}$$

$$\Delta\theta_{1|\gamma_k=\gamma_{k-1}} = \frac{\bar{d}}{L}\frac{\sin\gamma_k}{1+\cos\gamma_k} \tag{6}$$

$$\Delta\theta_{1|\gamma_k\neq\gamma_{k-1}} = \frac{\bar{d}}{L\Delta\gamma}(\ln(1 + \cos\gamma_{k-1}) - \ln(1 + \cos\gamma_k)) \tag{7}$$

$$\Delta\theta_2 = \tan(\gamma_k/2) - \tan(\gamma_{k-1}/2) \tag{8}$$

where the help variables $\bar{d}, \Delta\gamma, \overline{\Delta\theta}$ are defined as

$$\bar{d} = h\,(v_k + v_{k-1})/2 \tag{9}$$

$$\Delta\gamma = \gamma_k - \gamma_{k-1} \tag{10}$$

$$\overline{\Delta\theta} = (\Delta\theta_1 + \Delta\theta_2)/2 \tag{11}$$

Scheding, Dissanayake, Nebot and Durrant-Whyte (1997,1999), Madhavan, Dissanayake and Durrant-Whyte (1998) discuss autonomous navigation experiments in underground mines based on wheel slip estimation. The states are extended with slip angles for the front part and the rear part respectively and the rolling radius compared to the states used in HUNS.

HUNS was set in dead reckoning only pose estimation mode in the underground field trials in the LKAB Kiruna mine in 1996/97 in order to test the accuracy of the models used in the control loop. The LHD was ordered to start drive straight in the footwall drift and then, after approximately 25 meters, make a 90-degree or 106-degree turn into a cross drift and drive another 25 meters. The results of the tests were that the LHD managed to perform the runs without being close to collisions with the walls of the drifts. The conclusion from the tests were that the kinematic motion model was accurate enough to allow autonomous driving for shorter distances in sections of the drift with blocked retro-reflectors or sections lacking retro-reflectors, which implies dead-reckoning pose estimation only. The pose estimation safety system is discussed in section 2.3.1.

2.2.2 Guidance controller

The reference path consists of polynomial segments connected to points (nodes) in the layout of the production area. The segments are designed such that there are no discontinuities in the points where the segments are connected to each other. The end point of one segment in the reference path is the start point of the next segment. There can be more than one ingoing segment to a point and more than one outgoing segment from the point. As an example - one outgoing segment continuous in the footwall drift and another segment goes in to a cross drift. All segments of the production area are stored in HUNS, but it is the traffic control system that orders the segments to execute, see Andersson and Strömsten (2013).

A ghost vehicle, a tricycle, is used to guide the LHD along the reference path. The relation between the tricycle and the articulated vehicle is based on two assumptions.

The rear axis of the tricycle - or the extension of it - is assumed to go through the hinge of the articulated vehicle.

The other assumption concerns the relation of the rotational speed of the front frame and the rear frame of the articulated vehicle relative the tricycle. Let subscript f denote the front frame, subscript r denote the rear frame, γ denote the articulation angle, and ω denote the rotational speed, the assumption then implies that

$$\omega_f = -\omega_r = \frac{\dot{\gamma}}{2} \tag{12}$$

The assumptions make the relation between the physical and fictive vehicles unique and make it possible to analytically calculate the position of the fictive vehicle relative the physical vehicle in computational efficient manner.

Denote the transversal velocity and the heading of the front frame in the coordinate system of the fictive vehicle v_f and θ_f respectively, see figure 5. The velocity of the articulation hinge in the x and y direction respectively is then assuming no sideslip of the articulated vehicle

$$\dot{x}_j = v_f \cos \theta_f + \omega_f L \sin \theta_f \tag{13}$$

$$\dot{y}_j = v_f \sin \theta_f - \omega_f L \cos \theta_f \tag{14}$$

The first assumption implies that $\dot{x}_j = 0$, which gives

$$v_f = -\omega_f L \tan \theta_f \tag{15}$$

Inserting (15) in (14) gives after some manipulations

$$\dot{y}_j = -L\omega_f \frac{1}{\cos(\theta_f)} \tag{16}$$

The distance d in figure 5 can be calculated based on (16) as

$$d = \left| \int \dot{y}_j dt \right| = \left| -L \int \omega_f \frac{1}{\cos(\theta_f)} dt \right| = \left| -L \int \dot{\theta}_f \frac{1}{\cos(\theta_f)} dt \right| = \left| -L \ln \tan \frac{\Pi}{4} + \frac{\theta_f}{2} \right| \tag{17}$$

From the second assumption (12) we get

$$\theta_f = \int \omega_f \, dt = \int \frac{\dot{\gamma}}{2} dt = \frac{\gamma}{2} \tag{18}$$

which finally result in

$$d = \left| -L \ln \tan \frac{\Pi + \gamma}{4} \right| \tag{19}$$

The control point that follow active segment of the reference path is the mid point on the rear axis of the tricycle. The tricycle is aimed in the travelling direction of the LHD.

Five control variables are used in the high-level controller; $(\hat{d}_{err})$ is the lateral error, $(\hat{\theta}_{err})$ is the heading error, $(\hat{K}_c)$ and $(\hat{K}_{c\_T})$ are the curvature of the reference path corresponding to the current and the predicted pose of the control point, $(\frac{d\hat{K}_{c\_T}}{ds})$ is the change in curvature in the reference path corresponding to the predicted pose of the control point.

The set angle and the set angle speed for the fictive tricycle are calculated with the feedback gains l_d and l_θ, the wheelbase L_t and the speed v_t of the fictive tricycle as

$$\gamma_t^{set} = -l_d \hat{d}_{err} - l_\theta \hat{\theta}_{err} + L_t \hat{K}_c \tag{20}$$

$$\dot{\gamma}_t^{set}(T) = \frac{L_t}{1 + (L_t \hat{K}_{c\_T})^2} \frac{dK_{c\_T}}{ds} v_t \tag{21}$$

The set values for the fictive tricycle are transformed into the corresponding set values for the articulated vehicle.

The transformation of the set angle for the tricycle to the set angle for the articulated vehicle is based on the assumption of a common centre of rotation (CoR) for both vehicles, see figure 5.
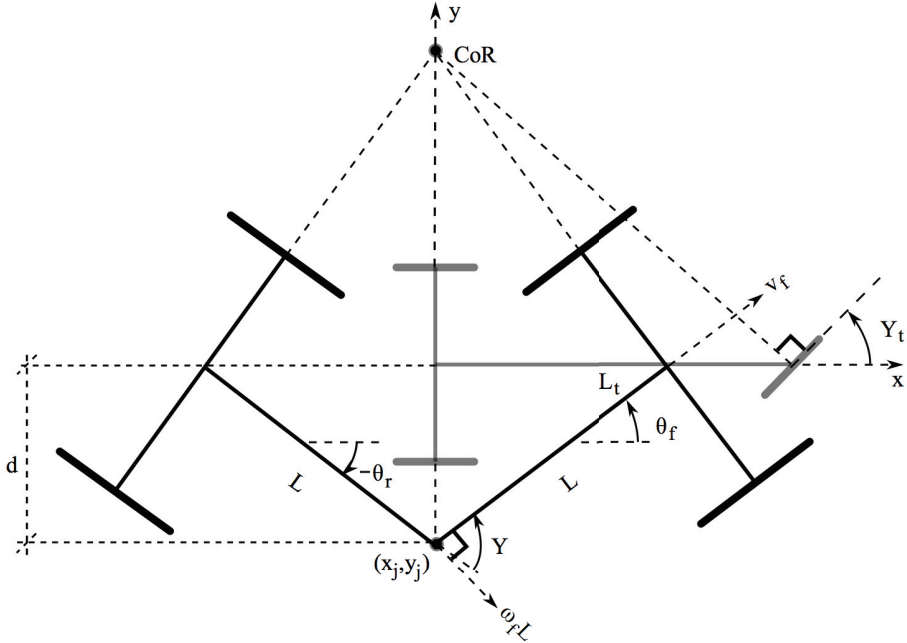
Figure 5. The relation between the physical articulated vehicle (black) and the fictive tricycle vehicle (grey) is illustrated in the figure.

The transformation is done using two equations; one of them solved numerically, see Andersson and Strömsten (2013).

Table 1. The distance d in meter for some values of the articulation angle γ is shown in the table for an articulated vehicle with wheelbase 2.55 meter (TORO2500E).

γ	0.0°	2.0°	5.0°	10.0°	20.0°	30.0°	40.0°	80.0°	160.0°
d	0.0	0.0445	0.1113	0.2228	0.4473	0.6753	0.9088	1.9454	6.2124
d / γ		1.2751	1.2754	1.2766	1.2815	1.2898	1.3017	1.3933	2.2247

A linear approximation can be used for practical values of the articulation angle.

The five steps used in the guidance controller are summarized in figure 6.
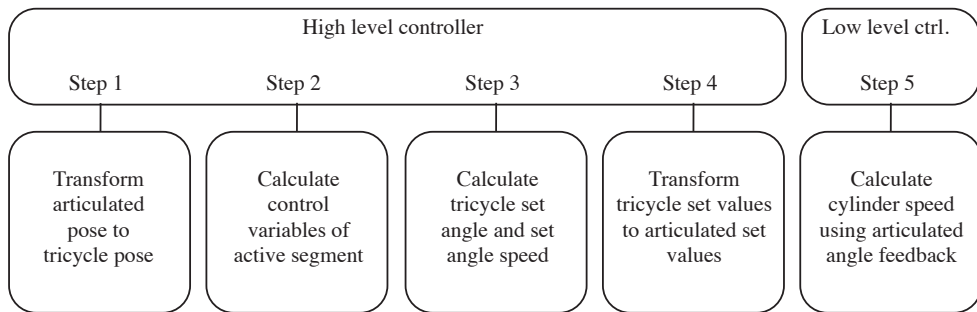
Figure 6. The control of the articulation angle is done in five steps as illustrated in the figure. The control of the drive speed of the vehicle is omitted.

Table 2. Characterization of high-level control variables.

Variable	Type	Control point	Path point
$\hat{d}_{err}$	Feedback	Current	Nearest
$\hat{\theta}_{err}$	Feedback	Current	Nearest
$\hat{K}_c$	Feed forward	Current	Nearest
$\hat{K}_{c\_T}$	Feed forward	Predicted, time based	Nearest
$\dfrac{d\hat{K}_{c\_T}}{ds}$	Feed forward	Predicted, time based	Nearest

The parameter values of the high level controllers were the same independently of LHD, of the load in the bucket, of the driving speed of the LHD and of the tyre wear implying that the solution proved to be robust. Careful tuning of the parameters during practical tests with the first commissioned LHD was necessary to gain acceptable performance during normal and provoked conditions.

The other task of the guidance controller is to control the drive speed of the vehicle, which is a straightforward task compared to the steering control.

Figure 7. The block diagram shows the control loop in HUNS.

2.2.3 Assisting system for loading

Low scoop weights of tele remote excavated buckets were early identified in the 10-year production period in the Kiruna mine. A driver assisting function was implemented to improve the situation. The function implies that the remote operator only controls the drive speed and articulation angle during the excavation. The control of the boom cylinders and the bucket cylinder is done automatically. The function emulates the skilled drivers excavation of the bucket in the muck pile. The function uses the measured speed of the LHD as the feedback control variable and the pose estimate to detect wheel spin.

Marshall, Murphy and Daneshmend (2008) refers to "muck" as

> "*Muck* typically refers to freshly blasted (fragmented) rock in an underground mine, which is ready for transport."

The loading part consists of five sequences.

Sequence 1. The bucket has been positioned in the correct position and the operator commands the LHD to drive forward on 1st gear. The driver-assisting function is initiated when the drive speed of the LHD is 1 m/s with some tolerance.

Sequence 2. The drive speed decreases when the bucket hits the muck pile. When the drive speed drops below v_{start} m/s, the bucket is lifted Δz_{start} mm in order to get a distribution of the load between the front axle and the rear axle of the LHD that prevents wheel spin, which is *traction control*.

Sequence 3. Tilting the angle of the bucket controls the drive speed of the LHD. If the drive speed drops below v_{min} m/s, the bucket cylinder speed is set to v_{bu_max} m/s in order to prevent the vehicle to come to a stop. If the drive speed exceeds v_{max} m/s, the bucket cylinder speed is set to zero in order to slow down the LHD. When the drive speed of the LHD, v, is between v_{min} and v_{max}, the bucket cylinder speed v_{bu} is

$$v_{bu} = \frac{v - v_{max}}{v_{min} - v_{max}} v_{bu\_max} \tag{22}$$

Sequence 4. When the bucket angle has reached its maximum value, the bucket is lifted Δz_{stop} mm in order to maximize the filling of the bucket.

Sequence 5. The function signals that the scooping is done. The operator starts reversing the LHD out from the muck pile. When the vehicle has moved Δx_{start} meter from the stop position of the scooping, the bucket is lowered to its lowest position and the bucket angle starts to change according to a saw-tooth shaped signal. The shaking of the bucket continues until the LHD has moved Δx_{stop} meter from the stop position of the scooping. The shaking of the bucket is done in order to remove loose rocks from the bucket.

When sequence 1 starts, dead reckoning only pose estimation is started in parallel to the ordinary retro-reflector based pose estimation. This makes it possible to detect wheel spin, which is highly unwanted during excavation. Spinning wheels will significantly reduce the filling and also damage the road. Denote the estimated distance travelled since the start of driver assisted excavation Δs_{dr} based on the dead reckoning and the estimated distance travelled since the start of driver assisted excavation Δs_{rr} based on the retro-reflector corrected pose estimation. Then if $\Delta s_{dr} - \Delta s_{rr} > \Delta s_{spinn}$, where Δs_{spinn} denotes the maximum allowed difference in calculated distance between the two methods, wheel slip is considered to be detected. If wheel slip is detected, the current driver assisted excavation sequence is interrupted and the bucket is lifted Δz_{spinn} meter. This is done in order to stop the wheels from spinning. If the spinning of the wheels continues after the lifting of the bucket, the driver assisted excavation sequence is aborted and the operator has to take over the controls.

Traction control to prevent wheel spin has a positive effect not only on the production but also on tyre wear.

If the remote operator starts to manoeuvres the joystick for the control of the bucket height and angle during excavation, the driver assisted excavation is aborted and the controls of the boom and bucket cylinders is handed over to the operator. One example when this is relevant is if there is a very large boulder in the muck pile requiring a completely different excavation technique.

The pose estimation is used in a safety system that prohibits excavation too far into the draw point. If the rock flow is stopped; the result is that the penetration of the muck pile is initiated further into the drifts for each loaded bucket. This is a dangerous situation since the LHD then drive into parts of the drift with no steady rock overhead. If the ore flow starts during excavation, the risk is that the LHD will be buried under the muck pile.

2.3 Discussion

The discussion in this section is based on experiences from the 10-year production period of the LHD automation system at the LKAB Kiruna iron ore mine and work in the SMIFU pre-study, RTC, Rock Tech Centre (2012).

2.3.1 Machine safety

No collisions occurred between the LHD's and the walls of the drifts when the LHD's were in automatic mode, camera tracking mode or semi-automatic mode implying that the implemented solution was robust from a machine safety perspective and at the same time allowed the LHD's to "do their job" as indicated by the KPI's, Andersson and Strömsten (2013).

Collisions between the LHD's and the walls of the drifts occurred when the LHD's were in remote control mode, which resulted in the development of the remote control safety system discussed in section 6.3.

The functions of the machine safety systems active in automatic mode, camera tracking mode and semi-automatic mode are summarized below.

2.3.1.1 Sensor safety

Doubled sensors are used for the measurement of some variables in the navigation function. The articulation angle (one sensor located in the upper hinge and the other in the lower hinge), the boom angle (one sensor located in the left hinge and the other in the right hinge) and the rpm of the longitudinal drive shaft.

The information from the doubled sensors is compared in each sampling instant. If the difference in measurements is greater than a maximum tolerance, the LHD is stopped.

The angle sensors were an "add-on" solution to the original design of the TORO2500E's. As it turned out, the mechanical couplings between the sensors and the LHD was a "weak" solution implying relatively frequent failure of the couplings resulting in an erroneous measurement. However, since the other sensor in the pair reported a correct measurement, the safety system would stop the LHD and an alarm was presented on the operators interface in the control room indicating a large deviation between the sensor measurements. At no time, the couplings of both sensors in a pair failed at the same time. The frequency of erroneous measurements of the rpm of the longitudinal drive shaft was much less frequent compared the angle measurements.

2.3.1.2 Pose estimation safety

The association of a measured bearing from the laser scanner to the object causing the reflection is a key function.

When the pose estimation safety system stopped the LHD, an alarm "*Navigation failure*" was presented on the operators interface in the control room. The cause of navigation failure was not presented since the underlying reason could have many different causes, one being sensor failure as discussed in the previous section since the average of the measured

variables were used in the pose estimator and if, for instance, one articulation angle sensor reported +10 degrees and the other -20 degrees, the resulting angle used for the dead reckoning update would be -5 degree resulting in that the measured bearing to a retro-reflector could not be associated to a retro-reflector position in the map.

If a measured bearing is wrongly associated to a retro-reflector in the reflector map and thereby used in the EKF to correct the pose estimation, it can have devastating consequences since the resulting pose estimate can be totally erroneous resulting in a collision with the wall of the drift.

Therefore, it is of utmost importance that the bearing used to correct the pose estimate in the EKF originates from the true retro-reflector with a correct position in the reflector map of the system.

The pose estimation safety system is based on the association type of the measured bearing or lack of measured bearing from the laser scanner. If a bearing is associated with a retro-reflector in the reflector map of the system, the navigation level is increased by 5%. If the increase will cause the navigation level to exceed 100%, the navigation level is saturated at 100%.

Bearings that cannot be used to correct the pose estimate, or lack of bearings will decrease the navigation level. For instance, bearings that are categorized as "FALSE" (originating from other reflective objects than retro-reflectors with surveyed positions or retro-reflectors significantly out of position) will decrease the navigation level with 20%. When the navigation level reaches 0%, the vehicle is stopped.

As an example, five consecutive sampling instances with FALSE associations will result in that the navigation level drops down from 100% to 0% in 0.125 seconds.

The association of measurements made by the laser scanner to be either "true" or "false" ensures the robustness of the pose estimation method. Only measured bearings to true reflectors are used in the correction of the pose estimate. Bearings being classified as "false" happens if the information from the navigation sensors is not consistent or too many reflectors are blocked or has erroneous positions compared to the reflector map.

Example.

This example describes an incident that occurred in the second production area for LHD automation at the Kiruna iron ore mine, referred to as level 765 meters road 33. The example illustrates the importance of machine safety systems.

> At one time, the pole of the laser scanner got hooked to a low hanging ventilation tube in the footwall drift of the production area when the automatic LHD was running on top gear. The result was that the pole with the laser scanner was ripped off the LHD and attached to the ventilation tube while the LHD continued to drive a few meters before the pose estimation safety system stopped it. The three alarms presented as a result of the incident on the operators interface in the control room were
> "*Navigation failure*"
> "*Laser scanner – no communication*"
> "*Pose initialization – too few measured bearings*"

2.3.1.3 Guidance safety

The guidance safety systems monitor the pose of the LHD relative the active segment. If the deviation is too large the LHD is stopped. The experience of the guidance safety systems is that stops by the system was mainly due to wear of the roadway or boulders on the drive way causing the estimated pose relative the segment to be outside the safety zone. The scanner is mounted 3.2 meters above the ground implying that unevenness in the roadway is amplified since the pose estimate is not transformed to the ground plane, which would have required fast reacting and very accurate inclination sensors. The wear of the roadway is a relatively slow process, which regular maintenance normally handles in opposite to spilled rocks from the bucket during hauling that creates a significant hinder instantaneously. In these cases, an obstacle detection system is necessary to avoid unnecessary wear of the LHD. If the rock is spilled while hauling in the rearward direction, the LHD will hit the rock driving in the forward direction with the bucket in front. To arrange sensors that can detect rocks on the roadway in this scenario is difficult because of the blocking nature of the bucket when sensing the roadway. Failures in the hydraulic system for the control of the articulation angle or the hydraulic system of the brakes were handled by the guidance safety system also. If, for instance, the brake system failed and the LHD was to make a change of driving direction at a point in the layout, the result would be that the target braking aiming at the reversing point would fail and the LHD would overshot the point. The overshoot would have been detected by the guidance safety system, which would have stopped the LHD by activating the E-brakes. This scenario occurred during the production period, especially in the early phase when the same oil tank were used for both the hydraulic system for the articulation angle, boom/bucket and the brake system. The alarm from the guidance safety system presented on the operators interface in the control room was either "*Guidance safety – outside zone sidewise*", "*Guidance safety – outside zone heading-wise*" or "*Guidance safety – outside zone length-wise*".

Two safety zones around the segment are used, the inner zone and the outer zone. The safety zones are defined as maximum allowed sidewise errors from the control point to the nearest point on the segment and maximum allowed differences between the heading of the ghost tricycle and the slope of the segment in the nearest point on the segment. The inner zone is narrower than the outer zone. The definition also includes a maximum distance error from the end point of the segment to the control point calculated in the lengthwise direction of the segment, which is used at reversing points or at end points where the vehicle shall stop. If the control point is inside the inner zone, the drive speed of the vehicle is set to the lowest value of what is defined in the segment, by the traffic control system or by the bucket safety system. For instance, the segment definition implies set speed corresponding to gear 4, but the traffic control system has limited the speed to gear 1, then gear 1 is used as the set value for the drive speed. The bucket is lifted as a function of the travelled distance on the segments during hauling to prepare for dumping when the LHD is close to the ore pass. If the bucket height or angle deviates from the set values with some tolerances, the allowed drive speed is limited to gear one. If the deviation in the bucket height or angle is significant, the LHD is stopped.

If the estimated pose of the tricycle is outside the inner zone of the segment but inside the outer zone of the segment, the drive speed is limited to gear 1.

If the estimated pose of control point is outside the outer zone of the segment, the LHD is stopped. The only way to move the vehicle then, is either by switching to remote control mode, or by moving the vehicle manually.

2.3.2 System development based on production experiences

The focus of the development work prior to the commissioning of the first LHD was on the automatic mode. As it turned out the cycle time of the LHD's in automatic mode when driving - hauling with load in the bucket and tramming with empty bucket – was comparable to manual driving.

Almost immediately after the system had been installed, the weakness of the technical solutions for the remote control showed up. The original remote function was simple tele-operation, implying that the same controls are used on the operator's desk as in the cabin of the machine. However, since the manual driver bases the control on 3D vision, audio and vibrations feedback compared to the remote operator that bases the control on only 2D video – slightly delayed – pure tele-operation of the LHD for the remote control was not sufficient.

The initial experiences from remote controlled scooping showed that the operators had difficulties in positioning the bucket in the correct position before the penetration of the muck pile begun based on only video information from the cameras on board the LHD. This resulted in low scoop weights and damaged roads at the draw points.

A number of collisions with the LHD's and the walls of the drifts occurred in remote control mode when the remote operator controlled the LHD based on video feedback information. The cabin of the LHD is more sensitive than other parts of the vehicle, implying that collisions involving the cabin did much damage. The remote control mode safety system was developed to minimize the collisions during remote operations of the LHD's.

Three functions were developed during the production period to assist the remote operator when scooping.

The bucket to load position function is an operator assisting function. By pressing a button on the operator's desk when the LHD is in remote control mode, the bucket is automatically position in the correct position for the scooping to start. The Auto Load function is another operator assisting function. Auto Load implies that the manoeuvring of the bucket during the penetration of the muck pile is done automatically. The function emulates a skilled manual driver. The remote control safety function stops the manoeuvring of the LHD in remote control mode if distance-measuring sensors, located on strategic positions on the LHD, measures the distances between the LHD and the walls of the drifts to be less than a certain limit.

2.3.3 Remote operators and service personnel

The remote operators had to base the scooping on only video feedback, compared to the manual driver with 3D vision feedback as well as audio and vibrations. This turned out to be more of a challenge for some of the remote operators. Student filled in as remote operators during the semester periods, many of them only working in the control room and never visiting the mine. It also turned out that the average weight of loaded bucket in remote mode compared to manual mode when the driver is sitting in the cabin of the LHD was a bit lower. The time it takes to load the bucket was also somewhat longer compared to manual operations. It reasonable to conclude that the limited feedback the remote operator had to base the control on was the main reason for this. The remote operator based the control on a

slightly delayed 2D video feedback from the LHD compared to the manual driver that bases the feedback on 3D vision, audio and vibrations of the LHD.

When the first LHD had been commissioned in the summer of 1999, LKAB found that the service personnel working with manual LHD's were lacking competence in computer systems, which is necessary for the service of an LHD automation system. For that reason, the author of this paper stayed in Kiruna and worked with service of the SALT4 system while LKAB started to build up internal competence that could handle the normal service and troubleshooting of the system, which took some years.

2.3.4 Manual, mechanized, remote controlled and automated operations

LKAB together with the Swedish mining company Boliden and the Polish mining company KGHM and major suppliers of underground mining equipment made a conceptual study in 2010 with the goal to develop a common vision for future underground mining, RTC (2010). The conceptual study was followed by a pre-study consisting of 14 work-packages addressing different technology areas, RTC (2012). Luleå University of Technology and Kraków University of Technology made contributions in this work. The result of the study is a strategic agenda for visions up to and beyond 2030 for underground mining. One of the work packages is called ZEPA – Zero Entry Production Ares. The goal with ZEPA was to identify technology development and research activities that make it possible to remove all humans from the production areas of the mines.

In order to systematically map activities to determine the current "case types" of work executed in the production areas, the work was divided into "*unit operations*" each consisting of a number of "*tasks*".

The tasks are divided into manual tasks, mechanized tasks, remote controlled tasks and automatic controlled task. As an example, the production loading with LHD's was identified as one unit operation consisting of tasks defined in table 3.

Table 3. The tasks of the unit operation "production loading" are defined in the table.

Task	Mechanized	Remote	Automatic
Bucket filling	X	X	
Hauling and Tramming	X	X	X
Waiting for rock breaker	X	X	X
Measuring of bucket weight	X	X	X
Dumping	X	X	X
Tramming	X	X	X

In all, 55 unit operations were identified in the three type mines studied consisting of 342 associated tasks categorized as

- Completely manual tasks: 107.

- Mechanized tasks: 235.

- Remote controlled tasks: 16.

- Automatic controlled tasks: 14.

The main part of unit operations and associated tasks were common for the type mines and thus independent of the caving methods. The type mines were

- Sub-level cave mine.

- Back-fill mine.

- Room and pillar mine.

An obvious conclusion from the result above is that the degree of remote and automatic controlled tasks is low compared to manual and mechanized tasks. One explanation to this is the difficulties in combing manual or mechanized work with remote controlled or automated work because of safety regulations.

An automated LHD operating in a production area requires area isolation system, which prohibits manual / mechanized types of tasks to be executed in the production area when the LHD is in automatic mode, which is in contrast to traditional AGV applications where the low speed of the vehicles in combination with external safety systems on-board the AGV's allows humans and AGVs to operate in the same areas.

Therefore, to fully utilize the potential of LHD automation other operations affecting or being affected by the production loading has to be changed, for instance automated or re-organized.

References

Andersson, U., Mrozek, K., Åström, K., & Hyyppä, K. (1997). Path design and control algorithms for articulated mobile robots. In *Proceedings of the International Conference on Field and Service Robotics*, 1997, Canberra, Australia.

Andersson, U., & Strömsten. M. (2013). Reflector based LHD automation at the LKAB Kiruna iron ore mine. Paper submitted to IEEE Robotics & Automation Magazine.

Eriksson, G., & Kitok, A. (1991). Automatic loading and dumping using vehicle guidance in a Swedish mine. In *International Symposium on Mine Mechanisation and Automation*, Colorado, pp. 15.33-15.40.

Duff, E., Roberts, M., & Corke, P. (2002). Automation of an underground mining vehicle using reactive navigation and opportunistic localization. In *Proceedings of the Australian Conference on Robotics and Automation*, 2002, Auckland, Australia. pp. 151–156.

Duff, E., Roberts, M., & Corke, P. (2003). Automation of an underground mining vehicle using reactive navigation and opportunistic localization. In *Proceedings of the IEEE/RSJ International Conference on Intelligent Robots and Systems, 2003, Las Vegas, NV, USA*. pp. 3775–3780.

Duff, E., & Roberts, M. (2003). Wall-following with constrained active contours. In *Proceedings of the 4th International Conference on Field and Service Robotics,* 2003, Japan.

Gustafson, A. (2011). Dependability assurance for automatic load haul and dump machines, pp. 11-12. Licentiate Thesis, Luleå University of Technology, Luleå, Sweden.

Hyyppä, K. (1993). On a laser anglemeter for mobile robot navigation, Doctoral thesis, Luleå University of Technology, Luleå, Sweden.

Jannok, D., & Petersen, M. (1992). Lasernavigering av midjestyrda gruvlastare. Master's Thesis, Luleå University of Technology, Luleå, Sweden.

Larsson, J., Appelgren, J., Marshall, J., & Barfoot, T.D. (2008). Atlas Copco infrastructure less guidance system for high-speed autonomous underground tramming, In *Proceedings of the 5th International Conference and Exhibition on Mass Mining on Field and Service Robotics*, Luleå, Sweden.

Larsson, J. (2011). Unmanned operation of load-haul-dump vehicles in mining environments. Doctoral thesis, Örebro University, Örebro, Sweden.

Larsson, J., Appelgren, J., & Marshall, J. (2010). Next generation system for unmanned LHD operation in underground mines. In *Proceedings of the SME Annual Meeting and Exhibition*, Phoenix, AZ, USA.

Larsson, U., Zell, C., Hyyppä, K., & Wernersson, Å. (1994). Navigating an articulated vehicle and reversing with a trailer. *In Proceedings of IEEE International Conference on Robotics and Automation*, San Diego, CA, USA.

Lundqvist, M. (1999). Reglering av skopposition på lastmaskin. Master's Thesis, Luleå University of Technology, Luleå, Sweden.

Marshall, J., Barfoot, T., & Larsson, J. (2008). Autonomous underground tramming for center-articulated vehicles. *Journal of Field Robotics*, 25(6-7):400-421.

Marshall, J.A., Murphy, P.F., & Daneshmend, L.K. (2008). Toward autonomous excavation of fragmented rock: full-scale experiments. *IEEE Transactions on Automation Science and Engineering*, 5(3):562–566.

Mäkelä, H. (2001a). Overview of LHD navigation without artificial beacons. *Robotics and Autonomous Systems*, 36:21–35.

Mäkelä, H. (2001b). Outdoor navigation of mobile robots. Doctoral thesis, Helsinki University of Technology, Espoo, Finland.

Nilsson, J-O., Wigdén, I., & Tyni, H. (2001). Mine automation at LKAB Kiruna, Sweden. In W. Hustrulid & R.C. Bullock (Eds.), *Underground mining methods: engineering fundamentals and international case studies*, (chapter 75). Society for Mining, Metallurgy, and Exploration: Littleton, Colo.

Roberts, J. M., Duff, E. S., & Corke, P. I. (2002). Reactive navigation and opportunistic localization for autonomous underground mining vehicles. *Information Sciences*, 145:127–146.

RTC, Rock Tech Centre. (2010). Final report MIFU – Smart mine of the future.

RTC, Rock Tech Centre. (2012). Sustainable mining and innovation for the future – research, development and innovation program.

Wylie, R. (1996). LKAB invests in the future. *Engineering and Mining Journal*:48-52.

CHAPTER 3

Part II - Traction control

3.1 Introduction

The subject of this part of the thesis is traction control for off-road construction vehicles.

The construction vehicles that are considered are the wheel loader and the hauler, which are both frame steered vehicles. Traction control implies control of the input torque to a driving wheel of the vehicle to the circumferential force in the tyre-soil contact patch. In certain situations, the control objective is to maximize the tractive forces (think of a loaded hauler climbing a steep hill) in other situations it might be to prevent the wheel to start spinning (think of a wheel loader ploughing snow), or in certain situations it might be to minimize the energy consumption (think of a hauler driving at constant speed on a flat road with good grip). The input torque to the driving wheels traditionally comes from one combustion engine. The engine torque is transmitted via a gearbox, shafts and power distributing units (PDUs) – commonly referred to as differentials - to the wheels. Different types of hybrid solutions where the combustion engine and electrical motors are used for the propulsion of the vehicle have been developed in recent years (Hori, 2004). Obviously, the control solutions differ between traction control systems for vehicles with mechanical drivelines and traction control systems for vehicles with individual wheel drives. The degree of freedom in control is higher for vehicles with individual wheel drives, Hori notes for instance that one of the possibilities that open up with individual wheel drives is local traction control system for each wheel.

The amount of articles that relates to on-road Ackermann steered single frame vehicles such as passenger cars is huge compare to articles related to off-road construction vehicles. Methods and results for single frame vehicles can in some cases directly be translated to articulated vehicles and in some cases not. A wheel loader for instance consist of two frames, each with its own center of gravity, which is a design that may cause snaking during certain driving conditions which does not exist in a passenger car. Snaking is a lateral stability problem, which influences the mobility performance, and thereby also the control of the traction forces (Azad 2005).

The definition of traction control is according to
http://www.thefreedictionary.com/traction+control (read 2013-09-26)

> "A method of preventing wheels from spinning when traction is applied by limiting the amount of power supplied to the wheel"

The definition does not say anything how to control the tractive forces. The definition is more like a constraint - "no wheel spin" - in the traction controller. The definition of traction control used in this thesis is *control of tractive forces*.

When studying literature that relates to traction control, it does not take long to come to the conclusion that some variables are very important such as

- Wheel slip.

- Power/Torque distribution.

- Efficiency.

The wheel slip transforms the input torque to a wheel into a tractive force in the contact patch between the wheel and the ground. The slip is caused by deflections of the treads of the tyre in the contact patch between the tyre and the ground. Too much slip implies spinning, which is highly unwanted. The slip in combination with the friction coefficient in the contact patch defines the maximum tractive force of the wheel before spin starts. The concept is illustrated in figure 1.
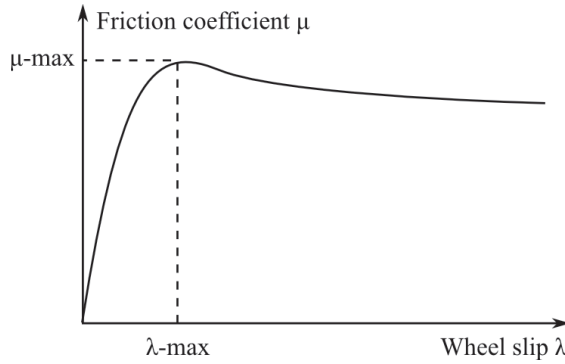
Figure 1. The figure shows a principal μ-λ relationship.

When the wheel slip is λ-max in figure 1 the friction coefficient is at its maximum (μ-max) implying that the maximum tractive force of the wheel is μ-max times the normal force (N) acting on the wheel. If the wheel slip exceeds λ-max, the wheel starts spinning and the traction is lost. It should be noted that the relation between the slip and friction coefficient depend on surface conditions, dry asphalt and ice has for instance completely different characteristics.

The wheel slip occurs in the longitudinal direction and the lateral direction of the tyre depending on the forces acting in the contact patch between the tyre and the ground. The wheel slip is divided into sideslip, which occurs if a lateral force acts in the contact patch, and longitudinal slip.

If we assume the sideslip to be zero, Kielce and Nielsen (2010) defines the longitudinal slip as

$$s_\delta = \frac{\omega_w r_w^r - V_x}{V_x}, \quad \omega_w r_w^r \le V_x \tag{1}$$

$$s_\delta = \frac{\omega_w r_w^r - V_x}{\omega_w r_w^r}, \omega_w r_w^r > V_x \tag{2}$$

The slip is defined by (1) when the wheel is braking and by (2) when the wheel is driving. The actual linear velocity of the wheel is V_x, comparable to GPS measured speed, the rotational speed of the wheel is ω_w and r_w^r is a reference value of the *rolling radius* of the wheel. The product $\omega_w r_w^r = V_t$ is the theoretical linear velocity of the wheel comparable to odometer-measured speed displayed on the speedometer in a passenger car for instance. The wheel slip is a value between -1 and 1. V_t equal to V_x implies that the slip is zero.

The rolling radius is defined as

$$r_w = \frac{V_x}{\omega_w} \tag{3}$$

The rolling radius is dependent of the input torque to the wheel as illustrated in figure 2.
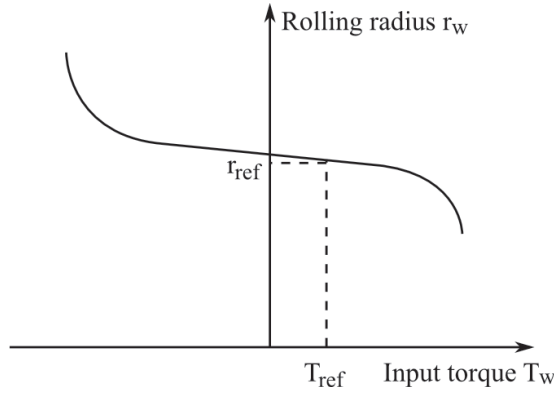
Figure 2. The rolling radius as a function of input torque to the wheel is illustrated in the figure.

If the input torque is T_{ref} in figure 2, the resulting rolling radius r_{ref} is the reference radius implying that the slip is zero. It should be noted that the relation between the input torque and the rolling radius depends on several variables such as temperature, normal load, inflation pressure of the tyre, etc.

The reference value of the rolling radius is not uniquely defined in the literature. Kiencke and Nielsen (2010) use the static wheel radius r_w^{stat} defined with the original radius of the tyre r_w^{org}, the stationary wheel ground contact force F_z, and the tyre spring stifness k_T as

$$r_w^{stat} = r_w^{org} - \frac{F_z}{k_T} \tag{4}$$

Andreev, Kabanau and Vantsevich (2010) use the rolling radius in *free mode* r_w^f as the refereence radius. The free mode implies that the input torque to the wheel corresponds to a tractive force equal to the rolling resistance of the wheel. For practical reasons, the rolling radius in *driven mode* r_w^0 can also be used. The input torque to the wheel is zero in driven mode.

3.1.1 Summary of work

A summary of the work done is that a significant amount of time has been spent on understanding the key mechanisms behind traction – slip, power/torque distribution and efficiency.

The sideslip has been studied by equipping a hauler with a GPS/INS system. This set-up makes it possible to estimate the sideslip based on the output from the GPS/INS system. The test vehicle ArtiTRAX has been used extensively in order to understand slip and energy efficiency as a function of torque distribution for vehicles with individual wheel drives. The focus has been on steady state conditions. Steady state in this case means that the speed and the articulation angle have been kept close to constant.

The work has been reported in a Masters' Thesis by Markdahl (2010) and in papers by Markdahl, Bortolin and Andersson (2010), Andersson, Bortolin, Backén and Gustafsson (2011), Andersson and Broström (2013).

3.2 Energy efficiency

3.2.1 Torque distribution methods

Articles from Yamakawa and Watanabe (2006), Yamakawa, Kojima and Watanabe (2007) and Senatore (2011) have been studied and serve as an inspiration to the initial experiments with ArtiTRAX regarding torque distribution between the driving wheels.

Yamakawa and Watanabe discuss a method to distribute the torque between the driving wheels in steady state when driving straight and in circles on flat surface. Steady state implies that the ground speed of the vehicle and the steering angle are constant. The model vehicle is a single frame vehicle with individual steered wheels with hub motors.

A minimisation problem is formulated for the steady state case. Determining the tractive forces - and thereby the torques - that minimises the cost function for a certain constant driving speed and load distribution between the wheels solves the minimisation problem.

It is shown in simulations that there is a close to linear relation between optimal torque and load distribution for the model vehicle when driving straight and in circles on flat ground.

It is noted that the (almost) linear relation does not hold for a reference vehicle – a four-wheel drive vehicle with a center differential and front two-wheel Ackermann steering – that is used for comparison.

Yamakawa and Watanabe find the optimal torque contribution for each wheel of the model vehicle to be approximately proportional to the ratio of vertical load on respective wheel.

Yamakawa, Kojima and Watanabe (2007) extend the work to electric off-road vehicles driving on rough ground. The *driving efficiency* of such vehicles is studied when driving in the pitch plane, which implies that only straight driving is considered.

The model vehicle studied is a four wheel driven single frame vehicle with individual wheel drives. The driving efficiency is defined as the average torque and frictional work done by all of the tyres.

Yamakawa, Kojima and Watanabe study the driving efficiency when driving over different ground profiles in simulations. The speed of the frame of the vehicle is controlled for the model vehicle. The output from the controller is the total torque to be distributed according to vertical load on the wheels. The model vehicle is compared to reference vehicles with a traditional mechanical driveline and a vehicle with hub motors where the speed of each wheel is individually controlled. In all but one simulation case presented, the reference vehicle is the most efficient, implying lowest averaged torque and frictional work.

The influence of different soils such as dry sand and moist loam is not discussed in the article. The rough terrain is only characterised by various ground profiles.

Senatore (2011) claims that optimal performance, regardless of the vertical load distribution, is achieved when the torque is biased toward the rear axle. The claim is based on simulations when driving straight with constant speed. Different soil characteristics are considered. The soil can influence the front tyres and the rear tyres in different ways if they travel in the same track. The front tyres packs loose soil, which means that the rear tyres travels on a stiffer ground compared to the front tyres.

The terms "*tractive efficiency*" and "*mobility*" are used. The tractive efficiency η_t is defined as

$$\eta_t = \eta_m \, \eta_s$$

where η_m is the efficiency of motion and η_s is the efficiency of slip. The definition of the efficiency of motion is

$$\eta_m = \frac{F_x R_l}{T}$$

where F_x is the drawbar pull, R_l is the rolling radius and T is the input torque to the wheel.

The definition of the efficiency of slip is

$$\eta_s = 1 - s_d$$

where s_d is the slip ratio defined as

$$s_d = 1 - \frac{V}{\omega R_l}$$

where V is the speed of the axle, ω is the rotational speed of the axle and R_l is the rolling radius.

The vehicle studied in simulations - FWD, RWD and AWD - all have mechanical drivelines.

The torque is split equal between left and right wheel and torque between front and rear axles can be varied in case of an AWD.

The speed of the vehicle is controlled by a PI controller, which output is the total torque required to maintain a certain speed. The total torque is varied from 0% to 100% between the front and rear axle of the AWD.

Simulations when driving on dry sand and on moist loam are presented. The simulation results are presented as driving power as a function of torque distribution to the rear axle. Difference in front and rear wheels slip ratio - Δs_d - is also presented.

There is one particular simulation example that can be compared with the proposed method by Yamakawa. In the example, the load distribution is 43,5% on the rear axle and 56,5% on the front axle for a vehicle driving on dry sand.

According to Senatore, the optimal distribution in this example is "*close to 50%F-50%R ratio*" (see figure 3).
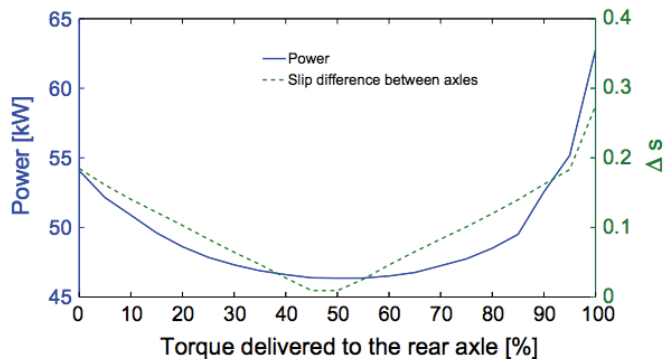
Figure 3. The figure is taken from Senatore (2011) and shows the efficiency in terms of driving power as a function of distribution of torque to the rear axle. The difference in slip ratio between the front and rear axles is also shown as a function of distribution of torque to the rear axle.

In the conclusions, it is stated that:

> "Static load distribution influences traction but does not have a significant impact on tractive efficiency: the best tractive efficiency, under a large range of operational conditions, is reached when the torque distribution is biased toward the rear axle. This operational condition helps to optimize the slip efficiency which dominantly influences the overall tractive efficiency".

It is worth noticing that Senatore does not present a method/guideline for how to bias the torque towards the rear axle. The claim by Senatore is in line with test results presented by Guy (2011).

3.2.2 Test with ArtiTRAX

The steady state velocity of ArtiTRAX has been 1 m/s during the tests. All effectiveness figures are based on measurements in steady state.

3.2.2.1 Indication of efficiency

The efficiency is shown in a number of figures below. Our indication of efficiency is based on Senatore (2011) with a slight modification that compensates for small variations of the ground speed in steady state.

Since the ground speed in steady state has some variations, the driving power is divided by the speed of the measuring wheel. The unit of the efficiency indication then becomes [W*s/m] = [J/s*s/m] = [J/m], which can be interpreted as the energy it takes to move ArtiTRAX one meter.

The average power during the period of steady state driving is divided by the average ground speed.

3.2.2.2 Influence of tyre pressure

The figure below shows the influence of varying pressure in the tyres. Three cases are shown:

- Low pressure in all four tyres.

- Low pressure in front tyres, normal pressure in rear tyres.

- Normal pressure in all four tyres.
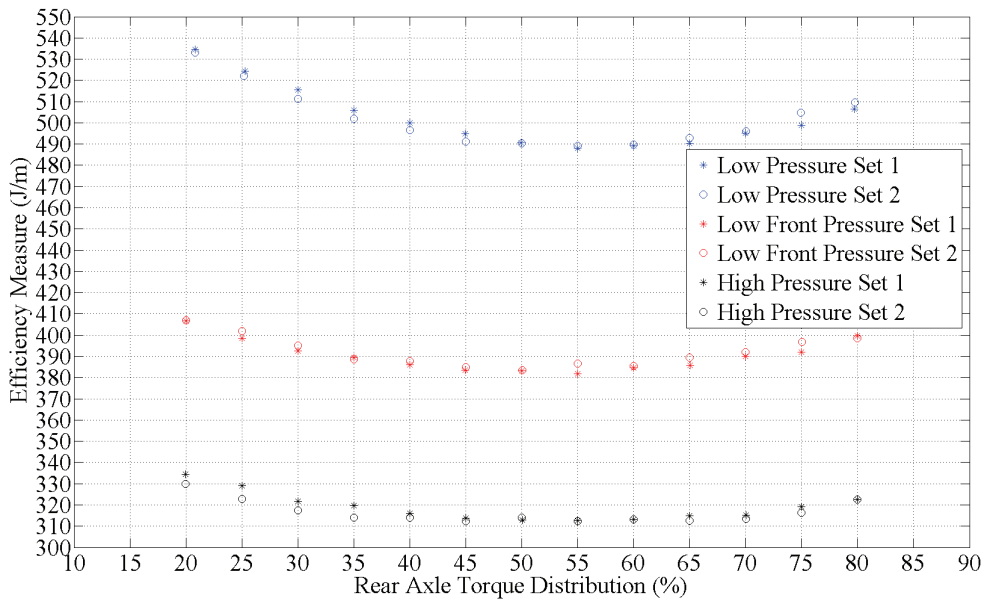
Figure 4. The figure shows the influence of tyre pressure on efficiency. A 75 kg passenger went with ArtiTRAX during the tests, which were done in a gymnasium. The vertical load distribution in this case is 44% on the front axle and 56% on the rear axle.

3.2.2.3 Load transfer
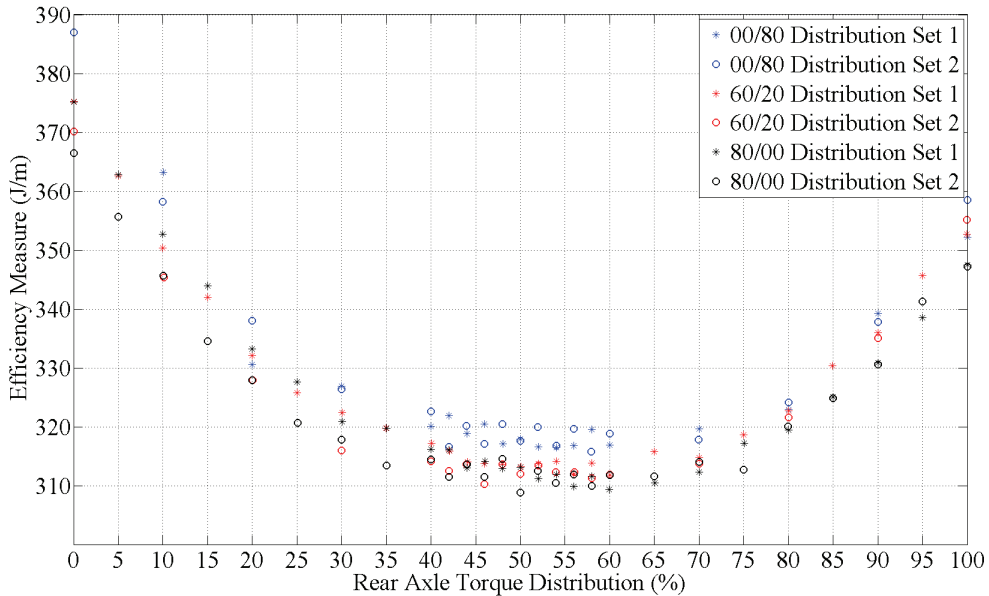
Figure 5. The figure shows the influence on the energy efficiency of different distributions of the load when driving straight with constant speed.

The runs presented in figure 5 were done with normal pressure in all four tyres with extra weights over the wheel axes according to table 1.

Table 1. Static axle loads for different distributions of extra weight.

Axle	F/R 80/0	F/R 60/20	F/R 0/80
Front	56%	50%	31%
Rear	44%	50%	69%

The following observations are made from figure 5.

- The efficiency curves for all distributions of extra weights are at a minimum in the torque distribution interval 45% to 70%. This region is very flat without distinctive minimums.

- Torque distribution in the intervals 0% to 20% and 80% to 100% is clearly less efficient for all distributions of extra weights.

- It is also clear in case of 2WD that rear wheel driving is more efficient than front wheel driving for all distributions of extra weights.

- The F/R load distribution 31/69 % is less efficient compared to the 56/44 % and 50/50 % load distributions.

46

3.2.2.4 Failing wheel drive
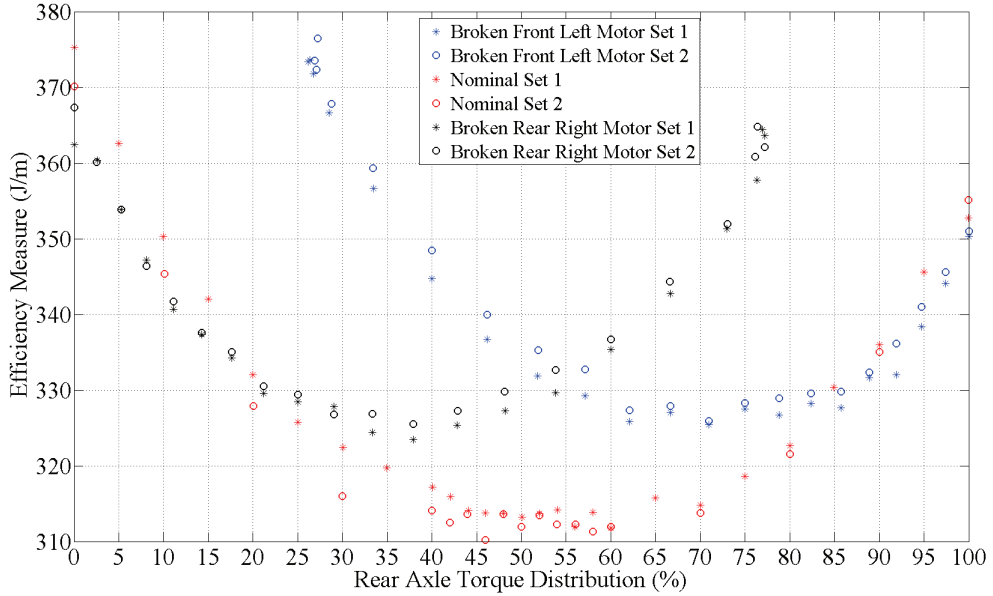
Figure 6. The figure shows the efficiency when one motor is turned off to simulate a drive failure.

The experiments presented in figure 6 are done with the front left motor turned off in two runs and with the right rear motor turned off in two runs. For comparison, the corresponding efficiency when all motors are running is also shown in the figure. The reason the marks are not on multiples of 5% on the x-axis when one motor is turned off is because the measured current is used when determining the distribution. The demanded distribution assumes all motors to be operating. The demanded distribution between the axles during the runs have been 0%-100%, 100%-0% in steps of 5%.

The efficiency curve in the case of one broken rear drive has a more distinctive minimum compared to the efficiency curve in case of one front drive broken. The efficiency curves indicate that a rule of thumb is to split the torque equal between the drives in operation in case if one failing drive.

3.2.2.5 Steering system inhibited

The importance of a proper torque distribution became evident when we tested to control the speed as well as the articulation angle of ArtiTRAX with only the individual wheel drives. Removing the chain connecting the motor for the articulation angle with the hinge made it possible to accomplish this scenario.

By using the kinematic model presented in chapter 1 as a control allocator (see section 3.5), we could use four individual wheel speed PI-controllers for each drive and still control the

speed of the vehicle and the articulation angle. The importance of proper distribution is illustrated in figure 7 and figure 8.

The main motivation for disconnecting the motor for control of the articulation angle is to study the efficiency in a transient mode, in this case during steering manoeuvres (the articulation angle is changed). Clearly, if the control of the wheel drives contradicts the control of the motor for the articulation angle, the fuel efficiency will not be optimal. Contradictory control will also lead to worsened traction performance.

Traction Control methods to handle transient modes (acceleration/deceleration) are discussed in Yin (2009) and Mutho (2011). Transient mode tests are not discussed in the thesis.
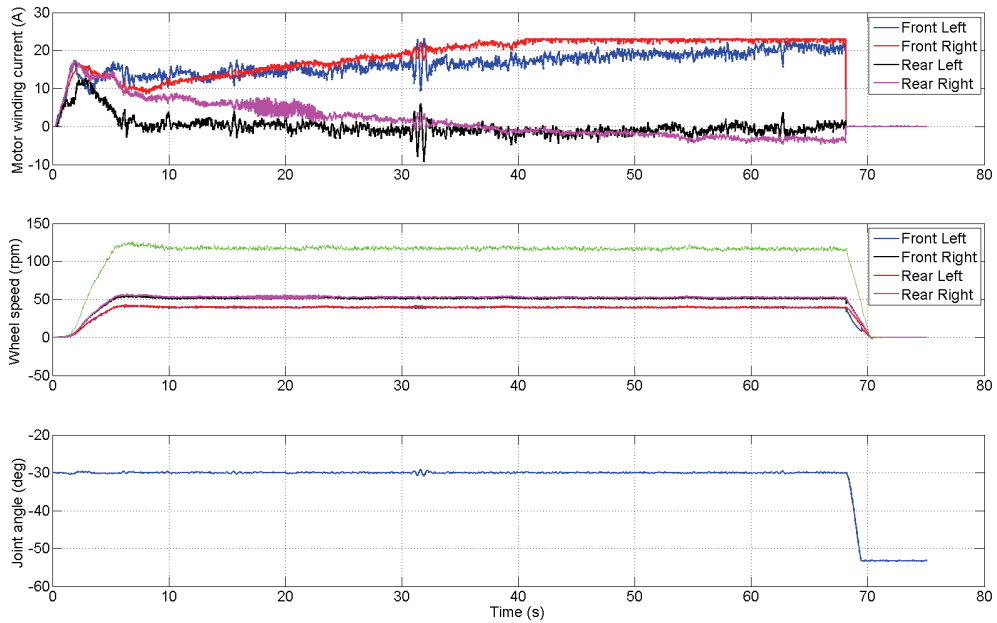
Figure 7. The figure is from a test when only the individual wheel drives were used to control both the speed of the vehicle - middle part (the green signal is the rotation speed of a measuring wheel) - and the articulation angle - lower part. The motor currents are shown in the upper part.

The motor currents drift apart as time goes by in figure 7. After approximately 40 seconds, the current to the front right motor becomes saturated and the rear right motor starts to brake (negative current). Still, the total control performance is excellent from a motion perspective since the speed of the vehicle and the articulation angle follows the set values perfectly. This implies that the set of input torques to the wheels that fulfil the control requirements contains a large number of possible combinations of torques.

48
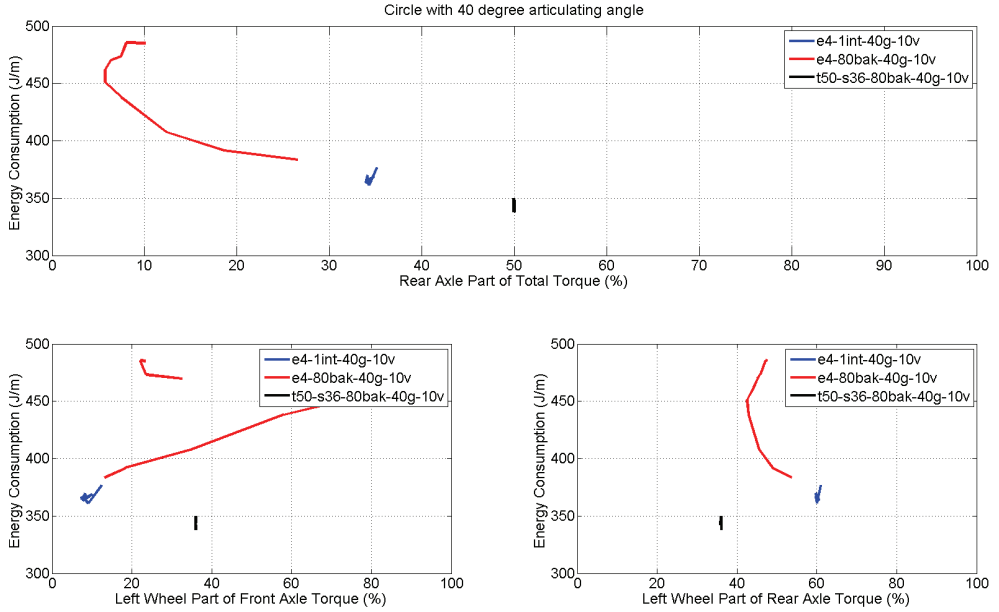
Figure 8. The resulting fuel efficiency from three different tests is shown in the figure when driving with an articulated angle of 40 degrees and a speed of 1.0 m/s. The red signal corresponds to the test in figure 7.

As is clear from the red signals in figure 8, the fuel efficiency worsens significantly over time. This is explained by windup in the integrators of the individual wheel speed controller's caused by model errors. The two other cases – blue and black signals – do not have the windup problem. This because the integral part of the individual wheel speed controllers were removed in one case (blue curve) and replaced by a common integral part in the outer loop for the control of the speed of the vehicle which is a control structure design less sensitive to model errors. In the other case (black curve), the motor for the articulated angle was connected to the hinge. The torque was distributed 50/50 % between the front and rear axle and 36/64 % between the inner and outer wheels on the same axle.

3.2.2.6. Discussion

The tests with ArtiTRAX have been done in an in-door gymnasium with a high friction carpet. The same gymnasium has been used in all tests, which means that the ground characteristics have been the same in all tests. ArtiTRAX has been "warmed up" according to a certain procedure before tests with the aim to have steady state working temperature during the tests. Since the test scenarios focus on steady state conditions (velocity and articulation angle), it is tempting to assume that the measured motor currents are proportional to the input torques to the wheels.

Based on the assumption that the measured motor currents are proportional to the input torques to the wheels, the indications from the test results so far is that the method proposed by Yamakawa et al. where the torque distribution is proportional to the load weight on the

wheels is not necessarily the optimal method in terms of fuel efficiency. The method proposed by Senatore where torque "is shifted slightly toward the rear axel" could be the optimal method in terms of fuel efficiency. It should be observed that the regions around the optimal torque distribution (see figure 5) are flat with a non-distinctive minimum.

Our plan is to map the motor currents to input torques in a test rig before doing further tests and drawing any type of conclusions.

3.3 Wheel slip

In Zoz (2003) the following question is raised, "which is the independent variable, pull or slip?" After spending some time on trying to understand the concept of slip and working with estimation of it, the question seems very relevant. Zoz points out that slip historically has been consider an independent variable but give arguments for that pull is the independent variable and that slip "happens". Our comment to this is that slip is important independently of how it is considered since it is a measure of the tractive performance.

3.3.1 Tests with Volvo A25E hauler

The characteristic of the sideslip of haulers is of interest when designing a traction control system. Tests based on a GPS/INS system were done with a Volvo A25E hauler, Andersson, Bortolin, Backén and Gustafsson (2011).
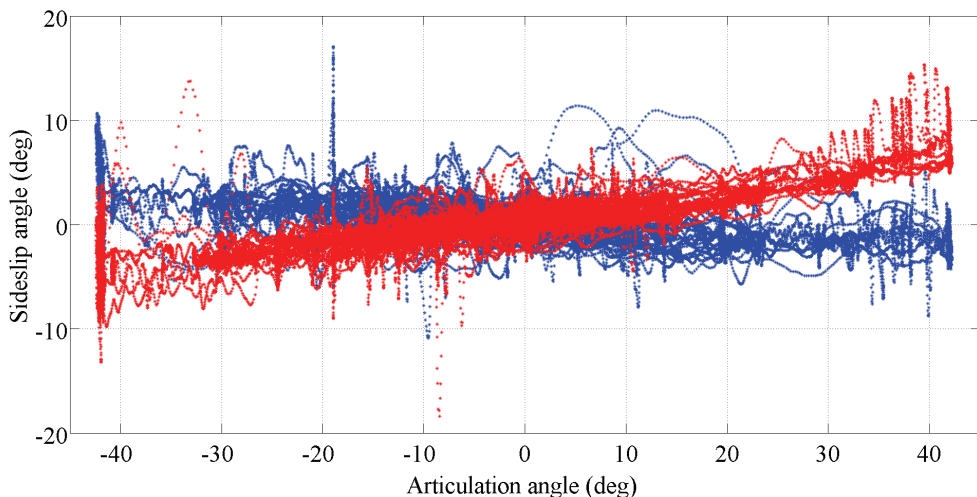
Figure 9. Estimation of sideslip angles of a Volvo A25E hauler as a function of the articulation angle. The blue signal is the sideslip angle of the tractor and the red signal is the sideslip angle of the trailer.

The tests result in figure 9 originates from runs on dry asphalt and gravel during summer conditions with an unloaded hauler. As a comparison, the corresponding result with a loaded

hauler driving on icy ground during winter conditions is shown in figure 10. The GPS/INS units were mounted in the centre of the hauler above the front axle on the tractor and above the forward bogie axle of the trailer.
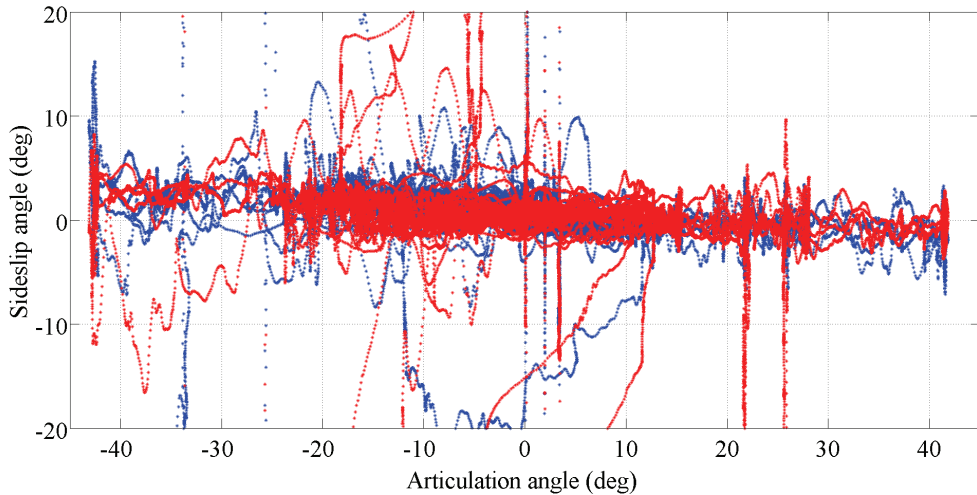
Figure 10. Estimation of sideslip angles of a Volvo A25E hauler as a function of the articulation angle. The blue signal is the sideslip angle of the tractor and the red signal is the sideslip angle of the trailer.

It can be noted that the sign of the sideslip angle of the trailer as a function of the articulation angle is changed when the hauler is loaded compared to when it is unloaded. The high amount of outliers in figure 10 compared to figure 9 is mainly explained by provoked driving on icy asphalt.

The test results with the A25E hauler were consistent with simulation results based on the ADAMS simulation model used in the work by Markdahl.

As a comparison to the test results from tests with the hauler, Scheding, Dissanayake, Nebot and Durrant-Whyte (1999) did a corresponding test with a centre articulated LHD in an underground mine where the pose of the LHD, the rolling radius and the slip angles for the front and rear frames were estimated. Instead of using a GPS receiver as the absolute senor, a laser senor measuring bearings to retro-reflectors on the walls of the drifts in the mine was used. The slip angles of the LHD in a ≈90 degree corner approached 6 degrees for the front frame and 20 degrees for the rear frame.

The kinematic model discussed in chapter 1 can be used to model sideslip and detect wheel spin, which is discussed by Markdahl, Bortolin and Andersson (2010).

3.3.2 Tests with ArtiTRAX

The individual wheel drives can be used to estimate the slip when driving at a constant speed. This can be done by for instance varying the motor current to one of the wheels and use the other three motors for speed control.
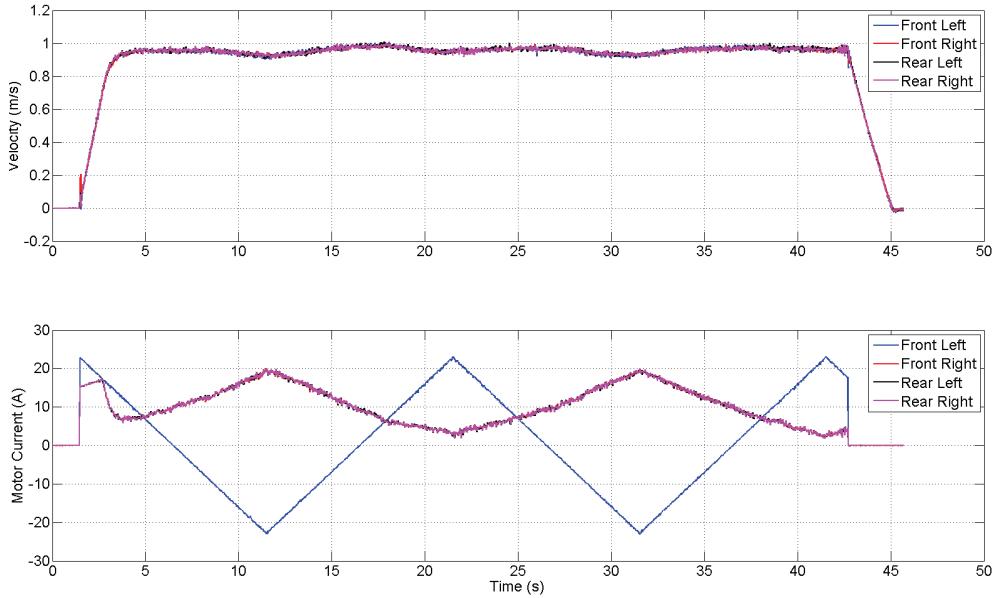
Figure 11. The figure shows vehicle speed – upper part – and motor currents – lower part - during a test in which the longitudinal slip was estimated.

During the test in figure 11, three of the motors were used to control the speed of the vehicle – the set speed is 1.0 m/s in this case – while the current to the fourth motor – in this case the front left motor – was varied as a saw tooth shaped signal between maximum and minimum current. The resulting slip estimates of the front left wheel are shown in the figure 12.

The blue signal in figure 12 is a numerical estimate of the slip based on the CVX-toolbox for Matlab. The green signal is a prediction of the slip based on the motor currents in figure 11, where the slip parameters used for the prediction has been estimated in an off-line procedure. The magenta signal is a Kalman filter based estimate of the slip, which can be implemented in real time. The slip levels are very low with indicates that the longitudinal elasticity coefficient of the tyre is very low Vantsevich (2005). The estimation methods are further discussed in Andersson and Broström (2013).
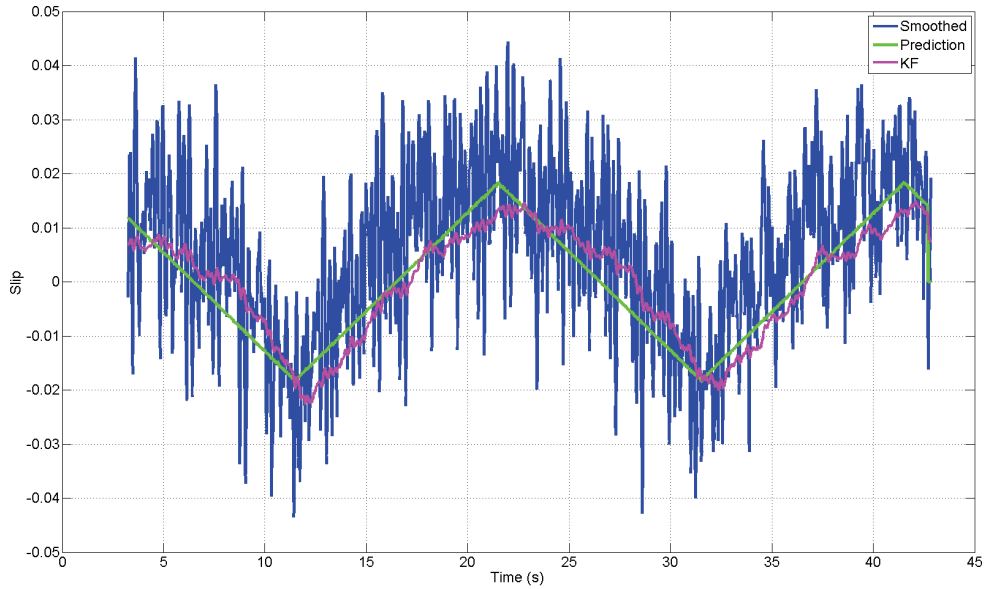
Figure 12. The figure shows the estimates of the longitudinal slip of the front left wheel when the motor currents and the velocity of the vehicle are according to figure 11.

3.4 Tyre parameter estimation

A method to estimate tyre parameters based on control of individual wheel drives was developed in the project. The method can be applied during steady state driving and does not interfere with the motion control of the vehicle, Andersson and Broström (2013). Huang and Wang (2013) point out that parameter estimation based on 4WD independent driven vehicles opens up the possibility for parameter estimation using redundant actuation without interfering vehicle motion control performance.

The method has the following properties.

- Maintains a constant actual velocity of the vehicle implying that no transfer of load occurs between the front axle and the rear axle that disturbs the tyre parameter estimates during the estimation phase.

- At the same time control the input torque to the wheel such that the estimates are consistent.

The parameters to be estimated are the rolling radius in driven mode (i.e. the rolling radius when the input torque to the wheel is zero) and the tyre longitudinal elasticity factor. The method is constrained to non-sliding conditions on firm roads and dense terrains.

See for instance Gustafsson (1997), Carlson (2005), Vantsevich (2005), Wilson, Siero, Kopchick and Vantsevich (2011) for further reading on estimation of the tyre longitudinal elasticity factor.

3.5 Control allocation

A vehicle propelled by individual wheel drives is en example of what in automatic control theory is referred to as an *over actuated system*. The *control allocation* method can be used to control such systems (Härkegård 2003). The concept is illustrated in figure 13.
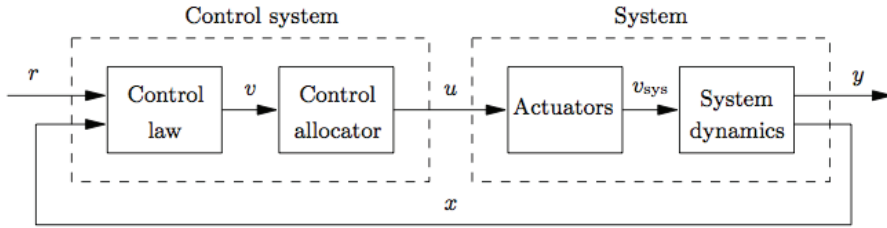
Figure 13. Block diagram of a system controlled based on the control allocation method. The figure is taken from Härkegård (2003).

The discussion in the following is based on discussions by Härkegård (2003), Laine (2007) and to some extent Xiong and Yu (2009).

The design is split into the design of a control law and a control allocator. A desirable property from a control law perspective is that the control allocator is designed such that the transfer function from the virtual control signal v to the system input v_{sys} (see figure 13) is a static function with unit gain. If this is the case, the control law can be designed based solely on the system dynamics. In practice, actuators are constrained and might contain dynamics that needs to be accounted for in the design of the closed loop either in the control law or in the control allocator as proposed by Härkegård.

The benefits with control allocation is

- Actuator constraints can be compensated for. If one actuator saturates, other actuators compensate for the lacking control effect (if we assume that enough power is available in the non-saturated actuators).

- Reconfiguration can be done in case of failing actuators without redesigning the control law. Reconfiguration can be done both on-line and off-line.

- The utilization of the actuators can be optimized based on the particular application.

The relation between the *virtual* control signal $v(t) \in \mathbb{R}^k$ and the *true* control signal $u(t) \in \mathbb{R}^m$, where $m > k$ is sought to be

$$g(u(t)) = v(t) \tag{5}$$

54

where $g: \mathbb{R}^m \mapsto \mathbb{R}^k$ is the mapping of the true control signal to the virtual control signal. Much of the literature in control allocation theory considers only the linear case for which the mapping becomes (dropping the time dependence)

$$Bu = v \tag{6}$$

where B k x m is the *control effectiveness matrix* with rank k, $k < m$. (The derivation of the matrix is exemplified in example 3 below.)

Laine (2007) use control allocation as a general approach to control the tractive forces in on-road hybrid vehicles. A constrained optimization formulation is used to separate the control law of motion from the allocation of the available motion actuators. Energy management and vehicle motion control is performed using the concept. The stability of the vehicle is prioritized over energy management. Limits in tyre forces and actuators (position and rate) are necessary to consider. The optimization method can be implemented in real-time.

The general optimization problem formulation with l_p-norm is

$$u = \arg \min_{u \in \Omega} \| W_u(u - u_{des}) \|_p$$

$$\Omega = \arg \min_{\underline{u} \leq u \leq \overline{u}} \| W_v(Bu - v) \|_p$$

where W_u and W_v are tunable weigthting matrices, $\underline{u}$ and $\overline{u}$ defines the constraints of the true control signal. u_{des} is the desired true control input determined by the energy management system (and also the steering in the case of steer-by-wire systems). The motion controller determines the virtual control signal v. It is higly likely that there will be conflicts between the desire to minimize the fuel consumption and the desired to keep the vehicle on track. Therefore a compromise has to be made which the tuneable weighting matrices do.

The general optimization problem becomes a Quadratic Programming (QP) problem possible to solve numerically if the l_2-norm is chosen. This type of problems is referred to as Sequential Least-Squares (SLS) and needs two steps to solve. SLS problems can be transformed to Weighted Least-Squares (WLS) problems, which are solved in one step and requires less computational power. A new tuning parameter w_γ is introduced in the WLS problem formulation, which is

$$u = \arg \min_{\underline{u} \leq u \leq \overline{u}} \| W_u(u - u_{des}) \|_2 + w_\gamma \| W_v(Bu - v) \|_2$$

The error in motion, $W_v(Bu - v)$, has to be prioritized over low fuel consumption for safety reasons implying that w_γ should be set to a high value.

The actuators constraints are defined by maximum values and maximum change rates, T_{max} and dT/dt_{max} in case of individual wheel drives where T denotes the torque. The rate limits can be approximated by position limits. The position limits at sampling instant k with maximum torque T_{max}, minimum torque T_{min} and maximum and minimum change in torque from one sampling instant to another ΔT_{max} and ΔT_{min} respectively, is the following constraints

$$\overline{u}_k = \min (T_{max}, u_{k-1} + \Delta T_{max})$$

$$\underline{u}_k = \max (T_{min}, u_{k-1} + \Delta T_{min})$$

The *active set method* implies that consideration is taken to saturated actuators. The different true control signals are divided into a set with saturated signals, named *the active set*, and unsaturated signals, named *the free set*, in the calculation of the true control signal at each sampling instant. Assuming that the weighted least squares method is used, the problem is rewritten as the least squares problem of the form

$$\| W_u(u - u_{des}) \|_2 + w_\gamma \| W_v(Bu - v) \|_2 = \| Au - b \|_2$$

$$A = \begin{pmatrix} \sqrt{w_\gamma}W_vB \\ W_u \end{pmatrix}, b = \begin{pmatrix} \sqrt{w_\gamma}v \\ W_u u_{des} \end{pmatrix}$$

The problem to solve is then

$$\min_u \| Au - b \|_2$$

$$\text{subject to } Bu = v, Cu \geq U$$

$$C = \begin{pmatrix} I \\ -I \end{pmatrix}, U = \begin{pmatrix} \underline{u} \\ -\overline{u} \end{pmatrix}$$

See Härkegård (2003, p. 135) and Laine (2007, p. 88) for further reading.

The conclusion from the discussion above is that the control allocation method can be used for traction control scenarios where a central controller is required. For example when a main objective is to minimize fuel consumption. The torque distribution method minimizing the fuel consumption defines the desired true control signal and the desired articulation angle speed and velocity of the vehicle defines the virtual control signal.

3.5.1 Kinematic model as control allocator

The kinematic model derived in chapter 1 can be interpreted as a control allocator if the actuator for the articulated angle is removed and the individual wheel drives used as the only actuators. The control allocator is then defined by

$$\begin{pmatrix} v_1 \\ v_2 \\ v_3 \\ v_4 \end{pmatrix} = \begin{pmatrix} -\left(\frac{e/2\cos(Y)}{1+\cos(Y)} + \frac{L\sin(Y)}{1+\cos(Y)}\right) & \left(1 - \frac{e/(2L)\sin(Y)}{1+\cos(Y)}\right) \\ \left(\frac{e/2\cos(Y)}{1+\cos(Y)} - \frac{L\sin(Y)}{1+\cos(Y)}\right) & \left(1 + \frac{e/(2L)\sin(Y)}{1+\cos(Y)}\right) \\ \frac{e/2}{1+\cos(Y)} & \left(1 - \frac{e/(2L)\sin(Y)}{1+\cos(Y)}\right) \\ -\frac{e/2}{1+\cos(Y)} & \left(1 + \frac{e/(2L)\sin(Y)}{1+\cos(Y)}\right) \end{pmatrix} \begin{pmatrix} \dot{Y} \\ v_r \end{pmatrix} \tag{7}$$

with the virtual control signal v and the true control signal u

$$v = \begin{pmatrix} \dot{\gamma} \\ v_r \end{pmatrix} \tag{8}$$

$$u = \begin{pmatrix} v_1 \\ v_2 \\ v_3 \\ v_4 \end{pmatrix} \tag{9}$$

Example 3: Design of control effectiveness matrix based on the kinematic model.

For the sake if simplicity, since the aim is to exemplify the design of the effectiveness matrix, we use $\gamma = 0$ in (7). We get

$$\begin{pmatrix} v_1 \\ v_2 \\ v_3 \\ v_4 \end{pmatrix} = \begin{pmatrix} -\frac{e}{4} & 1 \\ \frac{e}{4} & 1 \\ \frac{e}{4} & 1 \\ -\frac{e}{4} & 1 \end{pmatrix} \begin{pmatrix} \dot{Y} \\ v_r \end{pmatrix} \tag{10}$$

To design a control effectiveness matrix we use $v_1 + v_2 + v_3 + v_4$ from (10) which gives

$$\begin{pmatrix} \frac{1}{4} & \frac{1}{4} & \frac{1}{4} & \frac{1}{4} \end{pmatrix} u = v_r \tag{11}$$

and $v_3 - v_1 + v_2 - v_4$ which gives

$$\begin{pmatrix} -\frac{1}{e} & \frac{1}{e} & \frac{1}{e} & -\frac{1}{e} \end{pmatrix} u = \dot{Y} \tag{12}$$

(11) and (12) combined defines the control effectiveness matrix

$$B = \begin{pmatrix} \frac{1}{e} & 0 \\ 0 & \frac{1}{4} \end{pmatrix} \begin{pmatrix} -1 & 1 & 1 & -1 \\ 1 & 1 & 1 & 1 \end{pmatrix} \tag{13}$$

which fulfils the rank requirement since the rank is 2.

The unconstrained minimum l_2-norm control allocation problem

$$\min_u \| u \|_2$$

subject to $Bu = v$

has an explicit solution, which is

$$u = B^\dagger v$$

where $B^\dagger$ is the pseudoinvers of the control effectiveness matrix.

$$B^\dagger = B^T (BB^T)^{-1}$$

If we assume the actuators to be unconstrained in the example, which is not realistic but makes it possible to discuss the method in more detail, a control allocator can be designed based on the unconstrained minimum l_2-norm control allocation problem.

The pseudo invers of the control effectiveness matrix in the example is

$$B^\dagger = \begin{pmatrix} -\frac{e}{4} & 1 \\ \frac{e}{4} & 1 \\ \frac{e}{4} & 1 \\ -\frac{e}{4} & 1 \end{pmatrix} \tag{14}$$

which is a reasonable solution since it equals the kinematic model for $\gamma = 0$. A positiv value of $\dot{Y}$ implies that the rear part starts to rotate clockwise and the front part counter-clockwise, which gives a positive change in the articulation angle.

An actuator failure can often be approximately modelled as a change in the control effectiveness matrix, Härkegård (2003, p. 178). If we assume the front left motor (actuator) to be broken we get

$$u = \begin{pmatrix} v_2 \\ v_3 \\ v_4 \end{pmatrix} \tag{15}$$

From (10) we get

$$v_2 = v_r + \frac{e}{4}\dot{Y} \tag{16}$$

$$v_3 = v_r + \frac{e}{4}\dot{Y} \tag{17}$$

$$v_4 = v_r - \frac{e}{4}\dot{Y} \tag{18}$$

The design of a control effectiveness matrix based on $v_2 + v_3 + v_4$ and $v_2 + v_3 - v_4$ gives

$$\begin{pmatrix} 1 & 1 & 1 \\ 1 & 1 & -1 \end{pmatrix} \begin{pmatrix} v_2 \\ v_3 \\ v_4 \end{pmatrix} = \begin{pmatrix} \frac{e}{4} & 3 \\ \frac{3e}{4} & 1 \end{pmatrix} \begin{pmatrix} \dot{Y} \\ v_r \end{pmatrix} \tag{19}$$

The control efficient matrix is

$$B = \begin{pmatrix} \frac{1}{e} & 0 \\ 0 & \frac{1}{4} \end{pmatrix} \begin{pmatrix} 1 & 1 & -2 \\ 1 & 1 & 2 \end{pmatrix} \tag{20}$$

which fulfils the rank requirement since the rank is 2. The pseudo invers of the control effectiveness matrix is

$$B^\dagger = \begin{pmatrix} \frac{e}{4} & 1 \\ \frac{e}{4} & 1 \\ -\frac{e}{4} & 1 \end{pmatrix} \tag{21}$$

which is a reasonable solution since it equals the kinematic model for $\gamma = 0$. A positive value of $\dot{Y}$ implies that the rear part starts to rotate clockwise and the front right wheel increases the speed, which gives a positive change in the articulation angle.

As an alternative design of the control effectiveness matrix to compensate for the broken actuator we use $v_2 + v_3 + v_4$ and $v_2 - v_3 + v_4$ which gives

$$\begin{pmatrix} 1 & 1 & 1 \\ 1 & -1 & 1 \end{pmatrix} \begin{pmatrix} v_2 \\ v_3 \\ v_4 \end{pmatrix} = \begin{pmatrix} \frac{e}{4} & 3 \\ -\frac{e}{4} & 1 \end{pmatrix} \begin{pmatrix} \dot{Y} \\ v_r \end{pmatrix} \tag{22}$$

The control efficient matrix is

$$B = \begin{pmatrix} \frac{2}{e} & 0 \\ 0 & \frac{1}{2} \end{pmatrix} \begin{pmatrix} -1 & 2 & -1 \\ 1 & 0 & 1 \end{pmatrix} \begin{pmatrix} v_2 \\ v_3 \\ v_4 \end{pmatrix} \tag{23}$$

which fulfils the rank requirement since the rank is 2. The pseudo invers of the control effectiveness matrix is

$$B^{\dagger} = \begin{pmatrix} 0 & 1 \\ \frac{e}{4} & 1 \\ 0 & 1 \end{pmatrix} \tag{24}$$

which is a less reasonable solution since only one actuator, the motor for the rear left wheel, is used to control the articulation angle. The two alternatives to compensate for the broken actuator indicated that careful consideration has to be made in the design of the control effectiveness matrix.

3.5.1.1 Tests with ArtiTRAX

The chain connecting the articulation motor to the articulation hinge was removed from ArtiTRAX implying that the only way to control the motion of the vehicle was by using the individual wheel drives.

The outer loop contains one PI controller for the articulation angle and one PI controller for the velocity. The output from the controller for the articulation angle is the virtual control signal $\dot{\gamma}$. The output from the velocity controller is the virtual control signal v_r.
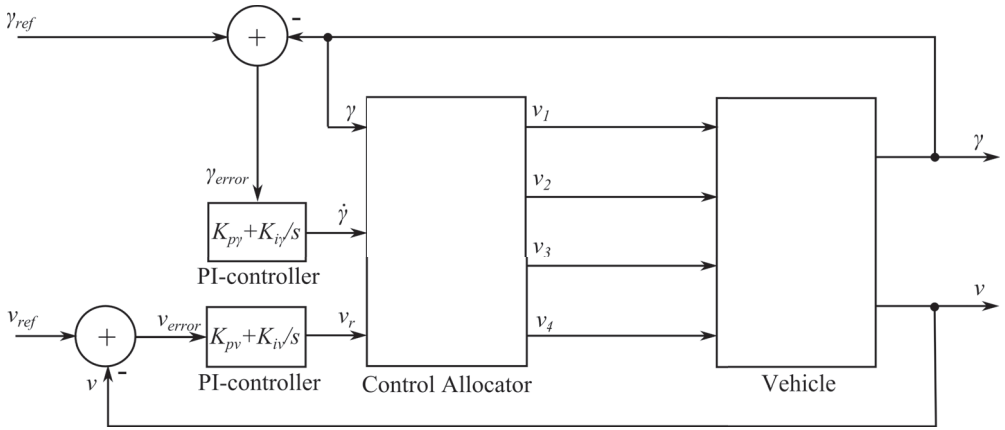
Figure 14. The figure shows the block diagram of the control system.

The velocity v in figure 14 is based on the mean value of the velocity of the rear wheels of ArtiTRAX. The articulation angle is measured with a potentiometer mounted in the articulation hinge.

The velocity of the measuring wheel could have been used in the feedback if the articulation angle between the measuring wheel and the rear frame of ArtiTRAX was measured, see chapter 1, section 2, equation (26).

The results from the tests are shown in figure 15-20.
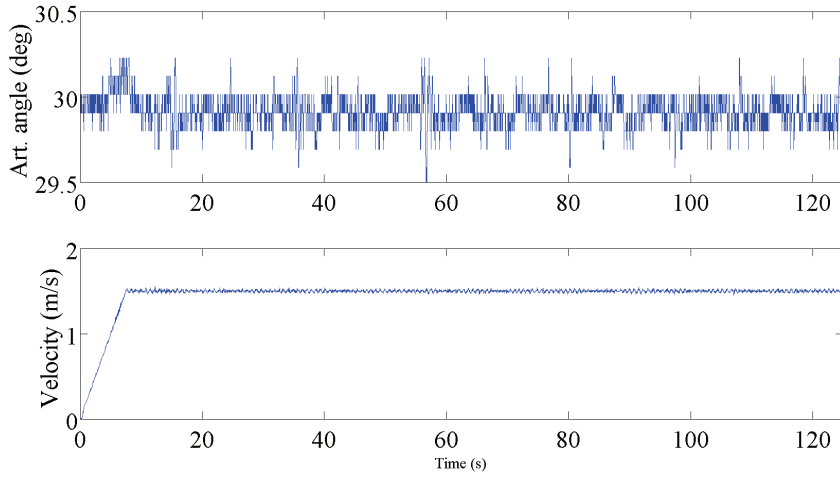
Figure 15. Measured values of the articulation angle and velocity, reference value of the articulation angle 30 degrees and reference value of the velocity 1.5 m/s.
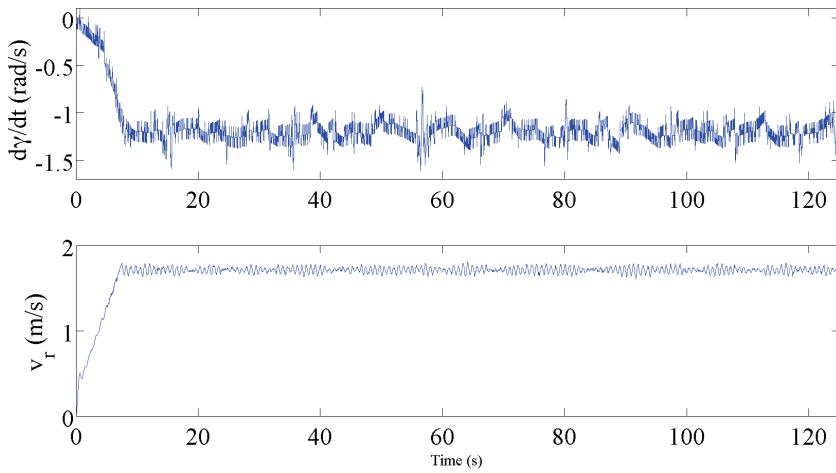
Figure 16. The virtual control signals, reference value of the articulation angle 30 degrees and reference value of the velocity 1.5 m/s.

60
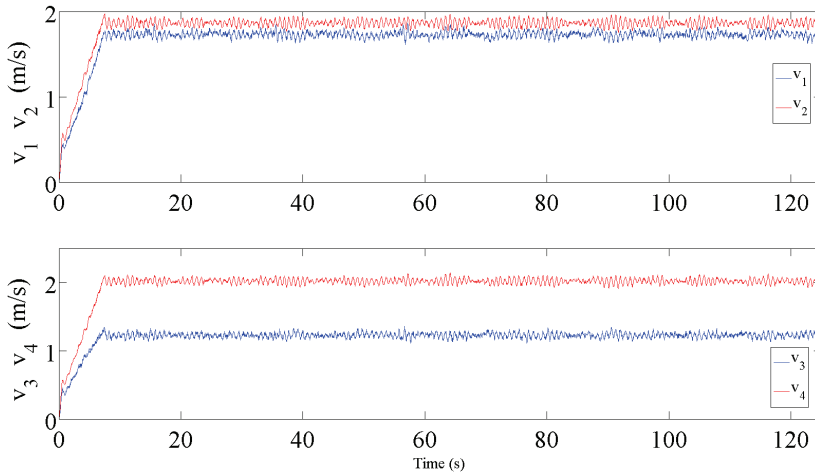
Figure 17. The true control signals, reference value of the articulation angle 30 degrees and reference value of the velocity 1.5 m/s.
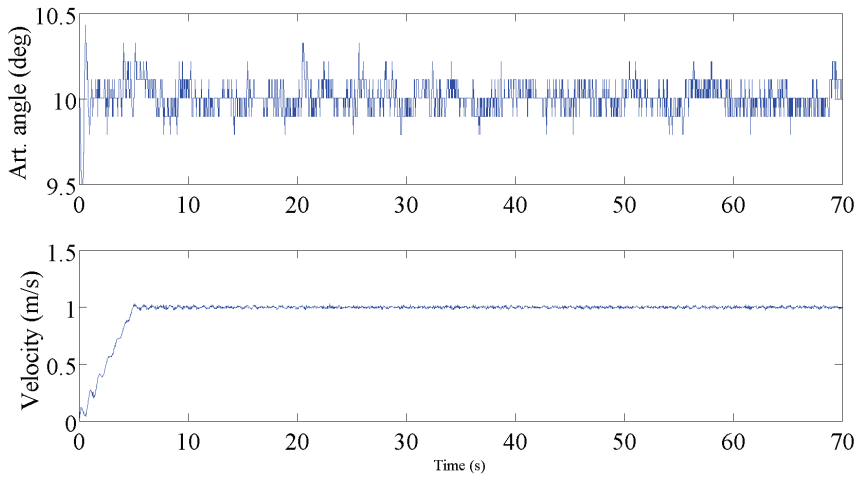
Figure 18. Measured values of the articulation angle and the velocity, reference value of the articulation angle 10 degrees and reference value of the velocity 1.0 m/s.

Articulation angle γ 30 degrees corresponds to driving in a circle with a diameter of approximately 4.6 meter neglecting the effect of sideslip. It takes approximately 10 seconds to complete one revolution in the circle if the velocity V of the vehicle is 1.5 m/s.
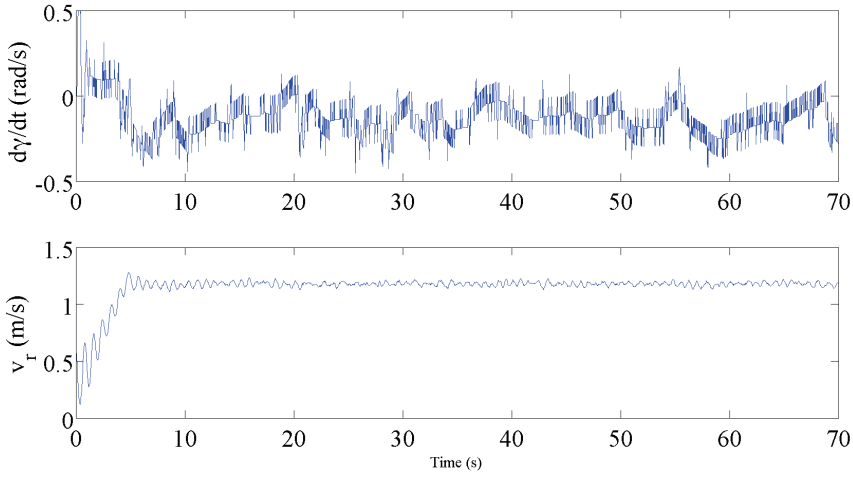
Figure 19. The virtual control signals, reference value of the articulation angle 10 degrees and reference value of the velocity 1.0 m/s.
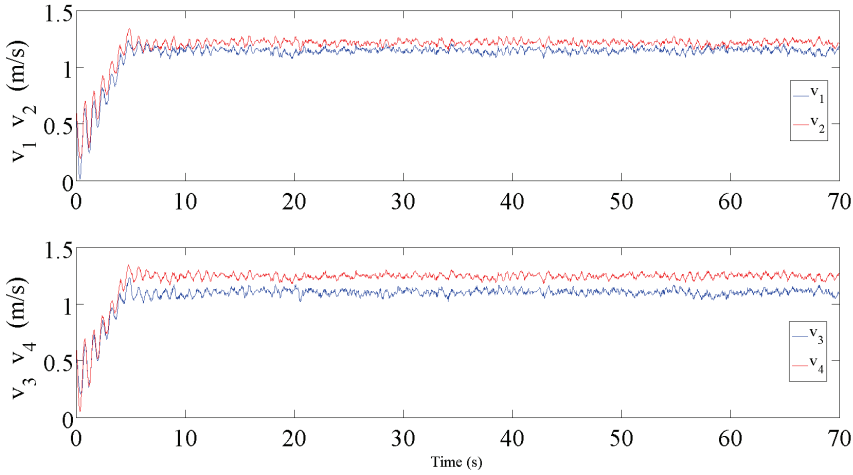
Figure 20. The true control signals, reference value of the articulation angle 10 degrees and reference value of the velocity 1.0 m/s.

Articulation angle γ 10 degrees corresponds to driving in a circle with a diameter of approximately 14.2 meter neglecting the effect of sideslip. It takes approximately 44 seconds to complete one revolution in the circle if the velocity V of the vehicle is 1.5 m/s.

The centrifugal force acting in the center of gravity is $F = m\omega^2 r$ where m is the mass, ω is the rotational speed and r is the rotational speed. The centrifugal forces acting in the center of gravity of the front frame F_f and in the rear frame F_r for the two tests are summarised in table 2.

The mass of the front frame m_f and the rear frame m_r are estimated according to the method discussed in chapter 1 section 3.

62

Table 2.

γ (°)	V (m/s)	m_f (kg)	m_r (kg)	ω (rad/s)	r (m)	F_f (N)	F_r (N)
30	1.5	174	146	0.63	2.3	159	133
10	1.0	174	146	0.14	7.1	24	20

The conclusion from table 2 is that the control system, the PI controllers and the control allocator, in the two tests handled centrifugal forces with a ratio of approximately 6.6.

The performance of the control system was satisfying in the both tests since the control errors in the articulation angle as well as the control errors in the velocity were small, see figure 15 and figure 18.

The parameters values of the PI controllers were the same during both tests implying that the control system automatically adapted to the differences in magnitude of the centrifugal forces.

The tests indicate that the kinematic model can be used as a control allocator for steady state driving.

3.6 Discussion

The design of the mechanical driveline of a four wheel drive (4WD) vehicle has to be a compromise that considers peripheral speed of the front and rear wheels, the difference in tractive conditions of the front and rear wheels caused by the front wheels "bulldozing" the track and the difference in radii when turning, Guy (2011).

By replacing the mechanical driveline with individual wheel drives, it should be – at least in theory – possible to design a tractive control functionality that is not a compromise between different demands exemplified by Guy.

Different scenarios have to be considered in practical applications in the design of the traction controller as exemplified below.

Example 1: A wheel loader penetrating a muck pile.

During the penetration phase of the muck pile, the optimal control of the traction to maximize the production would be to control the slip at the peak value of the friction coefficient for each driving wheel to advance as further as possible into the muck pile before the scooping starts.

An accurate estimate of the μ-λ relation is important in such a traction controller. Canudas-De-Wit, Tsiotras, Velenis, Basset and Gissinger (2003) discuss a method that is claimed to capture the transient behaviour of the changes in friction during abrupt braking and acceleration, which characterizes the behaviour of the wheel loader during the penetration of a muck pile with fragmented rock. Braking experiments with a passenger car on a flat and dry road is presented.

Yin and Hori (2010) discuss a method referred to as Maximum Transmissible Torque Estimation (MTTE). The method is applicable to electric vehicles (EVs). Only the torque

reference and the wheel rotation are needed to estimate the maximum transmissible torque to the road surface. Experimental results based on a commercial available vehicle EV "COMS" (2WD, 360 kg) is presented. It is concluded that the traction controller designed to co-operate with the MTTE estimator performed well regarding antislip (anti-spin) in various tyre-road conditions.

Magallan, DeAngelo and García (2011) propose an on-road strategy to control the torque of each of two electric motors to maximize the traction and at the same time avoid skidding (slipping). Jalali, Bode, Lambert and McPhee propose an on-road traction controller for a 4WD vehicle with individual drives that keeps the traction forces at the maximum while accelerating.

Example 2: A hauler hauling fragmented rock at steady state velocity on flat ground with high grip surface.

The total torque needed to keep the velocity is distributed to the driving wheels according to power distributing units (PDUs) in case of a vehicle with a mechanical driveline or an algorithm in case of a vehicle with individual wheel drives. It is likely that the resulting slip for each driving wheel is much less than the slip limit for wheel spin. In such a scenario, a reasonable optimal traction control is to distribute the torque among the driving wheels such that the fuel consumption is minimized.

Methods to minimize fuel consumptions are discussed by for instance Yamakawa and Watanabe (2005), Yamakawa, Kojima, and Watanabe (2007) and Senatore and Sandu (2011).

Mutoh, Suzuki and Kawaguchi (2011) discuss traction control of front and rear wheel independent drive type electric vehicle (FRID EV). The method uses the possibility to change the longitudinal tractive forces between the front and rear drives. This was found beneficial for energy saving during running. The method is based on μ-λ estimation, load movement compensation and slip ratio control. Experiments shows that it is possible to save 11% energy when accelerating a prototype FRID EV car up to 45 km/h. Further experiments is discussed by Mutho (2012) when driving on road with ultralow friction.

The examples cover two main requirements on the traction controller.

- Maximize the tractive force subject to some constraints.

- Minimize the fuel consumption subject to some constraints.

The constraints depend on the scenario, for instance the actuators in use to perform the action. The hydraulic steering system of an articulated vehicle is in use only when turning, which implies changes in the constraints compared to the steady state case.

The above reasoning implies in case of individual wheel drives, that the traction control cannot be performed isolated at each wheel. A central control function is necessary in some situations.

Applying input torque to the driving and braking wheels directly controls the traction. The following actuators are candidates for this control purpose.

- The brakes.

- The power-distributing units (PDUs) in case of a mechanical driveline.

- The engine or engines that propels the vehicle.

- The steering system.

The steering system as part of the traction control system might not be obvious, but the so called *duck walk* used when driving through muddy terrains with haulers is one example where the steering system is used as a part of the traction control system. The duck walk implies that the driver turns to the right and to the left with some frequency and amplitude to prevent the hauler to get stuck in the mud.

The field trials we have done so far with ArtiTRAX have raised some questions not only regarding control methods and slip estimation but also regarding efficiency measures. As a control engineer, it is tempting to design a traction controller that optimizes the efficiency, but then the question of what efficiency measure/measures to use in the control design rises

A typical work cycle of a construction vehicle consists of transient parts, steady state parts, driving on hard/soft ground, driving uphill/downhill, etc. In the case of a wheel loader and a hauler, their typical work cycles differs. The hauler spends a lot more time in steady state conditions.

In the field trials with ArtiTRAX, we have used an efficiency measure that is defined by the amount of fuel it takes to travel a certain distance. This is probably a relevant measure for the transport part of the working cycle of a construction vehicle, but is it a relevant measure when – for instance – filling the bucket of a wheel loader? (Probably not.)

Different efficiency measures are discussed in the literature, for instance in Vantsevich (2007). In Zoz (2002) it is pointed out that tractive efficiency (TE) of a single tractive device (wheel with hub motor in our case) is not necessarily the same as the tractive efficiency of the vehicle itself.

Efficiency measure functions relevant for construction machines (loaders and haulers) must be based on their typical work cycles consisting of steady state and transient operations. Examples of efficiency measures are a) energy, b) tyre wear, c) bucket filling degrees and d) traction. The weight(s) of the efficiency measures in the control law should depend on the operating status of the wheel loader. If, for instance, the loader is hauling on high friction surface; a) and b) will have high weights whereas c) and d) will have zero weights. On the other hand, if the loader is filling the bucket, c) and d) will have high weights and the other two measures will have low weights. The strategy can be formulated as an optimisation problem for energy consumption that satisfies all the relevant constraints.

An optimal controller will likely be too complex for real time operation. In such a case the optimal controller needs to be approximated without losing to much performance. For this purpose the so-called "bottom-up" strategy discussed in Åström and Hägglund (2001) can be used. The approach implies that the overall complex control system is built with simple building blocks such as PID, Feed forward controllers, Kalman filters, etc. Well defined type cases of driving scenarios (steady state driving, acceleration, turning, etc.), can be represented by relatively simple functions and that the overall control strategy will be to integrate the control of the type cases so that all possible combinations of type cases are handled in a stable and robust manner. The optimal controller can then be used as a reference for achievable performance.

References

Andersson, U., Bortolin, G., Backén, S., & Gustafsson, T. (2011) Estimation of Sideslip Angles of a Volvo A25E Articulated All-Wheel Drive Hauler Based on GPS/INS Measurements, *SAE Technical Paper Series 2011-01-2156*, Commercial Vehicle Engineering Congress, September 13-14, 2011, Chicago, Illinois, United States.

Andersson, U., & Broström, F. (2013). Tyre parameter estimation based on control of individual wheel drives. Paper submitted to International Journal of Vehicle Autonomous Systems.

Andreev, A. F., Vantsevich, V.V., & Lefarov, A. Kh. (1987) Differentials of Wheel Vehicles, *Mashinostroenie Publishing House*, Moscow, Soviet Union.

Andreev, A. F., Kabanau, K. I., & Vantsevich, V.V. (2010) *Driveline Systems of Ground Vehicles - Theory and Design*, CRC Press, Boca Raton, FL, United States.

Azad N.L., Khajepour, A., & McPhee (2005). Stability Control of Articulated Steer Vehicles by Passive and Active Steering Systems. *SAE technical paper series*, 2005-01-3573.

Carlson, C. R., & Gerdes, J. C. (2005) Consistent Nonlinear Estimation of Longitudinal Tire Stiffness and Effective Radius, *IEEE Transactions on Control Systems Technology*, Volume 13, Issue 6, pp. 1010-1020.

Gustafsson, F. (1997). Slip-Based Tire-Road Friction Estimation, Automatica, Volume 33, Issue 6, pp. 1087-1099.

Guy I.J., Crolla D.A., Godwin R.J., & White D.R. (2011). Axle torque distribution in four wheel drive tractors. *17th International Conference of the Society for Terrain-Vehicle Systems*, September 18-22, 2011, Blacksburg, Virginia, USA.

Hallowell, S.J., & Ray, L.R. (2003) All-wheel Driving Using Independent Torque Control of Each Wheel, *Proceedings of the American Control Conference 2003,* Volume 3, pp. 2590-2595.

Hori Y. (2004). Future vehicle driven by electricity and control – research on four-wheel-motored "UOT electric march II". IEEE Transactions on industrial electronics, Vol. 51, No. 5, October 2004.

Huang, X., & Wang, J. (2013). Longitudinal Motion Based Lightweight Vehicle Payload Parameter Real-Time Estimations, *Journal of Dynamic Systems Measurement and Control*, Volume 135, Issue 1, pp. 1183-1195.

Härkegård, O. (2003). Backstepping and control allocation with application to flight control. Doctoral Thesis, Department of Electrical Engineering, Linköping University, Linköping, Sweden.

Karlsson M. (2010). ArtiTRAX II, Master's Thesis, Department of Computer Science, Electrical and Space Engineering. Luleå University of Technology, Luleå, Sweden.

Laine, L. (2007). Reconfigurable motion control systems for over-actuated road vehicles. Doctoral Thesis, Department of Applied Mechanics, Chalmers University of Technology, Göteborg, Sweden.

Larsson, U., Zell, C., Hyyppä, K., & Wernersson, Å. (1994). Navigating an articulated vehicle and reversing with a trailer. *In Proceedings of IEEE International Conference on Robotics and Automation*, San Diego, CA, USA.

Markdahl, J. (2010). Traction control for off-road articulated vehicles. Master Thesis, Division of Optimization and Systems Theory, Royal Institute of Technology, Stockholm, Sweden.

Markdahl, J., Bortolin G., & Andersson U. (2010). Traction control for Articulated off-road vehicles. Reglermöte 2010, Lund, Sweden.

Mutho N., Suzuki K., & Kawaguchi, K. (2011). Front and rear wheel independent drive type electric vehicle (FRID EV) providing efficient running performance on various road surfaces. *IEEE Vehicle Power and Propulsion Conference (VPPC) 2011*, 1-6.

Rehnberg, A., Edrén, J., Eriksson, M., Drugge, L., & Stensson Trigell, A. (2011). Scale model investigation of the snaking and folding stability of an articulated frame steer vehicle. *Int. J. Vehicle Modelling and Testing*, Vol. 6, No. 2, 126-144.

Scheding, S., Dissanayake, G., Nebot, E. M., & Durrant-Whyte, H. (1999). An experiment in autonomous navigation of an underground mining vehicle. *IEEE Transactions on Robotics and Automation*, 15(1):85–95.

Senatore, C. (2010). Prediction of mobility, handling and tractive efficiency of wheeled off-road vehicles. Doctoral Thesis, Division of Engineering Science and Mechanics, Virginia Polytechnic Institute and State University (Virginia Tech), Blacksburg, Virginia, USA.

Senatore, C. & Sandu, C. (2011). Torque Distribution Influence on Tractive Efficiency and Mobility of Off-Road Wheeled Vehicles, *Journal of Terramechanics*, Volume 48, Issue 5, pp. 372-383.

Vantsevich, V.V., Barz, D., Kubler, J. & Schumacher, A. (2005). Tire Longitudinal Elasticity and Effective Rolling Radii: Experimental Method and Data, *SAE Technical Paper Series 2005-01-1823*, World Congress and Exhibition, April 11, 2005, Detroit, Michigan, United States.

Vantsevich V. V. (2007). Multi-wheel drive vehicle energy/fuel efficiency and traction performance- Objective function analysis. *Journal of Terramechanics*, vol. 44, 239-253.

Wilson, T., Siero, M., Kopchick, C., & Vantsevich, V.V. (2011). Terrain Truck: Control of Wheel Rotational Velocities and Tire Slippages, *SAE Technical Paper Series 2011-01-2157*, Commercial Vehicle Engineering Congress, September 13-14, 2011, Chicago, Illinois, United States.

Yamakawa, J., & Watanabe, K. (2005). A method of torque control for independent wheel drive vehicles on rough terrain. *Journal of Terramechanics*, vol. 43, 269-285.

Yamakawa, J., Kojima, A., & Watanabe K. (2007). A method of torque control for independent wheel drive vehicles on rough terrain. *Journal of Terramechanics*, vol. 44, 371-381.

Yin D. (2009). General approach to traction control for electric vehicles based on maximum transmissible torque estimation. Doctorial Thesis, Department of Electrical Engineering, University of Tokyo, Japan.

Zoz F.M., Turner R.J., & Shell L.R. (2002). Power delivery efficiency: A valid measure of belt and tire tractor performance. *Transactions of the ASAE*, Vol. 45(3), 509-518.

Zoz, F.M., & Grisso, R.D. (2003). Traction and Tractor Performance, *ASAE Distinguished Lecture Series #27*, http://bsesrv214.bse.vt.edu/Dist_Lecture_27/ (Accessed 6 June 2013).

Åström, K.J. & Hägglund, T. (2001), The Future of PID Control. *Control Engineering Practice*, Volume 9, Issue 11, pp. 1163-1175.

CHAPTER 4

Appended papers

[A] - AGV navigation by angle measurements

The author's main contribution: Guidance controller.

Comment: The author was the third to join the team. No one was working with control at the time.

AGV navigation by angle measurements

U Wiklund, U Andersson and **K Hyyppä**
Luleå University of Technology, Sweden

We describe an optical navigation system for the navigation and control of an autonomous guided vehicle (AGV). The navigation system consists of a low-power laser, a rotating mirror and the necessary optics. It is used to measure the angles to several identical reflective beacons. The position and heading of the AGV is recursively updated each time a valid angle is measured. It is easy to define and change the drive path which is a list of coordinates. The AGV follows straight lines between these coordinates. The system has been tested on an AGV prototype.

1 INTRODUCTION

In this paper we describe how an optical directional measuring system is used for the navigation of an autonomous guided vehicle (AGV). The directional measuring system consists of a low-power laser, a rotating mirror and the necessary optics. The measuring system is called anglemeter throughout this paper. The anglemeter is used to determine the direction to reference points, consisting of identical stripes of retro-reflective tape. The position and heading of the vehicle is determined recursively by using the angles measured to these reflectors. The vehicle used has three wheels where the single front wheel is used both for steering and traction.

For a non-moving vehicle, at least three reflectors have to be visible in order to determine the position. This requires that we know from which reflector each measured angle originates. Since the reflectors have no identity marks, we have to associate each angle with a reflector. There might also be false reflections from other objects. These false detections have to be detected and discarded.

If the initial position is unknown, there is no way that the association problem can be solved if only three reflectors are used. Therefore we have to use more reflectors than three to get redundancy in the pattern of measured angles. Our previous work concerned this topic - a method of how to find the initial position. We also made a prototype of the anglemeter and tested the system on an AGV prototype [1,2].

When the vehicle is operating in a production environment, only a fraction of the reflectors will be visible from its current position. Therefore many reflectors are needed for the determination of the position with high accuracy anywhere in the area of operation.

The main advantages of having passive reflectors of the type we use, are the flexibility and the economy. It is easy to change the transportation routes in a factory, compared with wires in the floor or painted lines. A change in the routes can be caused by a change in production or, simply, the planned route is obstructed. Since every reflector strip is inexpensive, the cost of the system is essentially proportional to the number of AGV's - not the present or future working area. The same navigation system can also be used to operate, say, a cleaning machine. The present system can be used outdoors if the surface it travels on is reasonably flat, or if the beacons are not too far away. Applications might be in mines, in agriculture, when cleaning airfields, for the positioning of a dredging boat etc.

In our current work we have taken the dynamics of the system into consideration. We have restricted our study to a single vehicle and describe the navigation system and guidance law that we use. A complete system will consist of several vehicles coordinated by a supervisory computer via radio communication.

1.1 Outline of the paper

The vehicle and the anglemeter are briefly described and analyzed in section two. We also give some suggestions on how to locate the reflectors.

Section three deals mainly with estimating the position when the vehicle is moving while angle measurements are made. In [1,2] we assumed that the speed of the vehicle was very low so three subsequent angles could be considered to be measured from the same point. The rotational speed of the anglemeter is 1 Hz. We now present a method (based on Kalman filtering) for updating the position each time an angle is measured. It is possible to use a high speed vehicle, typically 0.5-2 m/s. The association problem is solved preliminary using a windowing technique. To determine the initial position we use the method from [2]. We then give an overview of the different components in the navigation and guidance system.

In section four we turn to the control problem. The drive path of the vehicle consists of straight line segments between given points. The list of points can for instance be generated with a CAD-program on a personal computer. It is then simple to change the drive path that the vehicle is to follow.

Simulation results are presented in section 5.

2 SYSTEM DESCRIPTION

2.1 The vehicle

A picture of our vehicle is shown in fig 1. The upper part, which we call the "tower" is connected to the "frame" through thin legs leaving a 40 mm wide slit between them. This allows the anglemeter which is mounted in the center of the frame to have almost 360° of horizontal field of view. The dimensions of the vehicle are (w,l,h) 0.5m, 1.3m, 1.4m. The combined traction and steer unit is placed in front of the anglemeter in the frame. Both motors in it are of the permanent magnet 24 V DC type.

The tower contains, from the top: some push-buttons and control lights, a frame with a VME-back-plane containing all the electronics and at the bottom a battery box with two sets of lead-acid batteries. One set is used for the motors and the other for the electronics. The dangling cables seen in the figure goes to a personal computer which is used to test and simulate the system. More details of the electronics can be found in [1,2].

Fig 1. The test vehicle in our lab photographed with a flashlight to "light up" some of the beacons.

2.2 The anglemeter

There are many methods to measure angles to reflective beacons, our method take advantage of the known constraints in the measuring situation. It will gain orders of magnitude in receiver signal to noise ratio compared to other systems which use a vertical fan-shaped illuminating beam and a corresponding receiver field of view.

A picture of our prototype is shown in fig 2. A rotating mirror deflects a 1 mW laser beam to sweep in a horizontal plane. Before the laser beam hits the rotating mirror it travels through a hole in another deflecting mirror which is part of the optical receiver. The receiver is optically coaxial with the outgoing laser beam. The lens in the receiver has a focal length of 100 mm and a maximum aperture of 18 mm. The detector, which is placed on the optical axis in the focal plane of the lens, is a silicon photodiode with a diameter of 0.1 mm.

Fig 2 The prototype anglemeter. The rotating mirror is mounted under the flywheel in the right part of the photograph. The laser and part of the optical receiver can be seen in the lower left corner.

Our vehicle is moving on a reasonably flat floor, which means that we do not need to waste our illuminating laser power by spreading it out in a fan. We know at what height the laser beam will hit the wall and put our beacons at that height. This means that we can restrict the vertical field of view of the optical receiver in the anglemeter to the same order as the divergence of the illuminating laser beam. In this way we minimize the background noise and the probability of catching false beacons from strong external light sources. The divergence of the laser is 1 mrad. The discussion above is of course valid only if the scanning beam plane is parallel with the floor. The vertical length of the reflective stripes makes the anglemeter tolerate non-ideal i.e. real floors.

The improved signal to noise ratio will influence four parameters positively:

Longer range
Higher rotational speed of the mirror
Narrower reflective strips
Smaller error in measured angle

The reason to have mechanically moving parts in the anglemeter, which naturally makes it more fragile than e.g. a system built around CCD-cameras, is the precision level we want to reach. Our demand on almost 360° of horizontal field of view takes several CCD-cameras. The resulting adjustments and calibration of them and their non-ideal imaging optics will be very difficult.

The most important part of the anglemeter is the precision incremental encoder. The rotating mirror is attached to its axis. The error in measured angle to a beacon originates from:

Errors in the incremental encoder
Alignment errors
Noise in the receiver
Partly blocked beacons

The incremental encoder outputs two 90° shifted pulsetrains and a zero pulse. The pulsetrains contain 9600 pulses/revolution which gives a resolution of better than 0.2 mrad after electronic processing. The manufacturer does not state any absolute non-accuracy but we believe it is of the same order as the resolution. Its contribution to the total error is therefore negligible.

There are several alignments to be made in the anglemeter which can cause errors in the measured angle. The misalignment between the mirror rotational axis and the laser beam is the dominant one and will be discussed in some detail.

Fig 3 shows the rotating mirror, the laser beam, an attached coordinate system and the symbols which will be used. The mirror rotates around the vertical Z-axis. Its rotational angle is γ, which also is the angle of the reflected beam with no alignment error. The incoming laser beam can be assumed to lie in the XZ-plane and to hit the mirror in the origin of the coordinate system without loss of generality. The alignment error is β and the error in γ is $\Delta\gamma$. Observe that the reflected laser beam does not lie in the XY-plane and that $\Delta\gamma$ is the angle between the nominally reflected beam and the actual beams projection in the XY-plane.
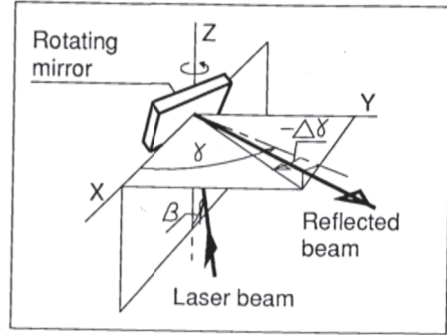
Fig 3 Coordinate system and symbols used to analyze the influence of the alignment error β on the measured angle error $\Delta\gamma$

Let n_0 be a unit vector normal to the mirror surface when $\gamma=0$.

$$n_0 = \frac{1}{\sqrt{2}} \cdot (1, \quad 0, \quad -1)^T \qquad (2.1)$$

This can be transformed to the rotating vector $n(\gamma)$ by premultiplying with the rotational matrix $R(\gamma)$.

$$n(\gamma) = R(\gamma) \cdot n_0 \qquad (2.2)$$

The rotational matrix is given by

$$R(\gamma) = \begin{pmatrix} c\gamma & -s\gamma & 0 \\ s\gamma & c\gamma & 0 \\ 0 & 0 & 1 \end{pmatrix} \qquad (2.3)$$

where we have used $c\gamma$ and $s\gamma$ as shorts for $\cos(\gamma)$ and $\sin(\gamma)$.
This gives

202

$$n(\gamma) = \frac{1}{\sqrt{2}} \cdot (c\gamma, \quad s\gamma, \quad -1) \tag{2.4}$$

The reflection of the laser beam can be modeled with a rotational matrix A, which is defined by

$$A(\gamma) = I - 2n(\gamma) \cdot n^T(\gamma) \tag{2.5}$$

This gives

$$A(\gamma) = \begin{pmatrix} s^2\gamma & -c\gamma \cdot s\gamma & c\gamma \\ -s\gamma \cdot c\gamma & c^2\gamma & s\gamma \\ c\gamma & s\gamma & 0 \end{pmatrix} \tag{2.6}$$

A unit vector p_{in} parallel with the incoming beam can be found by inspection

$$p_{in} = (s\beta, \quad 0, \quad c\beta) \tag{2.7}$$

A unit vector p_{out} parallel with the reflected beam is formed by premultiplying p_{in} with A.

$$p_{out} = A \cdot p_{in} \tag{2.8}$$

Which becomes

$$p_{out} = (s\gamma \cdot s\gamma \cdot s\beta + c\gamma \cdot c\beta, \quad -s\gamma \cdot c\gamma \cdot s\beta + s\gamma \cdot c\beta, \quad c\gamma \cdot s\beta)^T \tag{2.9}$$

Finally the projection of p_{out} in the XY-plane is p_{outp}

$$p_{outp} = (s\gamma \cdot s\gamma \cdot s\beta + c\gamma \cdot c\beta, \quad -s\gamma \cdot c\gamma \cdot s\beta + s\gamma \cdot c\beta, \quad 0)^T \tag{2.10}$$

this can also be written as

$$p_{outp} = k \cdot (\cos(\gamma + \Delta\gamma), \quad \sin(\gamma + \Delta\gamma), \quad 0)^T \tag{2.11}$$

After some manipulations where we have assumed that β and $\Delta\gamma$ are small we arrive at the result

$$\Delta\gamma = -\sin(\gamma) \cdot \beta \tag{2.12}$$

This is a systematic contribution to the total error in the measured angle and might also be the dominating one if the alignment is not done with outmost care.

Our present beacons have a horizontal width of 20 mm and one can ask the following question. To what part of the beacons do we measure our angles? The mirror rotates in the positive sense so that the laser beam crosses the beacon from right to left. Due to our high signal to noise ratio we can have a rather low threshold level in the receiver without introducing false detections as a result of electronic noise. Experiments have shown that the angle is measured to a point less than 1 mm from the right edge of the reflective tape. This is at a range of 10 m and at a rotational speed of 1 Hz. Thus the contribution to the error angle from the electronic noise is negligible.

From the discussion above it follows that if the right side of a beacon is blocked due to some obstacle we will get an error which could be significant. We would be better off if the beacon were completely blocked! The error is random with a positive mean.

2.3 Reflector maps

A large number of reflectors are needed in a production environment. It would be almost an impossible task to find the coordinates of all the reflectors with high accuracy in a global coordinate system. Therefore it is wiser to divide the area of operation into smaller areas. Different rooms in a factory is a simple example of this division. The area near a docking station is another. The approximate location of the local rooms in the global system can easily be found. The reflectors are then localized within these local coordinate systems with high accuracy. We use the anglemeter to do the localization of the reflectors.

If the reflectors are located in a local room with too much symmetry, there can be several solutions when the initial position is determined. Therefore the reflectors should be located randomly. We can however allow a symmetrical location of the reflectors in for instance a narrow corridor which the AGV only drives through, without docking at any specific points. Without knowing the actual position of the beacons, the symmetry in the measured angles could be used for navigation when the vehicle is passing the corridor.

3 ESTIMATING THE TRAJECTORY OF THE AGV

The position is updated each time a valid angle is measured. This means that all angles will be measured from different positions of the AGV. We therefore have to model the vehicle's motion between the measurements. In this section we start by deriving a motion model which will be used in the estimator design. We have chosen a first-order model instead of the more common second order models where acceleration is taken into account. To compensate for this model simplification, we assume that the values of the speed and steer angle are contaminated with additional noise. The control laws are also designed such that the changes in the set values to the servos between two sampling instants are small. This helps to justify our reduced order model.

The motion model can be used to update the position even if there are no angles available. This will however lead to large accumulated errors. We therefore need the angles to make corrections. But the measured angles have to be associated with reflectors or discarded as false. An association method is presented where we use the estimated position from the filter.

Before the filter can be used, the initial position has to be found. The method used at present will be described at the end of this section.

3.1 Motion model

We will study planar motion for a vehicle that moves with the translational velocity u_1 and the angular velocity u_2. The location of the AGV is described by the coordinates x,y and its orientation by the angle θ to the x-axis. In the description we have chosen the midpoint of the rear axis as reference point on the vehicle, cf. fig 4. The angle θ is also the heading of the AGV.

The differential equations for the motion are

$$\dot{x} = u_1 \cos\theta \qquad \dot{y} = u_1 \sin\theta \qquad \dot{\theta} = u_2 \tag{3.1}$$

On the vehicle we can control the speed of the front wheel, v, and the steer angle, α. In fig 4 we can see that there will be an instantaneous center of rotation for the motion of the vehicle.
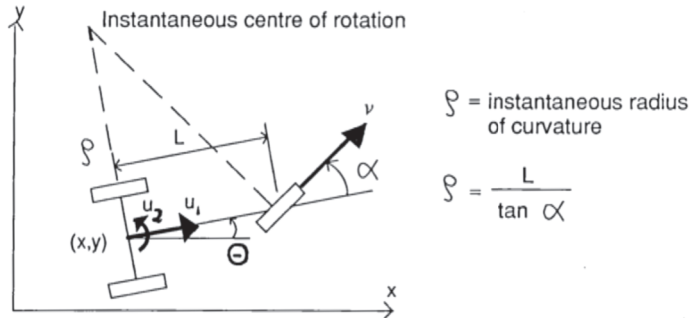
Fig 4. When the steer angle is constant, the motion of a three wheeled vehicle is along a segment of a circle.

Since the vehicle is a tricycle, we will get the following relations for our input signals u_1 and u_2

$$u_1 = v \cos\alpha \qquad\qquad u_2 = \frac{v}{L}\sin\alpha \tag{3.2}$$

204

78

where L is the distance between the steer axis and the rear axis. It is also possible to derive expressions for the input signals when the rear wheel movements are measured. In the future we will use incremental encoders to measure the wheel movements. This will increase the accuracy of the update of the motion model between the sampling instants. At present we do the assumptions that the input signals u_1 and u_2 are constant during the sampling interval. This means that we have assumed that the speed and steer angle only changes at the sampling instants and remain constant during the sampling interval, T. The equations of motion can be integrated between the sampling instants with constant input signals. This gives the non-linear discrete time model

$$x(k+1) = x(k) + \frac{u_1}{u_2}(\sin(\theta(k) + u_2 T) - \sin\theta(k)) \tag{3.3a}$$

$$y(k+1) = y(k) + \frac{u_1}{u_2}(-\cos(\theta(k) + u_2 T) + \cos\theta(k)) \tag{3.3b}$$

$$\theta(k+1) = \theta(k) + u_2 T \tag{3.3c}$$

Throughout this paper we will use k to denote the value of a variable at the discrete time instants t_k when sampling is made. For convenience, this will be omitted for the input signals.

The geometrical interpretation of (3.3), is that the motion is along a segment of a circle. For small changes $u_2 T$ in the heading, we can approximate the trajectory with a straight line.

$$x(k+1) = x(k) + u_1 T \cos\theta(k) \tag{3.4a}$$

$$y(k+1) = y(k) + u_1 T \sin\theta(k) \tag{3.4b}$$

$$\theta(k+1) = \theta(k) + u_2 T \tag{3.4c}$$

With a proper control law, the steer angle often will have a small variation around a nominal value needed to follow the current segment. The steer servo also has a short time constant. The neglected dynamics in the servos will introduce some uncertainties in the input signals. We will take these model errors into account by including noise signals in the discrete time model, i.e. we replace the idealization in (3.2) with the additive noise model

$$u_1 = (v + w_v)\cos(\alpha + w_\alpha) \qquad\qquad u_2 = \frac{(v + w_v)}{L}\sin(\alpha + w_\alpha) \tag{3.5}$$

This can now be inserted in (3.3) or (3.4) where we, after straightforward identification of terms, can find the coefficients for the noise terms. Only the first order terms are used. For sampling intervals of 0.2 s or shorter, the numerical values of the coefficients in the two cases are practically the same. We therefore use the coefficients from the second linearized case. We will now have a model of the type

$$x(k+1) = f_1(x(k), y(k), \theta(k), u_1) + g_{11} w_v + g_{12} w_\alpha \tag{3.6a}$$

$$y(k+1) = f_2(x(k), y(k), \theta(k), u_1) + g_{21} w_v + g_{22} w_\alpha \tag{3.6b}$$

$$\theta(k+1) = f_3(x(k), y(k), \theta(k), u_2) + g_{31} w_v + g_{32} w_\alpha \tag{3.6c}$$

where for instance

$$g_{11} = T \cos\alpha(k) \cos\theta(k) \tag{3.7}$$

The noise signals w_v and w_α are assumed to be independent zero mean white noise processes with covariance matrix Q.

We can write this motion model in a more compact way by introducing the state vector $X = (x, y, \theta)^T$ and noise vector $w = (w_v, w_\alpha)^T$.

$$X(k+1) = f(X(k), u_1, u_2) + G(k) w(k) \tag{3.8}$$

205

79

3.2 Measurement model

Reflector i is located at (x_i, y_i). The index i is used to denote the current reflector. The position of the midpoint of the rear axis is $(x(k), y(k), \theta(k))$. Using fig 5 we see that the angle to this reflector is

$$\gamma_i(k) = -\theta(k) + \arctan\left(\frac{y_i - y(k) - d\sin\theta(k)}{x_i - x(k) - d\cos\theta(k)}\right) + \upsilon(k) \tag{3.9}$$

where d is the distance between the anglemeter and the rear axis. We can write this as

$$\gamma_i(k) = h_i(X(k)) + \upsilon(k) \tag{3.10}$$

We assume that the sequence $\{\upsilon(k)\}$ is white noise with zero mean and covariance R and uncorrelated with the process noise. The real measurement noise was analyzed in section 2.2. There are also errors in the reflector coordinates. The white noise assumption on $\{\upsilon(k)\}$ has been chosen to simplify the estimator design.
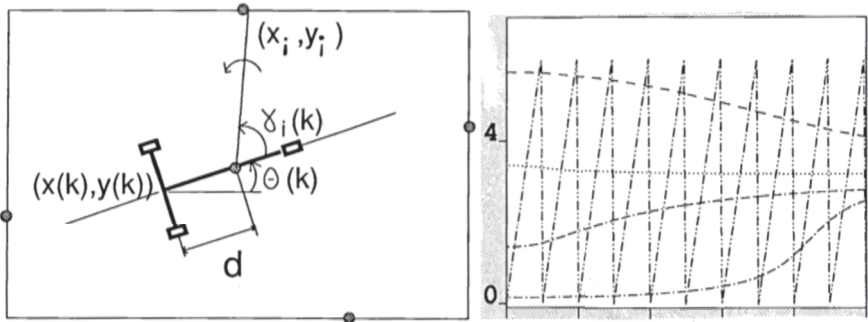
Fig 5. Principle of angular measurements and variation in the angles to four reflectors when the vehicle follows a straight line with the speed 0.5 m/s.

The mirror in the anglemeter rotates with one revolution per second. Suppose that the vehicle is moving straight forward in a room with four reflectors. In fig 5 we show the variation in the angles to the reflectors. The instantaneous angle $\gamma(t)$ of the anglemeter is also shown in the same figure. It is only possible to measure an angle to a reflector at those time instants when we have a crossing between the anglemeter curve and the corresponding reflector curve. If we get a detection or not, depends on if the reflector is obstructed or not. There can also be other objects that occasionally give false reflections. The detections will occur at a non-uniform sampling rate.

3.3 Estimator design

The position is updated with a discrete extended Kalman filter. Using the motion model (3.6) and measurement model (3.10), the design is straightforward. We will not rederive the filter equations here. They can be found in for instance [3] or [4] and in our forthcoming report [5]. In this paper we only describe the principles of the filter.

Suppose we want to estimate the state $(x, y, \theta)^T$ at time t_{k+1}. The previous state estimate was made at time t_k and determined by the measurements up to and including that time. We denote this estimate by $\hat{X}(k \mid k)$. This estimate and the motion model is used to predict the state at the time when the next sampling is made. The predicted state is notated $\hat{X}(k+1 \mid k)$ and is given by (3.3), or for short sampling intervals or small steer angles by (3.4). In general we can write this as

$$\hat{X}(k+1 \mid k) = f(\hat{X}(k \mid k), u_1, u_2) \tag{3.11}$$

At this stage we have to determine from which reflector the angle originates. At present we use a preliminary association method which is described in the next section. Let us assume that we have associated the angle γ_i with reflector j. The association problem is to make sure that $j=i$, where i is the true reflector number. No matter if the association was successful or not, the predicted measurement at time t_{k+1} will be

$$\hat{\gamma}_j(k+1\mid k) = h_j(\hat{X}(k+1\mid k)) \tag{3.12}$$

We then correct the prediction of the state according to

$$\hat{X}(k+1\mid k+1) = \hat{X}(k+1\mid k) + K(k+1)(\gamma_i(k+1) - \hat{\gamma}_j(k+1\mid k)) \tag{3.13}$$

where $K(k) = (K_1(k),\ K_2(k),\ K_3(k))^T$. If no angle is measured at time t_{k+1}, then the gain vector is $K(k)=0$, otherwise it is determined by linearizing the nonlinear system, given by (3.6) and (3.10), around a nominal value. In our case we choose the estimated state as nominal value. A Kalman filter is then designed for the linearized system. We then use the calculated filter gain on our nonlinear process.

3.4 Association of measured angles with reflectors

When an angle is measured, it has to be associated with a reflector or discarded. Only the angles that can be associated with reflectors are used for the update of the position. At present we use an association method based on knowledge of an approximate value of the position and orientation. This is determined using the motion model (3.11) with the set values of the control signals. The predicted angles to a number of reflectors is then determined with (3.12). If the measured angle falls into an angular tolerance band around the predicted angle to one reflector, we assume that this is the one.

This association routine will work satisfactory if we only have 6-7 reflectors in the room. The corresponding window to reflectors close to the vehicle can be allowed to be rather large, cf. fig 5. But if it is made too large, we will have problems with false detections.

3.5 Estimating the initial position

In this version of the system, the initial position is determined with a method proposed in [2]. From the unknown position the vehicle will only be able to measure the angle to perhaps 60-70% of the reflectors in the room. The rest will be obstructed by different objects. The position can be calculated using triangulation if we know the angles to three reflectors. So we start with assuming that the first three angles comes from the first three reflectors. This gives a position in the room. If this position is correct, there should be reflectors located in the directions given by the rest of the angles. In this way we try all possible combinations of angles and reflectors, until we find a position where we can associate all angles with reflectors.

To reduce the number of possible combinations, we assume that the number of reflectors in a room is limited to 15. All reflectors are located on the walls so the order between them never change. We also assume that there are no false detections among the measured angles. If there is a false value, the proposed method will fail. The vehicle then has to be moved and the procedure repeated. However, when we have made tests on our experimental setup, this problem seldom occurs. When the vehicle has found the initial position, false detections cause little problem.

3.6 System overview

An overview of the navigation and the control system is given in fig 6. We have already described the hardware and the navigation system. We will now briefly summarize each component in the system. In the next section we will turn to the control of the AGV, i.e. how the set values of the speed and steering angle are determined. These set values are used in the position estimator to predict the position of the AGV at the time instant when an angle is measured. The angle originates from reflector i. The predicted position and the map of reflector coordinates are then used to associate the measured angle with reflector number j and correct the estimated position. The estimated position is compared with the desired position and new set values of the control signals are determined. In this figure we can note that we do not need any measurements of the rear wheels movements. This will however be implemented in a future version of the system to increase the accuracy further.
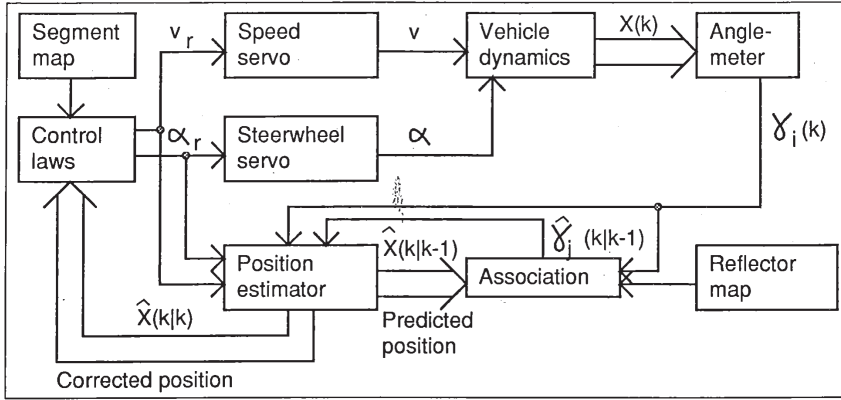
Fig 6. *Block scheme over the different components in the navigation and control system.*

4 CONTROL LAWS

The variables that are controlled, are the speed and the steer angle of the single front wheel. The control laws are designed to take the following requirements into account:

A   The vehicle should follow the drive path.
B   The speed should be as high as possible.
C   The change of the controlled variables from one sampling to another should lie within certain limits.

The first and second points are obvious. One reason for the third requirement is that the acceleration of the vehicle can cause slipping of some wheel. The estimator does not model the dynamics in the servos or slipping. If there are large changes in the set values to the servos or slipping occurs, this may result in poor estimates of the position and heading. Another reason is that large changes of the set values to the servos cause wear of the mechanical components of the vehicle.

4.1 Guidance control

The drive path is given in the memory of the onboard computer as a list of coordinates (x_s, y_s). It is defined by drawing straight lines between neighboring coordinates [6]. One such line is referred to as a segment. Since the vehicle is supposed to follow the segments, it is natural to transform the position and heading received from the estimator to a position (x_s^*, y_s^*) and heading θ_s^* in a local coordinate system around the segment s which the vehicle is following. $x_s^*(k)$ is the orthogonal projection of the position of the front wheel onto segment s, $y_s^*(k)$ is the perpendicular distance from the segment to the front wheel and $\theta_s^*(k)$ is the heading of the vehicle relative to the segment. This information is used in the guidance controller. The set value to the steer servo is given by

$$\alpha_r(k) = Atan2(-y_s^*(k), d_s) - \theta_s^*(k) \quad , \quad -\alpha_{max} \leq \alpha_r(k) \leq \alpha_{max} \tag{4.1}$$

The interpretation of (4.1) is that the steer wheel is aimed at a point on the segment which is the distance d_s away from the projection x_s^*. The aiming point is chosen such that large changes in the set value of the steer angle are avoided. α_{max} is the maximum allowed steer angle.

When the vehicle starts to follow the drive path, the distance d_s is small if the vehicle is far away from the segment so that the vehicle will travel almost perpendicular to it. When the vehicle is close to the segment and almost parallel to it, d_s can not be too small. If that is the case, or the speed compared to the sampling time is large, there will be oscillatory behavior in the control signal since the control is done in discrete time.

208

82

The way we define the drive path has the advantage that it is easy to design and that it will occupy a small amount of memory in the computer. The disadvantage is the sharp corners between the segments. It is not desirable that the vehicle makes such sharp turns. The vehicle starts to follow the new segment before the end of the old is reached to prevent overshoots in the path the vehicle is taking. If we call the distance from the end of the segment where the vehicle starts to follow the new segment l_s^e and the length of the segment l_s, we have the condition for switching between segments

$$x_s^{\bullet}(k) \geq l_s - l_s^e \tag{4.2}$$

The angle between segment s and segment $s+1$ is λ_s. l_s^e is calculated as

$$l_s^e = c \cdot | \lambda_s | \quad , \quad -\pi \leq \lambda_s \leq \pi \tag{4.3}$$

where c is chosen such that the vehicle makes a smooth turn when it starts to follow the new segment, $s+1$. To prevent a large change of the steer angle when a switch to a new segment is made, d_s depends on how the vehicle is located relative to the new segment and also on the steer angle at the time instant when the segment change is made. Fig 7 visualizes (4.1) and shows the aiming distance as a function of $y_s^{\bullet}$.
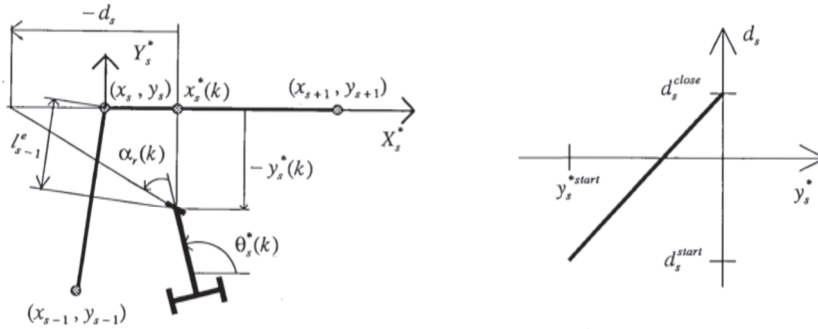
Fig 7. Here equation (4.1) is visualized. The guidance controller calculates at each sampling instant a set value to the steer servo such that the steer wheel is aimed the distance d_s away from the projection of the vehicle's position on the segment. In this figure we see the vehicle at the sampling instant when it leaves segment s-1 and starts to follow segment s. The segments are defined in the global coordinate system by the coordinates (x_{s-1}, y_{s-1}), (x_s, y_s) and (x_{s+1}, y_{s+1}). To the right we can see the aiming distance d_s on segment s as a function of the front wheel's perpendicular distance to it.

In fig 7 we see the vehicle at the sampling instant when it leaves segment s-1 and starts to follow segment s. The aiming distance is chosen at this sampling instant such that it is the distance between the projection $x_s^{\bullet}(k)$ on the new segment, (in this case segment s), and the point where the tangent of the front wheel crosses the x-axis of the new segment before the set value has been changed. This value of d_s is called d_s^{start} in the right figure, where we can see the aiming distance d_s on segment s as a function of the front wheel's perpendicular distance to it. $y_s^{\bullet start}$ is the value $y_s^{\bullet}(k)$ when the vehicle starts to follow the new segment. d_s can be positive or negative depending on how the vehicle is located relative to the segment and the steer angle when a switch is made to a new segment. d_s^{close} is the aiming distance when the perpendicular distance to the segment is zero. When the steer angle and heading to the segment are small one can linearize and discretize the closed loop system, assuming no dynamics in the servos. It turns out that $1/d_s$ and 1 are the feedback parameters in a state-feedback regulator. d_s^{close} is the value of d_s that gives the linearized closed loop system proper poles. Choosing d_s as in the right figure prevents large changes in the steer angle at switching time and at any other sampling instant if the sampling time compared to the speed is low.

4.2 Speed control

The linear and the angular accelerations of the vehicle depend on the steer angle, the speed of the front wheel and their derivatives with respect to time. One possible control strategy is to limit the acceleration to prevent slipping by choosing suitable set values to the servos. We have chosen to calculate the set value to the steer servo according to (4.1), which leaves the set value to the speed servo as the only

remaining variable left for limiting the acceleration. The guidance controller is designed such that the derivative of the steer angle is low. This property cooperates with the ambition of the speed controller to limit the acceleration, and also allows a higher speed since the acceleration partly depends on the derivative of the steer angle.

One can use models of the vehicle and the servos to predict the acceleration that a certain set value would give rise to and chose a set value to the speed servo that will not cause slipping. However, estimating the acceleration is not an easy task. Therefore we limit the acceleration using the rule of thumb.

The set value to the speed servo is calculated as a function of the set value to the steer servo as shown in fig 8. The angular velocity of the vehicle gives rise to forces acting perpendicular to the wheels. If these forces exceeds certain values, slipping occurs. Therefore the speed has to be reduced when the steer angle is large, at least when the maximum allowed speed is high.

Fig 8. The set value to the speed servo as a function of the set value to the steer servo.

There is also a restriction in the change of the set value to the speed servo from the previous sampling instant to the current sampling instant according to

$$| v_r(k) - v_r(k-1) | \leq \Delta v_{lim}$$ (4.4)

This is to limit the acceleration of the vehicle. This function is mainly active at start-up. At that time the speed is 0 m/s, and if the steer angle is 0°, the set value to the speed servo will be maximum speed according to fig 8. This can lead to slipping of the front wheel.

Calculation of the set value to the speed servo according to fig 8 and (4.4) guarantees that the speed control is smooth if the guidance control is smooth.

5 SIMULATION RESULTS

The navigation and the control system have been simulated and tested on our AGV prototype with the simulation and control program REGSIM, which is developed at Luleå University of Technology [7]. When simulating the system, we assumed that the speed and steerwheel servos in fig 6 were first order systems. The time constant was set to 0.2 s for the speed servo and 0.1 s for the steerwheel servo. The set value of the speed was set to 0.5 m/s. Equations (3.1) and (3.2) were used to simulate the vehicle dynamics.

The room has the dimensions 9x5.5 m^2. There are eleven reflectors on the walls, marked as dash-dotted lines in the fig 9, and five tables that the AGV should avoid to move. Since the mirror rotates with 1 Hz , the mean time between angle measurements would be approximately 0.1 s if only a few of the reflectors are obstructed. To simplify the simulation routines we assumed that angles were measured with the sampling interval 0.1 s. In tests on the prototype we have a non-uniform sampling interval.

In fig 9 and fig 10 we see the result from two different simulations. We assumed that the initial position had 50 mm error in the x- and y-coordinates and 0.05 rad error in the heading. In reality the initial position will be determined with high accuracy since it is determined using a lot of angles measured from one point.

In fig 9 we see the result when no angles were used for the update of the position. Neither the initial errors nor the accumulated errors due to model errors were removed. The estimated trajectory of the AGV is shown with a dashed line. We can also see the function of the guidance controller. The initial position is not on the first segment. The guidance controller will make the estimated position follow a smooth path until it reaches the segment. A change to the next segment is made before the end of a segment is reached. The control laws for guidance control and speed control are further described in [8].
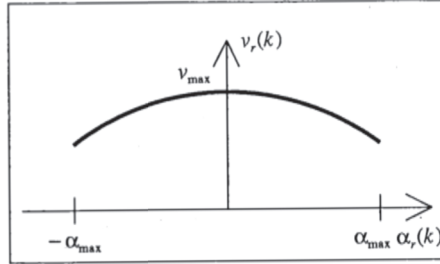
210

84

In fig 10 we see the result when measured angles were used to correct the estimated position. We assumed that the measured angles had been associated with the correct reflectors. Errors of the same magnitude as the assumed initial errors can however occur when the AGV is moving if an erroneous association is made. In this simulation the initial errors are reduced. This indicates that the system can handle up to around 10% false detections and erroneous associations. The errors in position is less than 50 mm during the 30 s simulation. The errors can be reduced by increasing the rotational speed of the anglemeter, i.e. have a shorter sampling interval, and measuring the rear wheel movements.
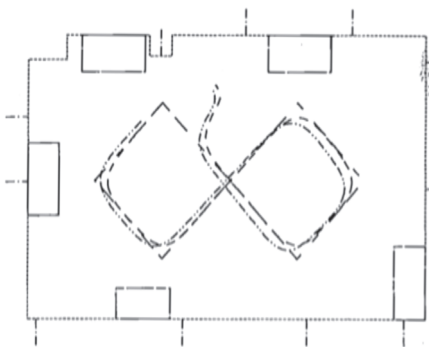
Fig 9.The estimated and simulated trajectory differs when no angles are used for the update of the position.
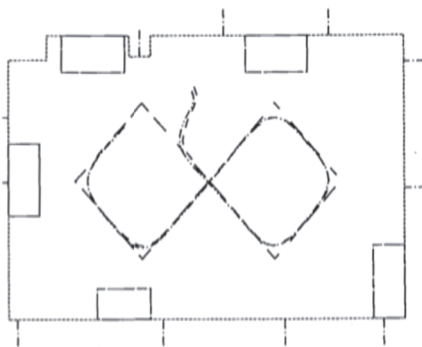
Fig 10. In this figure angles are used. We can also see how the vehicle follows and changes between segments.

6 SUMMARY

We have described an optical navigation system for an AGV based on directional measurements to several identical beacons. The position and heading of the AGV is updated recursively each time a valid angle is measured. The drive path that the AGV should follow consists of straight line segments between given points. This gives a very flexible system where it is easy to change the transportation routes. We also described the control laws that are used for segment following, segment change and speed control.

The system has been tested on an AGV prototype in the room shown in fig 9 and fig 10. It is however difficult to present any results from these tests, since we do not have any way to measure the position of the AGV when it is moving, except using the position estimator. At present we use a personal computer for all the calculations. This increases the computational times. Therefore we have only tested the system with the speed 0.3 m/s. In a future version we will use a Motorola 68020 with a 68881 floating-point coprocessor.

Our present research concerns a thorough error analysis of the position estimator, a new method to determine the initial position and a robust association method. The anglemeter will be redesigned to enable a rotational speed of at least 5 Hz.

7 ACKNOWLEDGMENTS

8 REFERENCES

[1] Hyyppä, K., "Optical Navigation System Using Passive Identical Beacons", Proc. Intelligent Autonomous Systems, Amsterdam, 8-11 December, 1986, pp 737-741, North-Holland (1987).

[2] Hyyppä, K. and Wiklund, U., "Optical Navigation System Using Passive Identical Beacons", Technical Report 1987:11T, Luleå University of Technology, S-951 87 Luleå, Sweden (1987).

[3] Jazwinski, H.J., "Stochastic Processes and Filtering Theory", Academic Press (1970).

[4] Anderson, B.D.O. and Moore, J.B., "Optimal filtering", Prentice-Hall (1979).

[5] Wiklund, U., "Navigation by Angle Measurements to Several Identical Beacons", Report, Luleå University of Technology, S-951 87 Luleå, Sweden, (to be published).

[6] Julliere, M., et al, "A guidance system for a vehicle which has to follow a memorized path", Proc. Automated Guided Vehicle Systems, Stuttgart, W.Germany, 7-9 June, 1983.

[7] Gustavsson, T., "REGSIM - User's manual", Report, Division of Automatic Control, Luleå University of Technology, S-951 87 Luleå, Sweden.

[8] Andersson, U., "A Control Strategy for Autonomous Guided Vehicles", Report, Luleå University of Technology, S-951 87 Luleå, Sweden, (to be published).

86

PAPER B

[B] - Path design and control algorithms for articulated mobile robots

The author's main contribution: Underground field trials.

Comment: The X4Y4 representation of the drive path was invented by Kalle Åström.

Path Design and Control Algorithms for Articulated Mobile Robots

Ulf Andersson, Kent Mrozek
Q Navigator AB
Aurorum 21B
SE-977 75 Luleå, Sweden

Kalle Åström
Dept. of Mathematics
Lund Institute of Technology
Box 118
SE-221 00 Lund, Sweden

Kalevi Hyyppä
Div. of Industrial Electronics
Luleå University of Technology
SE-971 87 Luleå, Sweden

Abstract

Experiments have shown that continuity of curvature of a reference path and of its derivative with respect to distance are particularly important for articulated mobile robots. The *X4Y4 curve* and a control algorithm for an articulated mobile robot following an *X4Y4 curve* are presented. Experiments with a 55 ton LHD vehicle in an underground mine have shown that the sideways repeatability when driving through a 106° curve at 2.8 m/s is within ± 100 mm, and when driving through a 10° curve at 5.1 m/s is within ± 50 mm.

1 Introduction

Path design is an important issue for real-world mobile robots. Ill-designed curves on a path can cause large guidance errors, and also result in high stress on servos, motors, bearings etc. in the robot.

Traditionally reference paths have been designed from lines and arcs, laid out to make the heading along the path continuous. We have however experienced, as others [Nelson and Cox, 1988], that it is not possible for most mobile robots to follow this kind of paths without errors.

The cause of errors is the discontinuity in curvature at the junctions between the lines and the arcs. A step-wise change of curvature demands infinite speed of the actuator controlling the curvature taken by the robot guide point. (The only exception is a tricycle-type mobile robot with the guide point placed under the steering wheel. This placement should however be avoided because of the resulting complex control of the orientation of the robot, and the wide swept area. The common placement of guide point is at the mid-point between the non-steered wheels for a tricycle-type mobile robot, and at the mid-point between the rear or front wheels of an articulated mobile robot.)

The importance of continuous curvature has been discussed extensively in   [Nelson, 1989] where quintic polynomial paths are proposed, and in [Kanayama and. Hartman, 1989] where cubic spiral paths are proposed. In the second paper a smoothness cost function is introduced which makes it possible to find the optimally smooth path. In [Graettinger and Krogh, 1989] time-scaling has been proposed to fulfill the dynamic constraints of a path.

In none of these papers has continuity of derivative of curvature with respect to distance along the path been discussed. The curvature is proportional to $\tan(\alpha)$ for a tricycle-type mobile robot and to $\tan(\alpha/2)$ for an articulated mobile robot. The angle α denotes the steering angle and the articulation angle respectively. Driving, with constant speed, along a path with a step change of the curvature derivative would demand a step change in the time derivative of α and therefor an infinite actuator torque of the steering mechanism of the mobile robot.

A rather different approach has been taken in [Steer, 1989] where the author proposes a gaussian shape of the steer angle versus time function of a tricycle-type mobile robot when driving in a curve. The gaussian function is infinitely differentiable, solving the problem with infinite actuator torque demand, but the path is complicated to find. In [Pin and Vasseur, 1990] a simple algorithm is presented to find the shortest path between two postures. Limitations of the steering rate is discussed.

In this paper we present and discuss the *X4Y4 curve*. It consists of two or three parts depending on the total heading change along the curve. The first part is called the closing part and the last part (second or third) is called the opening part. They are both characterized by

$$x^4 + y^4 = c^4 \qquad (1)$$

where *x* and *y* are the coordinates of the path in a global coordinate system and *c* is a positive scaling constant which controls the size of the curve. In the closing part the curvature goes from 0 to a finite value, and in the opening part the curvature returns from the same finite value to 0. The closing and opening parts are actually mirrored versions of each other: the *X4Y4 curve* is symmetric.

If the total heading change is > 90° the *X4Y4 curve* has a circular segment between the closing and opening parts. The radius of the circular segment is chosen such that the curvature is continuous along the whole *X4Y4 curve*.

The guidance controller on board the vehicle calculates set values to a servo which controls the articulation angle of the vehicle from measured errors in distance and angle. The distance error is defined as the distance from the guide point on the vehicle to the nearest point on the path, and the angle error as the angle between the heading of the vehicle guide point and the tangent to the path at the nearest point.

The calculation of the nearest point on the closing and opening parts of an *X4Y4 curve* can only be done numerically whereas the nearest point on the circular segment of an *X2Y2 curve* can be expressed in closed form.

To increase the performance of a guidance controller when driving the vehicle along an *X4Y4 curve* it is favorable to include a feed-forward part in the controller. This part is designed to be a function of the curvature at the nearest point. The function is dependent on the vehicle geometry.

The *X4Y4 curve* has been implemented on a navigation and guidance system on an articulated 55 ton mining vehicle driving at 5.3 m/s. Most of the development work was done using our test vehicle CALMAN [Larsson et al., 1994] which is a modified articulated lawn-mover of maximum speed 2.5 m/s. Figure 1 shows a photograph of CALMAN.

The navigation system onboard CALMAN is based on a laser scanner which measures headings to retroreflective beacons at known positions in the workspace. This scanner is visible in Figure 1 mounted on top of one of the boxes which houses the control system. The navigation system was developed at Luleå University of Technology [Hyyppä, 1986; 1989; 1993; 1994; Hyyppä et al., 1994; Wiklund et al., 1988]. It has been produced commercially for several years.

2 Properties of the *X4Y4 curve*

2.1 Desirable Path Properties:

- Continuous curvature $K(s)$. The variable *s* is the distance along the path.

- Continuous curvature change with distance dK/ds.

2.2 The *X4Y4 curve*

The *X4Y4 curve* is a symmetric curve consisting of three parts if the total heading change is more than 90° or of two parts if the total heading change is less than or equal to 90°. To make the curvature $K(s)$ continuous it is chosen to have the same value on both parts at the junction(s).

Total Heading Change > 90°

The first part is the *closing X4Y4* characterized by:

- heading change = 45°.

- $K = dK/ds = 0$ at the start point.

- $K \neq 0$ at the end point.

- $dK/ds = 0$ at the end point.

The middle part is a circular arc (*X2Y2*) characterized by:

- K = constant.

- $dK/ds = 0$.

The last part is the *opening X4Y4* characterized by:

- heading change = 45°.

- $K = dK/ds = 0$ at the end point.

- $K \neq 0$ at the start point.

- $dK/ds = 0$ at the start point.

Total Heading Change = 90°

As above but without the middle part (*X2Y2*).
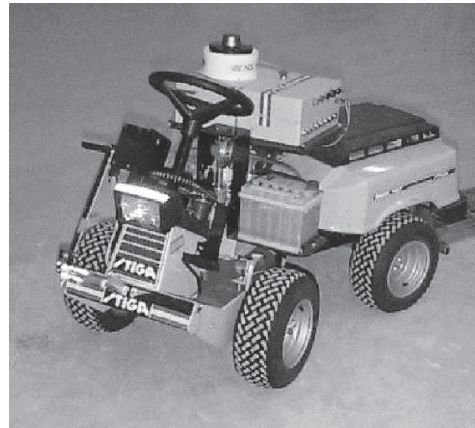
Figure 1. Photograph of our mobile robot CALMAN.

Total Heading Change < 90°

Only *closing X4Y4* and *opening X4Y4* parts with less than 45° heading change in both. The curvature is still continuous but at the joining point we get

$$\left(\frac{dK}{ds}\right)_{opening\ part} = -\left(\frac{dK}{ds}\right)_{closing\ part} \quad (2)$$

i.e. the curvature derivative with respect to distance is discontinuous. An alternative design is to include a small *X2Y2* part in the middle which instead of one jump gives two smaller jumps in *dK/ds*.

Examples of four alternatives for designing a 90° curve are shown in Figure 2.
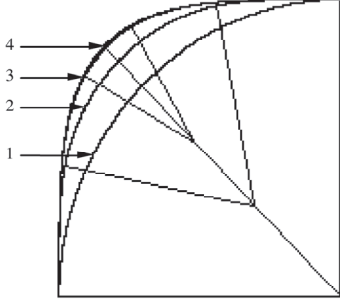
Figure 2. 90° curve examples.
1. *X2Y2(90°)*
2. *X4Y4(11.45°)-X2Y2(67.1°)-X4Y4(11.45°)*
3. *X4Y4(30°)-X2Y2(30°)-X4Y4(30°)*
4. *X4Y4(45°)-X4Y4(45°)*
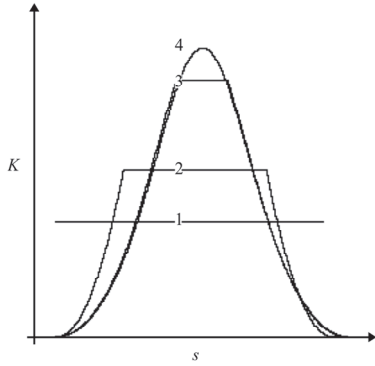
Figure 3. Curvatures *K(s)* from 90° curve examples. The symbol *s* denotes the distance along the curve.
1. X2Y2(90°)
2. X4Y4(11.45°)-X2Y2(67.1°)-X4Y4(11.45°)
3. X4Y4(30°)-X2Y2(30°)-X4Y4(30°)
4. X4Y4(45°)-X4Y4(45°)

Figure 3 shows that only the fourth alternative gives the desirable property of continuous *dK/ds* along the whole curve.

3 Controller for the *X4Y4 curve*

A block diagram of our proposed control system for articulated mobile robots is shown in Figure 4. The set value for the articulation angle α_{set} is calculated according to

$$\alpha_{set} = f(d_{path}, \Delta_{path}) + FF(K_n) \quad (3)$$

where

d_{path} is the sidewise error to the reference path, the sign is positive when the guide point is to the left of the curve, and negative when it is to the right of the curve;

Δ_{path} is the heading error to the reference path and

$$-\pi \le \Delta_{path} \le \pi;$$

K_n is the curvature at the nearest point on the reference path;

f is the error controller function (there are a number of standard controller structures to choose among);

FF is a feed-forward function of K_n which depends on vehicle geometry, rotation direction of the curve (clockwise or counter-clockwise), and the driving direction of the robot (forward or reverse).
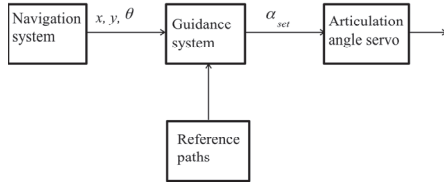
Figure 4. Block description of the proposed control system for articulated mobile robots.

3.1 Steps in Determining d_{path}, Δ_{path} and K_n on the *X4Y4* part.

It is assumed that the position and heading (*x, y, θ*) of the guide point in the global co-ordinate system is determined by a navigation system.

A normalised co-ordinate system is used as an aid in determining the variables d_{path}, Δ_{path} and K_n. Figure 5 shows an *X4Y4* part giving a heading change of 45° in normalised

form, together with some variables which are used for the calculations.
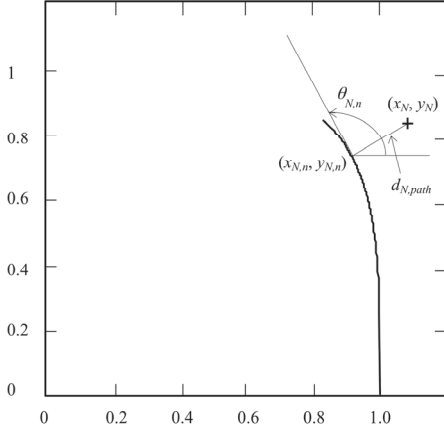
Figure 5. Normalised co-ordinate system of the *X4Y4* part with a heading change of 45°. The symbol '+' denotes the position of the mobile robot. Subscript *N* denotes 'normalised' and subscript *n* denotes the nearest point on the curve.

The steps to calculate d_{path}, Δ_{path} and K_n are:

1. Transform the *X4Y4* part and the global position (x, y) of the mobile robot guide point to the normalised co-ordinate system.

2. Use a numerical method, e.g. Newton-Raphson, to find the nearest point on the *X4Y4* part. Use appropriate start values.

3. Calculate the heading of the curve, i.e. the direction of the tangent, and the curvature at the nearest point.

4. Transform from the normalised co-ordinate system back to the global co-ordinate system i.e.
   $(x_{N,n},\ y_{N,n},\ \theta_{N,n},\ K_{N,n}) \rightarrow (x_n,\ y_n,\ \theta_n,\ K_n)$.

5. Calculate the guidance controller inputs.

$$\left| d_{path} \right| = \sqrt{\left(x - x_n\right)^2 + \left(y - y_n\right)^2} \qquad (4)$$

$$\Delta_{path} = \theta - \theta_n \qquad (5)$$

4   Design of *X4Y4 curves*

The design of the curves need to take into account the limitations of the vehicle which are:

- Maximum articulation angle.
- Maximum articulation angle speed.

The maximum articulation angle and the geometry of the vehicle limit the maximum curvature the vehicle can follow, which gives a maximum allowed curvature K_{max}.

The curvature speed K_v (i.e. the time derivative of the curvature for the vehicle when driving along a curve with a certain speed ds/dt) can be expressed as

$$K_v = \frac{dK}{dt} = \frac{dK}{ds} \cdot \frac{ds}{dt} \qquad (6)$$

The vehicle should drive with constant speed along the curve to get a smooth ride. This condition together with the maximum articulation angle speed and the geometry of the vehicle, limits K_v to $K_{v\,max}$.

The limits K_{max} and $K_{v\,max}$ should contain some safety margins.

4.1   A Design Example
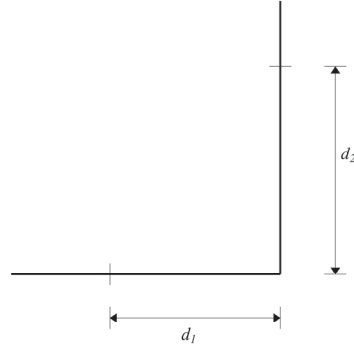
Figure 6. The basis for the path design is a polygon of straight lines, which could represent the centre lines for tunnels in a mine. In this example a curve should be designed within the limits defined by d_1 and d_2. If $d_1 < d_2$ then d_1 is the limit (and then also the scale factor c = d_1 in case of a 90° curve).

The design steps are:

1. Make a curve with the smallest possible curvature within the size limits.

2. Check that the maximum curvature does not imply an articulation angle greater than the limit of the vehicle.

3. If the maximum curvature speed implies an articulating angle speed of the vehicle greater than the limit of the vehicle, reduce the vehicle speed.

5 Experiences of the *X4Y4 curve*

5.1 Non-articulated Vehicles

The *X4Y4 curve* has for some time been used successfully in a number of AGV installations, and is commercially available. The vehicle types have been:

- Tricycle vehicles (single steer and drive unit).
- Diff vehicles (differential drives).
- Quad vehicles (dual steer and drive units).

The maximum speed of these AGV's is typically 1.0 m/s.

5.2 Articulated Vehicles

Lately, the curve has also been used for the following articulated vehicles:

- CALMAN, our modified 200 kg articulated lawn mover with maximum speed = 2.5 m/s.
- A 55 ton LHD vehicle with maximum speed = 5.3 m/s.

The main difference between AGV's and articulated vehicles is that the chassis parts do not rotate relative to each other when an AGV turns.

This difference becomes very clear in practice if there is a discontinuity in *dK/ds*. In an AGV, limited discontinuities is not noticeable due to the stiff chassis and the low speed. In an articulated vehicle, even small discontinuities in *dK/ds* becomes noticeable in the performance of the vehicle due to the two part chassis and the high speed.

CALMAN

Our mobile robot CALMAN has been used in several research projects [Larsson et al., 1994].

The control of the articulation joint is done with a DC-motor connected to the joint via spring tensioned wires. Due to the springs, the connection is not very stiff which requires high damping in the servo for the articulation angle.

The LHD Vehicle

The LHD (Load Haulage and Dump) vehicle is used for transporting rock in its bucket in underground mines. To our knowledge automatic (i. e. driverless) LHD vehicles have not yet been used commercially, although experiments with LHD vehicles following an optical guide line have been reported [Hurteau et al., 1992].

The LHD vehicle we have used has the following limitations:

- Maximum steering angle 33°.
- Maximum steering angle speed 18°/s.
- Electrically driven (1000 V, 3-phase AC) with 4 gear positions. Approximate speeds for the gear positions are:

- 1: 1.0 m/s.
- 2: 1.7 m/s.
- 3: 2.8 m/s.
- 4: 5.1 m/s.

The control of the articulation angle is done via a hydraulic system. The electrical interface to the hydraulic system has electrical proportional valves which are controlled by PWM-signals from the control system.

The Path Layout for the LHD Vehicle

The layout (see Figure 7) consisted of straight-line segments and curve segments of the *X4Y4* type. The straight-line segments were connected with the four curves 1, 2, 3 and 4 in Figure 7.

Curves 2 and 4 were designed to have a safety margin of approximately 5° in articulation angle and approximately 7 °/s in articulation angle speed. The design was made for a constant speed of the vehicle of 2.8 m/s along the curve.
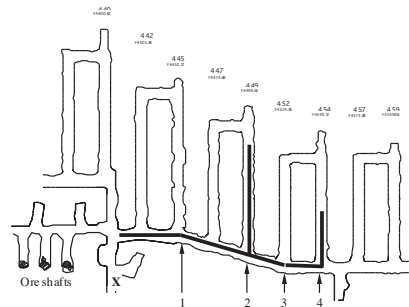
Figure 7. Layout for the 55 ton articulated LHD vehicle in an underground mine. The symbol X marks the position of the power supply unit for the vehicle. The x-axis of the global co-ordinate system points to the right in the figure. The distance, in the x-direction, from the supply unit to curve 4 is approximately 140 m. The curves are of the following types:

1. *X4Y4*(8°)-*X4Y4*(8°)
2. *X4Y4*(45°)-*X2Y2*(16°)-*X4Y4*(45°)
3. *X4Y4*(2.5°)-*X2Y2*(5.5°)-*X4Y4*(2.5°)
4. *X4Y4*(45°)-*X2Y2*(5.5°)-*X4Y4*(45°)

Curves 1 and 3 have heading changes less than 90° and therefor have discontinuities in *dK/ds* which made a "trial and error" design necessary. The designed speed for these curves is high (5.1 m/s) which demanded some fine tuning to give a satisfactory result.

Experimental Results

The logged position of the vehicle when driving through curve 4 is shown in Figure 8. The drag from the power supply cable influenced the path taken by the vehicle somewhat. When driving into the curve the drag was considerably higher than when driving out. The drag creates

a torque at the articulation joint which tries to decrease the articulation angle.

The path in the forward direction (left to right in Figure 7) is slightly uphill. Therefor the speed was somewhat lower when driving in the forward direction compared to when driving in the reverse direction. The maximum speed (5.3 m/s) was reached in the beginning of curve 1 when driving in the reverse direction. The logged speed of the vehicle when driving through curve 4 is shown in Figure 9. The speed was sampled with a rate of 40 samples/s.
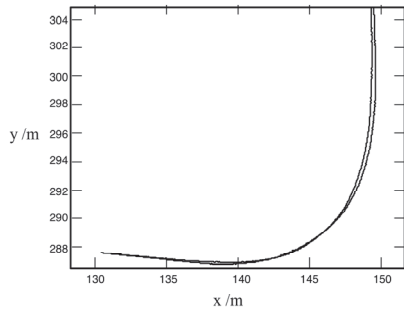
Figure 8. Logged position when running in and out of curve 4. The electric power supply cable mounted in the rear of the LHD vehicle introduced a force causing the LHD vehicle to take an "outer" curve when running in.
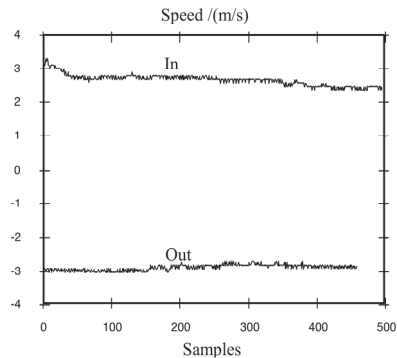
Figure 9. Logged speed (m/s) when driving in and out of curve 4. Sampling frequency = 40 Hz. Speed is positive when driving in and negative when driving out. It is slightly uphill when going in which explains the lower speed in that direction.

The logged articulation angles of the vehicle when driving in and out of curve 4 are shown in Figure 10 and when driving twice through curve 4 are shown in Figure 11.
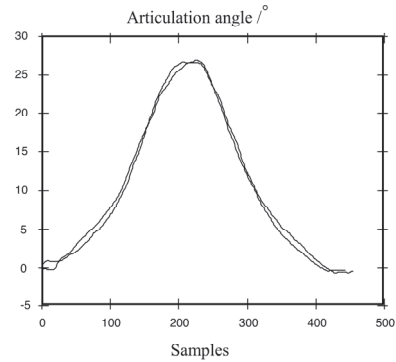
Figure 10. Logged articulation angle when running in and out of curve 4.
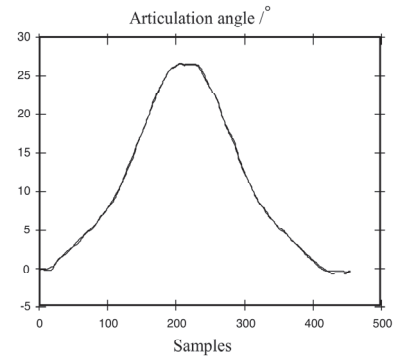
Figure 11. Logged articulation angle for two runs into curve 4. The small differences illustrates the high repeatability of the system.

Finally, the logged articulation angle of the vehicle when driving through curve 3 is shown in Figure 12. This curve has an *X2Y2* part which is visible in the figure as an almost constant articulation angle for the middle part of the curve.

94
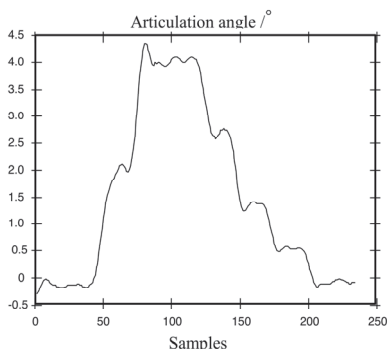
Figure 12. Logged articulation angle when driving into curve 3. The 5.5° *X2Y2* part in the middle shows up as an almost constant articulation angle between samples 80 and 130.

6 Conclusions

X4Y4 curves without discontinuities in *dK/ds* give excellent path-following performance of an articulated vehicle. The design does not require any trial and error. Practical tests have shown that safety margins of $\approx 5°$ for articulation angle and of $\approx 40\%$ for articulation angle speed make it possible to keep the guidance controller non-saturated in the curves.

X4Y4 curves with discontinuities (less than 90° curves) are possible for articulated vehicles, but demand a trial and error based design when driving at high speed.

After a large number of runs in the mine we have come to the conclusion that the repeatability in curve 2 and 4 is within ±100 mm. The repeatability on straight paths and the wider curves (curve 1 and 3) is within ±50 mm.

Curve 1 and 3 have a small discontinuity in *dK/ds*. The discontinuity is so small that it is not noticeable in practice. However, some care had to be exercised when deciding the scale factor *c* for these curves. There were lower limits for the two scale factors. Going below these limits caused the guidance controller to go into saturation when driving in 4:th gear.

References

[Graettinger and Krogh, 1989] T. J. Graettinger and B. H. Krogh, "Evaluation and Time-Scaling of Trajectories for Wheeled Mobile Robots", *Trans. Of the ASME*, vol. 111, pp. 222-231, June 1989.

[Hurteau et al., 1992] R. Hurteau et al., "Optical Guidance System for Underground Mine Vehicles", *Proc. Of the 1992 IEEE Int. Conf. On Robotics and Automation*, pp. 639-644, Nice, France, May 1992.

[Hyyppä, 1986] K. Hyyppä, "Optical navigation system using passive identical beacons", *Proc. Intelligent Autonomous Systems*, Amsterdam, December 1986.

[Hyyppä, 1989] K. Hyyppä, "Luleå Turbo Turtle (LTT)", *Proc. IEEE/RSJ International Workshop on Intelligent Robots and Systems `89*, Tsukuba, September 1989.

[Hyyppä, 1993] K. Hyyppä," On a laser anglemeter for mobile robot navigation", Doctoral Thesis 1993:117D, Luleå University of Technology 1993.

[Hyyppä, 1994] K. Hyyppä, "Design considerations in a laser navigation system for mobile robots", *Mechatronics*, vol. 4, no. 2, pp. 199-206, 1994.

[Hyyppä et al., 1994] K. Hyyppä, U. Wiklund, U. Andersson, Å. Wernersson, T. Gustafsson, G. Hillerström, and C. Zell, "Navigational experiments with the autonomous mobile robot LTT using angle measurements to identical beacons", *Tampere Int. Conf. on Machine Automation*, Tampere, February 1994.

[Kanayama and. Hartman, 1989] Y. Kanayama and B. I. Hartman, "Smooth Local Path Planning for Autonomous Vehicles", *1989 IEEE Int. Conf. on Robotics and Automation*, pp. 1264-1270, Scottsdale, Arizona, May 1989.

[Larsson et al., 1994] U. Larsson, C. Zell, K. Hyyppä and Å. Wernersson, "Navigating an Articulated Vehicle and Reversing with a Trailer", *1994 IEEE Int. Conf. on Robotics and Automation*, San Diego, May 1994.

[Nelson, 1989] W. L. Nelson, "Continuous Steering-Function Control of Robot Carts", *IEEE Trans. On Industrial Electronics*, vol. 36, no. 3, pp. 330-337, August 1989.

[Nelson and Cox, 1988] W. L. Nelson and I. J. Cox, "Local Path Control for an Autonomous Vehicle", *1988 IEEE Int. Conf. on Robotics and Automation*, pp. 1504-1510, Philadelphia, Pennsylvania, April 1988.

[Pin and Vasseur, 1990] F. G. Pin and H. A. Vasseur, "Autonomous Trajectory Generation for Mobile Robots with Non-Holonomic and Steering Angle Constraints", *Proc. IEEE Int. Workshop on Intelligent Motion Control*, pp. 20-22, Istanbul, August 1990.

[Steer, 1989] B. Steer, "Trajectory Planning for a Mobile Robot", *The Int. Journal of Robotic Research*, vol. 8, no. 5, pp. 3-14, October 1989.

[Wiklund et al., 1988] U. Wiklund, U. Andersson and K. Hyyppä, "AGV navigation by angle measurements", *Proc. 6th int. Conf. Automated Guided Vehicle System*, pp. 199-212, Brussels, October 1988.

PAPER C

[C] - LHD automation at the LKAB Kiruna iron ore mine

The author's main contribution: Team member, inventor of the driver assisting system for excavation of fragmented rock and "typing the text".

Comment: The paper spans work during a period of 15 years and discusses the automated production system from many viewing angles.

LHD automation at the LKAB Kiruna iron ore mine

Ulf Andersson

Division of Systems and Interaction, Luleå University of Technology, 971 87, Luleå, Sweden

Mats Strömsten

Luossavaara-Kiirunavaara Aktiebolag, LKAB, 981 86, Kiruna, Sweden

Abstract

This paper describes a reflector based LHD navigation system and a driver assisting system for remote controlled excavation of fragmented rock. The navigation system was first tested in underground field trials in 1996 and was later part of the LHD automation system in the LKAB Kiruna iron ore mine, which is one of the world's largest underground mines. The system was used in production from 1999 to 2009 and consisted at most of eight 75 tonnes automatic LHD's and seven production areas in the sublevel cave mine. Lower weights of tele remote excavated buckets compared to manual excavated buckets were early identified. The driver assisting system was developed to address the low bucket weights. The performance of the system is presented in terms of key performance indices (KPI's) based on significant amount of data from the 10-year production period. Such figures have not been found in the literature and are therefore a novelty contribution of this paper together with the driver assisting system for remote controlled excavation. A comparison is done with later developed navigation systems with focus on navigation algorithms and underground field trials. Few papers discussing navigation systems for LHD automation has been published in recent years. The majority of papers were published 10 to 15 years ago. Most of the papers published today discuss LHD automation from a commercial perspective, which is outside the scope of this paper.

1 Introduction

The LHD vehicle, where LHD stands for Load, Haul and Dump, is a type of wheel loader machine adapted for use in underground mines. The LHD is articulated frame steered to reduce the sweep area when turning. The main difference compared to a wheel loader is that the cabin is placed on the side of the machine to reduce the height.

The name of the vehicle actually defines what it does; namely it loads fragmented rock – a mix of ore and waste rock - in the bucket at the draw point, transports (hauls) the fragmented rock to the ore pass, dumps it in the ore pass and returns to the draw point. This cycle is repeated until, ideally, it is no longer profitable to continue loading, meaning that the amount of waste rock becomes too high.

- There are some typical benefits that motivates LHD automation, such as:

- Improvement of working conditions. Manual work is monotone, the operator in the cabin is exposed to vibrations, does not have access to daylight, etc.

- Improvement of working conditions in terms of job rotation. It is possible to alternate between remote controlled and manual loading if the LHD's still features a driver's cabin.

- Lower personnel costs since a remote operator can handle more than one machine.

- It is not necessary to ventilate poisonous gases in the production area, which means that the production can begin directly after blasting, thus increasing the utilization.

- Better control of the flow of ore through the mine since the loading done by the LHD system is completely computer controlled, which could be a part of the integrated process control of the mine.

- Better utilization of the LHD's since the stops due to changes of work shift personnel can be minimized.

In this context, it is also important to point out some "drawbacks" with LHD automation:

- The requirement on service personnel increases. The LHD automation system is a complex system that requires skills that traditional service personnel of the LHD usually lack.

- Fewer human senses can be used for feedback control during the loading. Typically, only video feedback is usually used for the remote operator meaning that, for instance, the vibrations and sounds of the machine that a manual operator in the cabin of the machine experience and uses for the control of the loading will be lost. This might result in lower scoop weights on the average when comparing the performance of an automatic LHD with a manual LHD. Supervision and removal of rocks spilled from the bucket during the transportation from the draw point to the ore pass also becomes more difficult.

- No humans in the production area that surveys the environment, for instance water leakages that an operator of a manual LHD can detect and take action against.

- Regulations might limit the access to the production area for other work forces compared to manual production. The possibilities for maintenance work in the production area are reduced.

- Increased amount of infrastructure in the production area such as communication systems, personal safety systems, navigation references, etc. leads to increased disturbance sensitivity. The disturbance sensitivity increases significantly for serial connected systems.

On a technical level, there are some important requirements typical for the application.

- Robust navigation.

- Low cycle time.

- Robust communication.

- Robust and easy to use area isolation systems.

100

The distances from the walls of the drifts to the machine are very small and unlike traditional AGV applications in factories / warehouses running at low speed (typically 1 m/s), it is not possible to have external safety systems that will stop the vehicle in case of navigation error unless the speed is limited. A limitation of the speed increases the cycle time and thereby the production, which is not acceptable.

It is, especially in production areas operated by only one LHD, important that it is possible to go with full speed. This means top gear on straight parts, and in curves a speed corresponding close to the maximum angular velocity of the steering mechanism of the articulation hinge. This requirement becomes less important in production areas with many intersections operated by several vehicles since there is a higher degree of conjunction. This, on the other hand, puts higher demands on the traffic control system to optimize the total transportation flow in the production area.

Since the loading is done via remote control, a low latency is important in the loop starting with the video signal, passing by the remote operator and ending with the control signals at the machine. It is also important that the communication system handles the reflection phenomena that typically occur in the drifts with uneven structure. If using wireless communication with several access points, the latency for the hand over between the access points must also be sufficiently low.

1.1 Background

A number of attempts to automate LHD's have been done since the 80's in underground mines, Mäkelä (2001a), Roberts, Duff and Corke (2002), Bakambu and Polotski, (2007), Marshall, Barefoot and Larsson (2008) and Gustafson (2011).

The Swedish mining company LKAB has since the late 80's conducted a series of LHD automation projects. A driving force has been the large-scale operations in the Kiruna sublevel cave iron ore mine, which is one of the world's largest underground mines. The projects discussed in this paper concern the adoption to LHD automation of a laser based navigation system originally developed for AGV applications. The adapted system, called HUNS, was later used as the navigation system during the 10-year production period. At its peak, the system consisted of eight LHD's operating in seven production areas in the sublevel cave mine.

Today, at least three major suppliers of underground mining equipment have developed LHD automation systems of their own that are commercially available. This is in contrast to the situation in the late 90's when mining companies had to develop their own systems, Wylie (1996).

1.2 LHD's

Two types of LHD's are considered in the paper. The type used in the field trials was a TORO501E Sandvik/Tamrock electric LHD with a nominal loading capacity of 13 tonnes. The eight LHD's used during the 10-year production period were of type TORO2500E from Sandvik/Tamrock with a nominal loading capacity of 25 tonnes.

Figure 1. The photograph shows the LHD used in the underground field trials. Eight retro-reflectors are lightening up by the camera flash.

Figure 2. The photograph shows one of eight 75 tonnes LHD's used in the 10-year production period. The laser scanner is placed above the rear axle in the centre of the vehicle and rotates the laser beam over the cabin roof 3.2 meters above the ground.

The electric motors of the LHD's runs at a constant rpm implying that the drive speed of the LHD's cannot be continuously controlled except when breaking. Four gears are used and the

typical speed corresponding to each gear is 1, 2, 3 and 5 [m/s] respectively. The speed of the top gear has a strong dependence of the inclination in the roadway.

1.3 Outline of the paper

We have identified some important properties based on extensive use of the LHD automation system. These properties are:

- The *cycle time*, the *robustness* and the *loading capacity* of a navigation system have a direct influence on the production.

- The *navigation accuracy* and the *navigation safety systems* are important because of the narrow drifts and the danger of collapse at the draw point.

- The navigation system should not cause increased *wear of the machine* compared to manual operation, for instance wheel spin during loading.

- The *system maintenance* should not require expertise knowledge of algorithms and sensors.

The focus in the paper is on technologies that addresses the two first points; it should be noted that remote controlled excavation of fragmented rock is considered being an integrated part of the automation system of the LHD. The reason simply being the completely integrated load, haul and dump functions of the machine itself. It is our opinion that systems controlling these functions have to be integrated for the cyclic operation to be efficient.

A literature review is presented in section 2.

It should be noted that few papers discussing navigation systems for LHD automation has been published in recent years. The majority of papers were published 10 to 15 years ago. Most of the papers published today discuss LHD automation from a commercial perspective, which is outside the scope of this paper. See for instance http://www.e-mj.com/index.php/features/2234-the-drivers-of-autonomy.html (read 2013-11-06).

Some details of the system architecture important for the integration of the driver assisting system for remote controlled excavation are discussed in section 3. Section 4 and 5 describes functions comparable to the reviewed techniques for automatic tramming and hauling. Section 6 describes the driver assisting system for remote controlled excavation of fragmented rock. Field test results are discussed in section 7. The key performance indices are presented in section 8. Conclusions are found in section 9. Details of the navigation algorithms are found in the appendix in section 10.

2 Litterature review

Driver assisted and automated excavation of fragmented rock in underground mines can be viewed as a sub-topic of the research field "*automatic/autonomous earthmoving*". A detailed state of the art discussion is found in Singh (2002) and a later – but briefer – in Hemami and

Hassani (2009). Bonchis, Hillier, Ryde, Duff and Pradalier (2011) divide the research field into a) systems (including systems of systems), b) traditional robotic topics and c) tool-ground interaction. Bonchis et al. discuss experiments in autonomous bulk material handling using a skid-steered Bobcat and a GPS/INS system. The work described is classified as scooping, which is a typical task of the LHD.

Marshall, Murphy and Daneshmend (2008) discuss experimental results from the excavation phase of fragmented rock with a full scale LHD with 10 tonnes loading capacity. The LHD was manual driven but equipped with sensors to measure external forces caused by the interaction between the bucket and the muck pile and internal forces acting in the hydraulic system of the boom/bucket. Sensors to measure the configuration of the loader at all times, boom/bucket cylinder positions and wheel rotation were also installed. Two types of excavation methods were studied during the trials a) *controlled excavation* and b) *aggressive excavation*. The difference between the methods is the strategy the driver uses when first penetrating and then scooping the muck pile. Marshall, Murphy and Daneshmend discuss an approach for automatic control of the scooping based on the results of the trials and suggest the need for force-based control that does not prioritize trajectory following by the bucket, which can be accomplished with *admittance control*. The suggested system is based on force feedback to an admittance controller that reacts to bucket-rock interaction forces by changing the bucket cylinder's retraction velocity rather than its position.

Translating the "Simultaneous Localization And Map building" (SLAM) concept to LHD automation implies that a navigation system based on SLAM continuously estimates a 3D map of the walls, roof and roadways of the drifts, spilled rocks on the roadways and infrastructure such as water tubes, ventilation tubes, electrical wires, cabinets, etc. and the LHD's pose relative the map. Dissanayake, Newman, Clark and Durrant-Whyte (2001) discuss a general solution to the SLAM problem. Applications in underground mines are considered by for instance Lavigne and Marshall (2012) who discuss large-scale mapping (2012). Still there is no general SLAM solution for underground applications, Le Cras (2012).

Path tracking for articulated vehicles is discussed by for instance Hemami and Polotski (1996), DeSantis (1997), Hemami and Polotski (1998), Altafini (1999), Polotski (2000) and Bolzern and Locatelli (2002). The use of a ghost vehicle to solve the tracking problem is discussed in Bolzern, DeSantis, Locatelli and Masciocchi (1998).

Corke and Ridley (2001) and Ridley and Corke (2001, 2003) discuss kinematics of articulated vehicles such as the LHD.

Scheding, Dissanayake, Nebot, and Durrant-Whyte (1997,1999), Madhavan, Dissanayake and Durrant-Whyte (1998) discuss autonomous navigation experiments in underground mines based on wheel slip estimation.

A detailed review is done in the following based on the discussions by Mäkelä (2001a, 2001b) – referred to as *Mäkelä* in the following, Duff, Roberts and Corke (2002, 2003), Duff and Roberts (2003), Roberts, Duff and Corke (2002) – referred to as *Duff et al.* in the following -, and Marshall, Barfoot and Larsson (2008) – referred to as *Marshall et al.* in the following. The remainder of the section is divided into sub-sections in order to structure the discussion.

2.1 Overview

One common factor that separates the hauling/tramming techniques discussed by Mäkelä, Duff et al. and Larsson et al. from HUNS is that these systems are referred to as *infrastructure free*. Such systems use the walls of the drifts as the references, and not artificial references such as retro-reflectors used by HUNS.

The hauling/tramming technique of HUNS and the hauling/tramming technique discussed by Mäkelä is classified as *absolute navigation*, implying that the absolute position of the autonomous vehicle is known at all times relative some fixed real-world co-ordinate system, Dragt, Camisani-Calzolari and Craig (2005). The hauling/tramming technique discussed by Duff et al. is referred to as *reactive navigation* implying that the LHD reacts to objects in its environment to continue to move forward.

Both Mäkelä and Marshall et al. discuss methods where the LHD is used to teach the route and create the localization references based on laser measurements to the walls of the drifts. The resulting localization map and reference path of the teaching procedure and office work is later used in the automated hauling and tramming of the LHD.

The weakness of the pure reactive navigation is the lack of path planning according to Duff et al., typically in intersections where the identity of the intersection is important and the action to take. The knowledge of occasional positions in the layout is referred to as *opportunistic localization*, a knowledge that makes it possible to compensate for the weakness of the pure reactive navigation.

The localization and the control are decoupled in the discussion by Duff et al. and the vehicle control is performed at a higher rate compared to the localization since the localization is not important for the control of the vehicle itself. The localization is mainly used for strategic decisions during automatic driving of the LHD. 2D laser scanners are used to measure the walls of the drifts.

Duff et al discuss a nodal map that can be constructed from a traditional mine map or by driving the LHD along the routes. Intersections and end points are defined as nodes and connected by segments. The reference path of the LHD is calculated online based on obstacle detection. The walls of the drifts are measured with the laser scanner and the walls are interpreted as obstacles to keep away from.

2.2 Preparation

Mäkelä discuss a method where the reference path is taught by driving the LHD in both directions. Teaching can be made either by a driver in the cabin or by a remote operator. The teach-in procedure includes recordings of the heading and the curvature of the LHD. The environment is also recorded during the teaching. The model for the environment is based on a set of points where the laser distance scanner has hit the wall of the drift. Two laser rangefinders are used to measure the walls of the drifts. An articulation angle sensor, an odometer and a gyroscope are used for dead reckoning calculations.

During the teaching, the environment model is built mainly relying on measurements by the range sensors perpendicular to the LHD. The resulting environment model is wall profiles of the drifts with a resolution of approximately 10 cm. The model of the environment differs in

forward and rearward driving direction since there might be a slight difference depending of the driving direction of the LHD.

The data from the teach-in procedure is post-processed for smoothing of the route based on the B-spline and speed profile determination. The reference trajectory consists of (x,y) points separated approximately 20 cm in which also the heading and curvature are defined together with the drive speed. Matching the start position with the end position does the correction of the dead-reckoning drift during teach-in. The speed profile is independent of the teach-in procedure and takes into account the curvature of the path.

To handle the complexity of a layout consisting of more than one draw-point and ore-shaft, the concept of route segment and nodes has been introduced since Mäkelä finds it impractical to teach all route combinations separately. Loading points, dumping points and intersections are examples of nodes, which are connected by segments. The function handles extension of the layout as new segments attached to existing segments.

The nodes discussed by Duff et al. as well as the segments can be supported by *hints* that are typically experience based after driving some cycles in co-pilot mode when the remote operator commands the LHD. Hints are specific for certain sections of the route and are for instance; maximum speed and drive left/right.

Marshall et al. discuss a teaching method where the LHD is driven along a desired route manually or tele-operated when data are logged from a hinge encoder, a drive shaft encoder and front/rear laser range finders. An IMU can also be used but is optional. The route is assumed to be collision free.

During route profiling, an off-line procedure, the logged data are processed into a format suitable for automatic driving. The result of the off-line procedure is the route profile that consists of four components; a path profile, a pause profile, a sequence of locally consistent metric maps and a speed profile. The path profile consists of equally spaced points, each 0.5 meter, containing the 2D pose and articulation angle.

The locally consistent metric, grid-type, maps of the mine environment along the path profile is generated based on odometer data and range finder data. Each cell of the grid is either "occupied" or "not-occupied" depending on the number of times the range sensor senses the wall at a location represented by the cell at certain distance. Marshall et al. use an atlas of metric maps attached along the path to form an overall route profile resulting in a globally consistent monolithic map. The speed profile specifies the speed of the LHD at each path point and takes into consideration travel direction, width of the drifts, and curvature. Pause profiles define for instance tasks such as bucket handling.

Re-profiling is only needed in case of major changes in the environment.

2.3 Initialization

The initialization procedure discussed by Mäkelä is dependent on a rough estimate of the real initial position at the start of the initialization for the wall profile-matching algorithm to work. Driving the LHD slowly in "wall following mode" in the middle of the drifts does the initialization of the pose estimate. After driving approximately 5 meters, the position is estimated, and then the driving continues for another five meters so that the heading can be estimated.

Marshall et al. can place the vehicle within five meters and 20 degrees of the taught start pose for the initialization to work.

2.4 Localization

The navigation technique discussed by Duff et al. relies mainly most of the time on *weak localization* (odometry), which is improved at nodes in the layout such as intersections, which are used as landmarks.

The pose estimators discussed are Kalman filter based; the filters are updated with either the turning rate (Mäkelä) or the steering rate (Marshall et al.) and the speed of the vehicle. The correction methods differ but are based on laser measurements to the walls of the drifts. The output from the filters is the 2D pose.

Mäkelä does the correction every meter based on a wall profile of five meters. The matching algorithm estimates the drift in the dead reckoning pose since the last pose correction by comparing the environmental model with the measured wall profile. The drift is used as the innovation in a "Kalman type of filter" to correct the states of the filter. The update of the dead reckoning is done at a rate of 25 Hz.

The localization (and control) algorithms discussed by Marshall et al. are updated at a rate of 25 Hz. The pose estimator is based on the Unscented Kalman Filter (UKF). Simulated range finder readings are calculated for each of the seven σ-points of the UKF to the "occupied cells" in the active metric map. A σ-point is a pose estimate of the vehicle at the current sampling instant with certain uncertainty. The σ-points are time update to the current sampling instant of the last corrected state and covariance. All seven σ-points and corresponding simulated readings are used in the calculation of the expected reading. The difference between the measured reading and the expected reading defines the innovation that is used to correct the states and the covariance of the UKF at the current sampling instant.

2.5 Control

The control points discussed for the guidance along the reference path are either the *current position of the control point* or a *predicted position of the control point*. The references path points discussed are either the *nearest point on the reference path* or a *selected point on the reference path ahead of the vehicle*. The control variables relates to the active part of the reference path and the control (navigation) point on the vehicle. The control variables are feed-forward, feedback or *follow-the-carrot,* Herbert (1997), variables. The input to the guidance controllers is the 2D pose estimate (Mäkelä and Marshall et al.), hints (Duff et al.) and the reference path. The control point is in the middle on the forward axis in the discussions by Mäkelä and Marshall et al.

An important function in the navigation technique discussed by Duff et al. is to find free space ahead of the LHD. A reference path ahead is calculated on line based on the free space determined. The reference path is based on an active contour method; the left wall of the drift and the right wall of the drift are regarded as obstacles that transmit energy. The area between them is the free space and the lowest energy field is somewhere in the middle of the

walls. The reference path, referred to as *snake*, is selected to be in the free space where the radiating field from the obstacles is low to minimize the risk of collisions between the LHD and the walls of the drifts. The reference path can be biased either to the right or to the left in the radiating field to prepare for cornering in an intersection for instance.

The control discussed by Duff et al. is based on the *follow-the-carrot* approach, implying that goal of the control is to aim the control point on the LHD to a point some distance a head on the references path. If the reference path starts to curve, the line between the aiming point and the control point on the LHD might not align with the reference path making the LHD shortcut the reference path.

Table 1. High-level control variables, Mäkelä.

Variable	Description
d_{adv}	The distance of the reference point ahead of the control point calculated as a time parameter multiplied with the speed of the vehicle.
c_{ref}	The reference curvature of the reference point ahead on the reference path.
d_1	The distance between the current position of the control point and the nearest point on the reference path.
h_{err}	The difference between the tangent of the reference point ahead on the reference path and the current heading of the control point.
d_2	The distance between a predicted position of the control point and the reference point ahead on the reference path. The prediction is based on the current heading of the control point.
d_3	The distance between a predicted position of the control point and the reference point ahead on the reference path. The prediction is based on the current curvature of the vehicle.

The parameters of the controller have to be tuned to adapt to the dynamics of the LHD such as delays in the hydraulic system for the steering in the discussion by Mäkelä. Therefore, the reference point for comparison is chosen to be a certain distance "ahead" of the current position. The output from the high level controller is the reference curvature (*cur*) and the speed. Mäkelä discuss the curvature of the vehicle, which is the reciprocal of the radius of the path the vehicle would drive with the current articulation angle.

The control law is $cur = c_{ref} + K_h h_{err} + K_1 d_1 + K_2 d_2 + K_3 d_3$, where K_i are tuning weights. The control law is a combination of linear feedback and feed forward.

Mäkelä uses low-level controllers to maintain the reference value of the articulation angle and the drive speed. The steering controller is a PI-type of controller.

Table 2. High-level control variables, Marshall et al.

Variable	Description
ε_L	The distance between the current position of the control point and the nearest point on the reference path.
ε_H	The difference between the predicted heading of the control point and the tangent in the nearest point to the predicted position on the reference path.

Marshall et al. handle the lateral errors and the heading errors of the forward frame of the articulated vehicle in the outer loop of the position controller. Because of the limited bandwidth of the steering system, it is necessary to look ahead along the reference path when calculating the heading error.

The control law corrects the steering rate as $\eta = -k_1\varepsilon_L - k_2 v \sin\varepsilon_H$, where k_i are tuning parameters and v is the speed of the LHD. The control law is a combination of linear feedback and non-linear feedback.

The input to the low level controllers discussed by Marshall et al. is the desired steering rate and the vehicle speed. Standard robust controllers are used for the low-level control, assuming decoupling between the steering and driveline dynamics. The low-level controllers runs at a higher frequency compared to the outer loop.

3 System details

The navigation system is connected to the traffic control system that issues high level commands relating to automatic tramming/hauling and dumping and at times to a remote operator desk in the control room. The commands are executed in HUNS and piped to the machine controller, see figure 3.

The system architecture implies that commands can be taken from both the traffic control system and the remote control system and mixed by HUNS in the control of the LHD. This is an important property for the driver assisting system for remote controlled excavation of fragmented rock where pure tele remote commands are mixed with automatic generated commands that are transmitted to the machine controller. The tele remote commands are for instance the steering, the gear selection and the brake command. The automatic generated commands are the speed of the boom cylinders and the speed of the bucket cylinder.
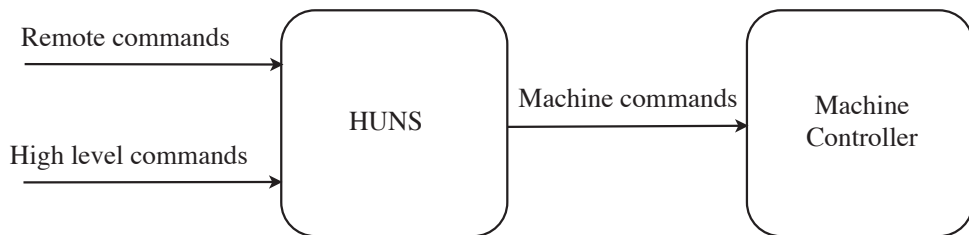
Figure 3. The navigation system HUNS and the machine control system. The inputs to the machine controller are the commands from HUNS if the LHD is in automatic mode. The inputs to the machine controller come from the controls in the cabin of the LHD if the LHD is in manual mode.

There are four operating modes.

- *Automatic mode*. The LHD is only connected to the traffic controller. The LHD navigates the layout in the drifts autonomously.

- *Camera-tracking mode*. The LHD is connected to a remote operator desk. The remote operator controls the cameras on the LHD.

- *Semi-automatic mode*. The remote operator controls the speed of the LHD and the bucket height and angle. The articulation angle is automatic controlled.

- *Remote control mode*. The remote operator has complete control of the LHD using the controls on the operator's desk. Remote controlled excavation is done in this mode.

4 Navigation references

The systems for the definition of the navigation references used is a CAD based tool *LDS* to define the reference paths of the production area and *AutoSurveyor* to survey the 2D positions of the retro-reflectors on the walls of the drifts, Åström (1991, 1993).

4.1 Reflector map

The reflector map contains the 2D position in a co-ordinate system of the production area of each retro-reflector, a single stripe of tape 25 mm in width and approximately 1 meter in length.

Figure 4. The photograph shows the SUV used for the surveying of the retro-reflector positions. The laser scanner for the retro-reflectors is mounted on a pole in the centre of the vehicle above the rear axis. The SUV was equipped with two distance measuring SICK LMS200 laser scanners and an IMU mounted on the roof for experimental purposes when the photograph was taken.

The heading is also defined for the retro-reflectors as a part of the association function of measured bearings to retro-reflectors. If the laser scanner is outside the sector defined by the heading of the retro-reflectors ±90 degrees, a measured bearing cannot originate from the retro-reflector. So called "walls" are also defined in the reflector map as another part of the

association function. Walls are typically used to separate cross-drifts from each other. If walls are not used, retro-reflectors in several cross-drifts can be in-line with the laser scanner and thus making it impossible to associate the measured bearing to one retro-reflector.

The retro-reflectors are surveyed using a SUV that is equipped with a laser scanner and encoders in the centre of the rear wheels so that the 2D positions of the retro-reflectors and the pose of the SUV can be estimated while driving in the production area. Definitions of walls and the heading of the reflectors are done off-line.

Madhavan and Whyte (2005) discuss a similar procedure to the surveying of the retro-reflectors except that natural landmarks are estimated instead of artificial landmarks (the retro-reflectors).

4.2 Segment map

The reference path consists of 7th order polynomial segments connected to points (nodes) in the layout of the production area. The reason for the change of representation compared to the field trials was the bigger LHD used in the production period. The X4Y4 representation could not be used to create collision free routes in all intersections. The segments are designed such that there are no discontinuities in the points where the segments are connected to each other. The end point of one segment in the reference path is the start point of the next segment. There can be more than one ingoing segment to a point and more than one outgoing segment from the point. As an example - one outgoing segment continuous in the footwall drift and another segment goes in to a cross drift.

All segments of the production area are stored in HUNS, but it is the traffic control system that orders the segments to execute.

The polynomial segment is defined as

$$y = p(x) = a_7 x^7 + a_6 x^6 + a_5 x^5 + a_4 x^4 + a_3 x^3 + a_2 x^2 + a_1 x^1 + a_0 x^0 \qquad (1)$$

Where the coefficients $a_i, i = \{0,1,2,3,4,5,6,7\}$ defines the curve shape.

Both the X4Y4 curve and (1) have properties for smooth path following, namely

- Continuous curvature $K(s)$. The variable s is the distance along the path.

- Continuous curvature change with distance Kd/ds.

The main difference is that continuous curvature change only holds for 90-degree curves in the case of the X4Y4 curve. The polynomial segment has no such limitations.

The user marks the start point and the end point of the segment in the drift on the 2D drawing of the production area, which is imported from the CAD mine map and selects the curvature in each point. If the start point is the end point of another segment, the curvature in the start point is set to the curvature of the end point of that segment The coefficients are automatically calculated such that the conditions for continuous curvature change holds also at the connecting point to other segments. The resulting segment is drawn on the screen.

The sweep area of the LHD can be simulated in LDS to check for collisions between the LHD and the walls of the drifts (measured by the mine surveyors), or the retro-reflectors that

are imported from AutoSurveyor. The user also defines the gear to use on the segment (1-4) and the driving direction. If the corresponding nominal speed of the selected gear implies a change of curvature that will require an articulation angle speed of more than the maximum articulation angle speed of the LHD plus some tolerance, the segment becomes "red marked" and the user has to use a lower gear. The segment will also be red-marked if the curvature somewhere on the segment corresponds to an articulation angle that exceeds the limitation of the LHD plus some tolerance. If this happens, the start point or end point of the segment has to be moved. The typical time it takes to define a segment map for the complete production area in the Kiruna mine is one or two days including the definition of the references for the control of the bucket height and angle.

Very seldom the segment map had to be redone after the first runs with the LHD in the production area, implying that the simulation tool in LDS is very effective.

5 Tramming and hauling

5.1 Pose estimator

The states of and output from the position estimator is the 2D pose of the mid point of the rear axis of the LHD in a local co-ordinate system of the production area.

The estimator is based on the Extended Kalman Filter (EKF) discussed by Wiklund, Andersson and Hyyppä (1988) and the kinematic model of articulated vehicles discussed by Larsson, Zell, Hyyppä and Wernersson (1994). The input to the estimator is the articulation angle and the speed of the LHD. If the difference between a measured bearing and an expected bearing is small enough, the measurement is associated to that retro-reflector, provided that there is only one candidate retro-reflector, and used to correct the pose estimate in the EKF, Hyyppä (1989, 1991). In case of no measurements or no measurement possible to associate to a retro-reflector in the map, the pose estimate is not corrected and simply updated by the dead-reckoning system to the next sampling instant.

A pose estimation safety system handles the lack of measured bearings or bearings that cannot be associated to retro-reflectors in the reflector map.

At blasting, the cross-cuts in the sub-level cave mine in Kiruna is shortened with three meters implying that retro-reflectors close to the draw point will disappear into the ore flow at some point, which is not a problem since the pose estimator is not dependent of measurements to particular retro-reflectors.

When the navigation system is powered on, the pose of the vehicle is unknown and an initialisation of the pose estimate is necessary. The initialization procedure requires the vehicle to be standing still during the time measured bearings from one revolution of the rotating head of the laser scanner are used to triangulate the pose, a method that requires at least four measured bearings. The triangulated pose is used as the initial 2D pose estimate of the vehicle. The initialization is done automatically without the requirement of a rough position defined by the remote operator or an external system.

The pose estimator is designed to be simplistic with a low computational demand. The rotational speed of the laser scanner is tuned so that during the sampling period of 0.025 second, the laser beam rotates approximately 100 degrees which, assuming well spread detectable retro-reflectors around the laser scanner, makes the angular difference between bearings used to correct the pose estimate almost perpendicular from one sample to another which will keep the variance in the estimated positions to a minimum.

The motion model used in the EKF is discussed in the appendix in section 10.

5.2 Guidance controller

The guidance controller calculates set values for the articulation angle, articulation angle speed and the drive speed of the vehicle.

A ghost vehicle, a tricycle, is used to guide the LHD along the reference path. The relation between the tricycle and the articulated vehicle is based on two assumptions.

The rear axis of the tricycle - or the extension of it - is assumed to go through the hinge of the articulated vehicle.

The other assumption concerns the relation of the rotational speed of the front frame and the rear frame of the articulated vehicle relative the tricycle. Let subscript f denote the front frame, subscript r denote the rear frame, γ denote the articulation angle, and ω denote the rotational speed, the assumption then implies that

$$\omega_f = -\omega_r = \frac{\dot{\gamma}}{2} \tag{2}$$

The assumptions make the relation between the physical and fictive vehicles unique and make it possible to analytically calculate the position of the fictive vehicle relative the physical vehicle in computational efficient manner.

Denote the transversal velocity and the heading of the front frame in the coordinate system of the fictive vehicle v_f and θ_f respectively, see figure 5. The velocity of the articulation hinge in the x and y direction respectively is then assuming no sideslip of the articulated vehicle

$$\dot{x}_j = v_f \cos \theta_f + \omega_f L \sin \theta_f \tag{3}$$

$$\dot{y}_j = v_f \sin \theta_f - \omega_f L \cos \theta_f \tag{4}$$

The first assumption implies that $\dot{x}_j = 0$, which gives

$$v_f = -\omega_f L \tan \theta_f \tag{5}$$

Inserting (5) in (4) gives after some manipulations

$$\dot{y}_j = -L\omega_f \frac{1}{\cos(\theta_f)} \tag{6}$$

The distance d in figure 5 can be calculated based on (6) as

$$d = \left| \int \dot{y}_j dt \right| = \left| -L \int \omega_f \frac{1}{\cos(\theta_f)} dt \right| = \left| -L \int \dot{\theta}_f \frac{1}{\cos(\theta_f)} dt \right| = \left| -L \ln \tan \frac{\pi}{4} + \frac{\theta_f}{2} \right| \tag{7}$$

From the second assumption (2) we get

$$\theta_f = \int \omega_f \, dt = \int \frac{\dot{\gamma}}{2} dt = \frac{\gamma}{2} \tag{8}$$

which finally result in

$$d = \left| -L \ln \tan \frac{\Pi + \gamma}{4} \right| \tag{9}$$

The control point that follow active segment of the reference path is the mid point on the rear axis of the tricycle. The tricycle is aimed in the travelling direction of the LHD.

Five control variables are used in the high-level controller; $(\hat{d}_{err})$ is the lateral error, $(\hat{\theta}_{err})$ is the heading error, $(\hat{K}_c)$ and $(\hat{K}_{c\_T})$ are the curvature of the reference path corresponding to the current and the predicted pose of the control point, $(\frac{d\hat{K}_{c\_T}}{ds})$ is the change in curvature in the reference path corresponding to the predicted pose of the control point.

The set angle and the set angle speed for the fictive tricycle are calculated with the feedback gains l_d and l_θ, the wheelbase L_t and the speed v_t of the fictive tricycle as

$$\gamma_t^{set} = -l_d \hat{d}_{err} - l_\theta \hat{\theta}_{err} + L_t \hat{K}_c \tag{10}$$

$$\dot{\gamma}_t^{set}(T) = \frac{L_t}{1 + (L_t \hat{K}_{c\_T})^2} \frac{dK_{c\_T}}{ds} v_t \tag{11}$$

The set values for the fictive tricycle are transformed into the corresponding set values for the articulated vehicle.
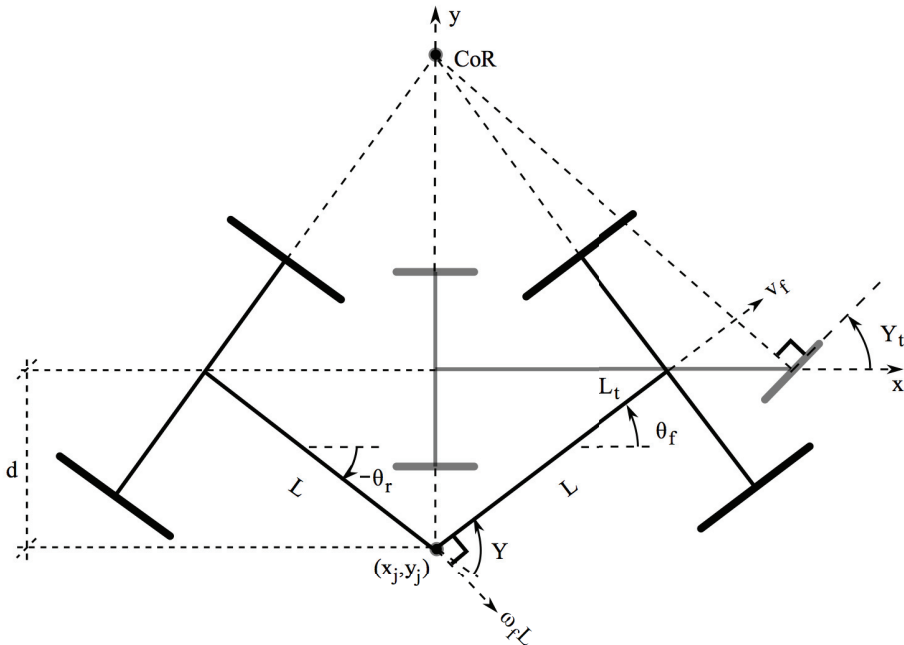
Figure 5. The relation between the physical articulated vehicle (black) and the fictive tricycle vehicle (grey) is illustrated in the figure.

The transformation of the set angle for the tricycle to the set angle for the articulated vehicle is based on the assumption of a common centre of rotation (CoR) for both vehicles, see figure 5.

The transformation is done using two equations; one of them solved numerically, see details in the appendix in section 10.

The five steps used in the guidance controller are summarized in figure 6.
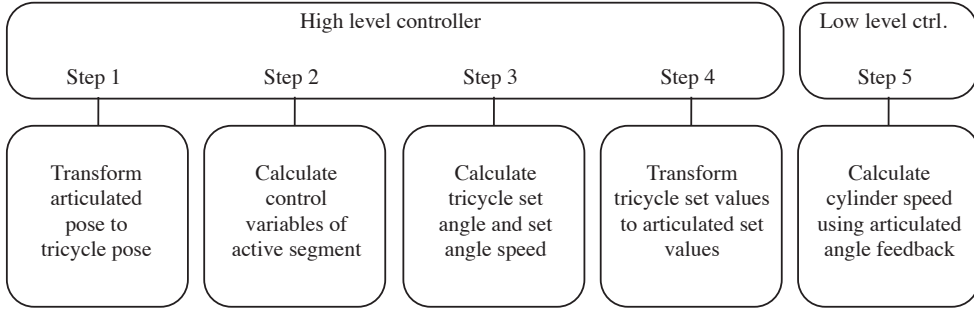
Figure 6. The control of the articulation angle is done in five steps as illustrated in the figure. The control of the drive speed of the vehicle is omitted.

Table 3. The distance d in meter for some values of the articulation angle γ is shown in the table for an articulated vehicle with wheelbase 2.55 meter (TORO2500E).

γ	0.0°	2.0°	5.0°	10.0°	20.0°	30.0°	40.0°	80.0°	160.0°
d	0.0	0.0445	0.1113	0.2228	0.4473	0.6753	0.9088	1.9454	6.2124
d / γ		1.2751	1.2754	1.2766	1.2815	1.2898	1.3017	1.3933	2.2247

A linear approximation can be used for practical values of the articulation angle.

Table 4. Characterization of high-level control variables as discussed in section 2.

Variable	Type	Control point	Path point
$\hat{d}_{err}$	Feedback	Current	Nearest
$\hat{\theta}_{err}$	Feedback	Current	Nearest
$\hat{K}_c$	Feed forward	Current	Nearest
$\hat{K}_{c\_T}$	Feed forward	Predicted, time based	Nearest
$\dfrac{d\hat{K}_{c\_T}}{ds}$	Feed forward	Predicted, time based	Nearest

The parameter values of the high level controllers were the same independently of LHD, of the load in the bucket, of the driving speed of the LHD and of the tyre wear implying that the solution proved to be robust. Careful tuning of the parameters during practical tests with the first commissioned LHD was necessary to gain acceptable performance during normal and provoked conditions.

The other task of the guidance controller is to control the drive speed of the vehicle, which is a straightforward task compared to the steering control.

A safety system will stop the LHD if the lateral error and/or heading error to the reference path exceed limits.

6 Assisting system for remote controlled excavation

Low scoop weights of tele remote excavated buckets were early identified in the 10-year production period in the Kiruna mine. A driver assisting function was implemented to improve the situation. The function implies that the remote operator only controls the drive speed and articulation angle during the excavation. The control of the boom cylinders and the bucket cylinder is done automatically. The function emulates the skilled drivers excavation of the bucket in the muck pile. The function uses the measured speed of the LHD as the feedback control variable and the pose estimate to detect wheel spin.

The excavation part consists of five sequences.

Sequence 1. The bucket has been positioned in the correct position and the operator commands the LHD to drive forward on 1st gear. The driver assisting function is initiated when the drive speed of the LHD is 1 m/s with some tolerance.

Sequence 2. The drive speed decreases when the bucket hits the muck pile. When the drive speed drops below v_{start} m/s, the bucket is lifted Δz_{start} mm in order to get a distribution of the load between the front axle and the rear axle of the LHD that prevents wheel spin, which is *traction control*.

Sequence 3. Tilting the angle of the bucket controls the drive speed of the LHD. If the drive speed drops below v_{min} m/s, the bucket cylinder speed is set to v_{bu_max} m/s in order to prevent the vehicle to come to a stop. If the drive speed exceeds v_{max} m/s, the bucket cylinder speed is set to zero in order to slow down the LHD. When the drive speed of the LHD, v, is between v_{min} and v_{max}, the bucket cylinder speed v_{bu} is

$$v_{bu} = \frac{v - v_{max}}{v_{min} - v_{max}} v_{bu\_max} \tag{12}$$

Sequence 4. When the bucket angle has reached its maximum value, the bucket is lifted Δz_{stop} mm in order to maximize the filling of the bucket.

Sequence 5. The function signals that the scooping is done. The operator starts reversing the LHD out from the muck pile. When the vehicle has moved Δx_{start} meter from the stop position of the scooping, the bucket is lowered to its lowest position and the bucket angle starts to change according to a saw-tooth shaped signal. The shaking of the bucket continues until the LHD has moved Δx_{stop} meter from the stop position of the scooping. The shaking of the bucket is done in order to remove loose rocks from the bucket.

When sequence 1 starts, dead reckoning only pose estimation is started in parallel to the ordinary retro-reflector based pose estimation. This makes it possible to detect wheel spin, which is highly unwanted during excavation. Spinning wheels will significantly reduce the filling and also damage the road. Denote the estimated distance travelled since the start of driver assisted excavation Δs_{dr} based on the dead reckoning and the estimated distance

travelled since the start of driver assisted excavation Δs_{rr} based on the retro-reflector corrected pose estimation. Then if $\Delta s_{dr} - \Delta s_{rr} > \Delta s_{spinn}$, where Δs_{spinn} denotes the maximum allowed difference in calculated distance between the two methods, wheel slip is considered to be detected. If wheel slip is detected, the current driver assisted excavation sequence is interrupted and the bucket is lifted Δz_{spinn} meter. This is done in order to stop the wheels from spinning. If the spinning of the wheels continues after the lifting of the bucket, the driver assisted excavation sequence is aborted and the operator has to take over the controls.

Traction control to prevent wheel spin has a positive effect not only on the production but also on tyre wear.

If the remote operator starts to manoeuvres the joystick for the control of the bucket height and angle during excavation, the driver assisted excavation is aborted and the controls of the boom and bucket cylinders is handed over to the operator. One example when this is relevant is if there is a very large boulder in the muck pile requiring a completely different excavation technique.

The pose estimation is used in a safety system that prohibits excavation too far into the draw point. If the rock flow is stopped; the result is that the penetration of the muck pile is initiated further into the drifts for each loaded bucket. This is a dangerous situation since the LHD then drive into parts of the drift with no steady rock overhead. If the ore flow starts during excavation, the risk is that the LHD will be buried under the muck pile.

7 Underground field trials

7.1 Driver assisted excavation

The evaluation of the driver assisted excavation function was done in production settings in the winter of 2002 with two LHD's in two production areas in the Kiruna mine.

Table 5. Excavation data.

Tele remote excavation			Driver assisted excavation				
Buckets	Av. wgt	Tonnes	Buckets	Av. wgt	Tonnes	LHD	Reading
32	20.57	658.24	87	24.08	2094.96	598	20020220
470	21.63	10166.10	260	23.08	6000.80	598	20020226
1169	21.68	25343.92	1095	21.89	23969.55	598	20020311
474	20.62	9773.88	979	22.11	21645.69	599	20020220
886	20.51	18171.86	470	21.28	10001.60	599	20020226
361	18.01	6501.61	299	19.28	5764.72	599	20020311

3392 buckets were tele remote excavated in total compared to 3190 driver assisted excavated buckets. The average weight of the tele remote buckets was 20,82 tonnes compared to 21,78 tonnes for driver assisted buckets. The difference is 4,6% increase of the weight in driver assisted buckets compared to tele remote buckets. The time spent excavating was roughly the same independent of method used. The remote operators were not instructed to use a particular excavation method; the choice of method was completely up to the remote operator. The reason to why a particular method was chosen is unknown.

7.2 Hauling/Tramming

The system discussed by Mäkelä was first tested in an open area and thereafter in a 190-meter tunnel. The speed of the LHD was up to 4.5 m/s on straight parts and 2.0 m/s in the steepest curves. The maximum deviation from the reference path was in the range of ±15 cm with the repeatability from one run to another better than that, typically ±5 cm. Smooth parts in the tunnels proved to be a tough situation for the matching algorithm to handle. However, it turned out that even small variations gave enough information for the longitudinal estimation of the position. The drift corrections based on the environmental model proved to be sufficient to compensate for slip and lack of accuracy in the used gyro. The LHD was able to negotiate the curves at a speed comparable to an experienced human driver. The field results are based on several hundred hours of driving.

Tests with the predictive part of the high level controller disabled were also performed at reduced speed. It was concluded that it is not enough to consider only the current position and heading, the reference path ahead of the LHD has to be taken into account.

Field test discussed by Duff et al. was done in an artificial test mine of 300 meter in length containing curves, sharp corners, a loop and a large "room". The conclusion of the field trials was that the LHD was driven along the 300-meter route including two 90-degree corners and a sweeping loop at speeds up to 18 km/h over a period of time of one hour without human interaction. During the test, the LHD "took better line" and reacted faster compared to a human operator who had an advantage in "blind corners" because of the memory of the corner profile from the previous run. Field test were also performed in an underground mine during two days, half a day were spent on acquiring hints in a tunnel of 150 meter in length. In the main test the LHD drove autonomously for an hour, periodically switching back to the tele remote system to dig and dump. At no stage during the underground trails did the LHD touch the walls of the drifts.

The system discussed by Marshall et al. was tested for several weeks in an underground mine with loaded and un-loaded bucket. The resolution used in the metric maps was 10 cm, which provided to be sufficient for the performance of the localization algorithms. The result of the field trials was that the system could drive the LHD on top gear (4th) and was faster than a human operator in some sections, typically on straight parts in narrow drifts, and slower at for instance direction switches. The positioning of the LHD was within the project goal of ±50 cm in all but one run.

HUNS tests were done in the southernmost production area in the Kiruna iron ore mine on level 740 meters in December 1996 and January 1997. Reflectors were mounted on the walls in the footwall drift and in two cross drifts in the ore body. This arrangement made it

possible to test high speed driving as well as cornering. The angle of the cross drift relative the footwall drift was 106 [degrees] and 90 [degrees] respectively.

The navigation system was tested during normal operational conditions.

- Driving straight and in curves.

- Driving with empty and full bucket (13 tonnes).

- Varying temperature of the oil in the system for steering and braking.

The navigation system was also tested during provoked operational conditions.

- Logs with height 0.15 [m] and depth 0.20 [m] were used as road bumps.

- Overloaded bucket (> 13 tonnes).

- Reflectors out of position compared to the reflector map.

- Blocked reflectors.

- Low tyre pressures.

The cycle time in automatic mode were compared to the cycle time in manual mode when an experienced driver drove the LHD.
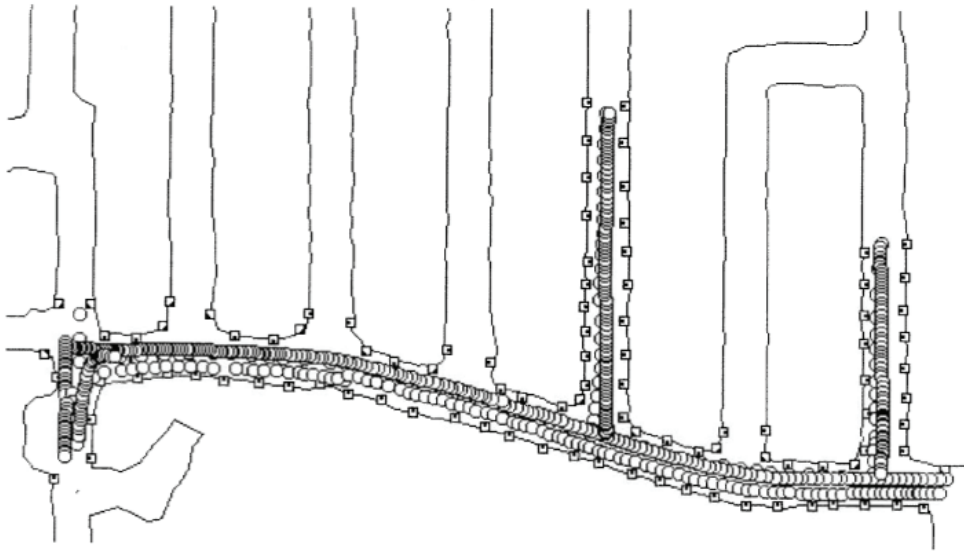
Figure 7. The figure shows the test area for the underground field trials.

Figure 7 is a screen dump from AutoSurveyor. The reflectors are represented by squares; the circles are the positions of the laser scanner where measurements were collected. The distance between the cross drifts, going into the ore body, is approximately 25 meters. The cross drifts are connected to the footwall drift which runs in parallel with the ore body. AutoSurveyor was later modified, so that the reflectors are surveyed while driving.

Initial field-testing of the system was carried out over a period of several weeks during December 1996 - January 1997.

The LHD was running on 4th gear when driving straight and 3rd gear in curves. The repeatability was within ± 0.05 meters at straight driving, within ± 0.10 meters in curves and within ± 0.05 meters at reversing points. The results were obtained by painting the roadway at check points, run the same path several times and then measure the deviation.

In order to test the cycle time, the automatic system was compared to a manual driver, one of the most experienced in the mine. The test cycle started in the entrance to the production area, continued into the rightmost cross drift in figure 7 and then back again.

The manual driver was approximately 12% faster than the automatic system mainly due to the "free wheeling" approach used in the curves. The manual driver did not gear down, instead he released the throttle and let the machine roll by itself and used the brakes to reduce the speed. The automatic system geared down from 4th to 3rd gear when negotiating the curve.

The manual driver had to make a quick correction when negotiating the second curve in one of the runs - at t≈60 seconds, the green curve in the figure below - implying that the margin of safety was too low, i.e. over speeding. Note the difference of the profiles in manual mode and the lack of difference in automatic mode.
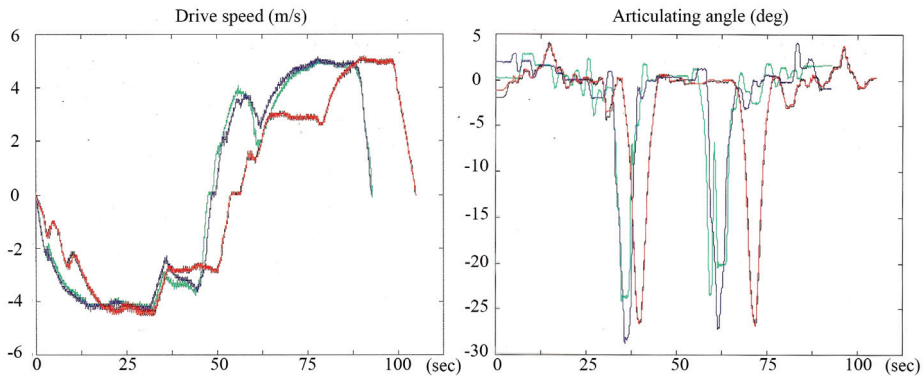
Figure 8. The figure shows the speed and articulation angle profiles during two runs in manual mode (blue and green curves) and two runs in automatic mode (red and black curves).

When driving over logs on 4th gear with loaded bucket, the rear wheels became airborne for a short while and thus moving the rear frame of the LHD to the side, see figure 9.
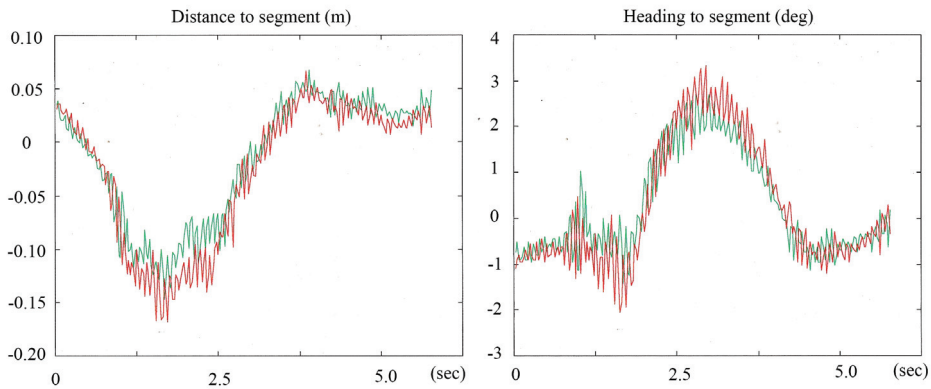
Figure 9. The figure shows the control errors in two runs with loaded bucket over a log on 4th gear, the front wheels hit the log first. Note the repeatability in the two runs.

In order to test the accuracy of the models used in the control loop, the navigation system was set in "blind mode" implying only dead reckoning based pose estimation. The LHD was ordered to start drive straight and then, after approximately 25 meters, make a turn either into a cross drift or into the footwall drift and drive another 25 meters. The result of the tests was that the LHD managed to fulfil the order without any collisions.

Some further discussions regarding the X4Y4 representation of the reference path and the LHD's ability to follow the path are found in Andersson, Mrozek, Åström and Hyyppä (1997).

8 Key performance indices

The key performance indices of the LHD automation system are presented in table 6. The figures are based on data from the 10-year production period 1999 to 2009. It is important to note that the KPI's are valid for the use of the LHD's in automatic mode.

We have not been able to find such figures when we have done the literature review. One of the later papers discussing navigation systems for LHD automation is the work by Marshall, Barefoot and Larsson (2008), who came to the same conclusion.

Citation from Marshall et al.

> "…This conclusion [widespread implementation of automatic tramming functionality in the mining industry yet to occur: our remark] is merely anecdotal because we are not able to cite any scientific reports that publicly divulge the performance of existing technologies in a true production setting..."

Therefore, the figures in table 6 are likely the first reporting of the performance of an LHD automation system in a production setting in a scientific paper.

121

The bucket payload is determined with a scale (LR810 Loadrite) based on measuring the hydraulic pressure in the lift cylinders, when the boom and bucket mechanism reaches a triggering position determined in the calibration procedure. The calibration of the scale is done using a known weight with the boom mechanism in the trig position.

The tramming distance is the one-way distance between the draw point and the ore pass, and is measured by the odometer and the navigation function. The instantaneous capacity is determined as the loaded tons during the time in operation. The average speed is calculated as the total trammed distance during the time in operation and thus including the whole loading cycle with bucket filling, tramming to ore pass, dumping and tramming back to the draw point.

The transport performance is defined as the loaded tons during time in operation times the tramming distance. The transport performance takes into consideration the influence of the tramming distance on the instantaneous capacity and can be used to roughly compare the loading performance in different production areas.

The utilization is the time in operation during 24 hours. The system availability is the time when all the system components are capable during the planned production time of 24 hours per day. The system components are the HUNS, the traffic control system LUCS, the remote control system LRCS, the communication system WUCS and the area isolation system. The LHD machine itself is excluded from the system availability.

It is important to keep in mind the planning of the overall ore flow in the Kiruna mine when studying the KPI's. The planning of the mine implies that some LHD's are not productive even though they are capable. The sublevel cave mine in Kiruna is divided into approximately 15 production areas that are all prioritized, each area operated mostly by one LHD or occasionally by two. The production of the highest prioritized area is first transported to the plants on the ground level. The production of the lowest prioritized area is last transported to the plants on the ground level. This implies that the ore passes of low prioritized production areas might be filled up having as a consequence that the LHD's stationed at those production areas during some periods have to be un-productive in stand-by mode. As an example, the production of one automatic LHD during 2004 was 1.587.729 tonnes, corresponding to approximately 74000 buckets, which indicates that the LHD mainly operated in high-prioritized production areas.

Table 6. The table shows the KPI's of the LHD automation.

KPI	Value	Unit
Average bucket payload	21.5	ton
Average tramming distance	152	m
Instantaneous capacity	226	ton/h
Average speed	3.2	km/h
Transport performance	34	ton*km/h
Utilization	59	%
System availability	>90	%

The average bucket weight of the manual LHD's of the same type, TORO2500E, during the period 2005 to 2009 was 25.3 tonnes. The difference is +3.8 tonnes compared to the average bucket weight of the automatic LHD's during the period 1999 – 2009.

The figures presented in this section are based on considerably more than 1.000.000 buckets excavated with manual LHD's and automatic LHD's.

9 Conclusion

We have presented key performance indices of an LHD automation system based on 10-years production with 75 tonnes automatic LHD's in one of the world's largest underground mines. This is to our knowledge the first time such figures are presented, which makes comparison with the performance of other LHD automation system impossible.

The evaluation of the driver assisting system for remote controlled excavation of fragmented rock indicates that such a system can increase the weights of the buckets, which is important. The function was implemented in all LHD's in the summer of 2002 and used for the remainder of the production period. The need of traction control to prevent wheel spinning during the excavation of the bucket was identified, the wear of the bucket have a strong influence of wheel spin tendencies.

The experience from the implementation of the driver assisting system was that the most important sequence to control for wheel spin not to occur was the second sequence where the bucket was lifted a bit when the speed had dropped to the trig level. In this context, it is important to note that the wear of the blade of the bucket plays an important role roll in this sequence. Experiences from the production period was that LHD's with new buckets or buckets with sharp retro-fitted blades positioned correct for the penetration to start, were not subject to wheel spin even though the initial lift of the bucket was not done. However, if the blade was worn, wheel spin occurred frequently if the initial lift of the bucket was not done. The tendency for wheel spin during the penetration of the muck pile is probably LHD type dependent. The eight TORO2500E's used all had a clear tendency for wheel spin.

The wheel slip experience indicates that the interaction of the driving wheels and the ground also must be considered in LHD automation applications. Traction control for off-road applications from a robotic perspective is discussed in for instance Waldron and Abdallah (2007). A review of traction control methods from a construction machinery perspective (haulers and wheel loaders) is found in Markdahl (2010).

Low bucket weights resulting from tele remote controlled excavation is a clear drawback for LHD automation. The results from the 10-year production period in the Kiruna iron ore mine does not come as a surprise since tele remote controlled excavation is based on a slightly delayed 2D video feedback for the remote operator that closes the loop compared to manual excavation where the driver bases the control of the bucket on non-delayed 3D vision, audio and vibration feedback.

The second and the third sequence of the driver assisting load function are comparable to the discussion by Marshall, Murphy and Daneshmend, (2008). Both the controller discussed in this paper and the admittance controller discussed by Marshall, Murphy and Daneshmend react to inputs by changing the velocity of the bucket cylinder. The difference is that the

controller discussed in this paper uses the speed of the LHD as the feedback to base the reaction on and not measured forces. An interesting question, based on the experiences of using the speed as the feedback, is how the speed correlates to the external forces caused by the interaction between the bucket and the muck pile. The speed sensors of the LHD only measures the component in the plane of the ground, whereas the measured external forces can be decomposed to forces acting in the plane of the ground and forces perpendicular to the plane of the ground. These forces influences the load transfer between the front and rear axle and thereby the maximum circumferential forces of the driving wheels of the front axle and the rear axle in the tyre-ground contact patch before wheel spin starts.

The field test scenarios discussed by Mäkelä, Duff et al. and Marshall et al. regarding tramming and hauling are similar to the tests with HUNS. The discussions are focused on "top speed", robustness and comparison between manual and automatic driving of the LHD. All teams managed to drive the LHD with a speed comparable to a skilled manual driver. No collisions with the walls of the drifts were reported.

Accuracy tests regarding the positioning of the LHD were done by Mäkelä, Marshall et al. and in the field tramming / hauling tests with HUNS. The positioning accuracy is important because of the narrow drifts. Tests with loaded and un-loaded buckets were reported by Duff et al., Marshall et al. and in the tests with HUNS. The load changes the dynamics of the LHD, which must be dealt with in a robust manner by the navigation system. Mäkelä made tests with the predictive part of the high-level controller disabled and showed that the predicted part of the controller plays an important role to handle dynamic properties. Tests running over obstacles were done in in the tests with HUNS in which the rear of the LHD became airborne. The system managed to control the LHD and continue the hauling which is an important property from a safety perspective. No collision between the walls of the drifts and the LHD's occurred in automatic/camera-tracking/semi-automatic mode during the 10-year production period, which proves the robustness of the system. The HUNS controller based on in-direct guidance of the LHD using a fictive tricycle (ghost) vehicle could handle wears of the LHD without need of re-parameterisation, which is important from a maintenance perspective.

The SLAM technique is relevant to use in cyclic applications such as LHD automation if the surrounding environment of the mobile robot changes. In the typical application of LHD's in large scale underground hard rock mines, the LHD will go back and forth the same route several hundred times. The chance that the environment changes much from one cycle to another is very low. Spilled rock from the bucket on the roadway during hauling occurs and can cause unnecessary wear of the LHD, but the bucket in front of the LHD makes it difficult to use sensors measuring the roadway. Rock outburst can occur, but when this happens, the mine or part of the mine has to be closed, infrastructure such as electrical wires repaired and the drifts reinforced before the production can be restarted.

The most interesting application of the SLAM technique for LHD automation is when the route is expanded into areas previous unknown to the system. The first development phase - *tunnel drifting* - of the production area in the sub-level cave operation in Kiruna is applicable to this scenario where LHD's are used for batch loading. (The other development phases are the *production drilling* and the *production loading*.)

Some lessons have been learnt over the years. The first was that the reference path representation is of importance when negotiating curves. Collision free paths could not be constructed for some intersections for the bigger LHD using the X4Y4 representation. Field

tests in production environments require careful planning and good communication with the remote operators. Paying attention to the remote operators opinions is important in the development of the system. The operators spend a significant time interacting with the system and quickly observe weaknesses that might not be relevant from an experimental perspective.

Our final conclusion is that driver assisted/automatic excavation is one of the most important topics to address in future research relating to LHD automation.

10. Appendix – Details on navigation algorithms

The time discrete state space model used in the pose estimator is, with k denoting the sampling instance

$$x_k = x_{k-1} + \Delta x \tag{A1}$$

$$y_k = y_{k-1} + \Delta y \tag{A2}$$

$$\theta_k = \theta_{k-1} + \Delta\theta_1 + \Delta\theta_2 \tag{A3}$$

where the increments $\Delta x, \Delta y, \Delta\theta_1, \Delta\theta_2$ depends on the velocity v, the sampling period h, the articulation angle γ and the distance between the articulating joint and the wheel axles L according to

$$\Delta x = \bar{d} \cos(\theta_{k-1} + \overline{\Delta\theta}) \, (1 - \overline{\Delta\theta}^2/6) \tag{A4}$$

$$\Delta y = \bar{d} \sin(\theta_{k-1} + \overline{\Delta\theta}) \, (1 - \overline{\Delta\theta}^2/6) \tag{A5}$$

$$\Delta\theta_{1|\gamma_k=\gamma_{k-1}} = \frac{\bar{d}}{L} \frac{\sin\gamma_k}{1+\cos\gamma_k} \tag{A6}$$

$$\Delta\theta_{1|\gamma_k\neq\gamma_{k-1}} = \frac{\bar{d}}{L\Delta\gamma} (\ln(1 + \cos\gamma_{k-1}) - \ln(1 + \cos\gamma_k)) \tag{A7}$$

$$\Delta\theta_2 = \tan(\gamma_k/2) - \tan(\gamma_{k-1}/2) \tag{A8}$$

where the help variables $\bar{d}, \Delta\gamma, \overline{\Delta\theta}$ are defined as

$$\bar{d} = h \, (v_k + v_{k-1})/2 \tag{A9}$$

$$\Delta\gamma = \gamma_k - \gamma_{k-1} \tag{A10}$$

$$\overline{\Delta\theta} = (\Delta\theta_1 + \Delta\theta_2)/2 \tag{A11}$$

The high level controller calculates set values for the articulation angle and the articulation angle speed. The task of the low level controller is to produce a steering cylinder velocity based on the set values from the high-level controller and feedback from the measured articulation angle.

Let the co-ordinate of the control point be (u, v), and let the co-ordinate of a point on the segment be (x, y) in the co-ordinate system of the segment with origin in the start point, the squared distance is then with $\Delta x = u - x$ using (1) given by

$$f(x) = (v - a_7 x^7 + a_6 x^6 + a_5 x^5 + a_4 x^4 + a_3 x^3 + a_2 x^2 + a_1 x + a_0)^2 + \Delta x^2 \tag{A12}$$

The nearest point fulfils

$$\frac{df(x)}{dx} = f'(x) = 0 \tag{A13}$$

which is solved numerically using the Newton-Raphson method

$$x_{n+1} = x_n - f(x_n)/f'(x_n) \tag{A14}$$

Denote the nearest point to (u, v) on the segment (x_c, y_c). The distance d_c and the slope θ_c is then

$$d_c = \sqrt{f(x_c)} \tag{A15}$$

$$\theta_c = \text{atan}\,(p'(x_c)) \tag{A16}$$

The curvature K and the change of curvature dK/ds are also used in the controller. The curvature is

$$K = \frac{p''(x)}{(1+p'(x)^2)^{3/2}} \tag{A17}$$

where $p(x)$ is according to (1) and the change in curvature where s denotes the distance from the start of the segment is

$$\frac{dK}{ds} = \frac{(1+(p'(x))^2)p'''(x) - 3p'(x)(p''(x))^2}{(1+(p'(x))^2)^3} \tag{A18}$$

Denote the wheelbase of the fictive tricycle L_t, the relation between the steering angle of the tricycle and the curvature of the segment is then

$$\gamma_t = \text{atan}\,(L_t K) \tag{A19}$$

$$\dot{\gamma}_t = \frac{L_t}{1+(L_t K)^2}\dot{K} \tag{A20}$$

where $\dot{K}$ can be expressed as

$$\dot{K} = \frac{dK}{dx}\frac{dx}{ds}\frac{ds}{dt} = \frac{dK}{ds}v_t \tag{A21}$$

where v_t is the speed of the tricycle along the segment.

The pose of mid point on the rear axle of the articulated vehicle (x, y, θ) - estimated by the pose estimator - can be transformed to the co-ordinate of the mid point on the rear axle of the fictive tricycle (x_t, y_t, θ_t), which is the control point, as a function of the articulation angle γ and the distance between the articulating joint and the wheel axles L according to

$$x_t = x + L\cos\theta - d\sin\theta_t \tag{A22}$$

$$y_t = y + L\sin\theta + d\cos\theta_t \tag{A23}$$

$$\theta_t = \theta + \delta \tag{A24}$$

where the help variables d and δ are defined as

$$d = L\ln\left(\tan\left(\frac{\pi+\gamma}{4}\right)\right) \tag{A25}$$

$$\delta = \tan^{-1}\frac{\sin(\gamma)}{1+\cos(\gamma)} \tag{A26}$$

The estimates of the distance to the segment $\hat{d}_c$, the slope of the segment $\hat{\theta}_c$, and the curvature $\hat{K}_c$ can then be calculated based on the pose estimate of the control point, summarized as

$$\left(\hat{x}_t, \hat{y}_t, \hat{\theta}_t\right)^T \rightarrow \left(\hat{d}_c, \hat{\theta}_c, \hat{K}_c\right)^T \tag{A27}$$

The estimates of the sidewise error, $\hat{d}_{err}$, and heading error, $\hat{\theta}_{err}$, used in the guidance controller are simply the distance to the segment and the difference between the heading of the tricycle and the slope of the segment. The curvature, $\hat{K}_c$, is also used in the in the guidance controller together with predictions, T seconds into the future, of the curvature, $\hat{K}_{c\_T}$, and the change in curvature, $d\hat{K}_{c\_T}/ds$.

Use the pose estimate of the articulated vehicle at current time as $(x_{k-1}, y_{k-1}, \theta_{k-1})^T$ in (2) - (4). The predicted pose, $\left(\hat{x}_T, \hat{y}_T, \hat{\theta}_T\right)^T$, is calculated using the current values of the articulation angle and drive speed T seconds into the future based on (5) - (7). The predicted pose of the control point, $\left(\hat{x}_{t\_T}, \hat{y}_{t\_T}, \hat{\theta}_{t\_T}\right)^T$, is then calculated using (28) - (30) based on the predictive pose of the articulated vehicle. The curvature, $\hat{K}_{c\_T}$, and change in curvature $d\hat{K}_{c\_T}/ds$ can then be calculated based on the predicted pose estimate of the control point, summarized as

$$\left(\hat{x}_{t\_T}, \hat{y}_{t\_T}, \hat{\theta}_{t\_T}\right)^T \rightarrow \left(\hat{K}_{c\_T}, d\hat{K}_{c\_T}/ds\right)^T \tag{A28}$$

The set values for the guidance along the segment can now be calculated in a number of steps.

The set angle and set angle speed of the tricycle is first calculated.

$$\gamma_t^{set} = -l_d \hat{d}_{err} - l_\theta \hat{\theta}_{err} + L_t \hat{K}_c \tag{A29}$$

where the gains l_d and l_θ are calculated based on a linear quadratic (LQ) criteria. Only the steady state values are used.

The predictive part T seconds into the future of the controller is

$$\dot{\gamma}_t^{set}(T) = \frac{L_t}{1+(L_t \hat{K}_{c\_T})^2} \frac{dK_{c\_T}}{ds} v_t \tag{A30}$$

The relations between the set values of the tricycle, $(\dot{\gamma}_t^{set}(T), \gamma_t^{set})$ and the set values of the articulated vehicle, $(\dot{\gamma}^{set}(T), \gamma_t^{set})$, are

$$\frac{L_t}{\tan(\gamma_t^{set})} = \frac{2\cos(\gamma^{set}/2)}{\sin(\gamma^{set})} - \ln\left(\tan\left(\frac{\pi+\gamma^{set}}{4}\right)\right) \tag{A31}$$

$$\dot{\gamma}^{set}(T) = \frac{L_t}{L} \frac{(1+\cos(\delta_1))^2 + \sin^2(\delta_1)}{1+\cos(\delta_1))} \frac{\sin^2(\delta_2)\cos(\delta_2)}{\sin^2(\delta_1)} \dot{\gamma}_t^{set}(T) \tag{A32}$$

where the help variables δ_1 and δ_2 are

$$\delta_1 = \tan^{-1}(L_t \hat{K}_{c\_T}) \tag{A33}$$

$$\delta_2 = \frac{\sin(\gamma^{set}(T))}{1+\cos(\gamma^{set}(T))} \tag{A34}$$

(A31) is solved numerically and (A32) analytically.

Define, with subscript k denoting the sampling instant

$$\gamma_k^{err} = \gamma_k^{set} - \gamma_k \qquad (A35)$$

$$z_k = e^{-h}z_{k-1} + (1 - e^{-h})(\gamma_{k-1}^{err} - \gamma_{k-2}^{err}) \qquad (A36)$$

where γ_i is the measured value of the articulation angle at sampling instants $k, k-1, k-2$, and h is the sampling time.

Finally, the guidance controller output, u_k, of the articulation angle speed at sampling instant k with gains k_1 and k_2 is

$$u_k = \dot{\gamma}_k^{set}(T) + k_1\gamma_k^{err} + k_2z_k \qquad (A37)$$

The relation between the output from the guidance controller and the steering cylinder speed input to the machine controller, is defined using four sets of linear relations for high speed counter clockwise turning, low speed counter clockwise turning, low speed clockwise turning and high speed clockwise turning. These sets are individual for each LHD and depend on, for instance, parameter settings in the machine controller for proportional valves in the hydraulic system for the steering.

References

Altafini, C. (1999). A path-tracking criterion for an LHD articulated vehicle. *International Journal of Robotics Research*, 18(5):435–441.

Andersson, U., Mrozek, K., Åström, K., & Hyyppä, K. (1997). Path design and control algorithms for articulated mobile robots. In *Proceedings of the International Conference on Field and Service Robotics*, 1997, Canberra, Australia.

Bakambu, J. N., & Polotski, V. (2007). Autonomous system for navigation and surveying in underground mines. *Journal of Field Robotics*, 24(10):829–847.

Bolzern, P., DeSantis, R.M., Locatelli, A., & Masciocchi D. (1998). Path-tracking for articulated vehicles with off-axle hitching. *IEEE Transaction on Control Systems Technology*, 6(4):515-523.

Bolzern, P., & Locatelli, A. (2002). A comparative study of different solutions to the path-tracking problem for an articulated vehicle. In *Proceedings of the 2002 IEEE International Conference on Control Applications,* Glasgow, Scotland, U.K.

Bonchis, A., Hillier, N., Ryde, J., Duff, E., & Pradalier, C. (2011). Experiments in autonomous earth moving. *IFAC Proceedings Volumes (IFAC-PapersOnline),* 18(PART 1):11588-11593.

Corke, P.I., & Ridley, P. (2001). Steering kinematics for a center articulated mobile robot. *IEEE Transaction on Robotics and Automation*, 17(2):215-218.

DeSantis, R. M. (1997). Modelling and path-tracking for a load-haul-dump mining vehicle. *Journal of Dynamic Systems, Measurement and Control*, 119:40–47.

Dissanayake, M.W.M.G., Newman, P., Clark, S., & Durrant-Whyte, H.F. (2001). A solution to the simultaneous localization and map building (SLAM) problem. *IEEE Transactions on Robotics and Automation*, 17(3):229-241.

Dragt, B. J., Camisani-Calzolari, F. R., & Craig, I. K. (2005). An overview of the automation of load-haul-dump vehicles in an underground mining environment. In *Proceedings of 16th IFAC World Congress*, Prague, Check Republic.

Duff, E., Roberts, M., & Corke, P. (2002). Automation of an underground mining vehicle using reactive navigation and opportunistic localization. In *Proceedings of the Australian Conference on Robotics and Automation*, 2002, Auckland, Australia. pp. 151–156.

Duff, E., Roberts, M. & Corke, P. (2003). Automation of an underground mining vehicle using reactive navigation and opportunistic localization. In *Proceedings of the IEEE/RSJ International Conference on Intelligent Robots and Systems, 2003, Las Vegas, NV, USA*. pp. 3775–3780.

Duff, E., & Roberts, M. (2003). Wall-following with constrained active contours. In *Proceedings of the 4th International Conference on Field and Service Robotics,* 2003, Japan.

Hemami, A., & Polotski, V. (1996). Problem formulation for path tracking automation of low speed articulated vehicles. In *Proceedings of the IEEE International Conference on Control Applications*, Dearborn, MI, USA.

Hemami, A., & Polotski, V. (1998). Path tracking control problem formulation of an LHD Loader. *The International Journal of Robotic Research*, 17(2):193-199.

Hemami, A., & Hassani, F. (2009). An overview of autonomous loading of bulk material. *26th International Symposium on Automation and Robotics in Construction, ISAR 2009*:405-411.

Hebert, M., Thorpe, C., & Stentz, A.T., editors. Intelligent Unmanned Ground Vehicles: Autonomous Navigation Research at Carnegie Mellon. Kluwer Academic Publishers, 1997.

Gustafson, A. (2011). Dependability assurance for automatic load haul and dump machines, pp. 11-12. Licentiate Thesis, Luleå University of Technology, Luleå, Sweden.

Hyyppä, K. (1991). Method of navigating an automated guided vehicle. European patent 0238615, Munich, July 1991.

Hyyppä, K. (1989). Method of navigating an automated guided vehicle. US patent 4811288, March 1989.

Larsson, J., Appelgren, J., Marshall, J., & Barfoot, T.D. (2008). Atlas Copco infrastructure less guidance system for high-speed autonomous underground tramming, In *Proceedings of the 5th International Conference and Exhibition on Mass Mining on Field and Service Robotics*, Luleå, Sweden.

Larsson, J., Appelgren, J., & Marshall, J. (2010). Next generation system for unmanned LHD operation in underground mines. In *Proceedings of the SME Annual Meeting and Exhibition*, Phoenix, AZ, USA.

Larsson, U., Zell, C., Hyyppä, K., & Wernersson, Å. (1994). Navigating an articulated vehicle and reversing with a trailer. *In Proceedings of IEEE International Conference on Robotics and Automation*, San Diego, CA, USA.

Lavigne, N.J., & Marshall, J.A. (2012). A landmark-bounded method for large-scale underground mine mapping. *Journal of Field Robotics*, 29(6):861-879.

Le Cras, J.R. (2012). A multisensor SLAM for dense map of large scale environments under poor lightning conditions. Doctoral thesis, Curtin University, Perth, Australia.

Madhavan, R., Dissanayake, M. W. M. G., & Durrant-Whyte, H. F. (1998). Autonomous underground navigation of an LHD using a combined ICP-EKF approach. In *Proceedings of IEEE Conference on Robotics and Automation*, Leuven, Belgium.

Madhavan, R., & Durrant-Whyte, H. F. (2005). 2D map-building and localization in outdoor environments. *Journal of Robotic Systems*, 22(1):45-63.

Markdahl, J. (2010). Traction control for off-road articulated vehicles. Master's Thesis, Royal Institute of Technology, Stockholm, Sweden.

Marshall, J., Barfoot, T., & Larsson, J. (2008). Autonomous underground tramming for center-articulated vehicles. *Journal of Field Robotics*, 25(6-7):400-421.

Marshall, J.A., Murphy, P.F., & Daneshmend, L.K. (2008). Toward autonomous excavation of fragmented rock: full-scale experiments. *IEEE Transactions on Automation Science and Engineering*, 5(3):562–566.

Mäkelä, H. (2001a). Overview of LHD navigation without artificial beacons. *Robotics and Autonomous Systems*, 36:21–35.

Mäkelä, H. (2001b). Outdoor navigation of mobile robots. Doctoral thesis, Helsinki University of Technology, Espoo, Finland.

Polotski, V. (2000). New reference point for guiding an articulated vehicle. In *Proceedings of IEEE International Conference on Control Applications*, Anchorage, AK, USA.

Ridley, P., & Corke, P. (2001). Autonomous control of an underground mining vehicle. In *Proceedings of Australian Conference on Robotics and Automation*, Sydney, Australia.

Ridley, P., & Corke, P. (2003). Load haul dump vehicle kinematics and control. Journal of Dynamic Systems, Measurements and Control, Transactions of the ASME, 125(1):54-59.

Roberts, J. M., Duff, E. S., & Corke, P. I. (2002). Reactive navigation and opportunistic localization for autonomous underground mining vehicles. *Information Sciences*, 145:127–146.

Scheding, S., Dissanayake, G., Nebot, E., & Durrant-Whyte, H. (1997). Slip modelling and aided inertial navigation of an LHD. In *Proceedings of IEEE International Conference on Robotics and Automation*, Albuquerque, New Mexico, USA.

Scheding, S., Dissanayake, G., Nebot, E. M., & Durrant-Whyte, H. (1999). An experiment in autonomous navigation of an underground mining vehicle. *IEEE Transactions on Robotics and Automation*, 15(1):85–95.

Singh, S. (2002). State of the art in automation of earthmoving, 2002. (2002). Robotics Institute. Paper 985.

Waldron, K.J., & Abdallah, M.E. (2007). An optimal traction control scheme for off-road operation of robotic vehicles. *IEEE/ASME Transaction on Mechatronics*, 12(2):126-133.

Wiklund, U., Andersson, U., & Hyyppä, K. (1988). AGV navigation by angle measurements. In *Proceedings of the 6th International Conference on Automated Guided Vehicle Systems*, Brussels, Belgium.

Wylie, R. (1996). LKAB invests in the future. *Engineering and Mining Journal*:48-52.

Åström, K. (1991). Where am I, and what am I seeing? Algorithms for a laser guided vehicle. Master's Thesis, Lund Institute of Technology, Lund, Sweden.

Åström, K. (1993). Automatic Mapmaking. In Proceedings of 1st IFAC International Workshop on Intelligent Autonomous Vehicles, Southampton, Hampshire, U.K.

[D] - Traction control for articulated off-road vehicles

The author's main contribution: Discussion partner.

Comment: Johan Markdahl derived the equations and "typed the text".

Traction Control for Articulated Off-road Vehicles

Johan Markdahl*, Gianantonio Bortolin†, and Ulf Andersson‡

*Dept. of Mathematics, Royal Institute of Technology, Stockholm, Sweden
†Dept. of Drivetrain Development, Volvo CE, Eskilstuna, Sweden
‡Dept. of Computer Science and Electrical Engineering, Luleå University of Technology, Luleå, Sweden

Abstract—**Certain off-road vehicles are equipped with a type of clutches referred to as differential locks. A driver may engage/disengage these locks to switch between two distinct operating modes: the closed mode is characterized by greater off-road traversability, while the open mode allows better manueverability. Many drivers lack the education and experience required to correctly judge the terrain ahead of the vehicle and therefore engage/disengage the locks in a suboptimal fashion. An automatic differential locking strategy is hence desired. This paper compares three such traction control algorithms of the on/off variety, all derived from the same underlying kinematic vehicle model but each relying on the availability of different output signals. The validity of the kinematic model and the algorithms' sensitivity to the values assumed by a couple of unobservable states, the wheel slip angles, is investigated by comparison to an existing articulated hauler model in ADAMS— an environment for simulation of multibody dynamics.**

1 Introduction

Articulated haulers are heavy equipment used to transport large quantities of loose materials such as sand, gravel or liquids. Unlike dump trucks, articulated haulers are designed to operate off-road. They may, for example, be employed at mines to transport ore over grounds not traversable by ordinary vehicles. The hauler's ability to take the shortest route on a load-haul-dump run minimizes fuel consumption and time expenditure.

A tire may sometimes lose its grip and slip rather than roll over the road, e.g. if subject to full throttle, icy road conditions or a steep road inclination. This is referred to as lost traction, traction being an adhesive friction force in tire/road interface that serves to drive the vehicle forward. Lost traction is undesirable since it reduces the vehicle's traversability and increases tire wear. Means must therefore be taken to curb wheel slip and regain lost traction, preferably before than after it is lost.

A differential is a driveline component that distributes power, i.e. torque and rotational speed, from an input shaft to two output shafts. There are many types of differentials: open, clutch-type limited slip, viscous coupling and locking differentials to name a few. The differentials on Volvo CE articulated haulers are of the locking type and has two distinct operating modes: open and closed. An open differential distributes rotational speed as needed, while the input torque is divided equally between the two output shafts. A locked differential forces the two output shafts to assume the same speed, while the torque is distributed as needed.

The basic type of differential is always open, allowing a left and right or front and rear wheel to rotate at different speeds. This is advantageous during cornering, but not during off-road driving. Volvo CE articulated haulers are therefore equipped with differential locks of the dog-clutch variety: a pair of face gears that are locked together pneumatically and pulled apart by a spring. These clutches force the differential output shafts to assume the same speed, thereby effectively removing the slip of a single wheel. A succession of locks may be engaged to curb the slip of multiple wheels.

A Volvo CE articulated hauler features 4 differential locks, one between each pair of wheels and a center differential lock between the tractor and trailer unit parts of the driveline. The vehicle may also be switched between 6×4 and 6×6 operating modes. The differential locks are either engaged/disengaged manually by the driver who turns switches on the dashboard or steps on a button on the floor, or governed by the automatic traction control (ATC) system.

Locking the differentials for extended periods of time builds up powerful wind-up torques, often exceeding the maximal engine torque by an order of magnitude. The presence of wind-up torques strains the driveline. Turning with locked differentials decreases manoeuvrability by forcing the tires to slip, thereby also increasing tire wear. Unnecessary engagements of the 6×6 operating mode worsen fuel economy due to inevitable power losses.

135

The locks should therefore be used sparsely. Logs from an automatic machine tracking information system (MATRIS) indicate that the ATC system outperforms even skilled drivers in this respect.

The ATC system works fine, but recent developments in hardware have paved the way for further improvements. This article explores the advantages that may be gained from utilizing the information obtained from a ground speed sensor (e.g. a ground speed radar or a GPS receiver) and individual wheel tachometers. Other quantities that would be interesting to measure include the articulation joint roll angle, the road inclination, the load mass and the center of mass acceleration, but evaluating the possible benefits of having access to such information lies outside the scope of this work.[1]

The control input considered is differential lock engagement. Since the engagement/disengagement of a dog-clutch may only switch between the open and closed operating modes of a differential, the system is hybrid and the control strategy must be of on/off type.[2] The traction control algorithms considered in this paper consist of the rules of differential lock engagement/disengagement.

2   Literature

There is a vast literature on automotive control system such as anti-braking lock systems (ABS), electronic stability control (ESC) and traction control systems (TCS), also known as anti-slip regulation (ASR). An often used vehicle model is the one-wheel model, consisting of two differential equations describing the translational and rotational motion of a wheel. They may be derived directly from a free body diagram of a tire using Newton's generalized second law. Each wheel may be considered in isolation from the rest thanks to the tachometers which measure and brakes that regulate the speed of each wheel.

Control algorithm designers concerned with the regulation of tire/road interface friction forces face three primary difficulties: i) the state equations involved are non-linear; ii) sensor output is limited to a few states and iii) road conditions are not given beforehand and may change drastically. The ABS algorithm presented in [1], for instance, deals with i) by linearizing the state equations around an operating point on an equilibrium manifold, with ii)

by using a proportional feedback of a convex combination of the hard-to-measure wheel slip and easy-to-measure wheel deceleration and address iii) by proving that the stability of the algorithm is guaranteed irrespective of the choice of operating point on the equilibrium manifold for certain convex combinations of the feedback.

Here, we will derive a model that is valid under normal operating conditions and assume that any deviation from that model is an indication of wheel slip, thereby addressing iii). Since the control algorithm is of an on/off type due to the particular actuators used, there is no need to concern ourselves with i). Hence, the main concern is to address the issue of ii), i.e. to find the minimum number of sensors needed to achieve a fast and robust algorithm.

3   Wheel slip

The wheel slip λ is often defined as a normalized function of the difference between the speed of the tire circumference and the ground as seen from a hub fixed coordinate system

$$\lambda \stackrel{\text{def}}{=} \frac{\omega r \cos\alpha - v}{\omega r \cos\alpha}, \tag{1}$$

where ω is the wheel angular speed, r the tire radius, α the tire slip angle, v the ground speed and the assumption $\omega r \cos\alpha > v$ holds, see for example [2]. As an alternative slip definition, consider the non-normalized quantity

$$\Delta\omega \stackrel{\text{def}}{=} \omega - v/r, \tag{2}$$

where $\Delta\omega r$ can be interpreted as the distance a slipping wheel slips per second.

Normalized slip quantities are of interest since they relate non-linearly to the tire/road interface friction coefficient $\mu(\lambda)$, as detailed in a large body of empirical studies, see for example [3]. A literature review of tire/road friction is provided in [4]. The friction coefficient $\mu(\lambda)$ enters the one-wheel model dynamics, but since the algorithms developed in this paper does not make use of tire dynamics, there little use in adopting λ as a measure of slip.

The non-normalized slip quantity has the advantage of be more directly related to tire wear. Consider two situations, one where $\omega = \epsilon > 0$, $v = 0$ and another where $\omega = 2M$, $v = M$, $\epsilon \ll M$. Definition (1) and $r = 1$, $\alpha = 0$ yields a $\lambda = 1$ in the former case and $\lambda = \frac{1}{2}$ in the latter. Definition (2) yields a $\Delta\omega = \epsilon$ in the former case and a $\Delta\omega = M$ in the latter, which is preferable since the latter case is much worse in terms of tire wear. Hence we use definition (2).

---

[1]The standard sensors do include an inclinometer, the information gained from it is however not utilized by the algorithms presented here.

[2]Other types of differential locks such as wet-disc clutches may operate in a sliding mode, producing a linear control system with the possibility of more diverse control action. Neither the brakes nor the retarder can be used to efficiently control wheel slip since their action is distributed equally over all wheels.

4 Control strategy

Certain output signals are hardly affected by rising slip levels while others may change rapidly. A GPS receiver's ground speed readings is an example of the former; tachometer measurements of the speed of some driveline shaft is an example of the latter. This notion of a static and a transient behavior of certain output signals at the onset of wheel slip form the basis of the traction control algorithms developed here.

The speed of a driveline shaft ω and the ground speed v are proportional to each other under the assumption of zero slip and a rigid driveline:

$$i\omega r = v, \qquad (3)$$

where i is a gear conversion ratio (possibly equal to 1) and r the tire radius. In the presence of wheel slip, the relation (3) is replaced by $\Delta\omega = i\omega r - v$, see equation (2).

Let $\boldsymbol{y}$ be the output signals and introduce $\boldsymbol{z}$ to denote states that are not measured, i.e. neither observable nor detectable. Let $g(\boldsymbol{y}, \boldsymbol{z})$ be a function of the states and suppose that an equation

$$g(\boldsymbol{y}, \boldsymbol{z})|_{\Delta\boldsymbol{\omega} = \mathbf{0}} = 0, \qquad (4)$$

holds true. The equality (4) is not guaranteed to withhold while $\Delta\boldsymbol{\omega} \neq \mathbf{0}$. Any contradiction of equation (4) can hence be used as an indicator of wheel slip.

Equation (4) is likely to be a kinematic relation; both Volvo CE and Caterpillar own patented traction control algorithms based on articulated vehicle kinematics [5, 6]. Ideally $g_i = \omega_i r_i - v_i, i \in \{1, \ldots, 6\}$, but unfortunately neither individual wheel tachometers nor ground speed sensors form a part of the basic sensors configuration.

As a more feasible example, consider

$$\omega_{dbx,f} - \omega_{dbx,r} = \begin{cases} 0 & \text{if } \gamma, \Delta\omega_i = 0, \forall i \\ f(\boldsymbol{y}, \boldsymbol{z}) & \text{otherwise,} \end{cases} \qquad (5)$$

where $\omega_{dbx,f}$ and $\omega_{dbx,r}$ are the dropbox output shafts angular speeds (sensors 5 and 6 in figure 1), γ the steering angle and f some function. Note that if $\gamma = 0$ and a tractor and trailer wheel should slip simultaneously, equation (5) would still hold.[3]

Introduce the functions $f^-(\boldsymbol{y})$ and $f^+(\boldsymbol{y})$ (preferably, but not necessarily, with the same sign as in their super index) and relax the no slip constraint (4) as

$$\begin{cases} g(\boldsymbol{y}, \boldsymbol{c})|_{\Delta\boldsymbol{\omega} = 0} \geq f^-(\boldsymbol{y}) \\ g(\boldsymbol{y}, \boldsymbol{c})|_{\Delta\boldsymbol{\omega} = 0} \leq f^+(\boldsymbol{y}), \end{cases} \qquad (6)$$

---

[3]I.e. $\Delta\boldsymbol{\omega} = 0 \Rightarrow g(\boldsymbol{y}, \boldsymbol{z}) = 0$ but $g(\boldsymbol{y}, \boldsymbol{z}) = 0 \nRightarrow \Delta\boldsymbol{\omega}$.

where $\boldsymbol{c}$ is some nominal value of $\boldsymbol{z}$. The functions f^- and f^+ ($f^\pm$) should be tuned from experimental data to account for setting $\boldsymbol{z} = \boldsymbol{c}$ but also to make the strategy more robust to the influence of estimation errors and unmodeled dynamics.

A trade off has to be made between functions $f^\pm$ with small magnitudes, which make control action fast but increase the risk of unnecessary engagements and functions with large magnitudes, which reduce the risk of unnecessary engagements but delay control action. Ideally, $g(\boldsymbol{y}, \boldsymbol{z}) = g(\boldsymbol{y}, \boldsymbol{c})$ so that the magnitude of the functions $f^\pm$ may safely be set to small values. If the chosen expression depends on unobservable states they will have to be set to some nominal values, probably requiring the functions $f^\pm$ to have large magnitudes.

5 Sensor configuration

The ATC system employs a steering angle sensor and shaft angular speed sensors—i.e. tachometers—positioned along the haulers driveline, see figure 1. The following sections will reveal that wheel slip angles are an integral part of articulated hauler kinematics. Measurement and/or estimation of wheel slip angles require sensors such as two-antenna GPS receivers, which are not available on articulated haulers in production. The slip angles are hence not observable using standard sensors.
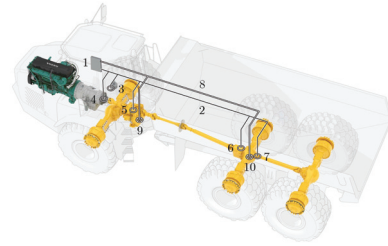
Figure 1: ATC system sensor and actuator configuration. The electronic control unit (ECU, 1) receives output signals (2) from steering angle sensor (3) and driveline tachometers (4, 5, 6, 7) and calculates an appropriate input signal (8) to the dropbox dog-clutch engagement/disengagement actuator (9) and 6×6 lock dog-clutch engagement/disengagement actuator (10).

6 Kinematic model

The kinematics of load-haul-dump vehicles (a kind of low set wheel loaders) is discussed in a body of

literature on path-tracking in underground environments. A model that includes wheel slip angles is found in [7]. This model cannot be used directly since the vehicle geometry of wheel loaders and articulated haulers differ.[4] A procedure for deriving kinematic models for the planar motion of articulated vehicles is presented in [8]. This paper generalizes the model of [7] by accounting for a broader range of ground vehicles, including but not limited to articulated haulers, using the technique from [8].

Consider the kth transverse axle of an articulated vehicle with n joints, as shown in figure 2. The velocity $\boldsymbol{v}_k = v_k(\cos\alpha_k, \sin\alpha_k)^T$ in the local coordinate origin O_k is related to the velocities v_{A_k} and v_{B_k} in the points A_k and B_k by the equations $\boldsymbol{v}_{A_k} = \boldsymbol{v}_k + \boldsymbol{\Omega}_k \times \boldsymbol{r}_{O_k A_k}$ and $\boldsymbol{v}_{B_k} = \boldsymbol{v}_k + \boldsymbol{\Omega}_k \times \boldsymbol{r}_{O_k B_k}$. The velocity $\boldsymbol{v}_{B_{k+1}}$ is equal to $\boldsymbol{v}_{A_k}$ rotated by γ_k degrees, see figure 2. These relations can be written on matrix form

$$\boldsymbol{\Psi}_k \overset{\text{def}}{=} \begin{pmatrix} v_k \\ \Omega_k \end{pmatrix},$$

$$\boldsymbol{v}_{A_k} = \begin{pmatrix} \cos\alpha_k & 0 \\ \sin\alpha_k & -a_k \end{pmatrix} \boldsymbol{\Psi}_k \overset{\text{def}}{=} M_{A_k} \boldsymbol{\Psi}_k,$$

$$\boldsymbol{v}_{B_k} = \begin{pmatrix} \cos\alpha_k & 0 \\ \sin\alpha_k & b_k \end{pmatrix} \boldsymbol{\Psi}_k \overset{\text{def}}{=} M_{B_k} \boldsymbol{\Psi}_k,$$

$$\boldsymbol{v}_{B_{k+1}} = \begin{pmatrix} \cos\gamma_k & -\sin\gamma_k \\ \sin\gamma_k & \cos\gamma_k \end{pmatrix} \boldsymbol{v}_{A_k} \overset{\text{def}}{=} R_{\gamma_k} \boldsymbol{v}_{A_k},$$

resulting in the system of equations

$$M_{B_{k+1}} \boldsymbol{\Psi}_{k+1} = R_{\gamma_k} M_{A_k} \boldsymbol{\Psi}_k, \tag{7}$$

which may be solved for Ω_k, v_{k+1} and Ω_{k+1} as functions of v_k, γ_k and $\dot{\gamma}_k$ by using the relation

$$\Omega_{k+1} = \Omega_k - \dot{\gamma}_k \tag{8}$$

and a few trigonometric identities.

The velocity v_i of a single wheel with slip angle α_i, expressed in the kth axle local coordinates, may be calculated as

$$\boldsymbol{v}_i = \begin{pmatrix} \cos\alpha_i & c_k \\ \sin\alpha_i & 0 \end{pmatrix} \boldsymbol{\Psi}_k$$

where α_i is the ith wheel slip angle. Note that the sign of Ω_k determines if a wheel i is inner or outer.

7   Articulated hauler kinematics

Picture an articulated hauler from a bird's eye view as displayed in figure 3 and note the likeness with

---

[4]The wheel loader vehicle geometry allows its rear wheels follow in the front wheel tracks, thereby increasing maneuvrability. This is not case with articulated haulers. The non-steerable wheels of the trailer unit bogie also make articulated haulers more prone to side slip.
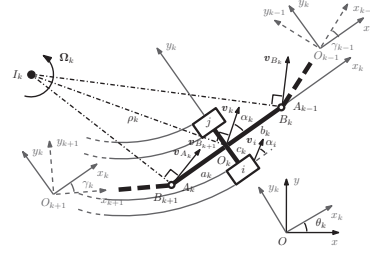

Figure 2: Kinematics of an articulated vehicle. I_k is the instantaneous center of rotation around which the kth axle rotates with velocity $\boldsymbol{\Omega}_k$. $\boldsymbol{v}_k$ is the translational velocity on the midpoint of the axle. A_k and B_k are two points on the longitudinal axle, situated at distances a_k and b_k from the origin O_k of the local coordinate system. $\boldsymbol{v}_{A_k}$ and $\boldsymbol{v}_{B_k}$ are the point's translational velocities. c_k is half the axle track. $\rho_k = \Omega_k/v_k$ is the turning radius. α_k is the slip angle and γ_k is the angle between the coordinate axes x_k and x_{k-1}. θ_k is the angle between the coordinate axis x_k and the x-axis of a global (i.e. ground-fixed) coordinate system with origin O.

figure 2. The corresponding system of equations (7) and (8) can be solved to yield

$$\begin{aligned} v_{34} = {}& \frac{(l_2 \cos(\gamma + \alpha_{12}) + l_1 \cos\alpha_{12})v_{12}}{l_2 \cos\alpha_{34} + l_1 \cos(\gamma - \alpha_{34})} \\ &+ \frac{l_1 l_2 \sin\gamma \dot{\gamma}}{l_2 \cos\alpha_{34} + l_1 \cos(\gamma - \alpha_{34})} \end{aligned} \tag{9}$$

$$\begin{aligned} \Omega_1 = {}& \frac{\sin(\gamma + \alpha_{12} - \alpha_{34})v_{12}}{l_2 \cos\alpha_{34} + l_1 \cos(\gamma - \alpha_{34})} \\ &+ \frac{l_2 \cos\alpha_{34} \dot{\gamma}}{l_2 \cos\alpha_{34} + l_1 \cos(\gamma - \alpha_{34})} \end{aligned} \tag{10}$$

$$\begin{aligned} \Omega_2 = {}& \frac{\sin(\gamma + \alpha_{12} - \alpha_{34})v_{12}}{l_2 \cos\alpha_{34} + l_1 \cos(\gamma - \alpha_{34})} \\ &- \frac{l_1 \cos(\gamma - \alpha_{34})\dot{\gamma}}{l_2 \cos\alpha_{34} + l_1 \cos(\gamma - \alpha_{34})}, \end{aligned} \tag{11}$$

where the notation is that of figure 2 and 3.

Introduce the functions

$$p(\alpha_{12}, \alpha_{34}, \gamma) = \frac{\sin(\gamma + \alpha_{12} - \alpha_{34})}{l_1 \cos(\alpha_{34} - \gamma) + l_2 \cos\alpha_{34}},$$

$$q(\alpha_{12}, \alpha_{34}, \gamma) = \frac{l_2 \cos(\alpha_{12} + \gamma) + l_1 \cos\alpha_{12}}{l_1 \cos(\alpha_{34} - \gamma) + l_2 \cos\alpha_{34}},$$

where p denote the inverse of the tractor unit steady state turning radius and q the quotient of
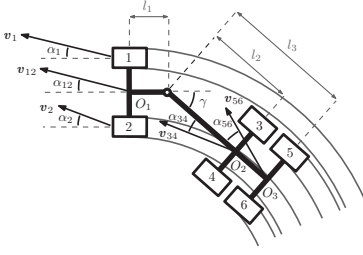
Figure 3: Articulated hauler kinematics. The points O_1, O_2 and O_3 correspond to the locations of the mean wheels in a three-wheel articulated bicycle model. $1, \ldots, 6$ are the actual wheels, l_k is the distance from point O_k, $k \in \{1, 2, 3\}$ to the hinge, $\boldsymbol{v}_{ij}$ is the vehicle translational velocity at point O_k, γ is the steering angle and α_{ij} is the kth mean wheel slip angle.

the tractor and trailer unit steady state turning radii.

The equations (9)–(11) may be tidied up by writing them as

$$v_{34} = q(\alpha_{12}, \alpha_{34}, \gamma)v_{12} + q(^{-\pi/2}, \alpha_{34}, \gamma)\dot{\gamma}l_1, \quad (12)$$
$$\Omega_1 = p(\alpha_{12}, \alpha_{34}, \gamma)v_{12} + p(-\gamma + \pi/2, \alpha_{34}, \gamma)\dot{\gamma}l_2,$$
$$\Omega_2 = p(\alpha_{12}, \alpha_{34}, \gamma)v_{12} + p(^{-\pi/2}, \alpha_{34}, \gamma)\dot{\gamma}l_1,$$

with e.g. $\dot{\gamma}l_1$ in equation (12) being interpreted as a tractor unit velocity with a $-90°$ slip angle.

To validate the kinematic model, we compare it to an existing articulated hauler model in ADAMS, an environment for simulation of multibody dynamics. The ADAMS model has previously been described in [9]. The ADAMS articulated hauler is run repeatedly on a curved road, see figure 4, varying the current gear and load mass.

We make use of two metrics,

$$d_1(x, \hat{x}) = \frac{1}{n}\sum_{k=1}^{n}|x_k - \hat{x}_k|, \quad (13)$$
$$d_\infty(x, \hat{x}) = \max_{k \in \{1, \ldots, n\}}|x_k - \hat{x}_k|, \quad (14)$$

to evaluate the discrepancy between a true value x and an estimate $\hat{x}$. k is a discrete time instance, and n the total number of time instances considered. Table 1 displays the accuracy of an estimate $\hat{v}_{34} = q(0, 0, \gamma)v_{12} + q(^{-\pi/2}, 0, \gamma)\dot{\gamma}l_1$ compared to v_{34}, on simulation output data from ADAMS.

8 Basic ATC system sensors

Equation (12) may be written as

$$\omega_{34}r - q(\alpha_{12}, \alpha_{34}, \gamma)\omega_{12}r - q(\pi/2, \alpha_{34}, \gamma)l_1\dot{\gamma} = 0$$

		α_{ij}, $\dot{\gamma} \stackrel{\text{def}}{=} 0$		$\alpha_{ij} \stackrel{\text{def}}{=} 0$, $\dot{\gamma} \in \mathbb{R}$		α_{ij}, $\dot{\gamma} \in \mathbb{R}$	
Load	Gear	d_1	d_∞	d_1	d_∞	d_1	d_∞
Zero	F1	1.2	14.6	0.2	1.6	0.1	0.6
	F2	2.1	22.0	0.5	2.4	0.2	0.7
	F3	3.2	25.6	1.3	5.7	0.2	0.7
Half	F1	1.6	11.6	0.6	3.1	0.1	1.0
	F2	2.8	17.6	1.4	6.9	0.2	1.4
	F3	4.1	20.7	2.4	11.2	0.2	1.6
Full	F1	2.0	10.0	1.2	5.9	0.3	1.7
	F2	3.5	16.2	2.3	10.6	0.3	2.4
	F3	4.9	22.5	3.5	15.5	0.3	2.5

Table 1: Mean and maximal relative trailer unit speed estimation errors, equations (13) and (14) with $x = v_{34}$ and $\hat{x}$ given by equation (12), as a function of setting the slip angles to zero, the three first forward gears F1, F2 and F3 (roughly corresponding to $v_{12} = 2$, 2.5 and 3 m s^{-1} respectively) and zero, half or full load (39 000 kg) using a steady state turning model ($\dot{\gamma} \stackrel{\text{def}}{=} 0$) or a transient state turning model ($\dot{\gamma} \in \mathbb{R}$). The units are cm s^{-1}. The gears are limited to F1, F2 and F3 since the vehicle is unlikely to turn on higher gears. The reverse gears have not been taken into account. The test road of figure 4 was used. Time instances with steering angles less than $1°$ were removed from consideration as they correspond to straight parts of the test road.

Figure 4: Test road in ADAMS. The articulated hauler runs from start to finish on the road centerline. The road lies in a plane (with the gravitational force $m\boldsymbol{g}$ as normal) and is mainly composed of curves. The greatest circle sector curvature corresponds to the maximal steering angle of $45°$.

under the assumption of zero slip, i.e. an expression like equation (4). The functions $f^\pm$ should be tuned to compensate for setting the unobservable slip angles α_{12} and α_{34} to zero.[5]

---

[5]On a side-note, consider the speed differences listed in table 1. The gear conversion ratios of the hub reduction and transverse differentials will amplify these speeds by a factor 18 approximately, depending on the make and model. An rpm difference Δn over the dropbox output shafts can be

Note that this approach is flawed since it cannot detect slip under all circumstance: if $\gamma = \dot\gamma = 0$ for instance, then $q(0,0,\gamma) = 1$ and

$$v_{34}/r + \Delta\omega_{34} - v_{12}/r - \Delta\omega_{12} = \Delta\omega_{34} - \Delta\omega_{12} = 0$$

whenever $\Delta\omega_{34} = \Delta\omega_{12}$. Hence this sensor configuration makes it difficult to detect simultaneous slip of the tractor and trailer unit wheels.

Also note that a slip of a front wheel, for instance, will have a less noteworthy effect on driveline shaft measurements of $\omega_{dbx,f} = i\omega_{12}$ than a direct measurement of ω_1 since

$$\omega_{12} = \frac{\omega_1 + \omega_2}{2},$$

by the workings of ordinary differentials (i being the differential and hub reduction gear conversion ratio). Notions of this kind will be further explored in section 11.

9   Ground speed sensor

GPS receivers and ground speed radars are examples of ground speed sensors. Output from a ground speed sensor can be compared to tachometer readings of the driveline shaft's angular speed to calculate the slip according to definition (2). An algorithm that knows the vehicle ground speed would hence be able to detect almost any type of wheel slip.

Assume that the speed is measured somewhere on the tractor unit and that it is recalculated to correspond to the speed at location O_1, see figure 3. The expression

$$\omega_{12}r - v_{12} = 0 \qquad (15)$$

is an equation of the type (4) which can be rewritten as a system of inequalities of the type (6) to detect a slip of the front mean wheel. A slip of the front bogie mean wheel is detected as

$$\omega_{34}r - v_{34} = \omega_{34}r - q(\alpha_{12},\alpha_{34},\gamma)v_{12}$$
$$+ q(-\pi/2,\alpha_{34},\gamma)\dot\gamma l_1 = 0, \qquad (16)$$

----

obtained as

$$\Delta n = 3 \cdot 6 \cdot |v_{34} - \hat{v}_{34}| \cdot 60/(2\pi).$$

An algorithm based on a steady state turning model and equation (16) would then have to tolerate an angular speed difference of about 40 rpm. 40 rpm is a considerable part of the speed difference limit above which safe engagement of a dog-clutch is no longer possible. The transient state turning model ($\dot\gamma \in \mathbb{R}$) reduce the difference to about 25 rpm and the slip angle model ($\alpha_{12}, \alpha_{34}, \dot\gamma \in \mathbb{R}$) to only 4 rpm. Hence, either the amount of tolerable slip or the risk of unnecessary engagements can be reduced by use of a more accurate kinematic model.

where $\omega_{dbx,r} = i\omega_{34}$ and

$$\omega_{34} = \frac{\omega_3 + \omega_4}{2}$$

under the assumption of a rigid driveline.

The main disadvantage of using ground speed sensors are the cost, but the expenses will be spread out if a GPS receiver is used since it has many other areas of application. Unfortunately, GPS receivers also have the downsides of having large sample times (1 s) and being useless underground in mining and tunnel constructions sites. If a ground speed radars is used, there is always a risk of it being rendered inoperable by mud.

10   Individual wheel tachometers

The ATC system tachometers do not measure wheel angular speed, but the angular speed of driveline shafts. These are proportional to the speeds of the mean wheels under the assumption of a rigid driveline. Measurements of the wheel angular speeds facilitate slip detection but are difficult to carry out since tachometers placed at those locations have low expected lifetime.[6] Here we do however assume that output from such sensors is readily available.

From $v_i = \omega_i r = \Omega_k \rho_i$, $v_j = \omega_j r = \Omega_k \rho_j$ and $\rho_i - \rho_j = a$ (see figure 2), we obtain the relations

$$\begin{cases} (\omega_1 - \omega_2)r - a\Omega_1 = 0 \\ (\omega_3 - \omega_4)r - a\Omega_2 = 0, \end{cases} \qquad (17)$$

where a denotes the axle track, i.e. the distance between a pair of wheels.

Since $\Omega_2 = \Omega_1 - \dot\gamma$, we may form the expression

$$[\omega_1 - \omega_2 - (\omega_3 - \omega_4)]r - a\dot\gamma = 0, \qquad (18)$$

which does not depend on slip angles at all. While this is precisely the type of expression on the form (4) we sought after, it cannot be used to detected all possible combinations of wheel slip.

To find all combinations of wheel slip that cannot be detected we write equation (18) on matrix form and calculate the null space as

$$\mathcal{N}([1\ {-}1\ {-}1\ 1]) = \mathrm{span}\left\{ \begin{bmatrix} 1 \\ 1 \\ 0 \\ 0 \end{bmatrix}, \begin{bmatrix} 0 \\ 1 \\ -1 \\ 0 \end{bmatrix}, \begin{bmatrix} 0 \\ 0 \\ 1 \\ 1 \end{bmatrix} \right\}.$$

Any combination of slip

$$\boldsymbol{\omega} + \Delta\boldsymbol{\omega} = (\omega_1, \omega_2\ \omega_3\ \omega_4)^T$$
$$+ (\Delta\omega_1, \Delta\omega_2\ \Delta\omega_3\ \Delta\omega_4)^T,$$

----

[6]One mud bath is enough to kill the sensors. To protect them, they need to encapsulated into the wheel hub.

is undetectable to the control strategy whenever $\Delta\boldsymbol{\omega} \in \mathcal{N}([1\ {-}1\ {-}1\ 1])$. Hence this criteria is most useful to detect the slip of a single wheel.

11 Evaluation

Unless the engine operating point is changed, a slipping wheel will have to take its excess speed from the remaining wheels, since the sum of angular speeds over all wheels is constant. Simulations in ADAMS indicate that equal amounts of speed is taken from each wheel. If, for instance, the first wheel should slip with $\Delta\omega_1 = \Delta\omega$, then

$$\Delta\boldsymbol{\omega} = (\Delta\omega,\ {-}\Delta\omega/3,\ {-}\Delta\omega/3,\ {-}\Delta\omega/3)^T. \qquad (19)$$

Assuming that a front wheel slips, we may calculate the effect upon the ATC system $g(\boldsymbol{y},\boldsymbol{c})|$ as

$$\begin{aligned}
g(\boldsymbol{y},\boldsymbol{0}) =&\ \frac{(\omega_3 - \Delta\omega/3 + \omega_4 - \Delta\omega/3)r}{2} \\
&- \frac{q(0,0,\gamma)(\omega_1 + \Delta\omega + \omega_2 - \Delta\omega/3)r}{2} \\
&- q(-\pi/2,0,\gamma)l_1\dot\gamma \\
=&\ -\frac{(1 + q(0,0,\gamma))\Delta\omega}{3} + \mathcal{O}(1),
\end{aligned}$$

where the correction term $\mathcal{O}(1)$ accounts for $g(\boldsymbol{y},\boldsymbol{c})|_{\Delta\omega=0} \neq 0$ due to $\boldsymbol{z} \neq \boldsymbol{c}$ is constant in the sense that it does not depend on $\Delta\boldsymbol{\omega}$. We also assume that only wheel angular speed is affected by wheel slip, i.e. that $\dot{v} \ll \dot{\omega}$, when calculating $g(\boldsymbol{y},\boldsymbol{c})$ for the ground speed sensor based algorithm.[7]

Table 2 lists the effects of various $\Delta\boldsymbol{\omega}$ on the functions $g(\boldsymbol{y},\boldsymbol{z})$. There is no column corresponding to all wheels slipping, since there would be no wheel left to steal the excess slip from in that case. The ground speed sensor based algorithm could detected that all wheels have lost traction as the vehicle decelerate over time, while the rest of the algorithms would remain oblivious to the fact.

12 Tuning

The parameters ϵ_1, ϵ_2 and ϵ_3 should be tuned so that no slip is detected during normal driving (i.e. no false positives) without delaying the detection of actual slip (i.e. minimize the amount of false negatives). This may be achieved by solving the

---

[7]There are circumstances under other quantities than ω and v are affected by wheel slip. If for example, both front wheels should slip, then the vehicle will tend to move forwards rather than turn, regardless of γ.

1	2	3	4	ATC system sensors	Ground speed sensor		Individual wheel tachometers		
1	-1/3	-1/3	-1/3	-1/3 - q/3	1/3	-1/3	4/3 - p/3		4/3
-1/3	-1/3	1	-1/3	1/3 + q/3	-1/3	1/3	p/3		-4/3
1/2	1/2	-1/2	-1/2	-1/2 - q/2	1/2	-1/2	p/2		0
-1/2	-1/2	1/2	1/2	1/2 + q/2	-1/2	1/2	-p/2		0
1/2	-1/2	1/2	-1/2	0	0	0	1		0
1/2	-1/2	-1/2	1/2	0	0	0	1		2
1/3	1/3	1/3	-1	-1/3 - q/3	1/3	-1/3	-p/3		-4/3
-1	1/3	1/3	1/3	1/3 + q/3	-1/3	1/3	4/3 + p/3		-4/3

Table 2: The first four columns of the table display slip in units of $\Delta\omega r$, i.e. slip per second, distributed over the four drive wheels—equation (19) provides an example. The last four columns display $g(\boldsymbol{y},\boldsymbol{c})$ in units of $\Delta\omega r$ where $q = q(0,0,\gamma) \in (0.86,1]$ and $p = p(0,0,\gamma) \in [0,0.18]$ for $\gamma \in [0,\pi/4]$. The headings with more than one column contain equations (15), (16), (17) (the tractor wheels) and (18). The trailer wheels slip calculation according to equation (17) gives the same result as the tractor wheels, except the rows should be switched—i.e. the missing column reads $p/3$, $4/3 - p/3$, ...

following linear program

$$\begin{aligned}
\min \sum_{i=1}^{m}&\ w_i^+ s_i^+ + u_i^+ t_i^+ + w_i^- s_i^- + u_i^- s_i^- \\
f^- &\leq g(\boldsymbol{y}_k,\boldsymbol{c}) \leq f^+, \forall k \in \{1,\ldots,n\} \\
-s_i^+ &\leq \epsilon_i^+ \leq t_i^+, \forall i \in 1,\ldots,m \\
-s_i^- &\leq \epsilon_i^- \leq t_i^-, \forall i \in 1,\ldots,m \\
s_i^+&, s_i^-, t_i^+, t_i^- \geq 0, \forall i \in 1,\ldots,m,
\end{aligned} \qquad (20)$$

where the $w_i^\pm, u_i^\pm$ are weights and the $s_i^\pm, t_i^\pm$ are help variables.

The problem (20) was solved in MATLAB over datasets from the road in figure 4 on the first three forward gears with varying load mass. The functions $f^\pm$ was set to

$$f^\pm = \epsilon_1^\pm + \epsilon_2^\pm|\gamma|, \qquad (21)$$

where terms like $|\dot\gamma|$, $\gamma\dot\gamma$ and γ^2 have been excluded since the optimal solution to problem (20) paid little or no mind to them. The weights used where $w_1^\pm = u_1^\pm = 1$, $w_2^\pm = u_2^\pm = 1/10$.

To obtain the amount of wheel slip per second $\Delta\omega r$ required for the algorithms to detect a slip of the front wheel, we solved

$$g(\boldsymbol{y},\boldsymbol{c}) = f^+ \qquad (22)$$

for $\boldsymbol{\omega}r = (\omega r,\ {-}\Delta\omega r/3,\ {-}\Delta\omega r/3,\ {-}\Delta\omega r/3)^T$ and simplified matters by using the values of $g(\boldsymbol{y},\boldsymbol{c})$ from table 2. The results are displayed in figure 5.
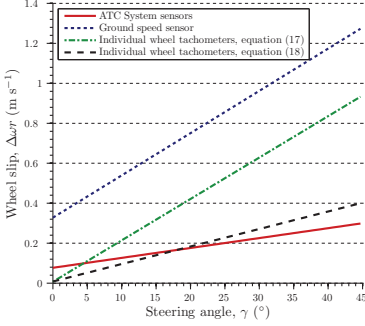
Figure 5: The amount of slip per second, $\Delta\omega r$, required for the different algorithms to detect a slip of the front wheel as a function of the steering angle, γ. These values are obtained as solutions to equation (22) where $g(\boldsymbol{y}, \boldsymbol{c})$ is taken from table 2 (or equation (19)) and f^+ have been determined by solving the problem (20) over simulation data from ADAMS with the articulated hauler being run repeatedly over the road in figure 4 on the first three forward gears with zero, half or full load mass (39 000 kg). The trailer unit velocity based algorithms (equations (16) and (17)) have been omitted since they are not primarily intented for detection of tractor unit wheel slip. The $\Delta\omega r$ curves were linearized to make the look of the graph clearer.

13   Conclusions and further work

While the results shown in table 2 speak in favor of the algorithm requiring individual wheel tachometers, those in figure 5 speak in favor of the algorithm based on ATC system sensors. The $\Delta\omega r = 0.4$ m s^{-1} < 75 rpm required to detect slip using equation (18) is well within acceptable limits. Non-planar motion, such as out of phase washboards, have not been taken into consideration wherefore the actual limits should be somewhat higher.

The algorithm based on equation (17) cannot fail to detect slip according to the results in table 2, yet still performs poorly based on the findings of figure 5. The ground speed sensor based algorithm also performs poorly. Note that the results in table 2 (and hence also in figure 5) underestimates the power of the ground speed based algorithms due to the $\dot{v} \ll \dot{\omega}$ assumption.

Better performance could perhaps be achieved by more careful tuning, using for example functions $f^{\pm}$ that are piecewise linear in γ and v, and setting the objective to $\sum_k f^+(\boldsymbol{y}_k) - g(\boldsymbol{y}_k, \boldsymbol{c})$. Also worth investigating is the possibility of esitmating v from

ω_i or having both individual wheel tachometers and a ground speed sensor and setting $g_i = \omega_i r - v_i$.

Further work include validating the kinematic model against an articulated hauler in the field. The measurements will be done using the ATC system sensors, two GPS reciever's and two inertial measuring units (IMU), one of each positioned at the two points O_1 and O_2 in figure 3.

14   Acknowledgements

References

[1] S. Savaresi, M. Tanelli, C. Cantoni, D. Charalambakis, F. Previdi, S. Bittanti, et al. Slip-deceleration control in anti-lock braking systems. In *16th IFAC World Congress*, 2005.

[2] U. Kiencke and L. Nielsen. *Automotive Control Systems For Engine, Driveline, and Vehicle*. Springer, Berlin, 2005.

[3] E. Bakker, H.B. Pacejka, and L. Lidner. A New Tire Model with an Application in Vehicle Dynamics Studies. *SAE paper*, 1989.

[4] L. Li, F.Y. Wang, and Q. Zhou. Integrated longitudinal and lateral tire/road friction modeling and monitoring for vehicle motion control. *IEEE Transactions on Intelligent Transportation Systems*, 2006.

[5] K. E. Olsson. Method for controlling rotation speed, 2008. US Patent 2008/0275615.

[6] B.J. Holt, J.E. Jensen, S. Marathe, and S.A. Marks. Electronic traction control system, 2003. US Patent 6,631,320.

[7] S. Scheding, G. Dissanayake, E. Nebot, and H. Durrant-Whyte. Slip modelling and aided inertial navigation of an LHD. In *IEEE International Conference on Robotics and Automation*, 1997.

[8] U. Larsson, C. Zell, K. Hyyppa, and A. Wernersson. Navigating an articulated vehicle and reversing with a trailer. In *IEEE International Conference on Robotics and Automation*, 1994.

[9] H. Illerhag and Sjögren F. Study of Driveline Functionality During off-road Driving of an Articulated Hauler. In *15th European ADAMS User's Conference*, 2000.

[10] J. Markdahl. Traction control for articulated off-road vehicles. Master's thesis, Royal Institute of Technology, 2010.

PAPER E

[E] - Estimation of sideslip angles of a Volvo A25E articulated all-wheel drive hauler based on GPS/INS measurements

The author's main contribution: Collecting and analysing data.

Comment: Staffan Backén pre-processed the raw data using the software tool from NovaTel and converted it to Matlab format. Fredrik Broström (not credited in the paper) developed the software for logging data.

Estimation of sideslip angles of a Volvo A25E articulated all-wheel drive hauler based on GPS/INS measurements

Ulf Andersson

Division of Systems and Interaction, Luleå University of Technology, 971 87, Luleå, Sweden

Gianantonio Bortolin

Volvo Construction Equipment AB, 635 10, Eskilstuna, Sweden

Staffan Backén

Division of EISLAB, Luleå University of Technology, 971 87, Luleå, Sweden

Thomas Gustafsson

Division of Systems and Interaction, Luleå University of Technology, 971 87, Luleå, Sweden

Abstract

We describe an off-line estimator for the sideslip angles of an articulated off-road vehicle based on measurements from Global Positioning System (GPS) and Inertial Navigation System (INS). The current implementation is a proof of concept and the intention is to develop a system that can be used as a reference for on-line estimators. By comparing measurements from two GPS/INS units, mounted on the front and rear part of the vehicle, it is possible to estimate the sideslip angles of both the front and rear part. The method has been tested on a Volvo A25E articulated all-wheel drive hauler equipped with two high precision GPS/INS units (NovAtel's SPAN-CPT). Tests have been performed when driving on asphalt, gravel and snow. The results from the tests are discussed.

1 Introduction

Improved traction control characteristics for 4x4 and 6x6 off-road construction vehicles, such as wheel loaders and articulated haulers, is one of the main goals of the research project "Traction control for off-road construction vehicles." which is a collaboration between Luleå University of Technology (LTU) and Volvo Construction Equipment (VCE), partially financed by the innovation agency Vinnova.

One of the aspects that we have analysed is the automatic engagement of differential locks in articulated haulers. One of the most challenging aspects is that a limited number of

sensors are available, i.e. the articulation angle, the transfer case in/out rotational speeds and the rotational speed of the third axel in the bogie of the hauler. At the moment there are no individual wheel speed sensors due to the harsh environment in which these vehicles operate.

One of the main results from [3,6] is the relationship between the front and back axle rotational speeds, the articulation angle and the sideslip angles of an articulated hauler according to

$$v_{34} = q(\alpha_{12}, \alpha_{34}, \Upsilon)v_{12} + q\left(-\frac{\pi}{2}, \alpha_{34}, \Upsilon\right)\frac{d\gamma}{dt}l_{12} \, , \tag{1}$$

$$q(\alpha_{12}, \alpha_{34}, \gamma) = \frac{l_{34}\cos(\alpha_{12}+\gamma)+l_{12}\cos(\alpha_{12})}{l_{12}\cos(\alpha_{34}-\gamma)+l_{34}\cos(\alpha_{34})}$$

Where α_{12}, α_{34}, γ, v_{12}, v_{34}, l_{12}, and l_{34} are according to figure 1 and q is the quotient of the steady state turning radii ($\frac{d\gamma}{dt} = 0$).
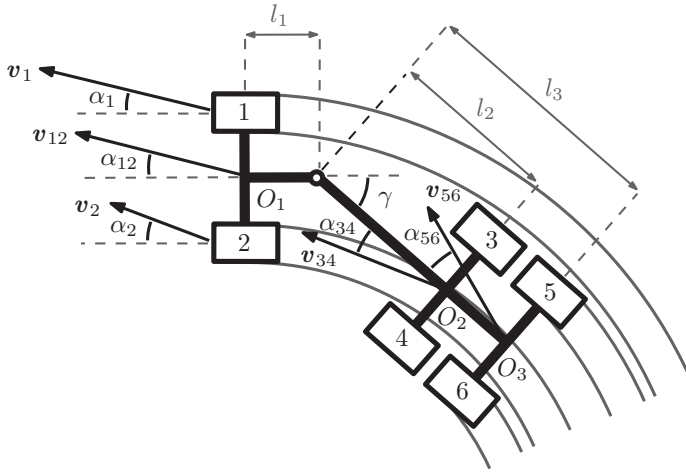
Figure 1. Sideslip angles of wheels, αI, and tractor/trailer parts, αij, of a hauler and the articulation angle γ are illustrated in this figure. The corresponding ground speed components are denoted vi and vij respectively.

The sideslip angle is the angle between the heading and the travelling direction, see figure 2. Sideslip angles depend on several variables, such as tire-road friction characteristics, load, speed, etc.

Equation (1) has been derived from kinematics considerations and partially validated using a 3-D model implemented in IMC Adams. Clearly, it would be very interesting to validate and further develop equation (1) by using measurement from a real vehicle in different road and load conditions.

The scope of this paper is to describe a NovAtel GPS/INS measurement system set-up that allows such kind of measurement, particularly the sideslip angles.

Next we are going to define wheel slip and sideslip angles more in detail as well as traction control and the GPS/INS. Section 2 describes our objective. In section 3 we describe the systems that we have used and the algorithms for estimation of the sideslip angles. Test

146

results are presented and discussed in section 4. The work we plan for the future is described in section 5. Some data about our test vehicle is described in section 6. References are found in section 7.

1.1 Wheel slip

Wheel slip is frequently mentioned in this paper and hence we need to give a formal definition. The force a tire receives from the road can be decomposed along three axes, i.e. the lateral force, the longitudinal force and the normal force. The presence of both longitudinal and lateral forces generates longitudinal and lateral wheel slips. There are different definitions in the literature, but in this paper we define the longitudinal slip in the direction of motion and the lateral slip at right angles to this, see Figure 1. The sideslip angle of a wheel is defined as the angle between the orientation (heading) of the tire and the orientation of the velocity direction. If the lateral slip is zero, then the sideslip angle is also zero and the heading and the drive direction are the same. Wheel slip depends on a number of variables. For instance, the friction between the tires and the surface, the tire characteristics, the steering / articulation angle, the load weight, the braking force, the accelerating force, etc. [15].

Generally, longitudinal wheel slip concerns traction control properties such as computation of reaction forces and wheel speed. Lateral wheel slip usually concerns stability properties such as turnability. Note however that the calculation of longitudinal wheel slip requires the sideslip angles since wheel slip is a vector.

It should be noted that wheel slip always occurs when rubber wheels are being used. Therefore it is important to distinguish between wanted and un-wanted slip. When the wheel spins, then un-wanted slip is present. In the continuing discussion, "slip" is synonymous with "un-wanted slip".
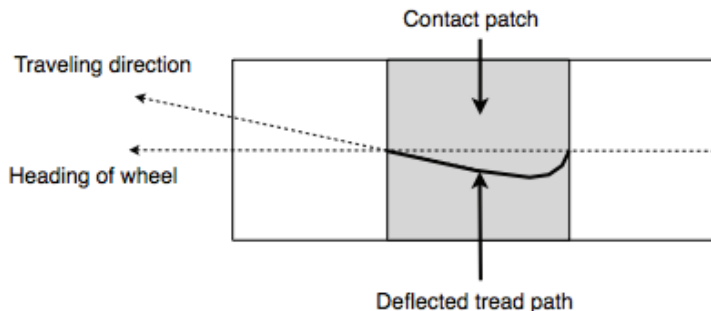

Figure 2. The sideslip angle is the angle between the travelling direction and the heading of the wheel. If the travelling direction and the heading of the wheel coincides, there is no sideslip.

1.2 Traction control

Traction control for off-road vehicles such as articulated all-wheel drive haulers is of great importance to improve the vehicle performance. A well-known method to reduce the slip and thereby improve the traction is to engage differential locks in the driveline of the vehicle. The drawbacks of differential locks that are engaged are for instance increased wear, increased fuel consumption but also reduced turnability of the vehicle [14]. Therefore, the differentials should be locked only when necessary, ideally only when slip occurs or is about to occur. A number of methods to detect slip have been reported in the literature. Some of them utilize dynamical models of the vehicle where sideslip angles are important inputs.

Traction control implies that the drive force of a driving wheel is controlled in some way. If the wheel starts to slip excessively, the drive force, which has a negative impact on the traction performance of the vehicle, is reduced.

Another method of traction control is to use combinations of braking control and engine control instead of control of differential locks. This method originates from anti-lock braking systems (ABS) developed in the car industry [16].

Volvo Construction Equipment has in the recent years initiated a number of development projects with the goal to have the traction control characteristics improved in both an optimal and robust way.

For the Volvo haulers, there is today one commercially available system for traction control called ATC [1]. The ATC system is based on information from sensors measuring the rotation speed in the forward and rearward driveline shaft respectively as well as a sensor measuring the articulation angle. The ATC system controls actuators for dog-clutch engagement /disengagement.

Traction control can be improved by refinements in the driveline design, and also by installing sensors and actuators with electronic interfaces allowing for computer control of the clutch. Additional sensors and/or more sophisticated algorithms may also increase the performance of an existing electronic traction control system.

In 2009, Volvo Construction Equipment and Luleå University of Technology (LTU) in Sweden started a co-operation within the field of traction control of off-road vehicles. One outcome of the co-operation so far is the system discussed in this paper.

Most of the research and development work seems to be aimed at on-road applications, mainly cars but also trucks to some extent. Less has been reported that relates to off-road applications [22,23,24,25,26,27,28,29,30,31,32,33,34]. There are some patents within the field of traction control of off-road vehicles [17,18,19,20,21].

A useful tool for analysis and development of control functions is simulation software. Complex models describing vehicle and tire dynamics can be implemented in software packages such as IMC Adams [4]. Control algorithms can be implemented and simulated in software packages such as Matlab/Simulink [5]. By combing these types of simulation tools in co-simulation mode, it is possible to simulate traction control of vehicles.

A simulation study on traction control properties of haulers has been carried out in a Master thesis work performed at VCE, [3]. The model of the hauler was implemented in ADAMS

and the traction control algorithms were implemented in Simulink, [6]. One of the main results of the simulation study is equation (1).

One conclusion from the simulation study was that sideslip occurs and has a negative impact on the estimation accuracy of wheel slip. This conclusion is valid if the only sensor information used is the articulation angle and the rpm of the forward and rearward driveline shaft respectively.

It is also noted in the paper that adding sensors that measures the rotational speed of each individual wheel improves the situation, but only some combinations of individual wheel slip can be detected depending vehicle parameters. See [6] for details. The main benefit with individual wheel sensors is that slip of a single wheel can more easily be detected.

To validate the simulation models, measurements of the wheel slip of a real hauler would be valuable. Unfortunately, slip is complicated to model accurately. Therefore it would be interesting to measure the slip to get an idea of for instance the magnitude of the sideslip angles during different driving conditions. This would also make it possible to compare measured sideslip angles with simulated ones.

Such measurements are also valuable in further analysis of complementary sensors needed for robust and accurate on-line estimation of wheel slip.

1.3 GPS/INS

GPS/INS units consist of a GPS receiver integrated with accelerometers and also gyros. If we assume that the accelerometer and gyros have three axles, the output from the GPS/INS includes for instance:

- Position in the co-ordinate axles of the earth (north, east, z).
- Ground speed components in the co-ordinate axles of the earth.
- Heading in the northeast plane parallel to the surface of the earth.
- Pitch angle, which is the angle - in the heading direction - between the GPS/INS unit and the northeast plane.
- Roll angle, which is the angle - perpendicular to the heading direction - between the GPS/INS unit and the northeast plane.

Some of these outputs can be used to estimate the sideslip angle of a wheel as illustrated in figure 1 and 2. This is due to the fact that we can estimate both the travelling direction and the heading. If we assume that the GPS/INS unit is mounted right above the center of the front axel wheels and that we are driving on a flat surface (for the sake of simplicity), we have

$$\theta_{O1w} = \theta_{gi} \tag{2}$$
$$\beta_{O1w} = tan^{-1}(\frac{v_{gin}}{v_{gie}}) \tag{3}$$
$$\alpha_{O1w} = \beta_{O1w} - \theta_{O1w} \tag{4}$$

Where the outputs θ_{gi} v_{gin} and v_{gie} are the heading, the north speed component and the east speed component of the GPS/INS unit. $\theta_{O1w}, \beta_{O1w}$, and α_{O1w} are the heading, the travelling direction and the sideslip angle of the wheel respectively.

2 Objective

The objective of this work has been to test a new measurement system set-up for off-line estimation of sideslip angles of an articulated off-road vehicle.

The motivation to the objective is as follows.

The difference between an on-line estimator and an off-line estimator is that an on-line estimator works in real-time in opposite to an off-line estimator. Off-line estimators process a set of (logged) data at one time.

The main advantage with off-line estimators is that it is possible to use statistical signal processing methods and computationally heavy algorithms that cannot be implemented in real time but improves the accuracy in the estimates significantly.

On the other hand, if the estimator should be used for control purposes, it has to work in real-time which limits the estimation methods to such that can be implemented in on-line estimators.

Therefore, an off-line estimator with high accuracy can be used to verify the performance of an on-line estimator. For instance, verify that requirements regarding accuracy in the estimation of wheel slip in a traction control system are fulfilled.

3 System description

The current implementation of the system is intended for proof of concept. Therefore, proven and commercially available sub-systems have been used where possible.

Two identical GPS/INS units were mounted on the rear and front part of the vehicle. Each unit consisted of an antenna and a GPS receiver integrated with three-axis accelerometers and also three-axis gyros. The GPS/INS units were connected to a PC aboard the vehicle logging the data output from each unit.
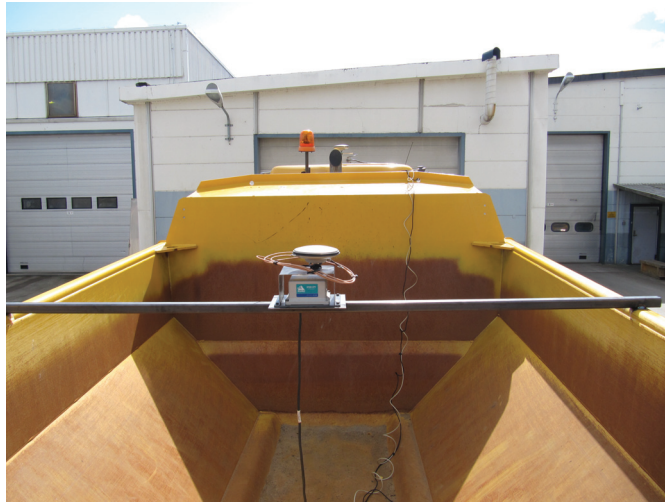
Figure 3. The two GPS/INS units mounted on the A25E hauler.

The system also consists of a local stationary GPS base station that is connected to another PC that logs the data from the base station. The base station is located in the test area.

The logged data is post-processed in two steps. The first step is to process the data for each unit individually in a software package that estimates pose, speed, etc. The information from the base station is used to improve the accuracy in the estimations by removing common mode errors. This result in highly accurate estimates, decimetre-level position accuracy and orientations accuracy within a small fraction of a degree, and can thus be considered as a truth-reference for the application described in this paper.

The second step is to combine the information from each unit. By comparing measurements from the units, it is possible to estimate the sideslip angles of both the front and the rear part of the hauler.

The post processing is described in detail below.

Additionally, if information from sensors integrated in the vehicle is logged in parallel to the GPS/INS data, it is possible to compare the measurements from the integrated sensors - for instance articulation angle and inclination - with the information from the system. It is also possible to compare the ground speed of the vehicle measured by the system with the drive speed based on rpm measurements.

3.1 System requirements

The basic system requirement is that it shall be possible to use the system on any vehicle, which means that the system itself must contain all the necessary sensors. The only requirement on the vehicle itself is the power supply.

Practical requirements:

- It shall be easy to mount the system on the vehicle.
- The system shall be adopted for use in the temperate climate zone.

- 220 V AC supply voltage, 12 or 24 V DC supply voltage.

3.2 System hardware

The most critical sub-systems for achieving sufficient accuracy in the estimates are the GPS/INS units on the vehicle. At present, NovAtel's SPAN-CPT systems are used which have the GPS and INS hardware integrated in one physical unit of dimensions 150x150x90 mm. The INS sends data periodically with 100 Hz; the GPS sends data periodically with 1 Hz [7].

The base station that has been used is NovAtel's DL-4 GPS receiver. The unit sends data with 1 Hz [8].

The antennas that have been used are NovAtel GPS-702L [9].

The antennas should be placed such that blocking of satellites is minimized. That implies that the antennas on the vehicle shall be placed on top of the vehicle and the antenna connected to the base station shall be placed in an open location.

The PC's that has been used for logging are UNO-2171 and UNO-2172 [10,11]. An important property of these PC's is that they have physical RS-232 ports for communication with the NovAtel units. They also support solid-state types of hard drives that can withstand the vibrations in the vehicle.

3.3 Data logging

The quality of the estimates from the post-processing of the GPS/INS data is greatly improved if a specific procedure is followed when logging data. Put simply, this allows for the calibration of several unknown parameters in a large Kalman filter.

The following procedure were devised and used when recording GPS/INS data.

1. Start logging both the GPS/INS units as well as the base station GPS unit.
2. Log for about five minutes with the vehicle at standstill. This data is used to find the absolute orientation of the INS by measuring the acceleration vector due to gravity and the rotation of the earth.
3. Drive in a wide "8-pattern", not too slow. This data is used to calibrate for the INS unit's orientation relative the frame of the vehicle.
4. Drive freely in any desired pattern – this is the data that are later used as a truth reference of the vehicle's position and orientation.
5. Repeat drive in a wide "8-pattern".
6. Log for about five minutes with the vehicle at standstill.
7. Turn off the logs.

Raw data from the units are logged.

3.4 Post processing of data

3.4.1 NovAtel post-processing software

A post-processing package for GPS/INS data, NovAtel Waypoint Inertial Explorer 8.3 [12], was used to process the recorded data. We will briefly describe this procedure, but first we will elaborate slightly on the features of the GPS receiver that were used.

The fundamental principle of satellite navigation relies on time of arrival. Each satellite transmits a time-stamped code and by comparing flight times of several such signals the receiver can solve for a position.

The GPS receivers used in this paper are high-accuracy, dual-frequency, carrier phase, and differential receivers. The GPS satellites transmit not only a signal known as C/A, which is what is used in all current mass-market receivers, but also an encrypted signal called P(Y). The latter have a much larger bandwidth and are also available on two separate frequencies. The increased bandwidth translated into a higher accuracy of the user-satellite distance measurements resulting in improved position estimates. By using measurements on two separate frequencies the accuracy is further increased.

By carrier-phase we refer to a receiver that use not only the code but also the carrier of the signal to solve for a position. Somewhat simplified, measurements of the code are absolute but noisy, while carrier-phase estimates are ambiguous but accurate.

Finally, differential refers to the use of two receivers, a stationary base and a moving rover. Rather than considering the user-satellite distances directly, the base-rover distance is used. With this technique, all common mode errors are removed.

At a rate of 1 Hz, The GPS receivers, base and rover, produces estimates of the pseudo-range (derived from code measurements) and the carrier-phase for both frequencies of all visible satellites. The INS delivers three-axis accelerometer and three-axis gyro data at a rate of 100 Hz.

Details about the processing are outside the scope of this paper, but it can be considered as a Kalman filter with a large number of states. All states are available as outputs, but for the purpose of this application, the main concern is position, velocity, acceleration, orientation, and angular velocity. Typical accuracies are around 1dm for position and a small fraction of a degree for the orientation.

An interesting application of the SPAN-CPT system is described in [35] where the interested reader can find more details about the system.

We refer the interested reader to [37] for a description of the Kalman filter and the ideas behind it.

3.4.2 Algorithms for estimation of sideslip angles of an articulated hauler

The outputs from the first post-processing step that are used in the estimation of the sideslip angles and the articulation angle are described in brief in the introduction. The outputs are divided into outputs for the tractor (front part) and outputs for the trailer (rear part) respectively.

Assume that the difference in pitch angle between the tractor and the trailer is so small that it can be neglected. Make the same assumption for the roll angle, as well as the difference in

speed in the z-direction. Also assume that the GPS/INS units are mounted in the intersections of the wheel axles and the lengthwise axles of the tractor and the trailer respectively. The intersections are denoted O_1, O_2 and O_3 in figure 1. Then we have:

- The travelling direction is the angle between the north axis speed component and the east axis speed component of the tractor, β_{12}, and the trailer, β_{34} / β_{56}, respectively.
- The sideslip angles are the difference between the travelling direction and the heading of the tractor, θ_f, and the trailer, θ_r, respectively (α_{12}, α_{34} and α_{56} in figure 3.)
- The articulation angle between the tractor and the trailer is the difference in the heading between the tractor and the trailer. (γ in figure 1.)

Formulated as equations we have (see figure 1):

$$\beta_{12} = tan^{-1}(\frac{v_{O1n}}{v_{O1e}}) \tag{5}$$

$$\beta_{34} = tan^{-1}(\frac{v_{O2n}}{v_{O2e}}) \tag{6}$$

$$\beta_{56} = tan^{-1}(\frac{v_{O3n}}{v_{O3e}}) \tag{7}$$

$$\alpha_{12} = \beta_{12} - \theta_f \tag{8}$$

$$\alpha_{34} = \beta_{34} - \theta_r \tag{9}$$

$$\alpha_{56} = \beta_{56} - \theta_r \tag{10}$$

$$\gamma = \theta_f - \theta_r \tag{11}$$

It should be observed that the heading is the same for all points on the tractor/trailer, which is not true for the speed components of the tractor/trailer. The travelling direction can not be calculated when the vehicle is not moving, but on the other hand wheel slip is not relevant in this case.

It should be noted that a complete estimate of the sideslip angles should also include the accuracy in the estimates. We have omitted this since it would require more knowledge about the statistical properties, for instance distribution functions, in the outputs from the NovAtel post-processing software. In this sense, the term "estimate" in the title might be somewhat misleading.

However, if the errors in the outputs have a small influence in the estimate of the sideslip angles, "patterns" should be possible to observe when, for instance, negotiating the same curve several times with un-changed driving condition (wheel to ground friction, load, etc.).

4 Test results

At present, the system has been used to estimate the sideslip angles of an A25E hauler under various driving conditions. Tests has been done when the hauler has been driving on asphalt, gravel and snow, loaded and un-loaded. The tests have been performed at the Volvo test facility in Eskilstuna, Sweden.

During the tests, the GPS/INS unit including the antenna of the front part have been mounted on top of the roof of the tractor such that the center of the antenna has been located right above the front wheel axis in the center of the vehicle. The GPS/INS unit including the antenna of the rear part has been mounted on a beam on top of the dump body of the trailer such that the center of the antenna has been located right above the front bogie axis in the center of the vehicle.

The articulation angle and sideslip angles that have been estimated during the tests are γ, $\alpha_{12\_tractor}$ and $\alpha_{34\_trailer}$ according to equations (11), (8) and (9) respectively.

Some results from the tests are illustrated and discussed in brief in the figures below.

Table 1. The accuracy, according to the NovAtel post-processing software, is summarized in this table for the GPS/INS unit on the tractor / trailer. The accuracy is defined in terms of min value, mean value and max value from the run illustrated in figure 5.

	Estimated position standard deviation (1-σ), east axis	Estimated position standard deviation (1-σ), north axis
Unit	[m]	[m]
Min	0.0070 / 0.0070	0.0040 / 0.0040
Mean	0.0115 / 0.0110	0.0072 / 0.0067
Max	0.0360 / 0.0350	0.0230 / 0.0230

	Estimated velocity standard deviation (1-σ), east axis	Estimated velocity standard deviation (1-σ), north axis
Unit	[m/s]	[m/s]
Min	0.0020 / 0.0020	0.0020 / 0.0020
Mean	0.0024 / 0.0024	0.0022 / 0.0022
Max	0.0040 / 0.0040	0.0040 / 0.0040

	Estimated heading accuracy
Unit	[degree]
Min	0.0119 / 0.0113
Mean	0.0170 / 0.0153
Max	0.0252 / 0.0208

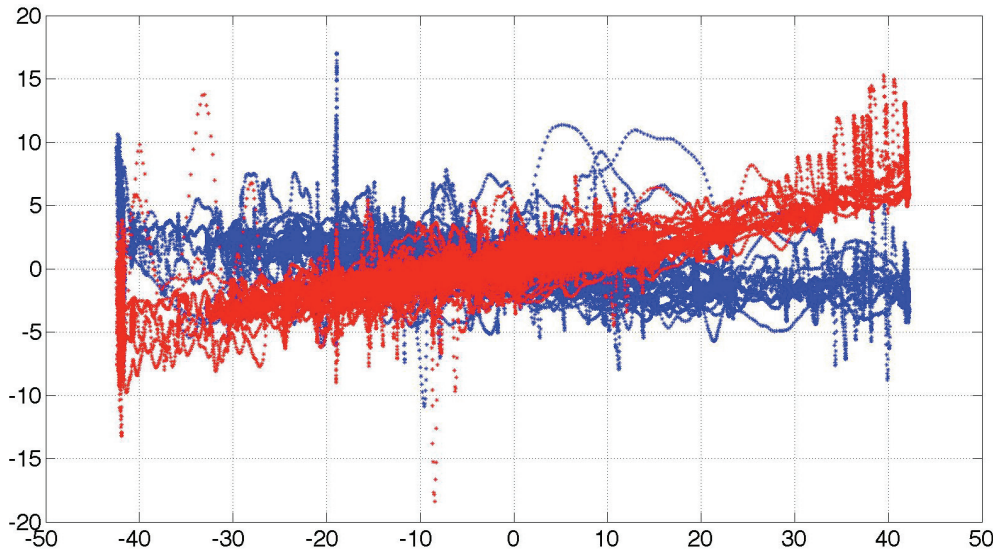Figure 4. Estimated sideslip angles for the tractor (blue) and the trailer (red) from the run illustrated in figure 5. The sideslip angles are plotted as a function of the articulation angle. The units for the sideslip angles and the articulation angle are degree.
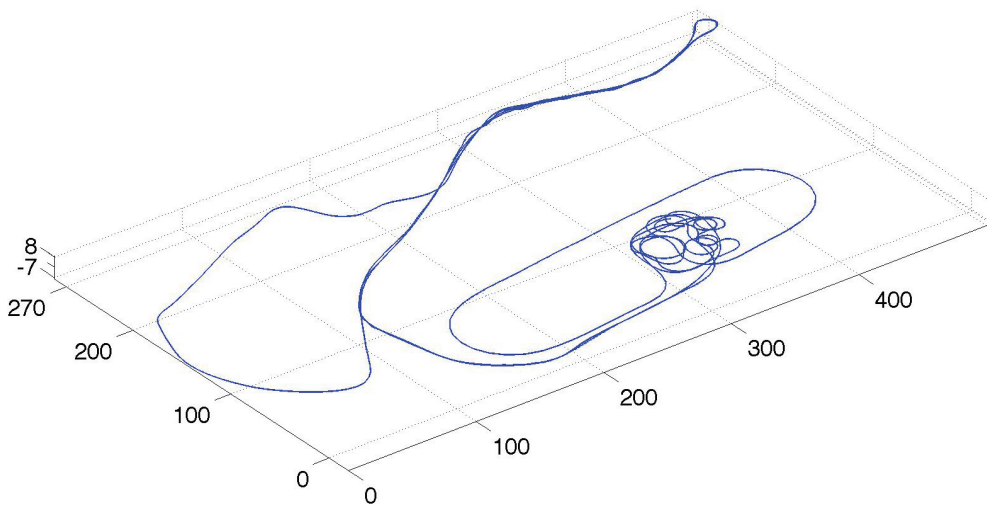
Figure 5. The sideslip angles in figure 4 originate from the path illustrated in this 3D plot. The units are meters. The surface consists of both asphalt and gravel.
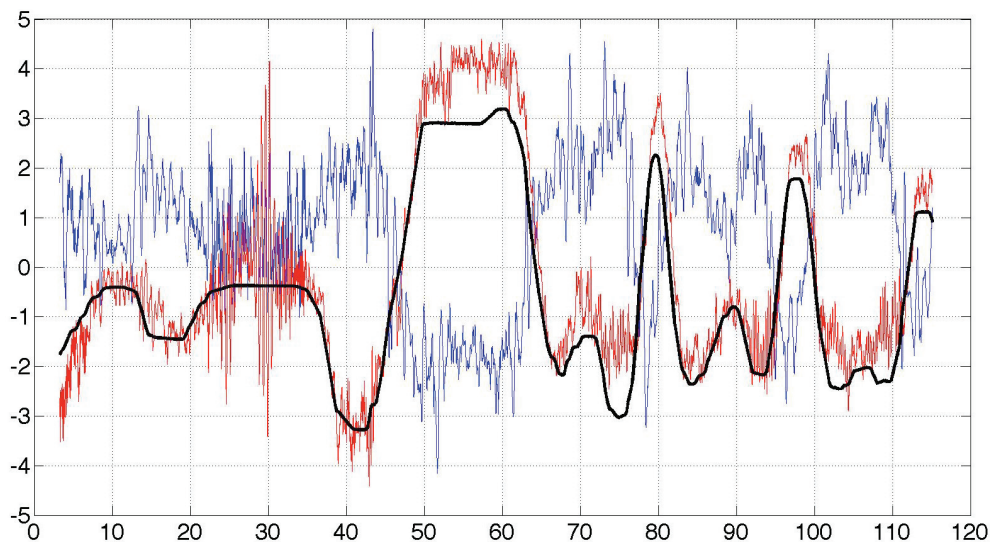
Figure 6. Detail from the run illustrated in figure 5. In this figure, the angles are plotted as a function of time. The blue line is the sideslip angle of the tractor and the red line is the sideslip angle of the trailer. The black line is the articulation angle down scaled by a factor 10. The detail is "part of circles" visible in figure 5. The "mirroring pattern" in the estimated sideslip angle for the tractor and the estimated sideslip angle for the trailer is repeated when driving several runs in this part of the test area. The ground in this part of the test area consists of asphalt. The asphalt was dry during the test.

Figure 7. The distance between the GPS/INS units as a function of the articulation angle during the run illustrated in figure 5 (blue). The theoretical distance is also plotted (red). The unit for the distance between the GPS/INS units is meter and the unit for the articulation angle is degree. There are outliers in the data, as is clear in this figure, that are explained in figure 8. The total number of samples is 83395 per GPS/INS unit. The "extreme" outliers are very few compare to the total number of sam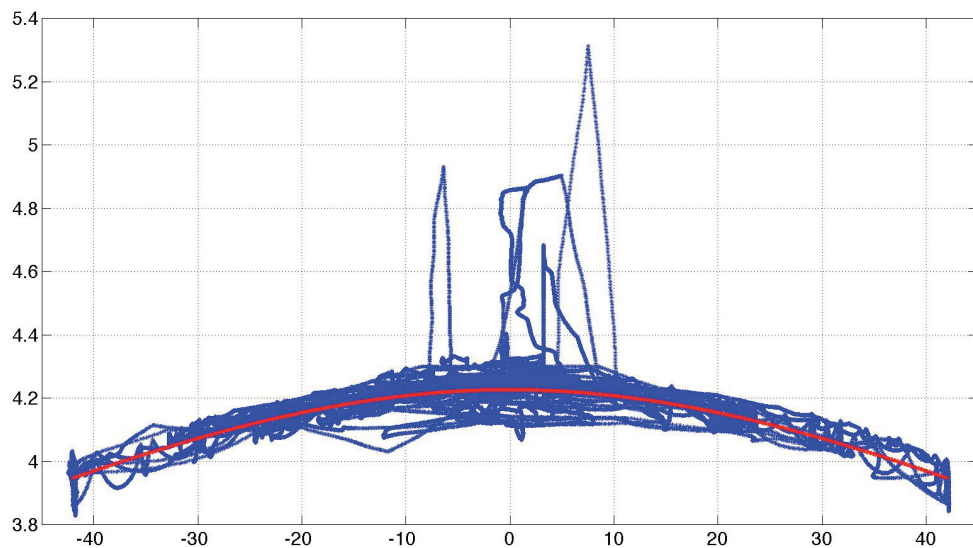ples. It should be observed that the data from each GPS/INS unit is processed separate. No consideration is taken in the processing to the fact that the actual distance between the units are known within a few centimetres. Therefore, this figure also gives a good illustration of the accuracy in the position estimations.
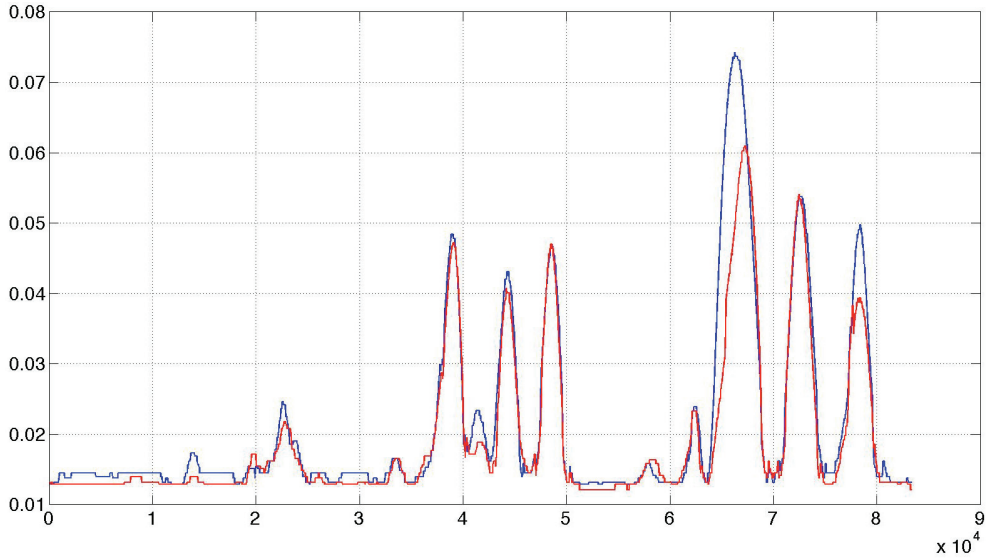
Figure 8. The standard deviation in the estimated positions as a function of sampling instant is illustrated in this figure. The blue curve is the standard deviation in the position estimate from the GPS/INS unit on the tractor and the red curve is the standard deviation in the position estimate from the GPS/INS unit on the trailer. The correlation between increasing standard deviation and outliers illustrated in figure 7 is high. When the standard deviation is low, the deviation from the theoretical distance between the GPS/INS units is also low. When the standard deviation increases so does the deviation from the theoretical distance between the units. The high correlation between the deviation from the theoretical distance and the standard deviations indicates that the estimators work properly. A corresponding 3D-plot to figure 5 were samples with standard deviation above a certain threshold was plotted in different colours reviles that the standard deviation increases when driving close to trees and in slopes. This is what we should expect since the probability of blocking of satellites increases in such areas. It is also interesting to note that the correlation between the standard deviation in the position estimate from the two GPS/INS units is high. This is also something that we should expect since they have approximately the same line of sight to the satellites.

158

5 Conclusions

A summary of the tests we have done so far is that the proposed method to estimate the sideslip angles looks promising. We have however only done a limited number of tests, all using the same vehicle.

To set up a test that results in a few hours of data demands - for practical reasons - very careful planning. We are hopeful that the method for off-line estimation of sideslip angles has good potential, but we want to base conclusions on more data - mainly data from other vehicles then our "test vehicle".

6 Future work

As is noted in the conclusions from the tests with the A25E, we need to have more data before we can draw conclusions regarding the proposed method for off-line estimation of sideslip angles. Data collection from other then the A25E we used in the tests is therefore a prioritized work.

We will also work to improve the accuracy in the post-processing estimation by doing this in one single step instead of two steps. The idea is to use the fact that the relative distance between the units mounted on the vehicle is known in the post processing. The motivation for this comes from the tests results. This will also make it possible to state statistical properties of the estimation errors. We will extend the off-line estimator to also estimate longitudinal slip.

The output from the first pre-processing step also includes an estimation of the 3D pose, which is not needed for the estimation of the sideslip angles but can be used to evaluate the movement pattern of the vehicle.

The system has been used to evaluate the pose estimation from a real-time GPS/INS based system that estimates the pose of a wheel loader on-line. The evaluation was a part of a master thesis work at Volvo CE reported in [36].

We are planning to continue to use the system to estimate the pose of articulated vehicles for evaluation purposes. One example is to compare the movement pattern of an articulated vehicle equipped with a traditional mechanical driveline with one that uses hub motors that are controlled individually. Vehicles with hub motors have a larger degree of freedom when it comes to control of the vehicle. It is important that the control of a single wheel does not counteract with the control of the other wheels and the control of the steering cylinders for the articulating joint.

We will use a small articulated vehicle with electric hub motors as a test platform for experiments. The vehicle is equipped with electric hub motors in each of the four wheels as well as an electric motor that controls the articulation angle [2].

7 The Volvo A25E hauler

A selected amount of specifications that relates to the content in this paper is presented below [13].

Engine: Volvo, V-act Tier III, 6-cylinder in-line, direct injected electronically controlled. SAE J1995 Gross power 305hp @ 35 r/s (2100 rpm). SAE J1995 Gross torque 1 700 Nm @ 20 r/s (1200 rpm).

Torque converter: Built-in Lock-up function. Transmission: Fully automatic Volvo PowerTronic planetary transmission with six forward gears and two reverse gears. Dropbox: Volvo-designed with high ground clearance. Axles: Heavy duty, purpose built Volvo design with fully floating axle shafts, planetary type hub reductions and 100% dog clutch type diff-lock. Operational mode: 6x4 or 6x6. Top speed forward 53 km/h (32.9 mph). Top speed reverse 13 km/h (8.1 mph).

Dual circuit system with air-hydraulic dry disc brakes on all wheels. Circuit division: One circuit for front axle and one for bogie axles. Retarder: Hydraulic, infinitely variable, integrated in transmission.

Steering system hydraulic cylinders: Two double-acting steering cylinders. Steering angle: 3,4 steering wheel turns lock-to-lock, ±45°.

Frames and Chassis: Box type design frames. 360° rotating, high positioned hitch. Independent wheel movement via a 3-point mounting system. Straddle mounted bogie beam.

Tires: 23,5R25.

Operating weight unloaded: Front 12 160 kg, rear 9 400 kg, total 21 560 kg, payload 24 000 kg. Operating weight loaded: Front 14 140 kg, rear 31 420 kg, total 45 560 kg.

Measures of length.

- Distance front wheel axle to articulating joint: 1 210 mm.
- Distance forward bogie axle to articulating joint: 2 965 mm.
- Distance rearward bogie axle to articulating joint: 4 635 mm.
- Gauge front wheel axle and bogie axles: 2 258 mm.
- Distance ground to top of cabin: 3 318 mm.
- Distance ground to top of dump body: 2 778 mm.

References

1. "Volvo Articulated Haulers A25E, A30E," Ref. No. 21 B 100 3154, September 2007.
2. M. Karlsson. "ArtiTrax II", Master's thesis, Luleå University of Technology, Sweden 2010.
3. J. Markdahl. "Traction control for articulated off- road vehicles", Master's thesis, Royal Institute of Technology, Sweden 2010.
4. "MBSSoft 4.0 for ADAMS User's Guide," 2001.

5. http://www.mathworks.com/.
6. J. Markdahl G. Bortolin and U. Andersson, "Traction Control for Articulated Off-road Vehicles", Proceedings of Reglermöte 2010, Lund, Sweden 2010.
7. "NovAtel SPAN-CPT Receiver User Manual," OM-20000122, Rev. 3, 2009/08/10.
8. "NovAtel DL-4 User Manual," OM-20000063, Rev. 1, 2001/08/24.
9. "NovAtel GPS-702L User Manual," OM-20000091, Rev. 2, 2005/09/01.
10. "UNO-2171 User Manual," Part No. 2003217101, 2nd Edition, August 2007.
11. "UNO-2172 User Manual," Part No. 2003217200, 1st Edition, June 2007.
12. "NovAtel Inertial Explorer User Guide," OM- 20000106, Rev. 7, 2010/04/08.
13. "Volvo Articulated Haulers A25E, A30E," Ref. No. 21 B 100 3154, September 2007.
14. A.F. Andreev, V.I. Kabanau and V.V. Vantsevich, "Driveline Systems of Ground Vehicles, Theory and Design", CRC Press, 2010.
15. H.B Pacejka, "Tire and Vehicle Dynamics", SAE International and Elsevier, 2005
16. H. Lee and M. Tomizuka, "Adaptive Vehicle Traction Force Control for Intelligent Vehicle Highway Systems (IVHSs)", IEEE Transactions on industrial electronics, vol. 50, no. 1, 2003
17. J. Smith and D. Suckow, "Differential lock control system," July 4 2000. US Patent 6,085,138.
18. B. Holt, J. Jensen, S. Marathe, and S. Marks, "Electronic traction control system," Oct. 7 2003. US Patent 6,631,320
19. J. Hosseini, M. Cobo, N. Rytter, and A. Verheyen, "Method and apparatus for controlling differentially driven wheel-slip for an articulated machine," July 9 1996. US Patent 5,535,124.
20. T. Murakami and Y. Sugano, "Control method of inter-axle differential and inter-axle differential apparatus," Mar. 26 2001. US Patent App. 09/816,369.
21. K. E. Olsson, "Method for controlling rotation speed," Nov. 6 2008. US Patent 2008/0275615.
22. U. Kiencke and L. Nielsen, Automotive Control Systems For Engine, Driveline, and Vehicle. Berlin: Springer, 2005.
23. S. Savaresi, M. Tanelli, C. Cantoni, D. Charalambakis, F. Previdi, S. Bittanti, et al., "Slip-deceleration control in anti-lock braking systems," in Proceedings of the 16th IFAC World Congress, Prague, Czech Republic, 2005.
24. Chen M-C, Wang W-Y, Li I-H, and Su S-F (2007). Dynamic slip ratio estimation and control of antilock braking systems considering wheel angular velocity. Proc. IEEE International Conference on Systems, Man and Cybernetics, pp. 3282-3287, Montreal, Que.
25. Hallowell S. J. and Ray L. R. (2003). All-wheel driving using independent torque control of each wheel. Proc. American Control Conference. Denver, Colorado, June 4-6, 2003, 2590-2595.
26. Hasemann J.-M. and Känsälä K. (1994a). A fuzzy controller to prevent wheel slippage in heavy duty off road vehicles. IEEE 44th Vehicular Technology Conference, 1994.
27. Hasemann J.-M. and Känsälä K. (1994b). An embedded distributed fuzzy logic traction control system for vehicles with hydrostatic power transmission. Proceedings, IEEE 7th Mediterranean Electrotechnical Conference, 1994.
28. Hasemann and Känsälä (1994), Avoiding slippage with fuzzy logic. Industrial Horizons, VTT Publications, Helsinki, 1994.
29. Jia Y. (2000). Robust control with declutch performance for steering and traction of 4WS vehicles under velocity-varying motion. IEEE Transactions on Automatic Control, vol. 8, no. 3, May 2000, 554-569.

30. Kachroo P., Tomizuka M. (1994). Vehicle Traction Control and its applications. Report UCB-ITS-PRR-94-08 California PATH Research Project, Dept. of Mechanical Eng., University of California, Berkeley.
31. Lee H., Tomizuka M. (1995). Adaptive Traction Control. Report UCB-ITS-PRR-95-32 California PATH Research Project, Dept. of Mechanical Eng., University of California, Berkeley.
32. Okubora T., Suhama M. and Kawamura A. (2002). Traction control characteristics of 4WD vehicle with anti-directional twin rotary motor. IEEE PCC 2002, Osaka, 588-592.
33. Sakai S., Sado H. and Hori Y. (1999). Motion control in an electric vehicle with four independently driven in-wheel motors. IEEE/ASME Transactions on Mechatronics, vol. 4, no. 1, March 1999, 9-16.
34. Verschoore R. and Duquesne F. (2001). Simulation of the influence of differential control on tractor work rate. Journal of Terramechanics, vol. 38, 221-233.
35. Kennedy S., Cosandier D., and Hamilton J, "GPS/INS Integration in Real-time and Post- processing with NovAtel's SPAN System", International Global Navigation Satellite Systems Society IGNSS Symposium 2007, The University of New South Wales, Sydney, Australia 4 - 6 December, 2007
36. R. Lilja, "A Localization and Navigation System for an Autonomous Wheel Loader", Master's thesis, Mälardalen University, Sweden 2011.
37. S. M. Kay, "Fundamentals of Statistical Signal Processing - Estimation Theory", Prentice-Hall PTR, 1993.

Contact information

Ulf Andersson (ulf.andersson@ltu.se) received his Master of Science in Industrial Electronics, Automatic Control, from Luleå University of Technology, Sweden in 1986. He received his Licentiate of Engineering degree in Automatic Control from the same university in 1989. The research work was done within the field of navigation methods for mobile robots. Between 1990 and 2009, Ulf Andersson has been working in the industry with laser based navigation systems for autonomous guided vehicles. During the later part, the work has been focused on autonomous and teleported mine vehicles. Ulf Andersson is currently working for Volvo Construction Equipment as a PhD student at Luleå University of Technology. His research interests are within the field of Traction Control for Off-Road Construction Vehicles.

Gianantonio Bortolin (gianantonio.bortolin@volvo.com) received his Master of Science in Electrical Engineering from the University of Padova, Italy, in 1999. He obtained the Pd.D. degree at the division of Optimization and System Theory, KTH, Stockholm in 2005. The main research topics were on process control and system identification. Since February 2006 he has been working at the Driveline Control group at Volvo Construction Equipment.

Staffan Backén (staffan.backen@ltu.se) obtained his Master of Science in electrical engineering from Luleå University of Technology in 2004. He defended his PhD thesis "On dynamic array processing for GNSS software receivers" in 2011 at Luleå University of Technology. His research interests mainly revolve around GNSS receivers with a focus on antenna arrays, receiver architecture, signal processing and sensor fusion.

Thomas Gustafsson (thomas.gustafsson@ltu.se) is Professor in Automatic Control at Luleå University of Technology, Sweden.

Acknowledgments

PAPER F

[F] - Tyre parameter estimation based on control of individual wheel drives

The author's main contribution: The idea to the method.

Comment: Fredrik Broström programmed ArtiTRAX and came up with the idea of multi-wheel estimation.

Tyre parameter estimation based on control of individual wheel drives

Ulf Andersson, Fredrik Broström, Thomas Gustafsson

Division of Systems and Interaction, Luleå University of Technology,

SE-971 87, Luleå, Sweden

Abstract

This paper describes a method to estimate tyre parameters for traction control applications based on control of individual wheel drives. The tyre parameters that are estimated are the rolling radius in driven mode (i.e. the rolling radius when the input torque to the wheel is zero) and the tyre longitudinal elasticity factor. The rolling radius in driven mode and the tyre longitudinal elasticity factor depend on several factors, among them the normal load. An important property of the method is that no transfer of load occurs during the estimation phase since the actual velocity of the vehicle is kept constant. Results from tests with ArtiTRAX, a 240 kg electric vehicle that carries 80 kg extra weight in three different front axle and rear axle distributions, are presented.

Keywords: Individual wheel drives, tyre parameter estimation, load transfer, rolling radius in driven mode, tyre longitudinal elasticity factor, traction control.

1 Introduction

1.1 Utilization of individual wheel drives

Provided that the drives that propel a vehicle with individual wheel drives are powerful enough, one drive is sufficient to control the actual velocity of the vehicle. Two or more drives can therefore be interpreted as redundant actuators, which raise the question of how this increased freedom should be used.

The contribution of this paper is the method proposed to estimate tyre parameters that make use of the increased freedom that individual wheel drives bring. The method has the following properties.

- A constant actual velocity of the vehicle is maintained during the estimation phase. This implies minimization of load transfer between the front axle and the rear axle. This is a desired property since load transfer disturbs tyre parameter estimates.

- The input torque(s) to the wheel(s) whose parameters are to be estimated are controlled such that the estimates are consistent.

The parameters that are estimated are the rolling radius in driven mode (i.e. the rolling radius when the input torque to the wheel is zero) and the tyre longitudinal elasticity factor. The method is constrained to non-sliding conditions on firm roads and dense terrains.

Huang and Wang (2013) has used a similar approach and point out that parameter estimation based on 4WD independent driven vehicles opens up the possibility for parameter estimation using redundant actuation without interfering vehicle motion control performance.

The redundant actuation can of course be used for other purposes. Hori (2004) lists the following possibilities: Antilock braking system, traction control system with local feedback control at each wheel, chassis motion control, estimation of road surface conditions. Laine (2007) propose a control allocation method, which separates the control law for the ground motion from the distribution of the desired motion forces among the available actuators. Senatore and Sandu (2011) propose that the freedom should be used to distribute torque between the drive axles so that the fuel consumption is minimized.

It is worth noticing in this context that it is possible to measure the motor current of electric wheel drives with high accuracy and thereby get an accurate estimate of the input torque to the wheel if the relation between the current and the torque is known. A simple approach is to use a linear relation between the torque and the motor current based on the specifications from the motor supplier. A more advanced approach is to map the current – torque relation of the motor in a test rig, such as the one in figure 1.
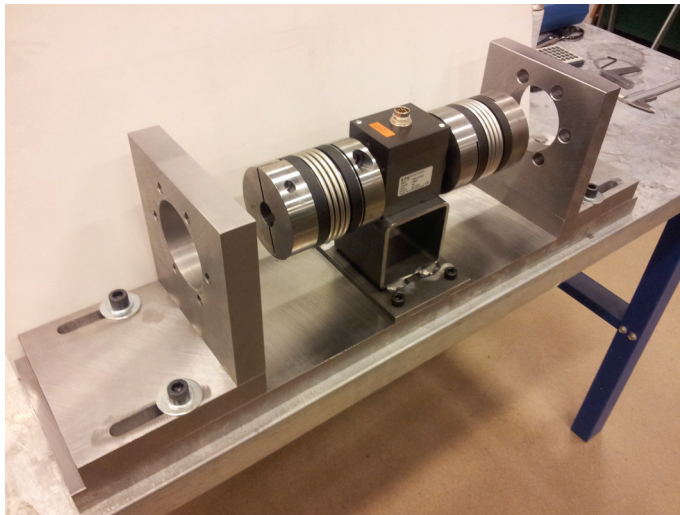

Figure 1. The photograph shows the test rig for mapping the motor parameters of our test vehicle ArtiTRAX. Two motors can be mounted in the rig. One motor is set in velocity mode and the other in current mode during the test. The shafts are connected via a torque transducer to measure the torque as a function of RPM and motor current.

1.2 Traction control

The proposed method originates from the development work of a traction control system for articulated off-road vehicles with individual wheel drives. The traction control problem is not addressed in the paper, but to put the estimation method in its context a brief background description is given below.

The typical work cycles of construction machinery such as the wheel loader and the hauler must be considered in the designing of a traction control system. A wheel loader working in a gravel pit compared to a hauler driving on a gravel road has different requirements on the traction control system. The loader is mostly in transient conditions, accelerating and decelerating, whilst the hauler often is driving with constant speed in steady state conditions. During certain situations, for instance during bucket filling with the loader or climbing a steep hill with the hauler, the traction should be maximized. Therefore, the traction control system must handle a number of optimization criteria depending on the actual working condition of the vehicle. Examples of these criteria are for instance maximum tractive force, energy efficiency, minimal tyre wear, etc.

A large number of traction control schemes have been published. Most of the papers are based on mechanical drivelines and on-road applications. Many methods depend on the wheel tyre-road friction coefficient. Rajamani, Phanomchoeng, Piyabongkarn and Lew (2012) present a review of such methods. Patterson, Gray, Bortolin and Vantsevich, (2013) discuss the fusion of a traction control system based on control of the driving and braking tyre operational mode of a 4x4 loader with the mechanical driveline to improve the traction. Slip control based on normal load and inflation pressure is discussed in Wilson, Siero, Kopchick and Vantsevich (2011). The idea is to control the rotational velocity of the wheels such that all wheels have the same slippage. On-road traction control of vehicles with individual (electric) wheel drives based on estimates of the slip and the friction coefficient is discussed in for instance Vasiljevic, Griparic, and Bogdan (2012).

1.3 Estimation method

The estimation method discussed in this paper mainly applies to the transportation phase of a work cycle during steady state conditions. The method is based on the bottom-up approach used in the design of complex systems. This approach often results in simple building blocks, Åström and Hägglund (2001).

The authors of this paper have over the years been involved in a number of industrial projects involving autonomously or remote controlled vehicles where the bottom-up approach has been used extensively. In these applications, often referred to as "mobile robotics", the use of simple building blocks has resulted in systems that have been used in real production.

The method consists of three basic building blocks that have been integrated. The building blocks are the PI controller, the feed forward controller and the Kalman filter.

There are at least two ways to control the actual velocity of a vehicle with individual drives, control the actual velocity of each wheel in local feedback loops at the wheels or control the actual velocity of the vehicle itself. Yamakawa, Kojima and Watanabe (2007) evaluate these two alternatives. Their conclusion is that the latter alternative is less sensitive to unevenness

in the ground resulting in higher energy efficiency compared to the first alternative. This is also the control strategy used in the proposed estimation method.

The estimator is based on a linear model that links input torque to the wheel to the circumferential force in the tyre-soil contact patch. The model was reported by Andreev, Vantsevich and Lefarov (1987) and is discussed in Vantsevich, Barz, Kubler and Schumacher (2005) and Andreev, Kabanau and Vantsevich (2010). The model is valid for firm roads and dense terrains. For wheel operating loads under road conditions and in some off-road operations, the relation between the input torque, T_w, to the wheel and the rolling radius in driven mode, r_w^0, can be expressed as

$$r_w = r_w^0 - \lambda_w T_w \tag{1}$$

where λ_w is the longitudinal elasticity factor of a tyre on the road or the combined longitudinal elasticity factor of a tyre and soil in off-road travel. The following relations holds on firm roads and dense terrains

$$\frac{T_w}{r_w^0} = F_x = \frac{1}{\lambda_w} \frac{r_w^0 - r_w}{r_w^0} = K_x s_\delta \tag{2}$$

where F_x is the wheel circumferenctial force, $K_x = 1/\lambda_w$ is the tyre longitudinal stiffness and $s_\delta = (r_w^0 - r_w)/r_w^0$ is the slip ratio used by Andreev, Kabanau and Vantsevich (2010).

It should be noted that there are several definitions that relates to radius of a pneumatic tyre, for instance static radius, dynamic radius and rolling radius. A description of such characteristics is found in Andreev, Kabanau and Vantsevich (2010).

There are other definitions of slip than the definition in (2). An alternative definition is to replace the rolling radius in driven mode with the rolling radius in free mode as discussed by Zoz and Grisso (2003). If the wheel is in free mode, the input torque to the wheel results in a circumferential force that equals the rolling resistance.

The longitudinal elasticity factor of a tyre is sensitive to variations in operating conditions such as temperature, inflation pressure, normal loading, tread depth and ground characteristics, Carlson and Gerdes (2005). Vantsevich, Barz, Kubler and Schumacher (2005) noted that the rolling radius in driven mode and the tyre longitudinal elasticity factor depend on the tyre pressure when performing tests with a dynamometer.

On-road methods to estimate the tyre longitudinal stiffness are for instance discussed in Gustafsson (1997) and Carlson and Gerdes (2005). The method proposed in Gustafsson is an on-line method based on a linear model. The bias in estimates based on linear models is discussed in Carlson and Gerdes who instead propose an off-line method based on a non-linear model.

The test results presented by both Gustafsson and Carlson and Gerdes are based on measurements of the rotational velocity of the driven and un-driven wheels and the actual velocity of the vehicle. 2WD vehicles without individual control of the wheels are used in the tests, implying that the actual velocity of the vehicle changes when the engine torque is changed or when the brakes are applied. These changes, that cause load transfer between the front axle and the rear axle due to the acceleration and the deceleration of the vehicle, are necessary to gain persistent excitation for the estimation of the tyre longitudinal stiffness.

If the circumferential force, F_x, and the rolling resistance force, R_x, are known, the resulting traction force, F_w, in the driving and the braking mode of the wheel can be calculated as

$$F_w = F_x - R_x \qquad (3)$$

On-line estimation of the rolling resistance force based on measurements of the actual velocity of the vehicle, the rotational velocity of the wheel and the engine torque is discussed in for instance Tannoury, Plestan, Moussaoui and Pita Gil (2012).

1.4 Outline of the paper

The outline of this paper is as follows. In section 2, the estimation problem is presented. In section 3, a control strategy is discussed that fulfils both the control of the actual velocity and the control of the input torque to the wheel for robust estimation. A brief description of the test vehicle ArtiTRAX is given in section 4. Some test results are presented in section 5 and finally in section 6, a discussion of the proposed method and some ideas about future work is presented.

2 Estimation problem

The requirement originating from the traction control system discussed in section 1.2, on the tyre parameter estimator is that the estimator shall be an integrated part of the traction control system, which means that the estimator has to work in real time.

2.1 Signals

The following signals are used to estimate the tyre parameters: The rotational velocity of the wheel, ω_w, the distance traveled by the wheel in the longitudinal direction, x_w, and the input torque to the wheel T_w.

The actual velocity of the wheel in the longitudinal direction, V_x, is used in estimators for comparision in section 5.

2.2 Parameters

The rolling radius, r_w, of the wheel can be expressed as

$$r_w = \frac{V_x}{\omega_w} \qquad (4)$$

(1) and (4) gives

$$\frac{V_x}{\omega_w} = \begin{pmatrix} 1 & -T_w \end{pmatrix} \begin{pmatrix} r_w^0 \\ \lambda_w \end{pmatrix} \qquad (5)$$

By using the "hat" symbol for estimated parameters, the relation between the estimated parameters and the measurements can be written

$$\frac{V_x(t)}{\omega_w(t)} = H(t) \begin{pmatrix} \hat{r}_w^0 \\ \hat{\lambda}_w \end{pmatrix} + e(t) \tag{6}$$

where $H(t) = (1 \quad -T_w(t))$ is the regression vector and $e(t)$ is the error term accounting for measurement errors and model mismatch.

2.3 Estimator

2.3.1 Kalman filter

The estimator is based on the following continuous time model

$$\begin{pmatrix} \dot{x}_w \\ \dot{r}_w \end{pmatrix} = \begin{pmatrix} 0 & \omega_w \\ 0 & 0 \end{pmatrix} \begin{pmatrix} x_w \\ r_w \end{pmatrix} + \begin{pmatrix} v_x \\ v_r \end{pmatrix} \tag{7}$$

$$z = (1 \quad 0) \begin{pmatrix} x_w \\ r_w \end{pmatrix} + e \tag{8}$$

where ω_w is the rotational velocity of the wheel, x_w in the state vector is the distance travelled by the wheel and r_w in the state vector is the rolling radius. $(v_x \quad v_r)^T$ and e is the process noise and the measurement noise respectively. The noise is assumed to be white with distribution $N(0, \sigma)$. A Kalman filter based on these models is used to estimate constant or slowly varying states, in this case the rolling radius r_w.

The observability matrix of the system is

$$O = \begin{pmatrix} 1 & 0 \\ 0 & \omega_w \end{pmatrix} \tag{9}$$

which has full rank if $\omega_w \neq 0$, implying that the states are observable as long as the vehicle is moving.

The method for the tyre parameter estimation is as follows

- Select a set of input torques, $T_{SET} = \{T_w^{min}, 0, T_w^{max}\}$, to the wheel whose tyre parameters shall be estimated. The minimum and maximum torques should be limited such that linear conditions hold according to (1),

- Estimate the rolling radius of the wheel for each member of the set during a period of driving with constant actual velocity. Select the steady state estimates of the rolling radius, denoted $\hat{r}_w^{Tmin}, \hat{r}_w^{T0}, \hat{r}_w^{Tmax}$, from each period as the values to base the tyre parameter calculations on,

- Calculate the tyre parameters; $\hat{r}_w^0 = \hat{r}_w^{T0}$, $\hat{\lambda}_w = \frac{\hat{r}_w^{Tmin} - \hat{r}_w^{Tmax}}{T_w^{max} - T_w^{min}}$.

Keeping the actual velocity constant during the estimation phase and at the same time controlling the torque estimation signal is realized using the control strategy discussed in section 4.

172

An alternate Kalman filter estimator based on Gustafsson (1997) is used for comparison in the discussion of test results in section 5. In this case the tyre parameters are estimated directly, implying that the state vector of the filter is $x(t) = (r_w^0(t) \quad \lambda_w(t))^T$. The quotient of the actual velocity and the rotational velocity of the wheel, $z(t) = V_x(t)/\omega_w(t)$, is used for the correction of the estimates. The filter is based on the following discrete time model

$$x(t+1) = x(t) + v(t) \tag{10}$$

$$z(t) = H(t)x(t) + e(t) \tag{11}$$

where $v(t), e(t)$ is the process noise and the measurement noise respectively. $H(t)$ equals the regression vector discussed in section 2.2.

A Kalman filter based on (10) and (11) results in estimates of the tyre parameters that is transformed to an estimate of the rolling radius according to

$$\hat{r}_w = \hat{r}_w^0 - \hat{\lambda}_w T_w \tag{12}$$

The Kalman filter equations are given by

$$\hat{x}^-(t) = A\hat{x}(t-1) + Bu(t-1) \tag{13}$$

$$P^-(t) = AP(t-1)A^T + Q(t) \tag{14}$$

$$K(t) = P^-(t)H^T(t)(H(t)P^-(t)H^T(t) + R(t))^{-1} \tag{15}$$

$$\hat{x}(t) = \hat{x}(t) + K(t)\big(z(t) - H(t)\hat{x}(t)\big) \tag{16}$$

$$P(t) = (I - K(t)H(t))\,P^-(t) \tag{17}$$

where A, B, H defines the state space model, the input model and the output model respectively. $P(t)$ is the covariance of the states, $Q(t)$ is the process noise covariance, $R(t)$ is the measurement noise covariance.

$Q(t)$ and $R(t)$ are often used as tuning parameters. They should of course reflect the statistical characteristics of the noise, but can also be used to keep the filter alive so that it will react to changes in driving conditions if the changes are detectable.

The initial values of $P(t)$ can also be regarded as tuning parameters. This is used in the estimation method and further discussed in section 5.

2.3.2 Least squares

The least square estimator is used for comparison in the discussion of test results in section 5. The least square estimates of the tyre parameters are given by

$$\begin{pmatrix} \hat{r}_w^0 \\ \hat{\lambda}_w \end{pmatrix} = (\textstyle\sum_{t=1}^{N} H^T(t)H(t))^{-1} \sum_{t=1}^{N} H^T(t)\frac{V_x(t)}{\omega_w(t)} \tag{18}$$

where N is the number of measurements. $H(t)$ equals the regression vector discussed in section 2.2. From (18), the following conditions are obtained for the least squares estimator to work

$$\omega_w(t) \neq 0 \tag{19}$$

$$\det \left(\sum_{t=1}^{N} H^T(t) H(t) \right) \neq 0 \tag{20}$$

Expansion of the determinant in (20) gives

$$\det \left(\sum_{t=1}^{N} H^T(t) H(t) \right) = N \sum_{t=1}^{N} T_w^2(t) - \left(\sum_{t=1}^{N} T_w(t) \right)^2 = N^2 \overline{Var}(T_w(t)) \tag{21}$$

If the variation in torque, $\overline{Var}(T_w(t))$, is small, the determinant will be close to zero resulting in poor excitation and thereby uncertain estimates, Söderström and Stoica (1989).

Remark. With independently controllable wheel drives, it is possible to maximize the variation in the torque over N samples subject to constraints such as maximum driving torque, maximum braking torque and maximum change speed.

Smoothing of the measurement data of the actual velocity of the vehicle is done in order to determine the window in time of constant actual velocity for the least squares estimation.

The smoothing of the raw data vector, $y \in R^n$, to the new vector, $x \in R^n$ is done by minimising the sum of the weighted norms over all feasible solutions numerically as

$$x = \arg \underbrace{\min}_{x \in \Omega} \left(\sum_{j=1}^{n} |x_j - y_j| + \gamma \left(\sum_{j=1}^{n} |D x_j|^2 \right)^{\frac{1}{2}} \right)$$

$$\tag{22}$$

subject to

$$\Omega = \left\{ x \mid x \in \mathbb{R}, y_1 = x_1, y_n = x_n, \sum_{j=1}^{n} y_j = \sum_{j=1}^{n} x_j \right\} \tag{23}$$

where the tuning parameter gamma is chosen to prioritise smoothing over curve following.

The differential operator, D, is defined as

$$D x_n \stackrel{\text{def}}{=} x_{n+1} - x_{n-1} \tag{24}$$

3 Controller

To limit the error sources in the estimation accuracy, a requirement on the controller is to keep the actual velocity constant during the estimation phase since acceleration or deceleration of the vehicle will cause load transfer between the front axle and the rear axle, which will disturb the estimates of the tyre parameters.

3.1 Control variables

The input torques to all wheels is assumed to be individually controllable.

In applications with electric drives, the input to the drive electronics could be a reference value for the motor current. In these cases, a transformation from reference torque to reference current has to be done by the control system.

3.2 Motion controller

The input to the motion controller is the difference between the reference velocity, V_{REF}, and the actual velocity, V_x, of the vehicle. The output from the controller, T_{MC}, is the torque to be distributed among the wheels. The structure of the controller and the distribution of torque between the wheels are further discussed in section 3.4.

The tyre longitudinal elasticity factor is a parameter that describes a property in the longitudinal direction of the wheel. The discussion regarding the motion control is therefore limited to only straight driving, i.e. turning is not considered.

3.3 Torque estimation signal

The torque estimation signal(s) to the wheel(s) whose tyre parameters are estimated can be selected arbitrarily as long as there is enough total torque left over for the motion control. The constraints in maximum driving torque, braking torque and the maximum change speed must also be considered.

Examples of easy to generate torque estimation signals are: Saw-tooth, sine and square wave. Details of the torque estimation signal such as shape, amplitude and periodicity should be based on the requirements of the tyre parameter estimator.

The saw-tooth wave and the sine wave are suitable for estimators that require excitation of the input torque to the wheel, for instance the least squares method and the Kalman filter based on the models (10) and (11). The square wave is suitable for the Kalman filter based on the models (7) and (8).

3.4 Overall control

The choice of control structure for the tasks outlined in section 3.2 and section 3.3 is a PI-controller in combination with feed forward control to compensate for the torque estimation signals to the wheels whose parameters are estimated.

In this context, the torque estimation signals can be interpreted as measurable disturbances that can be used in the feed forward controller in combination with the PI controller for the control of the actual velocity.

The computer algorithm, also shown as a block diagram in figure 1, in each sampling instant for the PI control, the feed forward control and the torque estimation signal is as follows (for the sake of simplicity limitations in torques and change speeds are not considered)

- Run the PI-controller, the output is the total torque T_{PI} for the drive speed of the vehicle,

- Determine the torque estimation signals $T_{ES1}, T_{ES2}, T_{ES3}, T_{ES4}$ for the wheels whose tyre parameters are estimated. The subscript 1-4 denotes the wheel identity,

- Determine the feed forward torque $T_{FF} = -(T_{ES1} + T_{ES2} + T_{ES3} + T_{ES4})$,

- Calculate the motion control torque $T_{MC} = T_{PI} + T_{FF}$,

- Distribute the motion control torque T_{MC} to the wheels, $(T_{MC1}, T_{MC2}, T_{MC3}, T_{MC4}) = TDfunc(T_{MC})$, where $TDfunc$ is the torque distribution function that fulfils $T_{MC} = (T_{MC1} + T_{MC2} + T_{MC3} + T_{MC4})$,

- Calculate the reference torques to each drive, $T_{DR1} = T_{MC1} + T_{ES1}, T_{DR2} = T_{MC2} + T_{ES2}, T_{DR3} = T_{MC3} + T_{ES3}, T_{DR4} = T_{MC4} + T_{ES4}$.
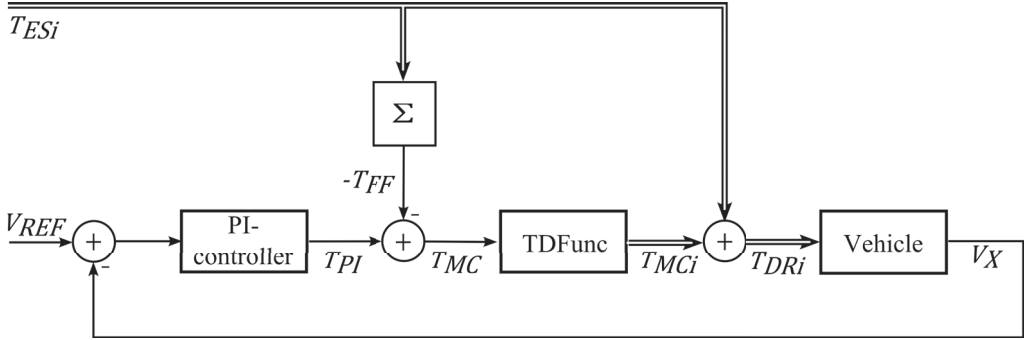

Figure 2. The figure shows a block diagram representation of the controller structure, where subscript *i* represent the wheel identity.

The control of some combinations of torque estimation signals is exemplified below.

3.4.1 1-wheel estimation

Assume that only the tyre parameters of wheel #1 should be estimated, then $T_{ES2} = T_{ES3} = T_{ES4} = 0$, $T_{FF} = -T_{ES1}$ and a possible distribution of the motion control is $T_{MC1} = 0$, $T_{MC2} = T_{MC3} = T_{MC4} = (T_{PI} + T_{FF})/3$.

The reference torques to the drives are $T_{DR1} = T_{ES1}, T_{DR2} = T_{DR3} = T_{DR4} = (T_{PI} + T_{FF})/3$

3.4.2 2-wheel estimation

Assume that the task is to estimate the tyre parameters of diagonal wheels, for instance the front left wheel (#1) and the right rear wheel (#4). Then it is possible to choose $T_{MC1} = T_{MC4} = 0$ and $T_{ES1} = -T_{ES4} = T_{ES}$ which gives $T_{FF} = 0$ since $T_{ES1} + T_{ES2} + T_{ES3} + T_{ES4} = 0$.

A possible choice for the motion control is $T_{MC2} = T_{MC3} = T_{PI}/2$.

This result in $T_{DR1} = T_{ES}, T_{DR2} = T_{PI}/2, T_{DR3} = T_{PI}/2, T_{DR4} = -T_{ES}$.

3.4.3 4-wheel estimation

If the tyre parameters of all wheels should be estimated at the same time, it is possible to use the same torque estimation signal for all wheels, except the sign is changed for two of them. For example $T_{ES1} = T_{ES2} = -T_{ES3} = -T_{ES4} = T_{ES}$.

The resulting feed forward torque is zero and $T_{MC1} = T_{MC2} = T_{MC3} = T_{MC4} = T_{PI}/4$ fulfills the requirement of the motion control.

The reference torques to the drives are $T_{DR1} = T_{PI}/4 + T_{ES}$, $T_{DR2} = T_{PI}/4 + T_{ES}$, $T_{DR3} = T_{PI}/4 - T_{ES}, T_{DR4} = T_{PI}/4 - T_{ES}$

4 ArtiTRAX

ArtiTRAX is a 240 kg articulated vehicle with 24 [VDC] electric motors. ArtiTRAX consists of two TRAX wheelchairs from the Swedish company Permobil. ArtiTRAX is developed at Luleå University of Technology in collaboration with Volvo Construction Equipment.

Many construction machines are articulated, for instance haulers and wheel loaders. ArtiTRAX is considered to be a downscaled version of such a vehicle in many test scenarios. The main advantage with ArtiTRAX is the small size, which makes initial tests easy to perform.

Figure 3. The picture shows ArtiTRAX during a test at the Arcus arena in Luleå, Sweden. The small wheel in the rear is the measuring wheel used to measure the actual velocity. Holders for weightlifting weights are placed above each wheel making it possible to change the static normal load in a controlled manner.

The two TRAX units are connected with a joint and thereby making ArtiTRAX articulated. The joint angle is controlled with an electric motor connected to the joint via a chain. Each

wheel has its own 500 [W] motor. The motor is connected to the wheel axle via a gearbox. The gearbox reduces the rotational speed of the motor 18 times. The controls of the motors are done in an on-board PC104 computer that sends the control reference values over a CAN bus to the drive electronic units of each motor. The drive electronic units control the motor currents.

ArtiTRAX is equipped with various sensors, the ones relevant for this paper are; Encoders that measure the rotational angle and velocity of the motors, encoder that measure the rotational angle and velocity of the measuring wheel and inbuilt sensors in the drive electronics that measures the motor currents.

The input to the drive electronic unit is a reference value for the motor current. The units control the motor currents with high accuracy. All five encoders are of the same type, an absolute encoder with a 12-bit single turn and 12-bit multi turn resolution.

The distance from the articulation joint to the front wheel axis and the rear wheel axis is 0.62 meters. The distance between the wheels on the same axis is 0.63 meter. The static wheel radius is approximately 0.21 meters. . The circumference of the measuring wheel is 0.5 meter.

5 Test results

The results presented in this section are based on tests with ArtiTRAX in an in-door gymnasium with a high friction carpet. The same gymnasium has been used in all tests, which means that the ground characteristics have been the same in all tests. ArtiTRAX has been "warmed up" according to a certain procedure before tests with the aim to have steady state working temperature during the tests.

A linear relation is assumed between the input torque (to the wheel) and the motor current during steady state driving. The linear relation can be used in an ideal case. It is important to note that comparison of estimates from different methods can be done even if the ideal case does not hold, since the estimates are based on the same data sets. It is also important to note that the focus of this paper is on the method that we propose and not on the absolute accuracy of the tyre parameter estimates.

Three weight distributions on the front axle and the rear axle has been used in the tests. The static front axle weight and rear axle weight for these cases is specified in table 1.

Table 1.

Axle	F/R 80/0	F/R 60/20	F/R 0/80
Front	180 kg	160 kg	100 kg
Rear	140 kg	160 kg	220 kg

If nothing else is stated, the weight distribution is 60 [kg] on the front axle and 20 [kg] on the rear axle and the reference value for the actual velocity is 1.0 [m/s].
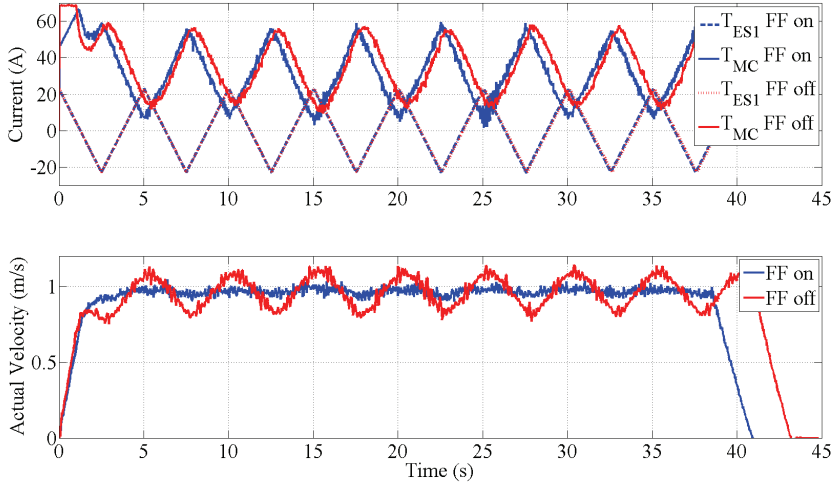
Figure 4. The figure shows the total motion control current (T_{MC}) and the motor current estimation signal of the front left wheel (T_{ES1}) during two runs together with the actual velocity of the wheel.

The feed forward control was turned on in one of the runs shown in figure 4 and turned off in the other run. If the feed forward control is not used in the controller, the actual velocity oscillates causing a transfer of load between the front axle and the rear axle during the estimation phase of the tyre parameters.

Figure 5. The figure shows least squares estimates of the rolling radius in driven mode and the tyre longitudinal elasticity factor of the front left wheel from 25 runs with feed forward control turned on and 25 runs with feed forward control turned off.

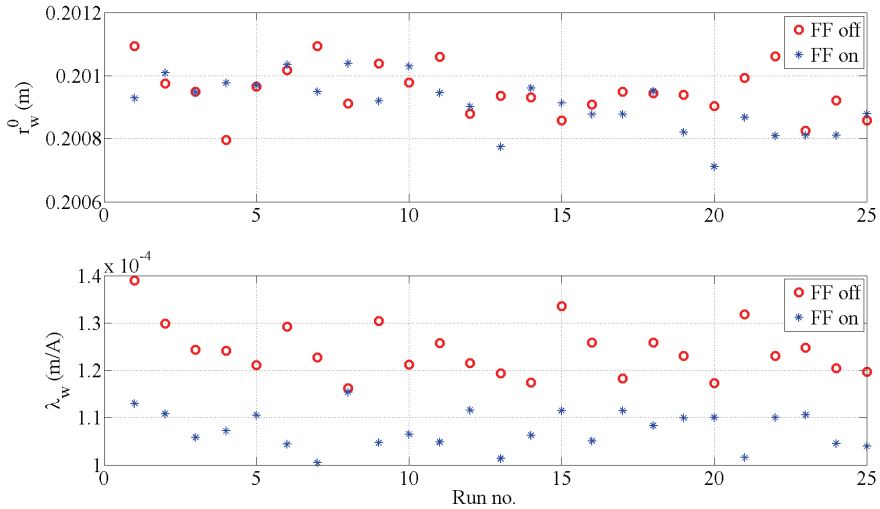It is clear from figure 5 that, on average, the estimate of the tyre longitudinal elasticity factor is larger when the actual velocity varies during the tyre parameter estimation phase, which is the case when the feed forward control is turned off.
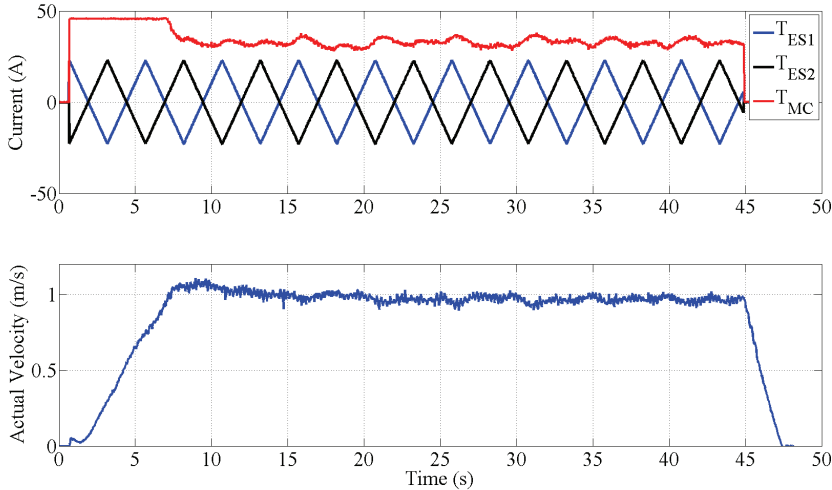
Figure 6. The figure shows controller signals and the actual velocity during a 2-wheel estimation test run when the tyre parameters of the front left wheel and the rear right wheel are estimated. The front right wheel and the rear left wheel are used for the motion control.
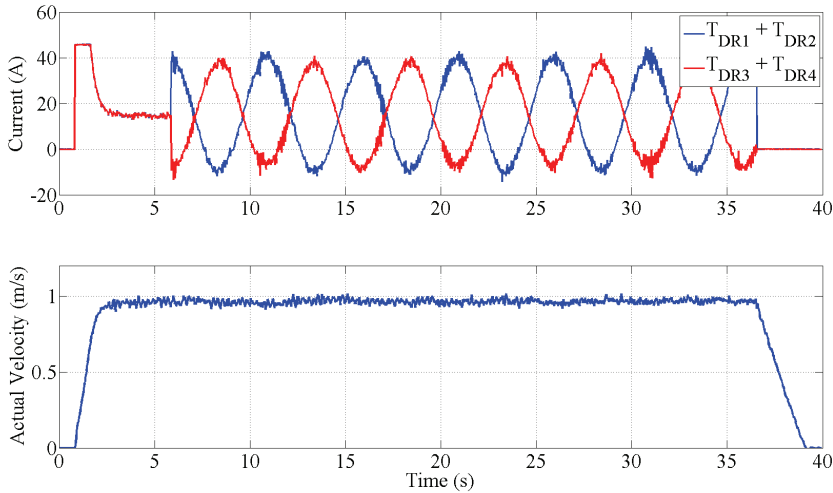
Figure 7. The figure shows controller signals and the actual velocity during a 4-wheel estimation test run, in this case using a sine wave shaped motor current estimation signal.

During 4-wheel estimation, as shown in figure 7, the tyre parameters of all wheels are estimated at the same time. All wheels are also used for the motion control. Because of this combination, the amplitude of the estimation signal had to be limited to be less than the

maximum current for each drive motor (23 [A]), otherwise the actual velocity would have been zero.
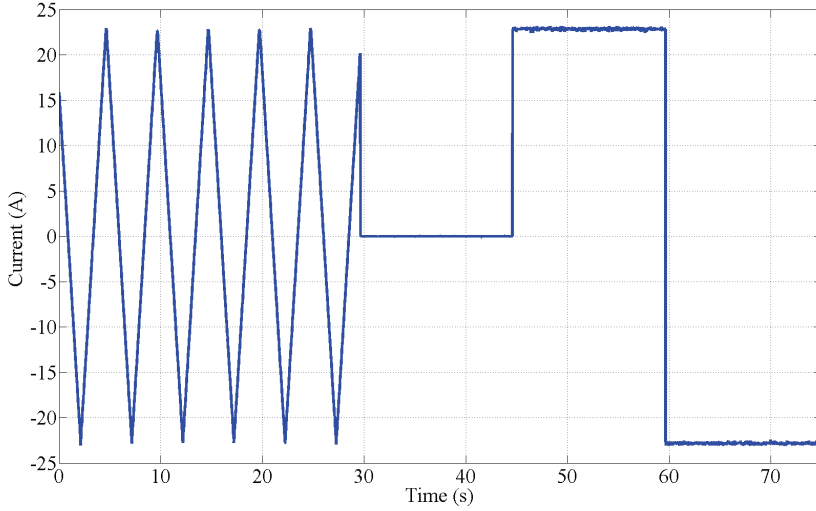
Figure 8. The motor current estimation signal is a combination of the saw tooth wave and the square wave.

The motor current estimation signal shown in figure 8 is used for the estimation of the tyre parameters of the front left wheel and to compare the two Kalman filter based methods discussed in section 2.3.1. In this case, the actual velocity was 0.5 [m/s] during the tests.

The Kalman filter that estimates the rolling radius in driven mode and the tyre longitudinal elasticity factor, "KF1", is updated during the first 30 seconds when the estimation signal is saw tooth shaped. The filter is not updated during the periods that follow when the estimation signal is square wave shaped due to poor excitation.

The Kalman filter that estimates the rolling radius directly, "KF2", estimates the rolling radius over the whole period but the covariance matrix, $P(t)$, of the states - see section 2.3.1 - is re-initiated to high values of the diagonal elements (and zeros to the off-diagonal elements) at time 0, 30, 45 and 60 seconds in order to make the filter adjust to new steady state conditions.

The two estimates of the rolling radius are shown in figure 9.

Figure 9. The figure shows the estimate of the rolling radius based on the two Kalman filter based methods discussed in section 2.3.1, when the motor current estimation signal is varied as in figure 8. The raw data, $(V_x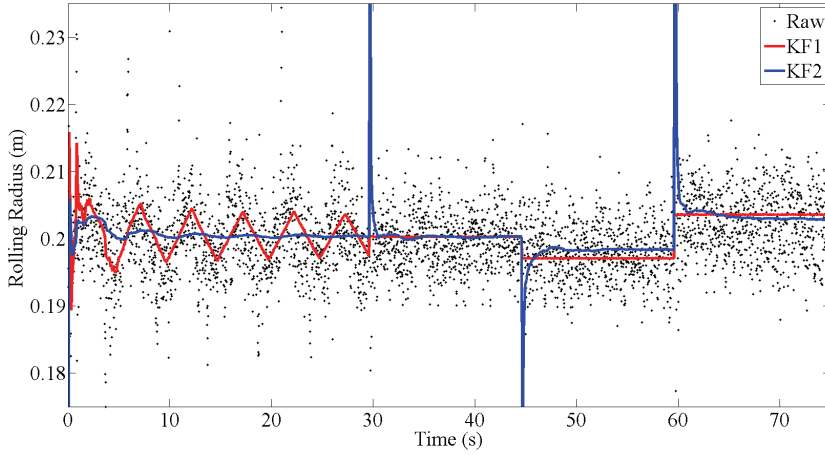/\omega_w)$, which is the quotient of the actual velocity of the wheel and the rotational velocity of the wheel is also shown.

From figure 9, it is clear that the Kalman filter that estimates the rolling radius directly is too slow to follow the saw tooth shaped variations in the estimation signal, but when it is re-initiated at the start of the periods with constant motor current, it finds a close to constant estimate of the rolling radius during each period.

The rolling radius estimate in driven mode is almost the same for both filters (30 to 45 seconds), but the estimate when the motor current is ± 23 [A] differs.

Note that the KF2 estimates converge to steady state values within approximately five seconds, implying that the period time could have been reduced. The tuning parameters of the filter are specified in table 2.

Table 2. The table specifies the tuning parameters of the two Kalman filters. Note that the covariance matrix of the "KF2" filter is reset to the value of P(0) at time 30, 45 and 60 seconds in the test.

Kalman filter	Q	R	$P(0)$
KF1	$\begin{pmatrix} 10^{-10} & 0 \\ 0 & 10^{-12} \end{pmatrix}$	10^{-1}	$\begin{pmatrix} 10^3 & 0 \\ 0 & 10^3 \end{pmatrix}$
KF2	$\begin{pmatrix} 10^{-4} & 0 \\ 0 & 10^{-4} \end{pmatrix}$	10^{-1}	$\begin{pmatrix} 10^3 & 0 \\ 0 & 10^3 \end{pmatrix}$

Table 3 shows the estimate of the rolling radius in driven mode and the tyre longitudinal elasticity factor from nine runs. For KF2, the estimate is based on the final values during each period with constant excitation signal that gives

$$\hat{r}_w^0 = \hat{r}_w(45^-) \tag{25}$$

$$\hat{\lambda}_w = \frac{\hat{r}_w(75^-) - \hat{r}_w(60^-)}{I_m(60^-) - I_m(75^-)} \tag{26}$$

where 45^-, 60^- and 75^- denotes the last value during the period when the motor current is zero, +23 and -23 [A] respectively. I_m is the motor current. For comparison, tyre parameter estimates based on the mean value during each period is included in table 3.

Table 3.

F/R	Run	KF1 $\hat{r}_w^0$	KF2 $\hat{r}_w^0$	Mean $\hat{r}_w^0$	KF1 $\hat{\lambda}_w 10^{-5}$	KF2 $\hat{\lambda}_w 10^{-5}$	Mean $\hat{\lambda}_w 10^{-5}$
	#1	0.2003	0.2003	0.2006	12.7	9.9	10.6
80/00	#2	0.2003	0.2003	0.1998	14.3	9.8	9.9
	#3	0.2004	0.2002	0.2012	10.9	9.8	9.8
	#1	0.2012	0.2013	0.2008	16.3	10.6	10.8
60/20	#2	0.2014	0.2013	0.2019	11.5	10.4	10.3
	#3	0.2012	0.2014	0.2013	13.7	10.2	10.7
	#1	0.2051	0.2051	0.2052	19.4	15.3	15.8
00/80	#2	0.2050	0.2050	0.2051	14.9	14.9	15.6
	#3	0.2051	0.2049	0.2051	19.6	15.8	16.4

The mean value parameters in table 3 has been calculated according to (25) and (26) with

$$\hat{r}_w(45^-) = \overline{\left(\frac{V_x(\{t\in\mathbb{R}|30<t<45\})}{\omega_w(\{t\in\mathbb{R}|30<t<45\})}\right)},$$

$$\hat{r}_w(60^-) = \overline{\left(\frac{V_x(\{t\in\mathbb{R}|45<t<60\})}{\omega_w(\{t\in\mathbb{R}|45<t<60\})}\right)},$$

$$\hat{r}_w(75^-) = \overline{\left(\frac{V_x(\{t\in\mathbb{R}|60<t<75\})}{\omega_w(\{t\in\mathbb{R}|60<t<75\})}\right)}.$$

It is clear from table 3 that both Kalman filter methods has little variation in the estimate of the rolling radius in driven mode and both methods gives almost the same results. The estimator based on the mean value has larger variations in the estimation of the rolling radius in driven mode for the distributions 80/00 and 60/20 of the extra weight. The estimation of the rolling radius in driven mode for the 00/80 distribution of the extra weight is almost the same for all three methods.

The Kalman filter methods differ in the estimate of the tyre longitudinal elasticity factor. KF1 estimates are larger than KF2 estimates and tends to vary more. The estimate of the tyre longitudinal elasticity factor based on the mean value is close to the corresponding KF2 estimate.

All methods results in estimates that are dependent on the load, the more load the lower estimate of the rolling radius in driven mode as well as lower estimate of the tyre longitudinal elasticity factor.
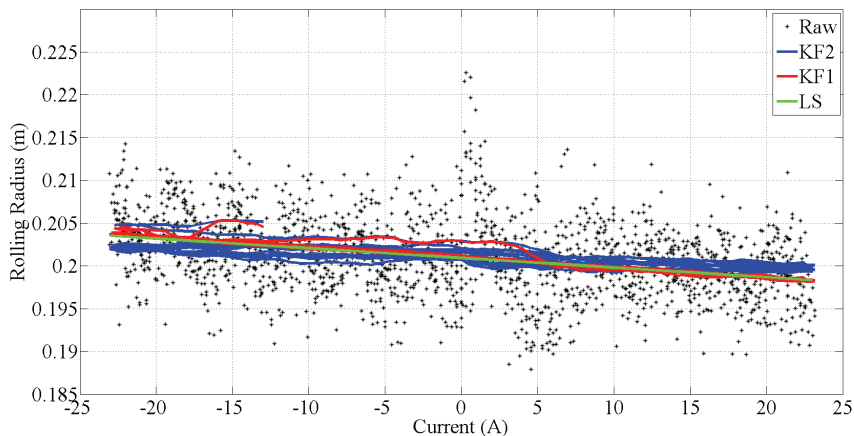
Figure 10. The figure shows the raw data from the encoders as a function of the motor current during a test run together with the least squares and Kalman filter estimates of the rolling radius.

The KF1 estimate shown in figure 9, converges to the off-line least squares estimate as time goes by which is not the case for the KF2 estimate. In this test, the quotient of the process noise covariance, $Q(t)$, and the measurement noise covariance, $R(t)$, of KF2 was tuned to get the filter response fast to be able to estimate the rolling radius when the motor current estimation signal was saw tooth shaped. As is clear from the figure, this is not a good approach since it makes the estimate noise sensitive.

6 Discussion

We have introduced a tyre parameter estimation method that eliminates the influence load transfer have on the tyre parameters by keeping constant actual velocity during the estimation phase.

Load transfer between the front axle and the rear axle occurs when the vehicle accelerates and decelerates. Changes occur in the rolling radius in driven mode and the tyre longitudinal elasticity factor if the load on the wheel is changed. This introduces disturbances in tyre parameter estimates.

The dependency of the load on the tyre parameter estimates has been verified in tests. It is therefore important to stress that the proposed method results in no transfer of load between the front axle and the rear axle since the acceleration and the deceleration of the vehicle is zero during the estimation phase.

By using a model that relates the input torque to the wheel to the rolling radius via the estimated parameters during non-sliding conditions, the slip can be calculated and controlled in a traction control system.

The method was tested in-door in a gymnasium using ArtiTRAX, a 240 kg articulated vehicle carrying 80 kg of extra weight in three different axle load configurations. This

implies good control of the load distribution and small variation in variables that influence the tyres such as temperature, ground characteristics, etc. during the tests.

The focus of this paper is on the proposed method and not on the result in terms of accuracy of the estimated tyre parameters. The next step of the future work is to map the motors of ArtiTRAX in the rig, as seen in figure 1, in order to study the accuracy.

We will also repeat the tests outdoor first with ArtiTRAX, and then later using a bigger vehicle with big tyres such as the wheel loader. This requires the use of an alternative sensor to measure the actual velocity compared to the measuring wheel used in the in-door tests. The plan is to use the combination of GPS and IMU. The occurrence of load transfer is expected in the case of a wheel loader even though the actual velocity is constant, since the vertical stiffness of the tyres are relatively low compared to the stiffness of the suspension which might result in a bouncing behaviour during steady state driving. This phenomenon must be addressed. It is also expected that the input torques to the wheels of a loader can be of such magnitude that the non-linear parts of torque – rolling radius relation has to be considered.

Torque distribution between wheels and axles with focus on energy efficiency is an interesting topic that can be explored in future work.

References

Andersson, U., Mrozek, K., Åström, K. and Hyyppä, K. (1997) Path Design and Control Algorithms for Articulated Mobile Robots, *Proceedings of the International Conference on Field and Service Robotics (FSR'97),* December, 1997, Canberra, Australia, Springer, London, pp. 390-396.

Andreev, A. F., Kabanau, K. I. and Vantsevich, V.V. (2010) *Driveline Systems of Ground Vehicles - Theory and Design*, CRC Press, Boca Raton, FL, United States.

Andreev, A. F., Vantsevich, V.V. and Lefarov, A. Kh. (1987) Differentials of Wheel Vehicles, *Mashinostroenie Publishing House*, Moscow, Soviet Union.

Carlson, C. R. and Gerdes, J. C. (2005) Consistent Nonlinear Estimation of Longitudinal Tire Stiffness and Effective Radius, *IEEE Transactions on Control Systems Technology*, Volume 13, Issue 6, pp. 1010-1020.

De Castro, R., Araujo, R.E. and Freitas, D. (2013) Wheel Slip Control of EVs Based on Sliding Mode Technique With Conditional Integrators, *IEEE Transactions on Industrial Electronics*, Volume 60, Issue 8, pp. 3256-3271.

Fredriksson, H., Andersson, U. and Hyyppä, K. (2010) Track Loader Kinematics*, Preprints: The Second IFAC Symposium on Telematics Applications*, TA2010, October 5-8, 2010, Timişoara, Romania.

Gustafsson, F. (1997) *Slip-Based Tire-Road Friction Estimation*, Automatica, Volume 33, Issue 6, pp. 1087-1099.

Gustafsson, F. (1998) *Monitoring Tire-Road Friction Using the Wheel Slip*, IEEE Control Systems, Volume 18, Issue 4, pp. 42-49.

Hallowell, S.J. and Ray, L.R. (2003) All-wheel Driving Using Independent Torque Control of Each Wheel, *Proceedings of the American Control Conference 2003*, Volume 3, pp. 2590-2595.

Hori, Y. (2004) Future Vehicle Driven by Electricity and Control – Research on Four-Wheel-Motored "UOT Electric March II", *IEEE Transactions on Industrial Electronics*, Volume 51, Issue 5, pp. 954-962.

Huang, X. and Wang, J. (2013) Longitudinal Motion Based Lightweight Vehicle Payload Parameter Real-Time Estimations, *Journal of Dynamic Systems Measurement and Control*, Volume 135, Issue 1, pp. 1183-1195.

Jackson, A., Crolla, D., Woodhouse, A. and Parsons, M. (2002) Improving Performance of a 6x6 Off-Road Vehicle Through Individual Wheel Control, *SAE Technical Paper Series 2002-01-0968*, World Congress and Exhibition, March 4, 2002, Detroit Michigan, United States.

Jalali, K., Bode, K., Lambert, S. and McPhee, J. (2008) Design of an Advanced Traction Controller for an Electric Vehicle Equipped with Four Direct Driven In-Wheel Motors, *SAE Technical Paper Series 2008-01-0589*, World Congress and Exhibition, April 14, 2008, Detroit, Michigan, United States.

Karlsson, M. (2010) *ArtiTRAX II*, Master's Thesis, Luleå University of Technology, Luleå, Sweden.

Laine, L. (2007) *Reconfigurable Motion Control Systems for Over-Actuated Road Vehicles*, Doctoral Thesis, Chalmers University of Technology, Göteborg, Sweden.

Magellan, G.A., De Angelo, C.H. and Garcia, G.O. (2011) Maximization of the Traction Forces in a 2WD Electric Vehicle, *IEEE Transactions on Vehicular Technology*, Volume 60, Issue 2, pp. 369-380.

Patterson, M.S., Gray, J.P., Bortolin, G. and Vantsevich, V.V. (2013) Fusion of Driving and Braking Tire Operational Modes and Analysis of Traction Dynamics and Energy Efficiency of a 4x4 Loader, *Journal of Terramechanics*, Volume 50, Issue 2, pp. 133-152.

Rajmani. R., Piyabongkarn, D., Lew, J.Y. and Grogg, J.A. (2012) Algorithms for Real-Time Estimation of Individual Wheel Tire-Road Friction Coefficients, *IEEE/ASME Transactions on Mechatronics*, Volume 17, Issue 6, p 1183-1195.

Rehnberg, A. and Drugge, L. (2010) Influence of Tyre Properties on the Ride Dynamics of Heavy Off-Road Vehicles. *Proceedings of the Joint 9th Asia-Pacific ISTVS Conference and Annual Meeting of Japanese Society for Terramechanics*, September 27-30, 2010, Sapporo, Japan.

Senatore, C. and Sandu, C. (2011) Torque Distribution Influence on Tractive Efficiency and Mobility of Off-Road Wheeled Vehicles, *Journal of Terramechanics*, Volume 48, Issue 5, pp. 372-383.

Söderström, T and Stoica, P. (1989) *System Identification*, Prentice Hall, Cambridge, Great Britain.

Tannoury, C. El., Plestan, F., Moussaoui, S. and Pita Gil, G. (2012) A Variable Structure Observer for an On-Line Estimation of a Tyre Rolling Resistance and Effective Radius, *12th International Workshop on Variable Structure Systems (VSS) 2012*, pp. 167-172.

Vantsevich, V.V. (2006) All-Wheel Driveline Mechatronics Systems: Principles of Wheel Power Management, *SAE Technical Papers Series 2006-01-0580*, World Congress and Exhibition, April 3, 2006, Detroit, Michigan, United States.

Vantsevich, V.V., Barz, D., Kubler, J. and Schumacher, A. (2005) Tire Longitudinal Elasticity and Effective Rolling Radii: Experimental Method and Data, *SAE Technical Paper Series 2005-01-1823*, World Congress and Exhibition, April 11, 2005, Detroit, Michigan, United States.

Vasiljevic, G., Griparic, K. and Bogdan, S. (2012) Slip-Based Traction Control System with an On-Line Road Condition Estimation for Electric Vehicles, *Proceedings of the IEEE International Conference on Control Applications (CCA) 2012,* October 3-5, Dubrovnik, Croatia, pp. 395-400.

Welch G., Bishop G. (2006) *An Introduction to the Kalman Filter*, Technical Report, University of North Carolina at Chapel Hill, NC, United States, http://www.cs.unc.edu/~welch/media/pdf/kalman_intro.pdf

Wilson, T., Siero, M., Kopchick, C. and Vantsevich, V.V. (2011) Terrain Truck: Control of Wheel Rotational Velocities and Tire Slippages, *SAE Technical Paper Series 2011-01-2157*, Commercial Vehicle Engineering Congress, September 13-14, 2011, Chicago, Illinois, United States.

Yamakawa, J., Kojima, A. and Watanabe K. (2007) A Method of Torque Control for Independent Wheel Drive Vehicles on Rough Terrain. *Journal of Terramechanics*, Volume 44, Issue 5, pp. 371-381.

Zoz, F.M. and Grisso, R.D. (2003) Traction and Tractor Performance, *ASAE Distinguished Lecture Series #27*, http://bsesrv214.bse.vt.edu/Dist_Lecture_27/ (Accessed 6 June 2013).

Åström, K.J. and Hägglund, T. (2001) The Future of PID Control. *Control Engineering Practice*, Volume 9, Issue 11, pp. 1163-1175.

[G] - Laser navigation system for automatic guided vehicles – From research prototype to commercial product

The author's main contribution: The idea to the report and "typing the text".

Comment: The discussions with Arne Hedström, Kalevi Hyyppä and Göran Netzler were very important for the content of the report.

Laser navigation system for automatic guided vehicles
From research prototype to commercial product

Ulf Andersson

Department of Systems and Interaction,

Luleå University of Technology, 971 87, Luleå, Sweden

Abstract

This report discuss the journey of a laser navigation system for Automatic Guided Vehicles (AGVs) developed in a research project at Luleå University of Technology in the late 80's up until today. The focus is on the commercialisation aspects of the system. The aim is to highlight and discuss the impact of certain events, circumstances and technical features that has influenced the current position of the laser navigation system in the market for Automatic Guided Vehicle Systems (AGVS). The innovation aspects are also discussed in the report.

1 Introduction

The reason to why the author of this report interrupted his research work at Luleå University of Technology in 1989 was the founding of the spinoff company AutoNavigator AB for which the author started to work.

The research project with the goal to develop a laser navigation system for AGVs had at the time managed to navigate a test truck and demonstrate it at a technical fair.

Almost 23 years has passed by since then so reflecting on commercial footprints made by the laser navigation system in the AGVS market is interesting from several perspectives. A question one can ask is if the laser navigation system is an innovation. We will look for an answer to that and also highlight and discuss the impact of certain events, circumstances and technical features that has influenced the current position of the laser navigation system on the AGVS market.

The European Union (EU) defines innovation in a glossary section on the web as cited below.

> Innovation
> "An innovation is the implementation of a new or significantly improved product (good or service), or process, a new marketing method, or a new organisational method in business practices, workplace organisation or external relation. The minimum requirement for an innovation is that the product, process, marketing method or organisational method must be new (or significantly improved) to the firm."

1.1 Method

Much of the discussions in the report are based on interviews with Mr Arne Hedström working for Kollmorgen Särö AB in Särö, Sweden. Mr Hedström has been in the AGV business working for NDC Netzler & Dahlgren Co AB, DanaherMotion Särö AB and now Kollmorgen Särö AB as a manager of technology development in different positions since the 70's until today.

The discussions are also based on interviews with Professor Kalevi Hyyppä at Luleå University of Technology. Professor Hyyppä was the inventor and the head of the research team working with the development of the laser navigation system in the 80's.

Mr Göran Netzler, former Managing Director of NDC Netzler & Dahlgren Co AB, and Chairman at NDC Automation Inc. (NASDAQ) has also given valuable inputs to the report.

1.2 Outline of the report

The outline of the report is as follows. In section 2, the AGV technology is discussed with focus on navigation techniques. In section 3, a historical background is given. Section 4 discusses events, circumstances and technical features that have influenced the position of the laser navigation system on the market for AGV systems. Some conclusions are presented in section 5.

2 AGV technology

2.1 Systems and vehicles

An AGV system (AGVS) is a material handling system that uses independently operated, self-propelled vehicles (AGVs) guided along defined pathways.

Barret Electronics of Grand Rapids, Michigan, USA is considered to be the first company that brought the AGV to the market in the 50's, Müller (1983). One of the first AGVs was a tow truck pulling a series of trailers that followed a wire in the floor instead of rails. The market for AGVs was small until the 70's when it started to expand in Europe.

The speed of the AGVs is low - typically 1 – 1.5 m/s - since AGVs often operates in areas where people work so that specially designed safety systems can stop them in a controlled manner. Mechanical bumpers were common earlier, but lately laser based sensors have become the standard solution.

Electrical drives are common, with large batteries as the energy source. Most AGVs are wheeled vehicles with solid tyres. The tricycle type is common, where the single front wheel is used both to control the steering angle and the speed of the vehicle. The load handling devices of the AGVs varies; forks and conveyor belts are two examples of common load handling devices.

The main applications of AGVs are according to Schultze and Zaho (2007), production, connection of different work areas, order picking, warehousing and assembly. AGVs are often used in cases of consistent material flow connections.

The warehousing and order-picking sector is characterized by high volume traffic from defined sources to defined drains. The AGVs employed in these applications typically has a high loading capacity and are designed to carry unit loads such as standardized pallets. AGV systems with more than 100 vehicles are common in warehousing and order-picking applications.

Inhomogeneous and changing loads characterize the assembly sector. The loading devices of the AGVs are often specific for the application and they often represent an assembly station of their own, the fitter riding along from one stationary assembly station to the next.

AGV systems with few vehicles are also common. Many of these applications can be handled without a central control unit. The systems are characterized by low investments and simple maintenance.

The original navigation technique (guidance technique) was based on wires buried in the floor that created a magnetic field that was detected by a receiver on the AGV. The task of the guidance controller was to follow the wire.

Later developed navigation technologies intended for industrial use is according to Schultz and Zaho (2007); laser, magnetic/ground matrix, optical guideline and "others".

Schultze and Zaho note that trends like laser guided vehicles and flexible software lead to other advanced application areas.

2.2 Laser navigation

A brief description of the laser navigation system is given in this section.

The detailed principal function of the navigation algorithms is discussed in Wiklund, Andersson and Hyyppä (1988). Technical details of the laser anglemeter are discussed in Hyyppä (1993c).

The AGV in figure 1 is in the outside yard carrying a roll between the factory and the warehouse at the Tetra Pak plant in the Jurong district in Singapore. The laser anglemeter is placed on the top of the AGV measuring angles to retro-reflectors. A retro-reflector is visible close to the downpipe on the warehouse. The AGV is a tricycle with the single front wheel used to control both the steering angle and the speed of the AGV. The plastic device in the front of the AGV is a mechanical bumper. The stop distance is less than the length of stroke of the bumper at full load, which limits the maximum drive speed to 1 m/s. The AGVs can be used to transport both rolls and pallets.

The system at Tetra Pak in Singapore is still in use and has been extended with four more AGVs since the original commissioning. The AGV control system has been upgraded a number of times, Hedström (2013).
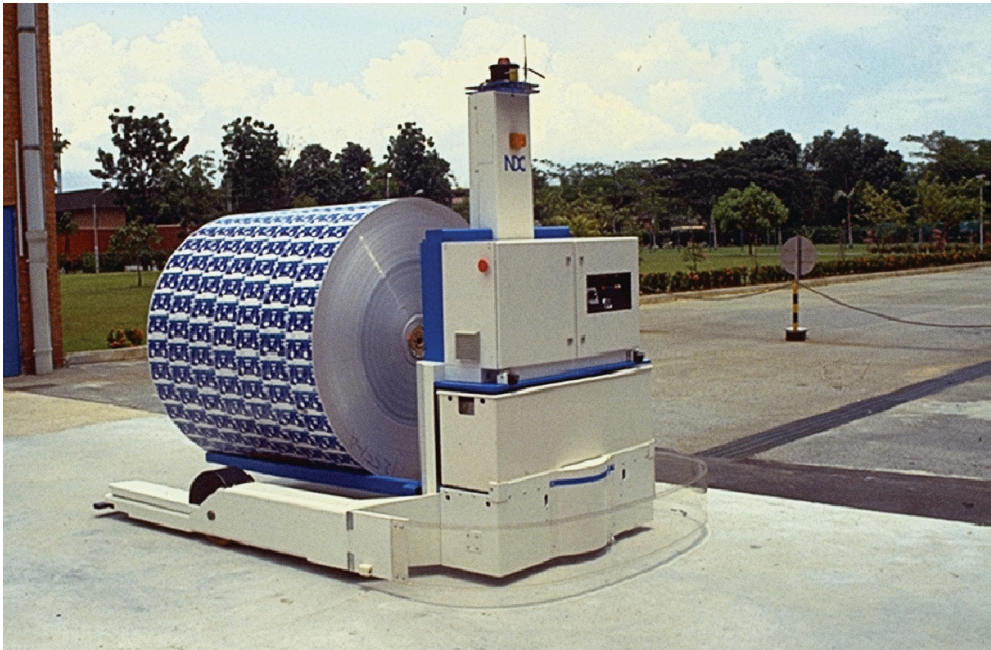
Figure 1. The photograph shows one of 10 laser guided AGVs that were installed at Tetra Pak in Singapore in 1991. The photograph is published with the permission of Kollmorgen Särö AB.

2.2.1 Pose estimator

The laser anglemeter rotates a laser beam counter-clockwise at 6 rev/s. When the laser beam hits a retro-reflector, a single stripe of tape, it is reflected back in the same direction, thus "hitting" the laser anglemeter which then registers the angle of the rotating head relative to the axis of the laser anglemeter. The measured angle is transmitted to the on-board navigation computer. Since the 2D positions of the retro-reflectors are known and stored in a reflector map, the measured angle can be associated to a retro-reflector in the map if the pose of the laser anglemeter is known or estimated with high accuracy.

An "abundance" of retro-reflectors can be installed since they are not space demanding to ensure redundancy in case of blocked or lost retro-reflectors.

When the navigation system is powered on, the pose of the vehicle is unknown and an initialisation of the pose estimate is necessary. The initialization procedure requires the vehicle to be standing still during the time measured angles from one revolution of the rotating head of the laser anglemeter are used to triangulate the pose, a method that requires at least four measured angles. The triangulated pose is used as the initial 2D pose estimate $(\hat{x}, \hat{y}, \hat{\theta})$ of the vehicle. (Estimates are denoted by the "hat" symbol.) It should be noted that the pose initialisation is done automatically with no requirements of complementing systems or that the vehicle should be positioned in certain spot as long as the laser anglemeter is surrounded by four well spread out retro-reflectors.

After the initial pose has been calculated, single measured angles are used one at a time to correct the estimated pose based on the Kalman filter method, which allows the vehicle to be

194

in motion. The difference between the measured angle and the expected angle to the retro-reflector causing the reflection is used to correct the pose estimate.

Figure 2. The sketch illustrates measurement of angles to retro-reflectors. Note that only one angle at a time is measured because of the rotation of the laser beam, implying that the pose of the vehicle changes between the measurements if the vehicle is in motion.

Measurements of the steering angle and the speed of the vehicle are used to update a kinematic model that describes the motion of the vehicle. The kinematic model is initiated to the pose estimate that was last corrected by a measured angle to a retro-reflector. A rough pose is then estimated, based on the kinematic model, at the time of the measured angle so that expected angles to retro-reflectors can be calculated. If the deviation between the measured angle and the expected angle to a reflector is small, the measured angle is associated to that reflector and the deviation is used to correct the rough estimate of the pose.

The association of a measured angle to the object causing the reflection is a key function in the navigation technique. There are several possible scenarios a few are listed below.

- The angle originates from a surveyed retro-reflector with a correct position in the reflector map.
- The angle originates from a stainless steel tube with a position not corresponding to the retro-reflector positions in the reflector map.
- The angle originates from a retro-reflector with a correct position in the reflector map but there are one or more reflector positions in the map giving the same expected angle.

- The angle originates from a retro-reflector that has been moved after the survey so that the measured angle and the expected angle differ significantly.

If a measured angle is wrongly associated to a retro-reflector in the map and thereby used for correction, the resulting pose estimate can be totally erroneous resulting in collisions with fixed installations at the site or with other vehicles. Therefore, it is of importance that the angle used for correction originates from the true retro-reflector with a correct position in the reflector map to avoid production disturbances.

A pose estimation safety system handles the lack of measured angles or angles that cannot be associated to retro-reflectors in the reflector map. Such measurements or lack of measurements causes the safety level to drop and when the level reaches 0% the vehicle is stopped. The vehicle will come to a stop in less than a second if consecutive measurements cannot be associated to retro-reflectors. Measured angles that are associated to retro-reflectors in the map increase the safety level up to 100%. The safety level is not updated if the safety level is at 100% and the measured angle is associated to a retro-reflector in the map.

Note that a measured angle can be disregarded even though it actually originates from a retro-reflector with a correct position in the map. This can happen if the sensors measuring the speed and steering angle gives inaccurate readings, resulting in incorrectly calculated expected angles to the retro-reflectors.

2.2.2 Guidance controller

The reference path of the vehicle is defined as a set of consecutive segments, where the end point of one segment is the start point of the next segment. A segment is mathematically defined as a 2D polynomial in the (x,y) plane of the plant.

The first step in the guidance control of the vehicle along the reference path is to transform the pose estimate to a local co-ordinate system of the active segment. The second step is to calculate the distance error and the heading error to the segment. The distance error is the distance between the control point of the vehicle and nearest point on the segment. The control point is typically somewhere on the centreline of the vehicle, for instance in the mid point of the rear axle in case of a tricycle vehicle. The heading error is the difference between the heading of the vehicle and the slope of the segment in the nearest point on the segment. The third step is to calculate the set value of the steering angle based on the distance and heading errors so that the vehicle follows the reference path smoothly. This is done by selecting appropriate weights of the distance error and the heading error to the segment in the guidance feedback controller. The wanted speed of the vehicle is given in the segment description and is used as the speed set value.

The guidance safety function will stop the vehicle if the control point is outside a safety zone around the active segment.

The laser guidance technique can be compare to a wire guided system; the only difference is that the wires are virtual and not physically embedded in the floor of the factory. In this context, it is important to note that the virtual wires do not have any limitations as the physicals wires have, for instance the magnetic field limiting the distance between them, implying that the virtual wires can be positioned arbitrarily in relation to each other.

Remark: The first representation of the segments were straight lines, Andersson (1989), but have later been modified to curved shapes to avoid discontinuities in the connecting points and for better control of the sweep area of the vehicle in curves.

2.2.3 Pros and cons

A minimal disruption of production is a key aspect demanded from end customers during commissioning. The impact during commissioning of a laser navigation system in on-going production environments is low. Retro-reflectors are easy to install. The survey of the reflectors has very little disruptive impact on the production system. Much of the traffic and order processing can be simulated off-line.

The most common plant layouts are of the "half-open" character, which is well suited for laser navigation with a typical distance between the laser anglemeter and the retro-reflectors of 5-15 meters.

There are no restrictions on the complexity of the traffic flow of AGVs and the reference paths that can be created since the paths are defined in a CAD system and the pose of the AGVs can be determined at every location in the plant.

Installation of a laser navigation system in environments with environmental requirements can be done with advantage, since no action is required in the factory to prevent dusting during the installation. Destructive action of the plant is necessary for systems that use, for example, navigation references in the floor, such as wire guidance systems. Examples of applications with high environmental requirements are the food and pharmaceutical industries.

An "abundance" of retro-reflectors can be installed since they are not space demanding to ensure redundancy in case of blocked or lost retro-reflectors.

The association of measurements made by the laser anglemeter to be either "true" or "false" ensures the robustness of the pose estimation method. Only measured angles to true reflectors are used in the correction of the pose estimate.

The pose initialisation, after, for instance, powering-on, is done automatically with no requirements of complementing systems or that the vehicle should be positioned in certain spot as long as the laser anglemeter is surrounded by a minimum of four well spread out retro-reflectors. The "self-healing" property regarding the localization is in contrast to other navigation techniques that require external systems for the initialisation of the pose or that the AGV is manually moved to certain spots in the plant.

Some environments are less suitable for the installation of retro-reflectors, for example, floor stacking areas where the line of sight is limited or the distance to walls / pillars / etc. is significant.

Outdoor setting with large distances between the AGVs and walls / pillars / etc. are not appropriate due to the reduction of the detection distance of retro-reflectors that fog inflicts.

2.3 Literature survey

A survey of navigation methods for AGVs and mobile robot applications is found in Hyyppä (1993c). A brief review of later work is given in this section with focus solely on computer

vision systems for AGV applications. The main argument for vision systems is that there is no need for special infrastructure to support the navigation function.

Computer vision based navigation techniques are nowadays commercially available, where typically cameras are used for the navigation of the AGV. An alternative to the camera as the vision sensor is a sensor that illuminates objects with a laser and calculates the distance based on the reflected light.

Kelly, Nagy, Stager and Unnikrishnan (2007), summarizes a five year project with the goal to develop a computer vision based AGV system that does not require supporting infrastructure for the navigation and can handle load that are not placed in exact positions, which typically occurs when humans handles, for instance, pallets. Kelly et al. claims that the developed system is the first instance of an AGV that has operated successfully in a relevant environment for an extended period of time without relying on any special infrastructure. The system consisted of a tug truck and a forklift truck. A downward looking camera was used on both AGVs for the navigation utilizing the "mosaic-based localization" technique as discussed in Kelly (2000). Four separate visions systems were installed on the forklift AGV, two systems for positioning and two systems for perception (fork hole location and stacking). The vision systems are based on cameras with the exception that the positioning system for trailer loading uses a laser sensor (LADAR).

Seelinger and Yoder (2006) discuss a method to automatically engage a forklift truck to a pallet based on a vision system using cameras. No supporting infrastructure for the identification of the pallet was used. The system managed to engage successfully in 98 cases out of 100 with varying localisations of the pallet.

Lecking, Wulf and Wagner (2006) discuss two laser based methods to locate and pick-up pallets. One method requires supporting infrastructure on the pallets (retro-reflectors) whereas the other method relies only on geometrical information of the pallet. The method based on the retro-reflectors is claimed to be robust and can locate and pick-up the pallet even if the position of the pallet is completely unknown. The method based only on the geometrical information can handle pose errors of the pallet of ±150 mm in both the x-direction and y-direction and ±15 degrees of orientation.

Baglivo, Biasi, Bellomo, Bertolazzi and Da Lio (2011) presents a method based on both laser and camera for the problem of identifying and localizing the pallet. A state-of-the art survey regarding other methods is also presented.

3 Historical background

A historical background is presented in this section. The discussion is split into two sections, the research project at Luleå University of Technology that resulted in the spinoff company AutoNavigator AB and the company NDC Netzler & Dahlgren Co AB that played a significant role in the commercialization of the laser navigation system that was developed in the research project.

3.1 The research project

Prior to the research project the inventor of the laser navigation system worked with the development of star sensors for sounding rockets that could detect the light emitted from bright stars. A sounding rocket spins around its own axis and when the emitted light from a star hits the photodiode of the star sensor, a pulse is generated. The attitude angles of the sounding rocket can be calculated in an off-line procedure based on recorded time instances of the pulses, Hyyppä (1993c).

Parts of the methods used in the sounding rocket application could be used for navigation of AGVs if the stars were replaced by retro-reflective stripes of tape and the illumination and detection of them was done by the laser anglemeter.

Figure 3. Luleå Turbo Turtle (LTT) in 2013. The design allows forks to be installed in the tower for load handling.

The inventor received funding from Carl Tryggers Stiftelse för Vetenskaplig Forskning to initiate work with the development of the laser navigation system. The Swedish business journal Dagens Industri, which monitored granted proposals from Carls Tryggers Stiftelse för Vetenskaplig Forskning, noted the project and interviewed the inventor, in an article entitled "He creates the unmanned truck that moves freely in the factory" (freely translated from "Han skapar den förarlösa trucken som kan röra sig fritt i fabriken"). The article was published on January 13, 1984. NDC Netzler & Dahlgren Co AB and a company that developed tailor made trucks contacted the inventor after the article was published.

The truck company received funding from Stiftelsen för Teknisk Utveckling to develop, in collaboration with the inventor, a laser navigating AGV to be installed in a plant for production of electronic systems. The collaboration resulted in a patent and a prototype AGV later referred to LTT, Luleå Turbo Turtle. The company that developed tailor made trucks went out of business before the research project was completed.

Urban Wiklund, Kent Mrozek and the author of this report were recruited to work in the research project. The Centek foundation at Luleå University of Technology contributed with additional funding in the later part of the project so that the software and the hardware could be updated. Johan Nordlander, Jan-Erik Moström and Lars Bergström were engaged for this work. The show-off off the Centek era in the project was at the Technical Fair in Älvsjö outside Stockholm Sweden in 1989 at which LTT was demonstrated.

The research project resulted in licentiate theses by Wiklund (1988) and Andersson (1989) and a doctoral thesis by Hyyppä (1993c) besides the founding of AutoNavigator AB.

3.2 NDC Netzler & Dahlgren Co AB

NDC Netzler & Dahlgren Co AB (referred to as NDC AB in the remainder of the report) was founded 1962 in Gothenburg, Sweden.

NDC AB became involved in the so-called Volvo Kalmar project in the early 70's, the first installation of AGVs in Sweden.

Volvo projected the Kalmar plant with the goal to create a flexible and ergonomic working environment. The assembly line was abandoned by the introduction of production cells. The cars under assembly were transported between the cells by AGVs. The design of the AGVs allowed the fitter to ride along and work with the car during the transport. NDC AB's role in the project was to develop the control systems for the two first prototype AGVs so that the concept could be tested. The concept fulfilled the requirements that Volvo had. The plant was built and the AGV system was installed in full-scale in 1972. NDC AB continued during the 70's to deliver control systems to other Volvo plants.

NDC AB was involved in a number of other AGV projects in Sweden in the 70:ies in addition to the Volvo projects. Notable is the first installation of AGVs at Tetra Pak in 1975 at the site in Lund, Sweden, for transport of paper rolls. The system had, for that time, the unique property that it was integrated with the business system of the factory. The integration implied that the transport tasks for the AGVs were automatically generated from the production planning system, although transport tasks could be generated or altered by the operators in the factory. The operators also had the possibility to change the route of the AGVs and also manually control the AGVs with a hand held device.

Figure 4. The photograph is taken at Volvo's plant in Kalmar, Sweden. Three out of 280 AGVs carrying car bodies under assembly are visible. The AGVs navigates by following magnetic fields generated in wires buried in the floor. The photograph is published with permission of Kollmorgen Särö AB.

The successes on the local Swedish market made NDC AB take the decision to develop their business model and introduce the technology on the international market. The business model implied that NDC AB provided a complete product line for AGV control with an architecture that made it easy for manufacturers of forklifts and material handling system to integrate and adapt the products to create customized transport solutions on their local markets. The model was based on a close and open collaboration with the supplier of the generic control technology (NDC AB) and companies utilizing the technology to continuously update the products with new functionality based on feedback from the suppliers needs. NDC AB limited its sales to a few partner companies within each market segment.

The first partner companies, the customers of NDC AB, were material handling companies in France and Germany, soon followed by companies in Finland and Switzerland. A company, NDC Automation, was founded in Charlotte, NC USA for the American market.

The business model is still in use, now by Kollmorgen Särö AB subsidiary to the American company Danaher who bought NDC AB in 2001.

4 The journey of the laser navigation system

4.1 AutoNavigator AB

The regional venture capital company Rödkallen AB acting in the county of Norrbotten, Sweden was in 1989 actively looking for investment cases as noted in the sub-annex 1 (p. 82) to the proposition from 1996 from Swedish National Audit Office. Rödkallen AB considered the research project to have business potential, which resulted in the founding of the spinoff company AutoNavigator AB

The business model used by Rödkallen AB to start spinoff companies from research projects at Luleå University of Technology was to found the companies together with the researchers from the university. Rödkallen AB was the main shareholder (>90%) and the researcher minority shareholders with an option to become major shareholders at a later stage when the spinoff company had started to take off.

AutoNavigator AB started its operations in 1990. The first business request came from NDC AB, which had been contacted by Tetra Pak regarding laser-navigating AGVs. Tetra Pak was considering laser-navigating AGVs at their plants in Dijon, France and in Singapore. The result of the request was the installation of 10 laser-navigating AGVs at the plant in Singapore in 1991.

Much work was done during the AutoNavigator era to adapt the navigation software and the laser anglemeter for production and for use in industrial applications. A rough estimate is that the software code ten folded during the period.

AutoNavigator AB was sold to the NDC group in 1992. The reason for the sale was the financial situation of the mother company Rödkallen AB as discussed in the sub-annex 1 (p. 82) to the proposition from 1996 from Swedish National Audit Office.

4.2 Collaboration with NDC AB

A close collaboration was early established between AutoNavigator AB and NDC AB who had developed a complete control system for AGV applications after the Volvo Kalmar project in the early 70's. The lacking component in the AGV system, NDC7, was the laser navigation functionality.

The main focus of the work was to integrate the laser navigation system in the NDC7 system. The first solution implied a stand-alone navigation computer for the navigation functionality. A few installations in addition to the Singapore system were delivered with this configuration. The navigation algorithms were later implemented in the NDC7 hardware.

4.3 The importance of patents

The method to associate a measured angle to an anonymous retro-reflector, a single stripe of retro-reflective tape, was patented by the inventor, Hyyppä (1988, 1989, 1991, 1993a, 1993b).

AutoNavigator AB in collaboration with NDC AB was not first to introduce laser navigation systems for industrial AGV applications on the commercial market. An earlier system used bar coded retro-reflectors where single stripes of retro-reflective tape with different spacing defined the code. A limited number of combinations were possible.

The team from Luleå University of Technology was contacted by representatives from the team behind the bar coded system at a conference on automated guided vehicle systems in 1988. The team behind the bar coded system claimed that the laser navigation system infringed a patent of theirs.

The claim remained unanswered until 1992; at a time when the NDC group had started to market the laser navigation system in USA and a US based company had started to market the bar coded system. The US based company contacted the NDC group and repeated the claim from the conference. A meeting was held to discuss the matter, in which a question was raised how to associate measured angles to retro-reflectors in big plants with multiple retro-reflectors with the same bar code. The reply was to use the knowledge of a pose estimate of the vehicle to distinguish the bar coded retro-reflector the measured angle originated from, which was the method patented by the inventor. This discussion changed the momentum since it became clear that the bar coded system likely infringed the patent of the inventor.

The successful outcome of the meeting was thanks to the patent by the inventor and implied that the NDC group could continue to market the laser navigation system in USA.

An analysis of the technical details that are distinctive is essential in preparing for a meeting as discussed above. The importance of the own patent becomes very clear during this type of work.

4.4 Business aspects

The Tetra Pak Singapore installation was important as a reference plant, but few laser navigation systems were sold and installed the years after. NDC put a lot of resources to market and push the technology to potential end customers during the years following the Singapore installation. The patent by the inventor played an important role in the marketing of the system. The patent could be used to make it credible to the end customers that the laser navigation system separated itself from other technologies, Netzler (2013).

It should be noted that the time it takes to establish a new complex technology, such as the laser navigation system, on a market with an existing and accepted solution, the wire guided system, is resource consuming and takes time. In this context, it is important to note that the end customers are more open to new technologies than the suppliers of the AGV systems and that the factual arguments does not necessarily coincide with the marketing arguments of the new technology. The time to market is illustrated by the sales of laser navigation units in table 1.

Table 1. The table shows sales of laser navigation units by NDC AB, DanaherMotion Särö AB and Kollmorgen Särö AB during the period 1991 - 2012. The data is published with permission of Kollmorgen Särö AB.

Period	Sold units
1991 – spring of 1998	1000
Summer of 1998 - 2012	9000

The laser navigation technology was new in the 90's compared to the wire guided based navigation technology with its roots in the 50's. The differentiation aspect – new vs. old technology - was especially noticeable in Japan, where the latest technology is used to a greater extent compared to e.g. Europe. An important event occurred in 1993 when a large Japanese company became partner to NDC AB, where the then new laser navigation technology that NDC AB could offer was an important contributor to the partnership.

4.5 Retrospective

It can be concluded that the increased capacity of the computer / memory capacity that emerged after the developments of the laser navigation algorithms in the latter part of the 80's was not used to further refine the algorithms when looking in the rear-view mirror.

One example of a potential refinement is the use of multiple angles instead of single angles in the correction of the pose estimate in the Kalman filter method, which can further increase the robustness of the pose estimation.

The complexity of managing systems products is one reason to why refinements are not done. Another reason is that it may be difficult to evaluate new ideas based on the commercial value.

The lesson is to constantly rethink the system based on new conditions and circumstances such as increased computing power and memory capacity.

4.6 Application outside the AGVS market

The laser navigation system was adapted to automation of the LHD vehicles at the LKAB Kiruna iron ore mine in Sweden in 1996. The navigation system was part of an LHD automation system used in production from 1999 to 2009, Wylie (1996), Nilsson, Wigdén, and Tyni (2001).

LHD automation systems were not considered to be part of the AGVS market. The necessary work to adapt the system to the application was therefore done by the company Q Navigator AB, founded to focus on mobile robotics in underground mine applications working in close collaboration with the NDC group.

Figure 5. The photograph shows one of eight automated LHD's at the LKAB iron ore mine. The photograph is published with permission of LKAB.

The LHD vehicle, where LHD stands for Load, Haul and Dump, is a type of wheel loader machine adapted for use in underground mines. The LHD is articulated frame steered to reduce the sweep area when turning. The main difference compared to a wheel loader is that the cabin is placed on the side of the machine to reduce the height.

The LHD in figure 4 is 14 meters long. The width of the bucket is approximately 4 meters. It weighs 77.5 tonnes un-loaded. The approximately 300-metre long cable of the machine is connected to a 1000 [VAC] outlet. The cable is rolled in or out depending on the travelling direction of the LHD, on a drum in the rear of the machine. It has a nominal loading capacity of 25 ton in a 10 [m^3] bucket. The rubber tyres are filled with both compressed air and water to reduce the explosion at puncture. The laser anglemeter for the navigation system is placed on the pole above the rear wheels and rotates the laser beam 3.20 meter above the ground. The height above the ground is selected so that the cabin of the LHD does not block the laser beam.

4.7 The current market

The current trend drives the technical development towards more flexible solutions especially for warehouse applications and at interfaces between automatic systems and manual operations.

The Automatic Guided Cart (AGC), a simple AGV based on magnetic tape navigation replacing stationary conveyor solutions, is expanding in the market.

A more complex system is the Automotive Intelligent Vehicle (AIV) for handling of goods such as containers in harbour areas.

The main suppliers on the world market for AGV systems are Kollmorgen Särö AB, IBEO, Götting KG and Guidance Navigation Limited.

The market of laser navigating systems in the world is estimated by Kollmorgen Särö AB to be in the interval of 1200-1600 units/year in which Kollmorgen Särö AB's share is about 50%.

The total market of AGVs in the world is estimated to be in the interval of 3000-4000 units/year.

The estimates imply that the laser navigation system has a market share in the interval of 15% - 27%.

5. Conclusion

The laser navigation system with its origin in a research project at Luleå University of Technology in the late 80's is today 2013 one of the leading technologies for AGV applications. There are some important events and circumstances that stand out when analysing the reasons for the success.

- The contact that was established between the inventor and NDC AB after the article in Dagens Industri 1984 turned out to be a key event in the commercialisation of the system.
- AutoNavigator AB did important work regarding the adaption to industrial applications of the system and the integration in a complete AGV system, NDC7. Therefore, the decision by Rödkallen AB to invest in the development of the system by founding AutoNavigator AB together with the researchers was a key contribution in the commercialisation of the system.
- The timing was optimal, since the system was developed at a time when the end customers of AGV systems started to ask for more flexible solutions than wire guided systems.
- AutoNavigator AB and NDC AB had developed complementing technologies and managed, although located in different regions of Sweden, to start a close collaboration that resulted in the integration of the laser navigation system in a complete AGV system, NDC7.
- NDC AB had the contacts with the end customers and had developed a business model in which the laser navigation system fit implying that NDC AB provided an efficient channel to the market for the system.
- The marketing campaign by NDC AB was sustained and turned out to be successful. The sales of laser navigation systems were low the years following the first installed system in 1991. It took several years of active marketing before the sales started to take off.
- The patent of the inventor turned out to be the key to get access to the American market. The patent prohibited a US based company to take legal action, claiming that the system infringed a patent of theirs, since the navigation system of the US based company likely infringed the patent of the inventor.

The National Audit Office concluded in 1996 that that the investments made by the mother company Rödkallen AB in AutoNavigator AB had an insignificant effect for the Norrbotten County and that the Swedish State lost 20 MSEK on the investment in Rödkallen AB.

The conclusion 17 years later is that the investment in AutoNavigator AB had a significant effect for the AGV systems industry in Sweden since the development of the now market leading technology has been based in Sweden ever since and has generated income to the Swedish State. It took several years to establish the laser navigation system on the market. The conclusion from the National Audit Office is therefore overhasty. The time to market for complex systems such as the laser navigation system has to be taken into account when analysing the outcome of the investment.

To analyse if the laser navigation system qualifies as an innovation, the Oslo Manual issued by OECD and Eurostat (2005) is used to interpret the definitions cited in section 1.

A common feature of an innovation is that it must have been *implemented* (§ 150), which means that it must have been introduced on the market, in this case the AGV systems (AGVS) market.

Diffusion is the way in which an innovation is spread through the market (§ 37), in this case the AGVS market, from the first implementation to different consumers, countries, regions, sectors, markets and firms. Without diffusion, the innovation has no economic impact.

An innovation must contain a degree of *novelty* (§ 205), which can be.

- *New to the firm* (§ 207), a product has been implemented by other firms but is new to the firm, in this case AutoNavigator AB.
- *New to the market* (§ 209), the firm is the first to introduce the innovation to the market. The market is the firm and its competitor and can include a geographical region or a product line. The geographical scope is defined by the firm's own view of its market, in this case the AGVS market.
- *New to the world* (§ 210), the firm is the first to introduce the innovation for all markets and industries, domestic and international.

A related concept to novelty is *radical* or *disruptive* innovation (§ 211), which is a concept that focuses on impact rather than novelty. A disruptive innovation has a significant impact on the market and the economic activity of firms in that market, in this case partner companies to Kollmorgen Särö AB active in the AGVS market.

The conclusion is that laser navigation system is *implemented.* It was introduced on the market in 1991. The system is also *new to the market.* The system was not the first laser navigation system in the market, but it was the first system using simple identical targets (anonymous stripes of retro-reflective tape). The system also fulfils the requirement of *diffusion* since it has been implemented in different consumers, countries, regions, sectors, markets and firms after the first implementation in Singapore at the Tetra Pak site. The system is also *disruptive* since it has a significant impact in terms of market shares and economic activity in partner firms to Kollmorgen Särö AB on the AGVS market.

The answer to the question in section 1 whether or not the laser navigation system is an innovation is: Yes it is an innovation. In addition to the minimum requirements (new to the firm and implemented), the innovation is new to the market, is disruptive and has an economical impact implying diffusion.

Technical features that proved important are the virtual guide paths (flexibility for the end user), the redundancy and the robustness of the system. The end user can create guide paths without destructive work in the factory. An abundance of retro-reflectors can be installed since they are not space demanding to ensure redundancy in case of blocked or lost retro-reflectors. The association of measurements made by the laser anglemeter to be either true or false ensures the robustness of the pose estimation method.

The localisation function of the system is self-healing which is an important feature for the usability of the system. The pose initialisation is done automatically with no requirements of complementing systems or that the vehicle should be positioned in certain spot as long as the laser anglemeter is surrounded by a minimum of four well spread out retro-reflectors.

References

Andersson, U. (1989). Trajectory estimation and control of autonomous guided vehicles. Licentiate thesis, Luleå University of Technology, Luleå, Sweden.

Baglivo, L., Biasi, F., Bellomo, N., Bertolazzi, E. and Da Lio, M. (2011). Autonomous pallet localization and picking for industrial forklifts: a robust range and look method. *Measurements Science and Technology*, 22(8).

European Union, http://ec.europa.eu/enterprise/policies/innovation/glossary/index_en.htm#i, read 2013-09-12.

Hedström, A., personal communication, April to September, 2013.

Hyyppä, K., personal communication, April to September, 2013.

Hyyppä, K. (1993c). On a laser anglemeter for mobile robot navigation, Doctoral thesis, Luleå University of Technology, Luleå, Sweden.

Hyyppä, K. (1993b). Menetelämä ohjaajattoman kulkuneuvon ohjaamisekis sekä siihen soveltuva ajoneuva. Finnish patent 88655, Helsinki, February 1993.

Hyyppä, K. (1993a). Fremgangsmåte for å navigere en automatisert, ledet farkost. Norwegian patent88655, Oslo, February 1993.

Hyyppä, K. (1991). Method of navigating an automated guided vehicle. European patent 0238615, Munich, July 1991.

Hyyppä, K. (1989). Method of navigating an automated guided vehicle. US patent 4811288, March 1989.

Kelly, A., Nagy, B., Stager, D. and Unnikrishnan, R. (2007). An infrastructure-free automated guided vehicle based on computer vision. *IEEE Robotics & Automation Magazine*, 14(3), 24-34.

Kelly, A. (2000). Mobile robot localization from large-scale appearance mosaics. *International Journal of Robotic Research*, 19(11), 1104-1125.

Lecking, D., Wulf, O. and Wagner, B. (2006). Variable pick-up for automated guided vehicles in industrial environments. In *Proceedings of IEEE Conference on Emerging Technologies and Factory Automation*, 1169-1174.

Müller, T. (1983). Automated Guided Vehicles. IFS (Publications) Ltd./Springer-Verlag, UK/Berlin.

Netzler, G., personal communication, September, 2013.

Nilsson, J-O., Wigdén, I., & Tyni, H. (2001). Mine automation at LKAB Kiruna, Sweden. In W. Hustrulid & R.C. Bullock (Eds.), *Underground mining methods: engineering fundamentals and international case studies*, (chapter 75). Society for Mining, Metallurgy, and Exploration: Littleton, Colo.

Oslo Manual: Guidelines for Collecting and Interpreting Innovation Data, 3rd Edition (2005), ISBN 978-92-64-01308-3.

Riksdagens revisorer (1996), Förslag till riksdagen 1996/97:RR2: Riksdagens revisorers förslag angående statligt engagemang i regionala investmentbolag.

Schultze, L. and Wüllner, A. (2006). The approach of automated guided vehicle systems. In *Proceedings of IEEE International Conference on Service Operations and Logistics, and Informatics*, 522-527.

Schultze, L. and Zaho, L. (2007). Worldwide development and application of automated guided vehicle systems. *International Journal of Service Operations and Informatics*, 2(2), 164-176.

Seelinger, M. and Yoder, J-D. (2006). Automatic visual guidance of a forklift engaging a pallet. *Robotics and Autonomous Systems*. 54(12), 1026-1038.

Segerfeldt, E., Jakten på innovationer, svenskt näringsliv, ISBN: 9789174378030.

Swedish Enterprise, http://www.svensktnaringsliv.se/english/about-us_16830.html, read 2013-07-13.

Wiklund, U. (1988). Algorithms for navigation of autonomous guided vehicles. Licentiate thesis, Luleå University of Technology, Luleå, Sweden.

Wiklund, U., Andersson, U. and Hyyppä, K. (1988). AGV navigation by angle measurements. In *Proceedings of the 6th International Conference on Automated Guided Vehicle Systems*, Brussels, Belgium.

Wylie, R. (1996). LKAB invests in the future. *Engineering and Mining Journal*:48-52.